Feedback adaptive compensation for active vibration control in the presence of plant parameter uncertainties

Abraham Castellanos Silva

UNIVERSITÉ DE GRENOBLE

THÈSE

Pour obtenir le grade de

DOCTEUR DE L'UNIVERSITÉ DE GRENOBLE

Spécialité : **Automatique-Productique**

Arrêté ministérial : 7 août 2006

Présentée par

Abraham CASTELLANOS SILVA

Thèse dirigée par **Luc DUGARD**
codirigée par **Ioan Doré LANDAU**

préparée au sein du **Laboratoire GIPSA-Lab**
dans l'**École Doctorale Électronique, Électrotechnique, Automatique et Traitement du Signal**

Compensation adaptative par feedback pour le contrôle actif de vibrations en présence d'incertitudes sur les paramètres du procédé

Thèse soutenue publiquement le **29 septembre 2014**,
devant le jury composé de :

M. Mohammed M'SAAD
Professeur, École Nationale Supérieure d'Ingénieurs de Caen, France, Président
M. Masayoshi TOMIZUKA
Professeur, Mechanical Engineering Department, University of California, Berkeley, États-Unis, Rapporteur
M. Alireza KARIMI
Maître d'enseignement et de recherche, EPFL, Lausanne, Suisse, Rapporteur
M. Luc DUGARD
Directeur de Recherche CNRS, Grenoble, France, Directeur de thèse
M. Ioan Doré LANDAU
Directeur de Recherche Emeritus CNRS, Grenoble, France, Co-Directeur de thèse

To Lili, Marilyn and my family

Acknowledgments

The work presented in this Ph.D. thesis has been done in the Control Systems Department of GIPSA-Lab, University of Grenoble, France, affiliated to the research team SLR (Systèmes Linéaires et Robustesse), and with the financial support of the National Council for Science and Technology of Mexico (CONACYT).

First of all, I would like to thank my two Ph.D. advisors, M. Ioan Doré Landau and M. Luc Dugard, from the University of Grenoble, for their constant support and help during my years of study. Both of them have shared their expertise and constantly encouraged me to become a better research scientist.

I would like to express my thanks to M. Mohammed M'Saad, president of the examination committee, and M. Alireza Karimi, member of the examination committee, for having accepted my invitation and also for their words of encouragement. I would like to express also my gratitude to M. Masayoshi Tomizuka and M. Alireza Karimi for having accepted to review my manuscript and write a report on my research work. Their remarks and suggestions were very significant and helpful to improve the work presented in this document, and to guide my future research activities.

I express my gratitude also to M. Gabriel Buche and the entire technical team at GIPSA-Lab; their help and expertise in the development and maintenance of the test bench on Active Vibration Control have been of great importance in obtaining the results presented in this manuscript. Thanks also for the administrative staff from GIPSA-Lab, for their help and guidance.

I would like to thank also Mme Alina Voda and M. John-Jairo Martinez-Molina for their support and the trust that they had on me, during the last year of my thesis, when they allowed me to be a Teaching Assistant at the University Joseph Fourier of Grenoble and the Polytechnic Institute of Grenoble, respectively.

My thanks go also to M. Mathieu Noé, Engineer Specialist at Paulstra-Vibrachoc, for having accepted to collaborate on an Active Vibration Control project.

I would like to express my thanks to my dear colleague and friend T.-B. Airimiţoaie for sharing with me his knowledge and friendship. A special mention goes to the community from the Worldwide Missionary Movement Church at Grenoble for their support, friendship, thrust and help all along these three years. Also, thank you to all my friends (in Mexico and France) for their advice and support.

Last but not least, I want to express my profound gratitude to both families in

Mexico and France, and to my beloved Liliane for having always stood by my side and encouraged me, even in the most difficult times.

Abraham Castellanos Silva

Contents

List of Figures

List of Tables

Glossary

ANC	Active Noise Control
ANVC	Active Noise and Vibration Control
AVC	Active Vibration Control
BSF	Band-stop Filter
CLOE	Closed Loop Output Error algorithm
AF-CLOE	Adaptive Filtered Closed Loop Output Error algorithm
F-CLOE	Filtered Closed Loop Output Error algorithm
FIR	Finite Impulse Response
IIR	Infinite Impulse Response
IMP	Internal Model Principle
OEFC	Output Error with Fixed Compensator algorithm
OEFO	Output Error with Fixed Observations algorithm
OEAFO	Output Error with Adaptive Filtered Observations algorithm
OEEPM	Output Error with Extended Prediction Model algorithm
PAA	Parameter Adaptation Algorithm
PSD	Power Spectral Density
Q	Youla-Kučera parameter
Q-FIR	FIR adaptive filter used in the Youla-Kučera parametrization
Q-IIR	IIR adaptive filter used in the Youla-Kučera parametrization
RELS	Recursive Extended Least Squares algorithm
RML	Recursive Maximum Likelihood algorithm
SPR	Strictly Positive Real
w.r.t.	with respect to
X-CLOE	Extended Closed Loop Output Error algorithm
YK	Youla-Kučera
YK-FIR	Youla-Kučera parametrization using FIR adaptive filters
YK-IIR	Youla-Kučera parametrization using IIR adaptive filters

List of Publications

The following list of publications has been the result from the work developed in this thesis with other two articles, the drafting of which is in progress.

International Journals with Peer Review

[J1] Direct Adaptive Rejection of Unknown Time-varying Narrow Band Disturbances applied to a Benchmark Problem (Castellanos Silva A., Landau I.D. and Airimiţoaie T.B.), European Journal of Control, 19(4):326 – 336 ([Castellanos Silva et al., 2013b]).

[J2] Indirect Adaptive Regulation Strategy for the Attenuation of Time Varying Narrowband Disturbances applied to a Benchmark Problem (Airimiţoaie T.B., Castellanos Silva A. and Landau I.D.), European Journal of Control, 19(4):313 – 325 ([Airimiţoaie et al., 2013]).

[J3] Benchmark on Adaptive Regulation - Rejection of Unknown/Time-varying Multiple Narrow Band Disturbances (Landau I.D., Castellanos Silva A., Airimiţoaie T.B., Buche G. and Noé M.), European Journal of Control, 19(4):237 – 252 ([Landau et al., 2013a]).

International Journals with Peer Review (under review)

[JUR1] Adaptive Attenuation of Unknown and Time Varying Narrow Band and Broad Band Disturbances (Landau I.D., Airimiţoaie T.B. and Castellanos Silva A.), submitted for review to International Journal of Adaptive Control and Signal Processing.

[JUR2] Robust Direct Adaptive Regulation of Unknown Disturbances in the Vicinity of Low Damped Complex Zeros - Application to Active Vibration Control (Castellanos Silva A., Landau I.D. and Ioannou P.), submitted for review to IEEE Transactions on Control Systems Technology.

International Conferences with Peer Review

[IC1] An Active Vibration Control System as a Benchmark on Adaptive Regulation (Landau I.D., Castellanos Silva A. and Airimiţoaie T.B.), Proceedings of the 12th European Control Conference (ECC), 2013 ([Landau et al., 2013b]).

[IC2] Direct and Indirect Adaptive Regulation Strategies for Rejection of Time Varying Narrow Band Disturbances applied to a Benchmark Problem (Airimiţoaie T.B., Castellanos Silva A. and Landau I.D.), Proceedings of the 12th European Control Conference (ECC), 2013 ([Airimitoaie et al., 2013]).

[IC3] Direct Adaptive Regulation in the Vicinity of Low Damped Complex Zeros - Application to Active Vibration Control (Castellanos Silva A., Landau I.D. and Ioannou P.), Proceedings of the 22nd Mediterranean Conference on Control and Automation, 2014 ([Castellanos Silva et al., 2014]).

National Conferences with Peer Review

[NC1] Stratégies directes et indirectes de régulation adaptative du rejet de perturbations variables à bande étroite appliquées à un Benchmark International (Castellanos Silva A., Airimitoaie T.B., Landau I.D., Dugard L., Buche G. and Noé M.), Proceedings of the 4émes Journées Démonstrateurs, 2013 ([Castellanos Silva et al., 2013a]).

[NC2] Algorithme de commande anticipatrice adaptative et contreréaction fixe pour le contrôle actif de vibrations en présence du couplage mécanique interne (Airimitoaie T.B., Landau I.D., Dugard L., Alma M., Castellanos Silva A., Buche G. and Noé M.), Proceedings of the 4émes Journées Démonstrateurs, 2013 ([Airimitoaie et al., 2013]).

Chapter 1

Introduction et Résumé Détaillé

Ce chapitre est consacré à la description des problèmes fondamentaux de contrôle actif du bruit (ANC) et de contrôle actif des vibrations (AVC) pour le rejet de perturbations à bande étroite. Il présente un résumé de l'histoire et les principaux progrès dans la littérature, une description de l'installation utilisée pour tester et valider les algorithmes développés, et au final un condensé sur les contributions originales de ce travail de recherche.

Le travail développé dans cette thèse a été fait dans le cadre du contrôle actif des vibrations grâce à des techniques de contrôle adaptatif robuste. L'objectif était de développer des algorithmes adaptatifs pour le rejet de perturbations, qui ont été mis en place et testés sur des plates-formes pilotes situées à GIPSA-Lab Grenoble.

1.1 Motivation

Dans cette section, les principes de base du contrôle actif de bruit et de vibration (ANVC) seront présentés. Le contexte de ce travail sera détaillé et des exemples seront utilisés pour poser le problème de commande associé.

Probablement l'un des premiers travaux sur le contrôle actif du bruit a été présenté dans le brevet français de Henri Coandă ([Coanda, 1930]), suivi peu après par le brevet US de Paul Lueg [Lueg, 1934] et par le travail de Harry F. Olson [Olson and May, 1953]. Dans ces travaux, l'idée de base était d'atténuer le bruit à l'aide d'une source secondaire électro-acoustique (haut-parleur). La mesure du bruit est obtenue par l'intermédiaire d'un microphone. Ces travaux se fondent sur le fait qu'il est possible de produire une interférence destructrice entre les champs sonores générés par une source primaire non contrôlée et par une source secondaire, dont la sortie acoustique peut être contrôlée.

L'interférence destructrice, en un point de l'espace, est obtenue lorsque la source secondaire génère une onde sonore ayant les mêmes caractéristiques de fréquence que le bruit, mais avec un décalage de 180^0 en phase. Tel est le principe du contrôle actif du bruit représenté sur la Figure 1.1, où l'effet d'une source sonore primaire est annulé par une source secondaire. La réduction du bruit du moteur dans les avions et les véhicules à moteur est une application possible de cette technique. Ce principe a été étendu à des applications dans le contrôle des vibrations, avec quelques différences comme expliqué dans ce chapitre.

Selon que l'énergie est injectée ou non dans le système, pour compenser le bruit ou les vibrations, on a pour les méthodes indiqués la classification suivante ([Fuller et al., 1997, Snyder, 2000]) : méthodes passives, semi-actives et actives.

La méthode *passive* consiste à ajouter de l'isolant ou d'amortissement. Il s'agit

d'une solution passive en ce que ni le contrôle ni l'énergie sont nécessaires. Parmi les avantages, on peut noter la mise en œuvre de solutions simples, fiables et robustes, tout en étant économiquement limitées en termes de poids et d'encombrement. En outre, étant donné qu'il n'est pas possible de cibler l'action de contrôle sur des objectifs particuliers, ses capacités de performance dépendent de la dynamique naturelle du système. Le résonateur de Helmholtz ([Olson and May, 1953, Fleming et al., 2007]) est un exemple de cette méthode.

Le procédé *semi-actif* a été développé pour surmonter les limites de la méthode passive. Cette méthode intègre l'utilisation d'actionneurs qui se comportent comme des éléments passifs, en autorisant uniquement le stockage ou la dissipation de l'énergie. La nouvelle fonction est l'ajustement de leurs propriétés mécaniques par un signal provenant d'un régulateur ([Karnopp et al., 1974]). Les amortisseurs de certains véhicules qui ont un coefficient d'amortissement visqueux commandé par ordinateur sont un exemple.

La méthode *active* utilise la capacité de fournir de l'énergie mécanique au système pour cibler l'action de commande sur des objectifs spécifiques. Cette thèse se concentre sur cette méthode de contrôle. Pour les applications au bruit, l'intérêt est porté sur des fréquences allant de 20 Hz à 20 000 Hz. Comme mentionné dans [Olson and May, 1953, Elliott and Nelson, 1993, Elliott, 2001], les méthodes passives ne fonctionnent généralement pas bien aux basses fréquences (inférieures à 500 Hz) car la longueur d'onde devient plus grande, ce qui nécessite des matériaux plus épais et plus lourds. Pour cette raison, beaucoup de problèmes acoustiques, en pratique importants, sont traités par les contributions actives de contrôle. Comme le montre la suite, cela posera de nouveaux problèmes de contrôle intéressants.

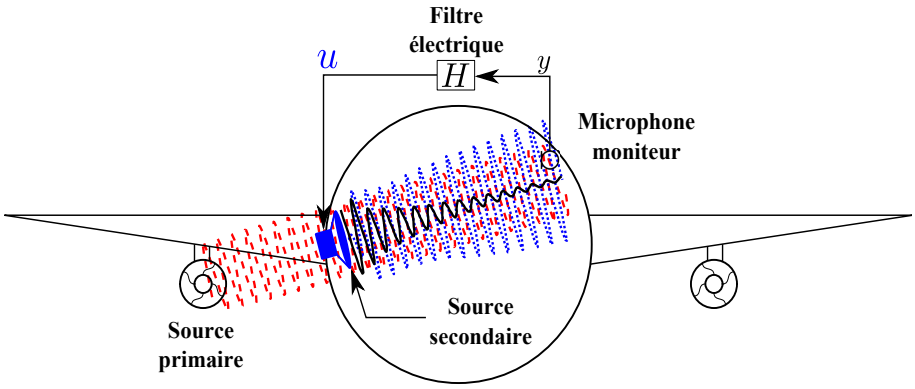

Figure 1.1: Annulation du bruit au moyen de l'ANC utilisé pour augmenter le confort acoustique des passagers dans un avion. Ligne pointillée rouge: source primaire, ligne pointillée bleue: source secondaire, ligne noire: onde acoustique mesurée par le microphone.

Les domaines d'application comprennent des domaines tels que l'automobile, l'aéronautique, la marine, les appareils où les machines rotatives et les moteurs créent des vibrations indésirables (voir [Chen and Tomizuka, 2014, Chen and Tomizuka, 2013a]). Un exemple d'annulation de bruit est illustré dans la Fig. 1.1, où la réduction du bruit engendré par les turbines d'avion est recherchée. Afin d'augmenter le confort des passagers, le bruit généré par les turbines d'avion est réduit le plus possible à l'aide d'une source secondaire (haut-parleurs) et d'un microphone utilisé comme capteur de bruit. Un autre exemple de réduction de vibration est représenté sur la Fig.1.2, où un système de commande active de châssis est disponible. Dans cette

application, l'objectif est de réduire les vibrations engendrées par le moteur au niveau du châssis. Au moyen d'actionneurs, une vibration contraire est introduite dans le châssis avec un déphasage de 180^0. Les vibrations sont généralement mesurées par des accéléromètres ou des capteurs de force. D'autres exemples sont donnés dans [Elliott and Nelson, 1993, Fuller and von Flotow, 1995, Guicking, 2007].

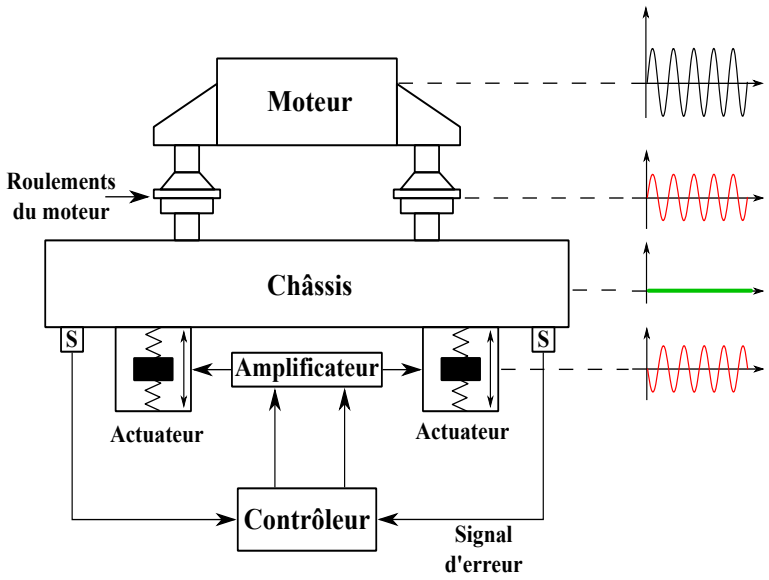

Figure 1.2: Contrôle actif de châssis utilisé pour réduire les vibrations engendrées par le moteur.

1.2 Description du Problème

Cette section fournit une brève description de l'un des problèmes de base pour le contrôle actif de bruit et vibrations (ANVC) qui seront traités plus tard dans cette thèse. L'objectif principal de commande est de réduire au mieux le niveau de vibrations (ou de bruits) à un endroit prédéfini.

Contrairement aux applications du contrôle actif du bruit, les applications au contrôle actif des vibrations sont très liées aux propriétés mécaniques de la structure considérée. En effet, dans une structure plusieurs types de mouvement d'onde peuvent causer des vibrations se propageant d'un endroit à l'autre. Les ondes acoustiques, évidemment, ne se propagent que longitudinalement dans les fluides à faible viscosité, tels que l'air. Dans les structures complexes souvent rencontrées dans les avions, vaisseaux spatiaux, navires et voitures, les différents types de mouvements ondulatoires structurels sont généralement couplés de façon assez complexe. Cela se traduit par des caractéristiques de fréquence du système présentant des modes de résonance et d'anti-résonance. Aux fins de régulation par rétroaction, les modes anti-résonants (générés par la présence de zéros complexes avec un faible amortissement) sont critiques pour la performance et la robustesse.

Une description linéaire du problème, quand toute l'information est disponible, sera utilisée comme point de départ pour améliorer les objectifs et les contraintes à résoudre. Cela permettra également de préparer le terrain pour les solutions adaptatives, requises par le manque d'informations sur les perturbations.

1.2.1 Régulation par rétroaction en présence de perturbations à bande étroite

L'un des problèmes fondamentaux pour l'ANC et l'AVC est de pouvoir atténuer des perturbations à bande étroite sans les mesurer. Cela peut se faire grâce à une approche de rétroaction. Même s'il y a deux configurations de contrôle (anticipation et rétroaction), dans cette thèse, seule la configuration de rétroaction sera considérée. La raison en est que le banc d'essai utilisé pour les expériences ne dispose que d'un seul mesure, alors que l'approche d'anticipation nécessite un deuxième capteur pour obtenir une *image* de la perturbation [Landau et al., 2011a].

La limitation de l'approche de rétroaction vient de l'intégrale de sensibilité de Bode [Doyle et al., 2013]. Cette intégrale stipule essentiellement que, quand une atténuation est obtenue à une certaine fréquence, une amplification se produit à une autre fréquence (connu aussi comme l'effet "*waterbed*"). Si le rejet de perturbations large bande est tenté avec une approche de rétroaction, des amplifications importantes se produiront car ce type de perturbations nécessite une *large* zone d'atténuation. Par conséquent, seules les perturbations à bande étroite seront considérées pour des approches de rétroaction. Pour le rejet de perturbations à large bande, des solutions ont été récemment été présentées, voir [Alma, 2011] et [Airimiţoaie, 2012].

Considérons le schéma de commande représenté sur la Fig. 1.3, où un système discret $G(z^{-1}) = \frac{z^{-d}B(z^{-1})}{A(z^{-1})}$ à une entrée et une sortie (SISO) est perturbé par un signal $p(t)$. La sortie perturbée est $y(t)$ et l'entrée du procédé est $u(t)$. Afin de forcer la sortie $y(t)$ vers zéro, c'est à dire annuler l'effet de la perturbation $p(t)$, un régulateur $K(z^{-1})$ est incorporé dans la boucle.

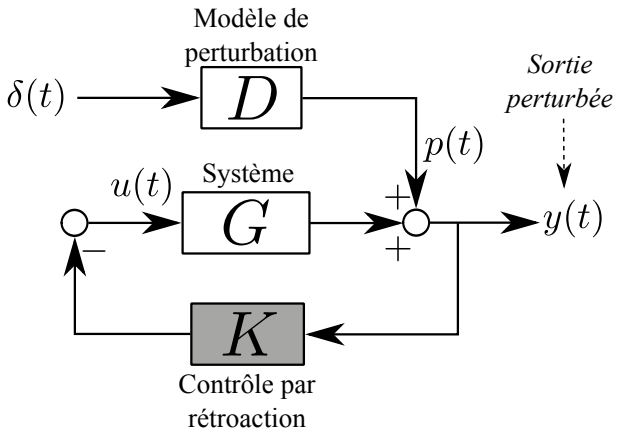

Figure 1.3: Système de rétroaction pour ANVC.

On suppose que le contrôleur K est une fonction de transfert de la forme :

$$K(z^{-1}) = \frac{R(z^{-1})}{S(z^{-1})}, \tag{1.1}$$

$R(z^{-1})$ et $S(z^{-1})$ étant des polynômes en z^{-1} avec la structure suivante

$$R(z^{-1}) = r_0 + r_1 z^{-1} + \cdots + r_{n_R} z^{-n_R} = H_R(z^{-1}) R'(z^{-1}), \tag{1.2}$$
$$S(z^{-1}) = 1 + s_1 z^{-1} + \cdots + s_{n_S} z^{-n_S} = H_S(z^{-1}) S'(z^{-1}), \tag{1.3}$$

où n_R et n_S sont l'ordre des polynômes R et S, respectivement et H_R et H_S sont des parties pré-spécifiées à des fins diverses, par exemple pour ouvrir la boucle à certaines fréquences ou intégrer le modèle d'une perturbation. Ce régulateur peut être calculé d'une manière linéaire par la méthode de *Placement de Pôles avec calibrage de fonctions de sensibilité*, par exemple[1]. Si le signal de perturbation $p(t)$ est connu, à savoir le modèle de la perturbation, il peut être utilisé à des fins de contrôle. Pour les perturbations à bande étroite, on suppose que $p(t)$ est le résultat du filtrage de l'impulsion de Dirac par un filtre $D(q^{-1})$:

$$p(t) = D(q^{-1})\delta(t) = \frac{N_p(q^{-1})}{D_p(q^{-1})}\delta(t) \tag{1.4}$$

où les racines de $D_p(z^{-1})$ sont sur le cercle unitaire.

La sortie du système en boucle fermée peut être écrite comme suit :

$$y(t) = \frac{1}{1+GK}p(t) = \frac{A(q^{-1})S(q^{-1})}{P(q^{-1})}p(t) \tag{1.5}$$

où $P(z^{-1}) = A(z^{-1})H_S(z^{-1})S'(z^{-1}) + z^{-d}B(z^{-1})H_R(z^{-1})R'(z^{-1})$ définit les pôles en boucle fermée. Si le polynôme $S(z^{-1})$ est sélectionné comme $S(z^{-1}) = D_p(z^{-1})S'(z^{-1})$, la sortie du système en boucle fermée devient

$$y(t) = \frac{A(q^{-1})D_p(q^{-1})S'(q^{-1})}{P(q^{-1})} \cdot \frac{N_p(q^{-1})}{D_p(q^{-1})}\delta(t) = \frac{A(q^{-1})S'(q^{-1})N_p(q^{-1})}{P(q^{-1})}\delta(t). \tag{1.6}$$

Si le dénominateur de (1.6) est asymptotiquement stable, à savoir $P(z^{-1}) = 0$, $|z| < 1$, la sortie du système en boucle fermée tend asymptotiquement vers zéro. Ceci est connu comme le *Principe du Modèle Interne* (IMP) [Francis and Wonham, 1976].

Les remarques suivantes peuvent être faites :

1. Pour le rejet d'une perturbation dans un contexte linéaire, il est nécessaire de connaître à la fois les modèles du système et de la perturbation. Généralement, le modèle du système peut être obtenu, par identification du système tandis que le modèle de perturbation est en général inconnu et peut varier dans le temps. Par conséquent, un schéma adaptatif est nécessaire.

2. Afin d'intégrer le modèle de la perturbation dans le régulateur, il est nécessaire que les racines de $D_p(z^{-1})$ ne soient pas racines de $B(z^{-1})$, c'est à dire que $D_p(z^{-1})$ et $B(z^{-1})$ soient premiers entre eux. Lorsque les racines des deux polynômes se rapprochent, cette caractéristique est réduite. Il est à noter que les systèmes de compensation qui ont des zéros complexes peu amortis compliquent cette situation. Cela est dû au fait que la solution devient des moins en moins copremière; et que la stabilité du système en boucle fermée est compromise. Cela sera examiné plus tard.

3. Même si le dispositif expérimental utilisé dans cette thèse a déjà été présenté dans des travaux antérieurs tels que [Landau et al., 2005] et [Landau et al., 2011b], actuellement, il présente d'importants changements qui résultent de la nouvelle structure mécanique qui introduisent de nouvelles caractéristiques et défis.

[1] D'autres techniques de conception de commande peuvent aussi bien être utilisées.

4. Il existe plusieurs méthodes pour introduire le modèle de perturbation dans la structure du dispositif de commande; parmi elles, la paramétrisation de Youla-Kučera fournit des fonctionnalités utiles pour la stabilité, la robustesse et la performance.

Il est bien connu que, dans les régulateurs de rétroaction, l'IMP peut conduire à une augmentation inacceptable de la valeur maximale de la fonction de sensibilité de sortie (qui rend le système proche de l'instabilité). Cela devient encore plus évident lorsque le rejet de plusieurs perturbations à bande étroite est effectué. Cependant, au voisinage de zéros complexes amortis faiblement, même le rejet d'une seule perturbation à bande étroite peut être difficile à réaliser. Étant donné que le dispositif de commande proposé est basé sur le modèle, un modèle du système identifié plus précis est nécessaire, spécialement dans la bande de fréquence où le rejet de perturbation est effectué.

En outre, même si toute l'information est disponible (modèle du système, modèle de perturbation, etc), la conception du régulateur linéaire n'est pas une tâche triviale. La difficulté augmente lorsque la perturbation est inconnue et variable dans le temps. Par conséquent, le problème réside dans la conception d'*algorithmes de commande adaptative robustes pour le rejet de perturbations inconnues et multiples à bande étroite, éventuellement variant dans le temps en présence de zéros complexes avec un amortissement faible.*

1.3 Revue de la littérature

Cette section fait une revue des contributions importantes de la littérature pour l'identification des zéros à phase non-minimale et pour la régulation par rétroaction de bruit ou de vibrations.

1.3.1 Identification des zéros à phase non minimale

Suivant [Söderström and Stoica, 1988] et [Ljung, 1999], l'identification des systèmes est le domaine de la modélisation des systèmes dynamiques à partir de données expérimentales. Ceci est illustré dans la Fig. 1.4 , où un système dynamique est excité par les entrées $u(t)$ et perturbations $v(t)$ et où certaines variables $y(t)$ sont mesurées.

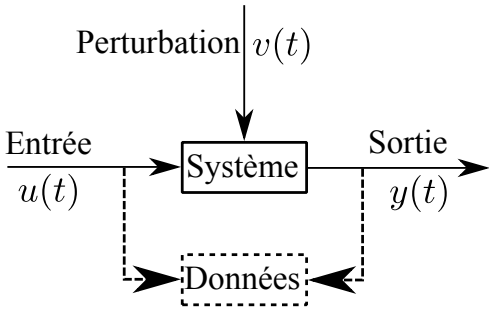

Figure 1.4: Schéma général d'un système dynamique où les entrées, les perturbations et les sorties sont affichées.

En utilisant les données collectées, on peut estimer/identifier les paramètres d'une expression mathématique qui représente la relation entre les entrées (sous contrôle), les perturbations (non contrôlées) et les sorties (mesurées). L'expression mathématique est connue comme *modèle*. La structure du modèle dépend de l'hypothèse faite sur les perturbations (qui ne peuvent être ni contrôlées ni mesurées). Le modèle mathématique représente

la relation entre les entrées et sorties, la représentation par fonction de transfert est utilisée le plus souvent ([Ljung, 1999, Söderström and Stoica, 1988, Landau and Zito, 2005]).

Dans la communauté du contrôle, les modèles sont souvent utilisés pour l'analyse et la synthèse. L'objectif global de l'identification pour le contrôle en effet est de fournir des modèles appropriés pour la conception de commande. Les travaux de [Gevers, 1993] et [Van Den Hof and Schrama, 1995] présentent un aperçu de ce domaine.

La bande passante réalisable par la boucle fermée est un problème majeur dans la conception du régulateur à partir d'un modèle. Ceci est particulièrement critique pour les systèmes qui contiennent des limitations de performance comme les zéros à phase non-minimale et les retards. Cette limitation augmente en temps discret, puisque dans [Åström et al., 1984] il a été prouvé que pour différentes valeurs de période d'échantillonnage, dans de nombreuses applications, des zéros instables apparaissent quand la période d'échantillonnage diminue, même si tous les zéros du modèle du système continu sont stables.

La configuration standard pour effectuer une identification de système est obtenue lorsque le système fonctionne en boucle ouverte (pas de commande en boucle fermée) [Ljung, 1999],[Landau and Zito, 2005]. Une théorie et des techniques ont été développées permettant d'identifier les systèmes en boucle fermée. Plusieurs contributions ont été faites dans ce domaine. Dans [Van Den Hof and Schrama, 1995] et [Hjalmarsson et al., 1996], il a été souligné que les conditions expérimentales en boucle fermée ne doivent pas être considérées comme dégradées ou défavorables, pour identifier les systèmes dynamiques. Si les algorithmes appropriés sont utilisés, de meilleurs modèles de commande peuvent être obtenus par identification en boucle fermée. Puis, dans [Landau and Karimi, 1997], une présentation unifiée des algorithmes récursifs pour l'identification de modèles du système en boucle fermée a été faite, avec des applications en temps réel. Des travaux tels que [Gustavsson et al., 1977], [Van den Hof, 1998] et [Forssell and Ljung, 1999] présentent des articles généraux où il est prouvé que la précision et les performances des modèles obtenus ont été améliorées par rapport aux modèles précédents obtenus en boucle ouverte.

Récemment, pour une identification plus précise des zéros posant problème (phase non-minimale ou avec faible facteur d'amortissement), [Martensson et al., 2005] ont présenté un procédé de synthèse d'entrée, pour optimiser le signal d'entrée. [Mårtensson and Hjalmarsson, 2005] et [Mårtensson and Hjalmarsson, 2009] exploitent l'analyse de la variance des zéros à phase non-minimale estimés et concluent que l'usage des modèles sur-paramétrés n'augmente pas la variance des zéros.

Bien que les travaux précédents traitent spécifiquement des zéros "restrictifs", la technique de synthèse des signaux d'entrée a été développée pour les modèles auto-régressifs avec entrées exogènes (ARX) et les modèles de réponse impulsionnelle finie (FIR). De plus, les conclusions majeures pour l'identification de système en boucle fermée des pôles instables et des zéros à phase non-minimale concernait les modèles sur-paramétrés. Les travaux présentés ici exploitent les résultats présentés dans [Landau and Karimi, 1997] et [Landau and Karimi, 1999] pour l'identification en boucle fermée en modifiant le régulateur, afin d'accroître la sensibilité du système aux fréquences ciblées.

1.3.2 Rejet de multiples perturbations à bande étroite

L'approche de contrôle par rétroaction devient le seul choix quand il n'est pas possible d'utiliser un second transducteur pour mesurer l'image d'une perturbation. Cela se

produit souvent dans la pratique. Si l'on considère les restrictions imposées par l'intégrale de sensibilité de Bode ([Åström and Murray, 2008],[Zhou et al., 1996]), nous ne pouvons atténuer les perturbations que sur une bande de fréquence finie. Par conséquent, cette partie de la thèse est axée sur le rejet de plusieurs perturbations sinusoïdales variant dans le temps. Pour une analyse comparative du rejet par rétroaction et par anticipation, voir [Elliott and Sutton, 1996].

Avant de présenter le résumé des méthodes existantes pour le rejet de perturbation à bande étroite, nous allons commenter les différences des deux paradigmes dans ce domaine. Récemment, dans [Landau et al., 2011c], il a été souligné que dans le paradigme de la *commande adaptative* classique, l'objectif est le suivi ou l'atténuation des perturbations en présence des paramètres inconnus et variables dans le temps du modèle du procédé. Par conséquent, l'adaptation se fait par rapport à des variations dans les paramètres du modèle du procédé. Les modèles de perturbations sont supposés constants et connus.

Contrairement au paradigme de commande adaptative, le paradigme de la *régulation adaptative* traite le rejet asymptotique (ou l'atténuation) de l'effet des perturbations inconnues et variables dans le temps. On suppose que les paramètres du modèle du système sont connus et presque invariants. Une commande robuste peut être appliquée pour faire face à d'éventuelles petites variations (incertitude) sur ses paramètres. Ensuite, l'effort est concentré sur le modèle de perturbation, pas sur le modèle du procédé. Une remarque concernant ce paradigme est que la perturbation doit être située dans la région de fréquence où le modèle du système a assez de gain (pour des raisons de robustesse qui seront expliquées plus tard).

Comme l'objectif de cette thèse est le rejet (ou l'atténuation) de perturbation, le problème de la régulation adaptative sera considéré. L'hypothèse courante est que la perturbation est le résultat d'un bruit blanc ou une impulsion de Dirac qui a traversé le *modèle de la perturbation*. Plusieurs solutions ont été proposées pour rejeter son influence sur la sortie du système. L'une d'elle est le *Principe du modèle interne* (IMP), rapporté dans [Amara et al., 1999a], [Amara et al., 1999b], [Gouraud et al., 1997], [Hillerstrom and Sternby, 1994], [Valentinotti, 2001, Valentinotti et al., 2003], [de Callafon and Fang, 2013], [Chen and Tomizuka, 2013b], [Karimi and Emedi, 2013], [Wu and Ben Amara, 2013], [Castellanos Silva et al., 2013b]. L'idée derrière ces méthodes est que le modèle de la perturbation est incorporé dans le régulateur ([Bengtsson, 1977], [Francis and Wonham, 1976], [Johnson, 1976], [Tsypkin, 1997]). Ses paramètres doivent être estimés de façon continue afin d'être en mesure de répondre à d'éventuels changements dans les caractéristiques des perturbations. Cela conduit à un algorithme de commande adaptative indirecte ([Airimiţoaie et al., 2013], [Aranovskiy and Freidovich, 2013]). Cependant, il a été montré dans [Landau et al., 2005, Landau et al., 2011c] que l'adaptation directe est possible si on utilise la paramétrisation de Youla-Kučera de tous les régulateurs stables.

Une autre idée qui a été utilisée est de construire et intégrer un observateur adaptatif dans le régulateur [Ding, 2003, Marino et al., 2003, Serrani, 2006, Marino and Tomei, 2007]. Toutefois, cette approche semble être principalement axée sur les perturbations qui agissent sur l'entrée du système. Des hypothèses supplémentaires doivent être prises en compte avant de l'appliquer à des perturbations sur la sortie (le système doit avoir des zéros stables, ce qui est rarement le cas pour les modèles de systèmes à temps discret). On peut noter que, bien que le Principe du modèle interne ne soit pas explicitement pris en compte dans ce schéma, l'intégration de l'observateur dans le contrôleur signifie que le Principe du modèle interne est implicitement utilisé.

Une approche directe qui utilise le principe d'une boucle à verrouillage de phase est présentée dans [Bodson and Douglas, 1997] et les résultats expérimentaux sont donnés [Bodson, 2005]. Il peut être appliqué pour le rejet de perturbations sinusoïdales dont les fréquences sont inconnues. L'estimation de la fréquence de perturbation et l'annulation de la perturbation sont réalisées simultanément en utilisant un signal d'erreur unique. La réponse en fréquence du procédé dans la plage de fréquence d'intérêt est nécessaire.

Récemment, dans [Landau et al., 2013a], les résultats d'une compétition sur un benchmark international sur la régulation adaptative des perturbations à bande étroite inconnues et variables dans le temps ont été présentés. Ces résultats regroupaient les travaux de [Aranovskiy and Freidovich, 2013], [de Callafon and Fang, 2013], [Chen and Tomizuka, 2013b], [Karimi and Emedi, 2013], [Wu and Ben Amara, 2013], [Airimiţoaie et al., 2013] et [Castellanos Silva et al., 2013b]. Le nombre élevé de participants à cette compétition prouve l'intérêt et la pertinence de ce genre de problèmes pour la communauté de recherche sur la commande. Il a été constaté également que la quasi-totalité des contributions utilisaient (explicitement ou non) le Principe du modèle interne.

1.4 Contributions

L'objectif principal de la thèse est le développement d'algorithmes adaptatifs pour l'atténuation des vibrations dans les systèmes mécaniques. Les algorithmes ont été testés sur le système de suspension active disponible au GIPSA-Lab de l'Université de Grenoble.

Dans la partie I de la thèse, le problème de l'incertitude des paramètres dans le système de vibration actif est considéré. Les contributions les plus importantes sont :

1. L'identification du modèle en boucle fermée de l'actionneur en présence de pôles et de zéros complexes avec faible amortissement. Une modification sur les algorithmes d'identification en boucle fermée est présentée et testée sur le système AVC réel.

2. L'analyse de performance robuste est présentée dans le contexte de la régulation par rétroaction.

Les contributions de la partie II de cette thèse sont les suivantes :

1. L'amélioration de la robustesse de l'algorithme adaptatif direct présenté dans [Landau et al., 2005], afin de maintenir le module de la fonction de sensibilité de sortie sous une certaine valeur.

2. Le développement de nouvelles méthodes de contrôle par rétroaction pour rejeter les perturbations à bande étroite sur la base de l'IMP en utilisant le paramétrage de YK et un filtre Q IIR.

Les résultats expérimentaux présentés confirment les résultats de l'analyse théorique. Bien que développés pour un système de contrôle actif des vibrations, les algorithmes sont également applicables au contrôle actif du bruit.

1.5 Plan du Manuscrit de Thèse

Dans la **Partie I** de la thèse, l'incertitude portant sur les paramètres du système avec zéros complexes faiblement amortis est traitée et étudiée. Tout d'abord, le **Chapitre 3** présente

le système AVC sur lequel les algorithmes ont été testés. Le système expérimental, construit en collaboration avec le centre de recherche sur le contrôle actif de vibrations et bruit, PAULSTRA SNC (Dept. VIBRACHOC), s'inspire des problèmes rencontrés dans l'industrie. Une particularité de ce système est la présence de zéros complexes faiblement amortis pour le modèle de la structure mécanique. Les deux chapitres suivants, analysent l'identification en boucle fermée du modèle du système et les contraintes de robustesse.

Le **Chapitre 4**, analyse le problème du contrôle linéaire de la régulation à rétroaction lorsque des perturbations à bande étroite sont appliquées au système. Les objectifs de contrôle ont été donnés afin d'évaluer la qualité de la performance du contrôleur. Dans ce chapitre, la paramétrisation de Youla-Kučera des régulateurs polynômes RST est présentée. Le Principe du modèle interne (IMP) est appliqué par ce paramétrage. Dans le contexte linéaire, c'est à dire quand les deux modèles du système et de la perturbation sont connus, les contraintes de robustesse sont établies par l'application de l'IMP.

Le **Chapitre 5** présente une version modifiée d'un algorithme d'identification en boucle fermée. La modification s'inspire de l'idée donnée dans l'algorithme *Maximum Recursive Likelihood* afin d'intégrer les avantages des algorithmes de [Landau and Karimi, 1997] et [Landau and Karimi, 1999], compte tenu de la présence de zéros complexes faiblement amortis.

Dans la **Partie II**, le **Chapitre 6** présente deux solutions pour le rejet de perturbation à bande étroite. La première correspond à une version améliorée de l'algorithme adaptatif direct présenté dans [Landau et al., 2005]. Les améliorations sont obtenues à travers la conception du régulateur central. La seconde solution est un algorithme mixte direct/indirect adaptatif pour l'atténuation de perturbations multiples à bande étroite utilisant un filtre Q-IIR. La procédure mixte est basée sur une première étape d'estimation du modèle de perturbation et d'une deuxième étape de mise à jour du filtre Q. Les deux solutions sont basées sur la paramétrisation de Youla-Kučera. Enfin, le **Chapitre 7** présente les résultats en simulation et en temps réel de l'exemple de benchmark international pour la régulation adaptative. Les résultats correspondent à la deuxième solution (les résultats de la première solution ayant déjà été publiés dans [Castellanos Silva et al., 2013b]). Grâce aux critères du benchmark, une évaluation comparative des résultats présentés dans ce chapitre est faite entre les différentes contributions présentées dans [Landau et al., 2013a].

Les conclusions et les orientations pour la recherche future sont données dans le **Chapitre 8**.

1.5.1 Description du système

La **Partie I** présente une étude sur l'incertitude des paramètres pour des systèmes avec zéros complexes faiblement amortis. Tout d'abord, le **Chapitre 3** décrit le système réel sur lequel les algorithmes proposés dans cette thèse ont été testés. Les figures 1.5 et 1.6 montrent le banc d'essai pour le contrôle actif des vibrations. Il utilise des actionneurs inertiels pour la génération de vibrations et de compensation. La structure est représentative d'un certain nombre de situations rencontrées en pratique. Dans la Fig.1.5, les actions de base pour le contrôle et pour la perturbation sont représentées.

Le système est composé d'un amortisseur passif, d'un actionneur inertiel, d'une structure mécanique, d'un transducteur de la force résiduelle, d'un dispositif de commande, d'un amplificateur de puissance et d'un shaker. L'actionneur inertiel crée des forces vibratoires qui contrecarrent l'effet des perturbations vibratoires introduites par le shaker.

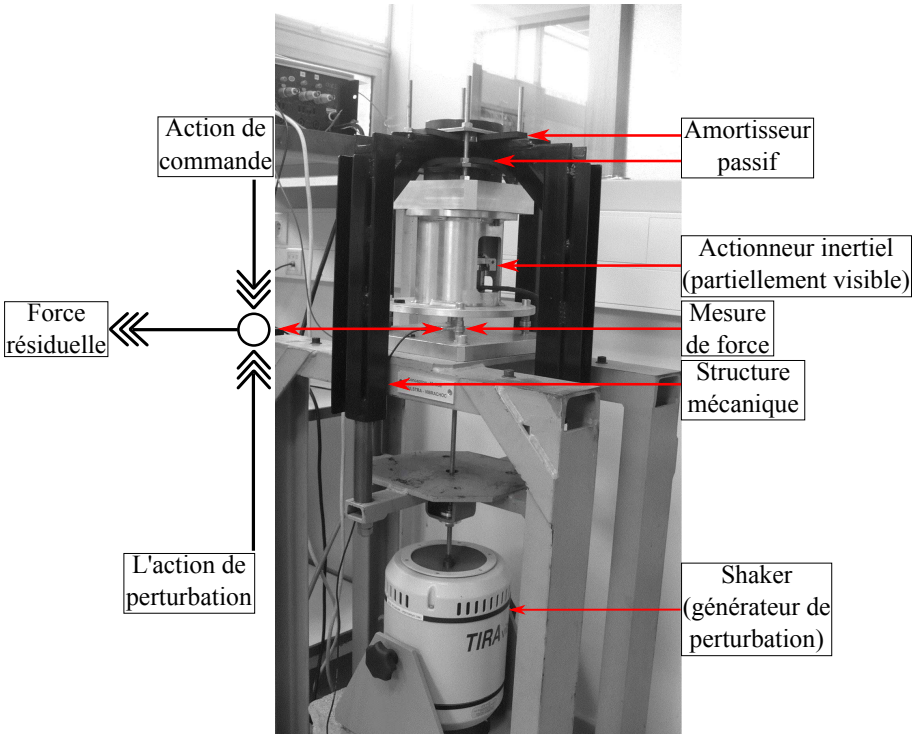

Figure 1.5: Le système de suspension active (AVC) utilisé pour des expériences - photo.

Les actionneurs inertiels utilisent un principe similaire à celui des haut-parleurs (voir par exemple [Marcos, 2000, Landau et al., 2011b]). La Figure 1.6 donne une vue générale du système, y compris le matériel de test. L'objectif est de minimiser la force résiduelle mesurée $y(t)$.

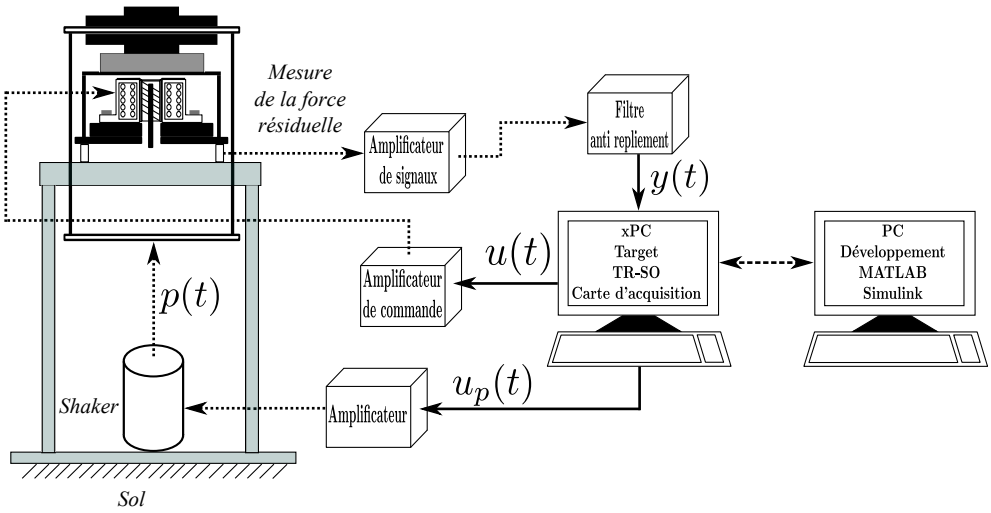

Figure 1.6: Vue générale du système AVC, y compris l'équipement d'essai.

Bien que développés pour un système de contrôle actif de vibrations, les algorithmes sont également applicables pour les systèmes de contrôle actif du bruit. Le diagramme correspondant à un fonctionnement en boucle fermée est présenté à la Fig 1.7. Le compensateur en contre-réaction dispose, comme entrée de la variable de performance $y(t)$, et sa sortie est représentée par $u(t)$ tel que décrit dans la Sous-section 2.2.1. Le

signal de commande appliqué à l'actionneur par un amplificateur est :

$$u(t) = -K(q^{-1}) \cdot y(t), \tag{1.7}$$

où $K(z^{-1})$ est la fonction de transfert à temps discret du contrôleur synthétisé. La fonction de transfert $G(z^{-1})$ (le chemin secondaire) caractérisant la dynamique de la sortie du compensateur $u(t)$ pour la mesure de la force résiduelle (amplificateur + actionneur + dynamique du système mécanique). La fonction de transfert $D(z^{-1})$ entre $\delta(t)$ et la mesure de la force résiduelle (en boucle ouverte) caractérise la voie primaire[2].

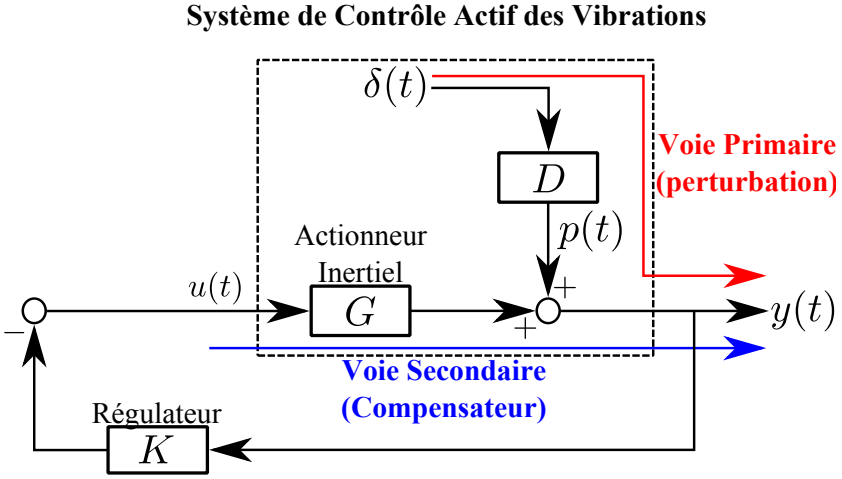

Figure 1.7: Régulateur par rétroaction pour l'AVC avec régulateur fixe.

La structure du modèle à temps discret linéaire invariant dans le temps de la voie secondaire utilisée pour la conception du contrôleur est :

$$G(z^{-1}) = \frac{z^{-d}B(z^{-1})}{A(z^{-1})} = \frac{z^{-d-1}B^*(z^{-1})}{A(z^{-1})}, \tag{1.8}$$

où

$$B(z^{-1}) = b_1 z^{-1} + ... + b_{n_B} z^{-n_B} = z^{-1}B^*(z^{-1}), \tag{1.9}$$
$$B^*(z^{-1}) = b_1 + \ldots + b_{n_B} z^{-n_B+1}, \tag{1.10}$$
$$A(z^{-1}) = 1 + a_1 z^{-1} + \ldots + a_{n_A} z^{-n_A}. \tag{1.11}$$

où $A(z^{-1})$, $B(z^{-1})$, $B^*(z^{-1})$ sont des polynômes en la variable complexe z^{-1} et n_A, n_B et $n_B - 1$ représentent leurs ordres respectifs[3]. Le modèle identifié de la voie secondaire est noté $\hat{G}$, ayant pour numérateur et dénominateur $\hat{B}$ et $\hat{A}$, respectivement.

Comme le système AVC est focalisé sur la régulation, c.à.d. minimiser ou rejeter l'effet de la perturbation à la sortie, le régulateur qui doit être synthétisé est un régulateur

[2]Dans la Fig. 1.6, l'entrée de l'amplificateur de perturbation est notée $u_p(t)$, alors que pour le système de rétroaction (Fig. 1.7), elle est notée $\delta(t)$, la différence provient du fait que pour le schéma du matériel, $u_p(t)$ est un signal généré par l'ordinateur et $\delta(t)$ est considérée comme l'impulsion de Dirac utilisée pour l'analyse.

[3]La variable complexe z^{-1} sera utilisée pour caractériser le comportement du système dans le domaine des fréquences et l'opérateur de retard q^{-1} sera utilisé pour décrire le comportement du système dans le domaine temporel.

de type polynomial RS (ou de façon équivalente un régulateur dans l'espace d'état + observateur, voir [Landau et al., 2011d],[Landau and Zito, 2005]).

La sortie du système $y(t)$ et l'entrée $u(t)$ peuvent s'écrire

$$y(t) = \frac{q^{-d}B(q^{-1})}{A(q^{-1})} \cdot u(t) + p(t); \tag{1.12}$$

$$u(t) = -\frac{R(q^{-1})}{S(q^{-1})} \cdot y(t) = -K(q^{-1}) \cdot y(t), \tag{1.13}$$

où q^{-1} est l'opérateur de retard de décalage ($x(t) = q^{-1}x(t+1)$) et $p(t)$ est la perturbation additive sur la sortie du système. $R(z^{-1})$ et $S(z^{-1})$ sont des polynômes en z^{-1} d'ordres n_R et n_S, respectivement, avec les expressions suivantes :

$$R(z^{-1}) = r_0 + r_1 z^{-1} + ... + r_{n_R} z^{-n_R} = R'(z^{-1}) \cdot H_R(z^{-1}), \tag{1.14}$$

$$S(z^{-1}) = 1 + s_1 z^{-1} + ... + s_{n_S} z^{-n_S} = S'(z^{-1}) \cdot H_S(z^{-1}), \tag{1.15}$$

où $H_R(z^{-1})$ et $H_S(z^{-1})$ sont des éléments pré-spécifiés du régulateur (utilisés par exemple pour intégrer le modèle interne d'une perturbation ou pour ouvrir la boucle à certaines fréquences).

1.5.2 La problématique de la commande linéaire

En supposant qu'une seule fréquence doit être annulée dans une région de fréquences loin de la présence de zéros complexes faiblement amortis et que les modèles du système et de la perturbation sont connus, la conception d'un régulateur linéaire est relativement simple, en utilisant le principe du modèle interne.

Le problème devient beaucoup plus difficile si plusieurs perturbations sinusoïdales doivent être simultanément atténuées, avec des fréquences proches de celles de certains zéros complexes faiblement amortis du système.

Les vibrations à atténuer sont situées dans la plage comprise entre 50 et 95 Hz. La voie secondaire (compensateur) dispose d'une caractéristique de fréquence comprise dans la région entre $0f_s$ et $0.5f_s$, où f_s est la fréquence d'échantillonnage (800 Hz dans notre cas).

Afin d'évaluer la qualité du régulateur, il est nécessaire de définir les objectifs de contrôle à remplir. Ces objectifs sont liés au nombre de fréquences des vibrations. Il existe trois niveaux de difficulté correspondant à une, deux ou trois fréquences dans la plage d'intérêt (50 à 95 Hz). Les objectifs de contrôle pour tous les niveaux sont résumés dans le Tableau 1.1. Le niveau 3 est particulièrement difficile en termes d'amplification tolérée (à d'autres fréquences que celles des perturbations) et des exigences transitoires. Un ensemble d'indicateurs de performance a été défini pour évaluer la performance à l'état stable. Plusieurs indicateurs ont été définis pour la performance transitoire mais le plus important est la durée transitoire. En effet, il est inutile d'examiner la performance transitoire si la performance d'atténuation n'est pas satisfaisante.

En supposant un contexte de synthèse par placement de pôles, les polynômes R' et S' (Eqs. (1.14) et (1.15)) sont les solutions de degré minimal de l'équation de Bezout suivante

$$\begin{aligned} P(z^{-1}) &= A(z^{-1})S(z^{-1}) + z^{-d}B(z^{-1})R(z^{-1}), \\ &= A(z^{-1})H_S(z^{-1})S'(z^{-1}) + z^{-d}B(z^{-1})H_R(z^{-1})R'(z^{-1}), \end{aligned} \tag{1.16}$$

Table 1.1: Les objectifs de contrôle dans le domaine fréquentiel.

Objectifs de contrôle	Niveau 1	Niveau 2	Niveau 3
Durée transitoire	$\leq$ 2 sec	$\leq$ 2 sec	$\leq$ 2 sec
Atténuation globale	$\geq$ 30 dB*	$\geq$ 30 dB	$\geq$ 30 dB
Atténuation de perturbation minimale	$\geq$ 40 dB	$\geq$ 40 dB	$\geq$ 40 dB
Amplification maximale	$\leq$ 6 dB	$\leq$ 7 dB	$\leq$ 9 dB

* À ce niveau, la spécification est de 30 dB pour la plage comprise entre 50 et 85 Hz, 28 dB pour 90 Hz et 24 dB pour 95 Hz.

où $P(z^{-1})$ est utilisé pour définir les pôles désirés en boucle fermée et où les degrés de $P(z^{-1})$, $R'(z^{-1})$ et $S'(z^{-1})$ vérifient :

$$n_P \leq n_A + n_B + d + n_{H_S} + n_{H_R} - 1,\ n_{S'} = n_B + d + n_{H_R} - 1,\ n_{R'} = n_A + n_{H_S} - 1.$$

La solution existe, si AH_S et BH_R sont premiers entre eux, (A et B définissent le modèle du procédé en temps discret). La sortie du système peut s'écrire :

$$y(t) = G(q^{-1})u(t) + p(t) = \frac{A(q^{-1})S(q^{-1})}{P(q^{-1})}p(t). \tag{1.17}$$

Les inconnues S' et R' peuvent être calculées en mettant (1.16) sous une forme matricielle (voir aussi [Landau et al., 2005]). La dimension de l'équation matricielle qui doit être résolue est

$$n_A + n_{H_S} + n_B + n_{H_R} + d - 1 \times n_A + n_{H_S} + n_B + n_{H_R} + d - 1.$$

Observation : la théorie ne dit rien sur ce qui se passe si la partie fixe H_S a des racines à proximité des racines de B. Si l'ordre du système est élevé comme c'est le cas du système de suspension active présenté dans la section précédente où $n_A = 18$, $n_B = 21$ et $d = 0$, l'équation matricielle à résoudre nécessite une puissance de calcul élevée.

Supposons que $p(t)$ est une perturbation déterministe, $p(t)$ peut donc s'écrire sous la forme

$$p(t) = \frac{N_p(q^{-1})}{D_p(q^{-1})}\delta(t), \tag{1.18}$$

où $\delta(t)$ est une impulsion de Dirac et $N_p(z^{-1})$ et $D_p(z^{-1})$ sont des polynômes premiers entre eux en z^{-1}, dont les ordres sont n_{N_P} et n_{D_P}. Nous sommes intéressés par le rejet de perturbations à bande étroite et dans ce cas, les racines de $D_p(z^{-1})$ sont sur le cercle unitaire.

Puisque l'objectif est d'annuler l'effet des perturbations, il est logique d'utiliser le ***Principe du modèle interne*** [Francis and Wonham, 1976], qui indique que les effets de la perturbation $p(t)$ sur la sortie $y(t)$ seront annulés si la partie fixe du polynôme $S(z^{-1})$ est choisie comme suit

$$S(z^{-1}) = D_p(z^{-1})S'(z^{-1}). \tag{1.19}$$

Grâce à la paramétrisation de Youla-Kučera [Anderson, 1998] (appelé aussi paramétrisation Q), il est possible de réduire l'ordre de l'équation matricielle à résoudre. Cela nous

permet aussi d'utiliser le principe du modèle interne. Le paramètre Q peut être représenté à la fois comme un filtre FIR ou comme un filtre IIR. Sous cette paramétrisation, les polynômes du régulateur RS sont définis comme suit. Pour un filtre IIR :

$$R(z^{-1}) = A_Q(z^{-1})R_0(z^{-1}) + A(z^{-1})H_{S_0}(z^{-1})H_{R_0}(z^{-1})B_Q(z^{-1}), \tag{1.20}$$

$$S(z^{-1}) = A_Q(z^{-1})S_0(z^{-1}) - z^{-d}B(z^{-1})H_{S_0}(z^{-1})H_{R_0}(z^{-1})B_Q(z^{-1}). \tag{1.21}$$

Pour un filtre FIR, les polynômes sont définis comme suit :

$$R(z^{-1}) = R_0(z^{-1}) + A(z^{-1})H_{S_0}(z^{-1})H_{R_0}(z^{-1})Q(z^{-1}), \tag{1.22}$$

$$S(z^{-1}) = S_0(z^{-1}) - z^{-d}B(z^{-1})H_{S_0}(z^{-1})H_{R_0}(z^{-1})Q(z^{-1}). \tag{1.23}$$

Grâce à la paramétrisation YK des contrôleurs RST, le principe du modèle interne (IMP) peut être utilisé pour rejeter l'effet des perturbations à bande étroite avec une réduction de la charge de calcul. Une autre caractéristique importante de cette paramétrisation est que, comme indiqué ci-après, il est possible de représenter la différence de performance entre un régulateur optimal, soit un polynôme optimal Q_{opt} et un autre régulateur, soit un polynôme $\widehat{Q}$, dans une équation montrant explicitement la différence entre Q_{opt} et $\widehat{Q}$. Cela va ouvrir la voie à la construction d'un système de régulation adaptative directe.

De l'IMP, par les équations (1.19) et (1.23) nous avons

$$D_p(z^{-1})S'(z^{-1}) = S'_0(z^{-1}) - z^{-d}B(z^{-1})H_{R_0}(z^{-1})Q(z^{-1}), \tag{1.24}$$

résolvons S'_0, l'équation (1.24) est réécrite

$$D_p(z^{-1})S'(z^{-1}) + z^{-d}B(z^{-1})H_{R_0}(z^{-1})Q(z^{-1}) = S'_0(z^{-1}), \tag{1.25}$$

l'équation diophantienne précédente a un ordre de

$$n_{D_p} + n_B + n_{H_{R_0}} + d - 1 \times n_{D_p} + n_B + n_{H_{R_0}} + d - 1,$$

où $n_{S'} = n_B + n_{H_{R_0}} + d - 1$ et $n_Q = n_{D_p} - 1$ et la réduction obtenue est de $n_A + n_{H_{S_0}}$. Il est à noter que l'ordre du filtre Q (n_Q) dépend de l'ordre du modèle de perturbation, pas de l'ordre du modèle du système.

Deux des restrictions sur la robustesse du système ont été déduites à partir des fonctions de sensibilité et du type d'incertitude.

1.5.3 Identification du système de contrôle actif des vibrations

Le **Chapitre 5** décrit l'identification du système de contrôle actif des vibrations. Une attention particulière est portée à l'identification du système en boucle fermée, où une contribution originale a été faite. Chaque procédure (boucle ouverte et boucle fermée) est effectuée en utilisant, comme entrée d'excitation, un signal binaire pseudo-aléatoire (PRBS).

La procédure d'identification en boucle ouverte est effectuée en l'absence de régulateur et de signal de perturbation à bande étroite. L'idée est de construire un prédicteur réglable (modèle) dont la sortie $\widehat{y}(t)$ correspond à la sortie mesurée $y(t)$. Dans le cas de l'identification en boucle fermée, la différence réside dans la présence d'un régulateur. Par conséquent, l'objectif est de construire en parallèle un prédicteur réglable qui minimise les différences entre les deux boucles fermées, celle mesurée et celle simulée. Les principales contributions de cette section sont les suivantes :

- La modification de l'algorithme d'identification en boucle fermée, présenté dans [Landau and Karimi, 1997].
- L'application sur le système de suspension active en présence de zéros complexes faiblement amortis.

La procédure d'identification en boucle fermée est basée sur les méthodes *d'erreur de sortie en boucle fermée* dont le principe est de trouver le meilleur modèle du système qui minimise l'erreur de prédiction $\epsilon_{CL}(t)$ entre la sortie mesurée du système en boucle fermée et la sortie prédite en boucle fermée.

Ainsi, pour améliorer le modèle identifié en boucle ouverte dans les régions de fréquences critiques pour le contrôle, deux actions sont proposées: *1)* la conception d'un régulateur spécifique qui augmente la sensibilité du système à de telles fréquences et *2)* une initialisation différente pour un algorithme basé sur l'erreur de sortie en boucle fermée.

Le régulateur conçu devrait augmenter la sensibilité du système dans les régions de fréquence où se trouvent des zéros complexes faiblement amortis. Cela ne signifie pas nécessairement que le régulateur sera *bon* en termes de performance de contrôle (de rejet de perturbation, de suivi, etc), mais seulement qu'il ne va pas déstabiliser le système. De plus, le dispositif de commande permet d'obtenir une meilleure approximation dans les régions critiques à des fins de commande (près des modes de résonance et d'anti-résonance). A cet effet, l'amortissement des pôles qui se trouvent à proximité des zéros complexes faiblement amortis est augmenté (ceux autour des fréquences de 50 et 100 Hz). La marge de module est maintenue à la valeur recommandée de $\Delta M = 0,5$ pour assurer la stabilité du système en boucle fermée.

Généralement de bons résultats en termes de validation sont obtenus avec l'algorithme X-CLOE. Considérant néanmoins la distribution de biais, si l'objectif est d'améliorer la précision du modèle dans les régions de fréquences critiques pour la synthèse, les algorithmes F-CLOE et AF-CLOE sont des méthodes plus appropriées : en effet, ces méthodes ne sont pas affectées par les caractéristiques du bruit de la mesure et permettent de discriminer plus précisément le modèle du système du modèle estimé dans la région de fréquence désirée. Donc, la procédure d'identification a été focalisée sur ces algorithmes.

Pour AF-CLOE, l'initialisation *standard* du filtre adaptatif $\widehat{P}(t) = \widehat{A}(t)S + q^{-d}\widehat{B}(t)R$ à $t = 0$ est de prendre $\widehat{A}(0) = 1$ et $\widehat{B}(0) = 0$. Une autre initialisation pour AF-CLOE est proposée : au lieu d'utiliser les valeurs initiales standard, il est proposé d'utiliser un modèle initial comme pour F-CLOE. L'adaptation du filtre n'est pas activée jusqu'à ce que l'horizon de l'estimation soit atteint. Cela signifie que pour certaines itérations (la longueur de l'horizon), les observations sont filtrées par un filtre $S/\widehat{P}$ constant et une fois que l'horizon est atteint, le filtre est conçu avec les estimations actuelles de $\widehat{A}(t)$ et $\widehat{B}(t)$. L'objectif est de permettre à l'algorithme AF-CLOE de démarrer dans le voisinage des paramètres optimaux, comme pour l'algorithme Maximum Recursive Likelihood. Cette action vise à combiner les améliorations des méthodes F-CLOE et AF-CLOE.

1.5.4 Régulation adaptative directe et robuste de perturbations à bande étroite inconnues

Le **Chapitre 6** développe les algorithmes robustes adaptatifs directs pour le rejet de perturbations inconnues à bande étroite dans une approche par rétroaction. Les algorithmes exploitent les capacités d'un régulateur robuste en ajoutant des fonctionnalités adaptatives. Elles sont basées sur la paramétrisation de Youla-Kučera et le régulateur robuste

central est calculé à partir du placement de pôles avec mise en forme des fonctions de sensibilité. Le schéma de base pour les algorithmes est montré dans la Figure 1.8. L'algorithme adaptatif direct pour un filtre Q FIR a été présenté dans [Landau et al., 2005]; le cas d'un filtre Q IIR est présenté ici.

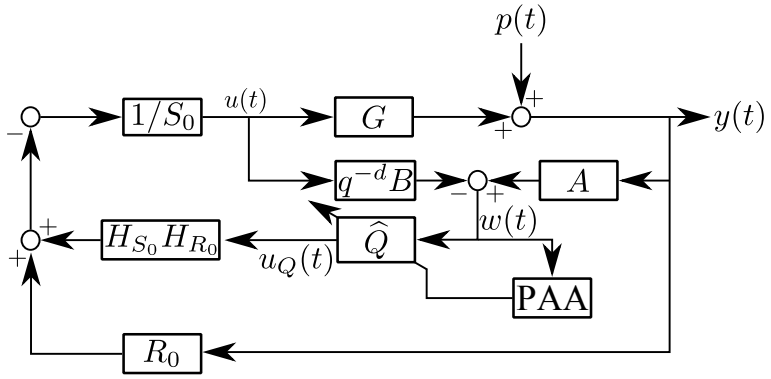

Figure 1.8: Schéma de base pour la commande adaptative directe.

Le cas FIR

L'objectif est de trouver un algorithme adaptatif qui estime directement les paramètres du modèle interne dans le régulateur en présence d'une perturbation inconnue (mais de structure connue) sans modifier les pôles en boucle fermée. De toute évidence, la paramétrisation Q est une option possible quand une représentation de filtre à réponse impulsionnelle finie (FIR) est prise en compte. Les modifications du polynôme Q n'affecteront pas les pôles en boucle fermée. Un aspect clé de cette méthode est l'utilisation de l'IMP. Afin de construire un algorithme d'estimation, il est nécessaire de définir une *équation d'erreur* qui reflète la différence entre la valeur optimale de Q et son estimation actuelle. Ceci est donné par l'équation suivante :

$$\epsilon_{FIR}(t+1) = \left[\theta^T - \widehat{\theta}^T(t+1)\right] \cdot \phi_{FIR}(t) + \upsilon(t+1), \tag{1.26}$$

où le polynôme estimé $\widehat{Q}(q^{-1},t)$ est défini comme $\widehat{Q}(q^{-1},t) = \widehat{q}_0(t) + \widehat{q}_1(t)q^{-1} + \cdots + \widehat{q}_{n_Q}(t)q^{-n_Q}$ et le vecteur de paramètre estimé associé: $\widehat{\theta}(t) = \left[\widehat{q}_0(t), \widehat{q}_1(t), \cdots, \widehat{q}_{n_Q}(t)\right]^T$. Le vecteur de paramètres fixes correspondant à la valeur optimale du polynôme Q est défini comme $\theta = \left[q_0, q_1, \cdots, q_{n_Q}\right]^T$. Le signal $\upsilon(t+1)$ est donné par l'équation suivante

$$\upsilon(t+1) = \frac{S'(q^{-1})D_p(q^{-1})}{P_0(q^{-1})}w(t+1) = \frac{S'(q^{-1})A(q^{-1})N_p(q^{-1})}{P_0(q^{-1})}\delta(t+1). \tag{1.27}$$

Ce signal tend asymptotiquement vers zéro, le polynôme $P_0(z^{-1})$ étant asymptotiquement stable (calculé à partir du régulateur central).

Le vecteur $\phi_{FIR}(t)$ est défini par

$$\phi_{FIR}^T(t) = \left[w_2(t), w_2(t-1), \cdots, w_2(t-n_Q)\right], \tag{1.28}$$

où

$$w_2(t) = \frac{q^{-d}B^*(q^{-1})H_{S_0}(q^{-1})H_{R_0}(q^{-1})}{P_0(q^{-1})}w(t). \tag{1.29}$$

L'erreur d'adaptation *a priori* est définie par

$$\epsilon^0_{FIR}(t+1) = w_1(t+1) - \widehat{\theta}^T(t)\phi_{FIR}(t), \tag{1.30}$$

et l'erreur d'adaptation *a posteriori* est obtenue à partir de

$$\epsilon_{FIR}(t+1) = w_1(t+1) - \widehat{\theta}^T(t+1)\phi_{FIR}(t), \tag{1.31}$$

où

$$w_1(t+1) = \frac{S_0(q^{-1})}{P_0(q^{-1})} w(t+1). \tag{1.32}$$

L'éq. (1.26) possède la forme standard d'une erreur d'adaptation *a posteriori* ([Landau et al., 2011d]), ce qui suggère l'utilisation de l'algorithme d'adaptation paramétrique (PAA) suivant

$$\epsilon_X(t+1) = \frac{\epsilon^0_X(t+1)}{1 + \Phi^T(t)F(t)\Phi(t)} \tag{1.33}$$

$$\hat{\theta}(t+1) = \hat{\theta}(t) + F(t)\Phi(t)\epsilon_X(t+1) \tag{1.34}$$

$$F(t+1) = \frac{1}{\lambda_1(t)}\left[F(t) - \frac{F(t)\Phi(t)\Phi^T(t)F(t)}{\frac{\lambda_1(t)}{\lambda_2(t)} + \Phi^T(t)F(t)\Phi(t)}\right] \tag{1.35}$$

$$0 < \lambda_1(t) \leq 1; \quad 0 \leq \lambda_2(t) < 2 \tag{1.36}$$

où $X = \{FIR, IIR, D_p\}$. Le vecteur d'observation (ou des mesures) $\Phi(t)$ est défini selon l'algorithme utilisé.

La contribution à l'égard du travail précédent présenté dans [Landau et al., 2005] se situe dans la synthèse du régulateur central, c'est à dire des polynômes R_0 et S_0. Le régulateur central joue un rôle très important dans cette approche.

Le cas IIR

L'algorithme précédent utilise une structure FIR pour le filtre Q. Dans cette section, un nouvel algorithme est développé, en utilisant une structure IIR. Une caractéristique essentielle de cette approche est que dans ce cas les pôles de la boucle fermée sont modifiés par le dénominateur du filtre Q. Les pôles de la boucle fermée sont définis par

$$P(z^{-1}) = A_Q(z^{-1})\left(A(z^{-1})S_0(z^{-1}) + z^{-d}B(z^{-1})R_0(z^{-1})\right). \tag{1.37}$$

Les polynômes dans la parenthèse sont les pôles définis par le régulateur central. Pour cette raison, il est nécessaire que le dénominateur de Q, c.a.d. A_Q, soit stable.

En supposant que le modèle du système correspond au système réel dans la plage de fréquences où les perturbations à bande étroite sont introduites, il est possible d'obtenir une estimation de $p(t)$, dénommée $\widehat{p}(t)$, en utilisant l'expression suivante

$$\widehat{p}(t) = \frac{1}{A(q^{-1})} w(t). \tag{1.38}$$

On suppose que la perturbation a la forme

$$\widehat{p}(t) = \sum_{i=1}^{n} c_i \sin(\omega_i t + \beta_i) + \nu(t). \tag{1.39}$$

où $\{c_i, \omega_i, \beta_i\} \neq 0$, n est le nombre de perturbations à bande étroite et $\nu(t)$ est un bruit affectant la mesure. On peut vérifier que, après deux étapes de transitoire $(1 - 2\cos(\omega_i)q^{-1} + q^{-2}) \cdot c_i \sin(\omega_i t + \beta_i) = 0$ [Chen and Tomizuka, 2012]. Ensuite, sur la base de l'idée donnée par les filtres coupe-bande, on peut estimer le polynôme $D_p(z^{-1})$, à partir du signal $\widehat{p}(t)$, pour être utilisé dans la structure de $A_Q(z^{-1})$. Si $A_Q(z^{-1})$ a ses racines sur la même ligne radiale que les racines de $D_p(z^{-1})$, à l'intérieur du cercle unitaire et donc stable, l'effet "*waterbed*" sur la fonction de sensibilité à la sortie peut être minimisé.

Pour cette raison et comme $D_p(z^{-1})$ a une structure de type miroir[4], la structure de $A_Q(z^{-1})$ peut être choisie comme suit

$$A_Q(z^{-1}) = D_p(\rho z^{-1}) = \prod_{i=1}^{n} \left(1 + \rho\alpha_i z^{-1} + \rho^2 z^{-2}\right) \tag{1.40}$$

où $0 < \rho < 1$ est un nombre réel positif inférieur à mais proche de un et $\alpha_i = -2\cos(2\pi\omega_i T_s)$ et T_s c'est le temps d'échantillonnage. Les racines de $A_Q(z^{-1})$ sont situées sur un cercle de rayon ρ. Cela rend $A_Q(z^{-1})$ stable, ce qui sera utile à l'algorithme d'adaptation des paramètres plus tard.

Ensuite, il est nécessaire de développer un algorithme qui estime les paramètres de D_p (α_i) pour une utilisation ultérieure dans la structure de A_Q. Pour cela l'équation suivante, qui concerne la vraie valeur de D_p correspondant à la valeur estimée $\widehat{D}_p$, est utilisée

$$\epsilon_{D_p}(t+1) = \left[\theta_{D_p}^T - \widehat{\theta}_{D_p}^T(t+1)\right] \cdot \psi(t), \tag{1.41}$$

où le vecteur de paramètres θ_{D_p} et sa version estimée $\widehat{\theta}_{D_p}(t)$ sont utilisés, avec les définitions suivantes

$$\theta_{D_p} = [\alpha_1, \cdots, \alpha_n]^T, \tag{1.42}$$

$$\widehat{\theta}_{D_p}(t) = [\widehat{\alpha}_1(t), \cdots, \widehat{\alpha}_n(t)]^T, \tag{1.43}$$

et en définissant le vecteur d'observation $\psi(t)$

$$\psi(t) = [\widehat{p}(t) + \widehat{p}(t-2n+2), \cdots, \widehat{p}(t-n+1)]^T, \tag{1.44}$$

nous pouvons utiliser le PAA défini dans les éqs. (1.33) - (1.35).

En comparant avec l'algorithme précédent (cas FIR), afin de mettre en œuvre l'estimation de B_Q (le numérateur de Q), la différence apparait sur le vecteur d'observation $\phi_{IIR}(t)$ qui consiste essentiellement à filtrer le signal $w_2(t)$ défini dans l'éq. (1.29) par le filtre $\frac{1}{A_Q(q^{-1})}$ (en supposant que A_Q est constant). Le signal de commande est calculé à partir de (voir Fig. 1.8):

$$S_0 u(t) = -R_0 y(t+1) - H_{S_0} H_{R_0} \widehat{B}_Q(t) w(t+1) - A_Q^* u_Q(t). \tag{1.45}$$

1.5.5 Évaluation comparative des algorithmes proposés

Le **Chapitre 7** présente les résultats de plusieurs expériences effectuées sur le système de contrôle actif des vibrations présenté dans le Chapitre 3. Des signaux multiples à bande étroite avec fréquences inconnues et pouvant varier dans le temps sont considérés.

[4]Cela est une condition nécessaire pour trouver les racines de D_p sur le cercle unitaire.

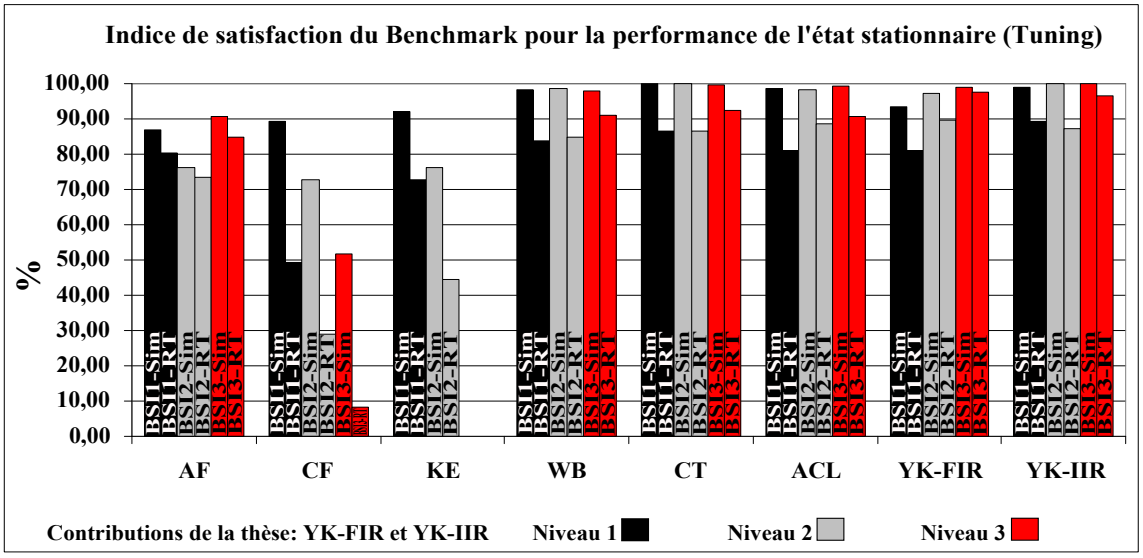

Figure 1.9: Indice de satisfaction du benchmark (BSI) pour tous les niveaux et résultats en simulation et en temps réel.

La difficulté est accrue par le fait que le système compensateur possède plusieurs modes de résonance et d'anti-résonance à la fréquence de la bande d'intérêt pour le rejet de perturbations multiples à bande étroite. La comparaison a été faite dans le contexte d'une compétition internationale (benchmark) lorsque les spécifications de contrôle et d'indice de performance ont été définies.

Pour tous les participants, la comparaison de la performance à l'état stationnaire est réalisée au moyen de l'indice de satisfaction de benchmark (BSI) défini dans l'éq. (A.5) et le critère global de la performance à l'état stable pour chaque niveau (J_{SS_k} dans l'Eq. (A.4)). Le BSI concernant tous les niveaux et tous les contributeurs pour les résultats en simulation et en temps réel est représenté graphiquement sur la Fig. 1.9. Bien que, en général, de faibles valeurs de J_{SS_k} indiquent en *moyenne* de bonnes performances, le BSI_k permet une meilleure caractérisation de la performance par rapport aux diverses spécifications du benchmark. Les résultats de simulation sont pertinents pour indiquer les capacités d'une méthode de synthèse pour répondre aux spécifications du benchmark. Il est également important de rappeler que le niveau 3 de l'indice du benchmark est le plus important.

Selon les résultats de la Fig. 1.9, l'algorithme YK-IIR répond pratiquement à toutes les spécifications de référence pour tous les niveaux. Le méthode de conception de [Chen and Tomizuka, 2013b] (notée CT) montre une performance équivalente. Le YK-FIR a une performance proche, spécialement au niveau 3. Dans la Fig. 1.9, on remarque qu'il y a des différences entre les résultats de simulation et les résultats en temps réel. Cependant, l'algorithme YK-IIR reste parmi les meilleures méthodes de conception. A travers les résultats en temps réel, plus exactement la différence entre les résultats en simulation et en temps réel, on peut caractériser la robustesse de la performance par rapport à des incertitudes sur le modèle de conception et le modèle de bruit.

Pour évaluer la perte de performance, la *perte de performance normalisée* et son indice global sont utilisés. Ils sont définis dans les équations (A.6) et (A.7), respectivement. L'algorithme YK-FIR a le deuxième meilleur résultat pour le niveau 1 et le meilleur résultat pour les niveaux 2 et 3. L'algorithme YK-IIR obtient la meilleure (plus petite)

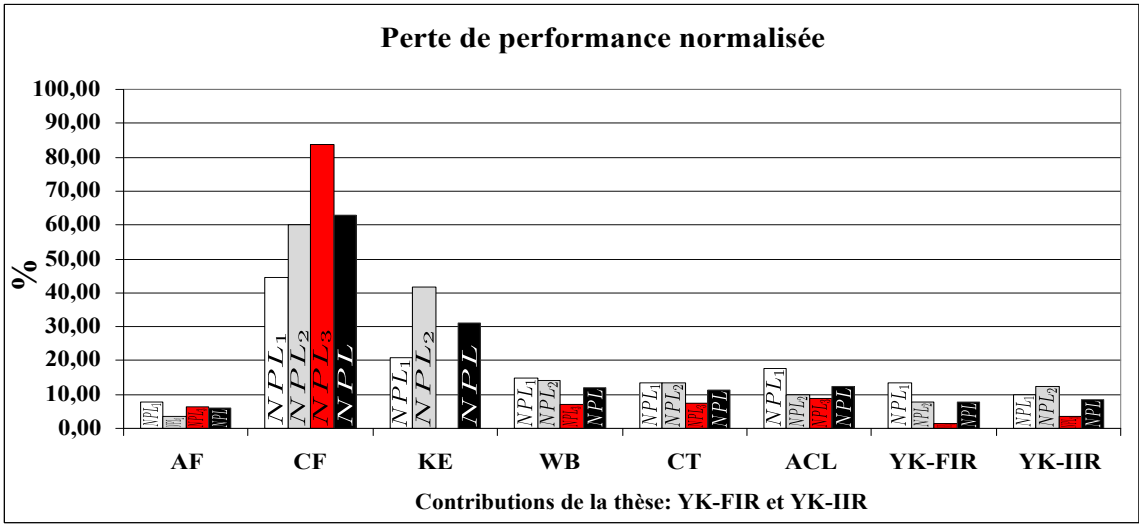

Figure 1.10: Perte de rendement normalisée (NPL) pour tous les niveaux (petits = meilleurs).

perte de performance pour le niveau 1, le troisième meilleur résultat pour le niveau 2 et le deuxième meilleur résultat pour le niveau 3.

En ce qui concerne les résultats globaux, le YK-FIR est la meilleure méthode de conception (7,62% de la perte de performance) et le YK-IIR est la deuxième meilleure méthode de conception (8,63% de la perte de performance). Ceci est représenté graphiquement sur la Fig. 1.10. Les contributions dénotées AF et CF ne sont pas prises en compte car elles ont utilisé des régulateurs différents pour la simulation et en temps réel.

Lors de la compétition internationale, l'algorithme donné dans la Section 6.3 (noté YK-FIR) avec la synthèse améliorée du régulateur central a été testé et comparé avec différentes méthodes de conception. Les améliorations permettent d'atteindre l'une des meilleures performances avec une complexité plus faible et une bonne robustesse contre les différences entre le simulateur et le système réel (des incertitudes). Le principal inconvénient de cette approche est que l'effet "*waterbed*" devient très difficile à réduire lorsque les fréquences de perturbation sont proches les unes des autres (comme proposé dans le nouveau protocole d'essai).

En comparaison, l'algorithme de la Section 6.4, a montré qu'il peut améliorer ce qui a été fait par l'algorithme YK-FIR en termes de robustesse et de performance. Néanmoins, l'inconvénient est la complexité (temps de calcul) de ce schéma.

Chapter 2

Introduction (english)

This chapter is dedicated to the description of the basic problems in Active Noise Control (ANC) and Active Vibration Control (AVC) for narrow band disturbance rejection which motivated the research and presents a summary of the history and main advances in the literature.

The work developed in this thesis has been done in the framework of Active Vibration Control through Robust Adaptive Control techniques. The objective was to develop adaptive algorithms for disturbance rejection, which were implemented and tested on real pilot-plants located at GIPSA-Lab Grenoble.

2.1 Motivation

In this section the basic principles of Active Noise and Vibration Control (ANVC) will be presented. The context of this work will be detailed and some examples will be used to state the associated control problem.

Probably one of the first works in Active Noise Control is the one presented in the french patent by Henri Coandă ([Coanda, 1930]). Shortly after that, Paul Lueg present his US patent in [Lueg, 1934] followed by the work of Harry F. Olson in [Olson and May, 1953]. In these works, the basic idea was silencing the noise field using an electro-acoustic secondary source (loudspeaker). The sound measurement is obtained through a microphone. These works rely on the fact that it is possible to generate destructive interference between the sound fields generated by the original *primary* source and that produced by a *secondary* source, whose acoustic output can be controlled. The destructive interference, in a particular point in space, is achieved if the secondary source generates a sound wave with the same frequency characteristics as the noise but with a 180^0 shift in phase. This is the principle in Active Noise Control and is shown in Figure 2.1, where the effect of a primary acoustic source is canceled with a secondary source. The reduction of engine sound in airplanes and motor vehicles are mentioned as possible applications of these techniques. This principle was extrapolated to applications in vibration control, nevertheless some differences arise as will be explained latter in this chapter.

According to whether or not energy is injected into the system to compensate noise or vibrations, the literature makes the following classification ([Fuller et al., 1997, Snyder, 2000]): passive, semi-active and active methods.

The first one is the classical solution which consists in adding insulation or damping materials. It is termed as passive because neither control nor energy are needed. Among the advantages, we found simple implementation and robust reliable solutions. However

it is economically limited in terms of weight and bulk. Besides, since it is not possible to target the control action to particular objectives, their performance capabilities depend on the natural system's dynamics. The Helmholtz resonator ([Olson and May, 1953, Fleming et al., 2007]) is an example of this method.

The semi-active method was developed to overcome the limitations of the passive method. This method incorporates the use of actuators which behave as passive elements, by allowing only storage or dissipation of energy. The new feature is the adjustment of their mechanical properties by a signal derived from a controller ([Karnopp et al., 1974]). As an example, the shock-absorbers in some vehicles have a computer controlled viscous damping coefficient.

The third method is termed *active* since it uses the ability to supply mechanical power to the system and to target the control action towards specific objectives. This thesis is focused on this control method. For noise applications, the interest is led to the frequencies range from 20 Hz to 20,000 Hz. As mentioned in [Olson and May, 1953, Elliott and Nelson, 1993, Elliott, 2001], passive methods generally do not work well at low frequencies (under 500 Hz) since the wavelength becomes larger, requiring thicker and heavier materials. For this reason, a number of practically important acoustic problems are dominated by active control contributions. As shown later, this will raise some interesting and new control problems.

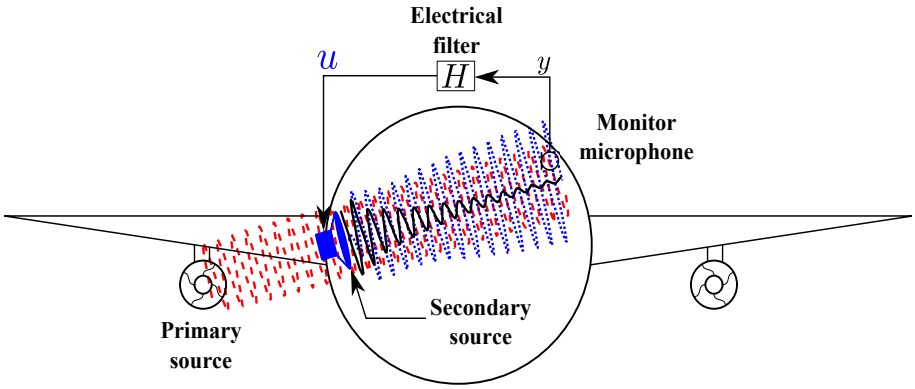

Figure 2.1: Acoustic cancellation by means of ANC used to increase passenger's comfort inside an airplane. Red dashed line: primary source; dotted blue line: secondary source; solid black line: acoustic wave measured by the microphone.

The application domain includes areas such as automotive, aircraft, marine, industrial equipment and appliances where rotatory engines and motors create unwanted vibrations (see [Chen and Tomizuka, 2014, Chen and Tomizuka, 2013a]). An example for noise cancellation is given in Fig. 2.1, where an airplane turbines noise reduction application is depicted. In order to increase the comfort of the passengers, the noise generated by the airplane turbines is minimized by means of a secondary source (loudspeakers) using a microphone as a noise field sensor. A vibration reduction example is depicted in Fig. 2.2, where an active chassis control scheme is shown. In this application, the objective is to reduce the vibrations created by the motor at the level of the chassis. By means of actuators, an opposite vibration is introduced to the chassis with a shift phase of 180^0. The vibrations are usually measured by accelerometers or force sensors. A more extensive background can be found in [Elliott and Nelson, 1993, Fuller and von Flotow, 1995, Guicking, 2007].

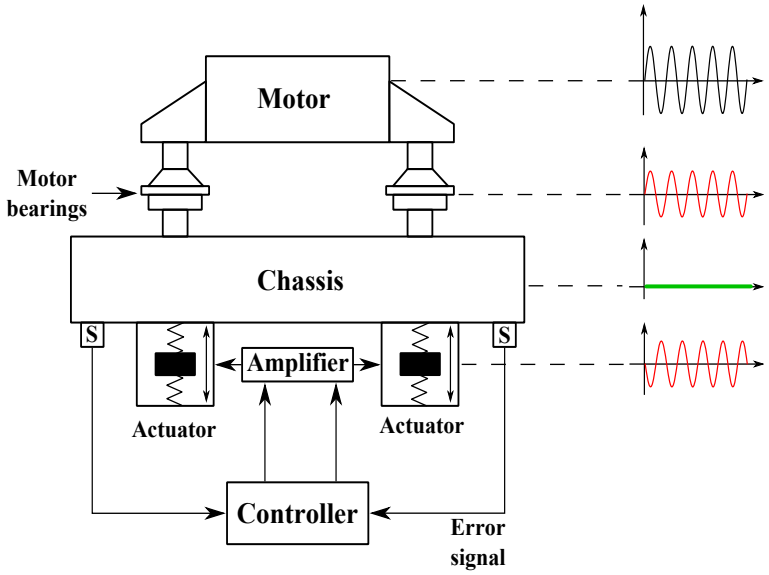

Figure 2.2: Active chassis control used to reduce the vibrations generated by the motor.

2.2 Problem Description

This section provides the reader with a brief description of one of the basic problems for Active Noise and Vibration Control that will be treated later of this thesis. The main control objective is to reduce the level of vibration (or noise) at a predefined location of interest.

Unlike the Active Noise Control applications, Active Vibration Control applications are highly related to the mechanical properties of the considered structure. Indeed, in a structure there are many different types of wave motion, which can cause vibrations propagating from one place to another. Acoustic waves, of course, only propagate as longitudinal, compressional waves in fluids with low viscosity such as the air. In the complicated structures often encountered in aircraft, spacecraft, ships and cars, the different types of structural wave motions are also generally coupled together in rather complicated ways [Junger and Feit, 1972]. This is reflected in the frequency characteristics of the system where resonant and anti-resonant modes can be found. For feedback regulation purposes, the anti-resonant modes (originated by the presence of complex zeros with low damping) are critical for performance and robustness issues.

A linear description of the problem, when all the information is available, will be used as set-up for enhancing the objectives and the challenges to be solved. This will also pave the way for the adaptive solutions required by the lack of information about the disturbances.

2.2.1 Feedback regulation in the presence of narrow band disturbances

One of the basic problems for ANVC is the strong attenuation of narrow band disturbances without measuring them. This can be done through a feedback approach. Even though in ANVC there are two control configurations (feedforward and feedback), in this thesis, only the feedback configuration will be considered. The reason is that the test bench used for the experiments features only one measurement, and

the feedforward approach requires a second sensor to obtain an *image* of the disturbance [Landau et al., 2011a].

The limitation for the feedback approach is due to the Bode's Sensitivity Integral [Doyle et al., 2013]. This integral basically states that when an attenuation is introduced at some frequency, an amplification will occur at another frequency (this is known also as *waterbed* effect). If broad band disturbance rejection is attempted with a feedback approach, important amplifications will be reflected since this type of disturbance requires a *wide* attenuation area. Therefore only narrow band disturbances will be considered for feedback approaches. For broad band disturbance rejection, recent solutions have been presented in [Alma, 2011] and [Airimiţoaie, 2012].

Consider the control scheme shown in Fig. 2.3, where a single-input single-output (SISO) discrete plant $G(z^{-1}) = \frac{z^{-d}B(z^{-1})}{A(z^{-1})}$ is disturbed by a signal $p(t)$[1]. The *disturbed* output is $y(t)$ and the plant input is $u(t)$. In order to force the output $y(t)$ to go to zero, i.e. the effect of the disturbance $p(t)$ is canceled, a controller $K(z^{-1})$ is incorporated into the loop in a negative feedback.

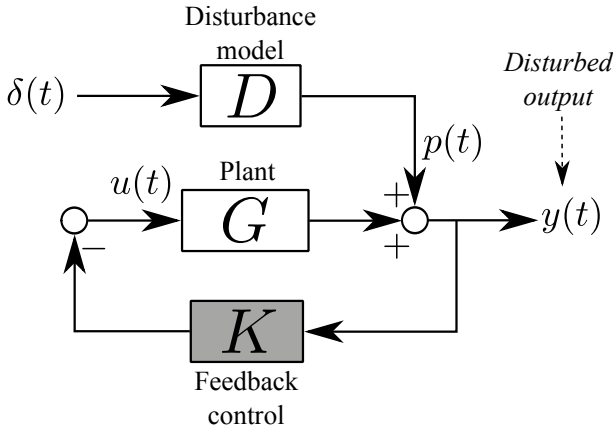

Figure 2.3: Feedback scheme for ANVC.

Assume that controller $K(z^{-1})$ is a transfer function where

$$K(z^{-1}) = \frac{R(z^{-1})}{S(z^{-1})}. \tag{2.1}$$

$R(z^{-1})$ and $S(z^{-1})$ are polynomials in z^{-1} with the following structure

$$R(z^{-1}) = r_0 + r_1 z^{-1} + \cdots + r_{n_R} z^{-n_R} = H_R(z^{-1})R'(z^{-1}), \tag{2.2}$$

$$S(z^{-1}) = 1 + s_1 z^{-1} + \cdots + s_{n_S} z^{-n_S} = H_S(z^{-1})S'(z^{-1}), \tag{2.3}$$

where n_R and n_S are the order of the polynomials R and S, respectively and H_R and H_S are pre-specified parts with various purposes, e.g. to open the loop at some frequencies or incorporate the model of a disturbance. This controller can be computed in a linear way by the Pole Placement technique, for instance[2]. If the disturbance signal $p(t)$ is known, i.e. the model of the disturbance, it can be used for control purposes. For narrow band disturbances it is assumed that $p(t)$ is the result of filtering a Dirac's impulse through a filter $D(q^{-1})$

$$p(t) = D(q^{-1})\delta(t) = \frac{N_p(q^{-1})}{D_p(q^{-1})}\delta(t) \tag{2.4}$$

[1] In the next chapter, a detailed description of the plant model and disturbance model will be given.
[2] Although other control design techniques can be used as well.

where the roots of $D_p(z^{-1})$ are on the unitary circle.

The closed loop plant output can be written as follows

$$y(t) = \frac{1}{1+GK}p(t) = \frac{A(q^{-1})S(q^{-1})}{P(q^{-1})}p(t) \tag{2.5}$$

where $P(z^{-1}) = A(z^{-1})H_S(z^{-1})S'(z^{-1}) + z^{-d}B(z^{-1})H_R(z^{-1})R'(z^{-1})$ defines the closed loop poles. If the polynomial $S(z^{-1})$ is selected as $S(z^{-1}) = D_p(z^{-1})S'(z^{-1})$, the output of the closed loop system becomes

$$y(t) = \frac{A(q^{-1})D_p(q^{-1})S'(q^{-1})}{P(q^{-1})} \cdot \frac{N_p(q^{-1})}{D_p(q^{-1})}\delta(t) = \frac{A(q^{-1})S'(q^{-1})N_p(q^{-1})}{P(q^{-1})}\delta(t). \tag{2.6}$$

If the denominator of (2.6) is stable, i.e. $P(z^{-1}) = 0$, $|z| < 1$, the output of the closed loop system will go asymptotically towards zero. This is known as the *Internal Model Principle* (IMP) [Francis and Wonham, 1976].

Here the following remarks can be done:

1. For disturbance rejection in a linear context, it is necessary to know both plant and disturbance models. Usually the plant model can be obtained by means of system identification, nevertheless the disturbance model is in general unknown and possibly time-varying. Therefore an adaptive scheme is required.

2. In order to incorporate the model of the disturbance in the controller, it is necessary that the roots of $D_p(z^{-1})$ are not contained in $B(z^{-1})$, i.e. they have to be coprime. When the roots of both polynomials get closer, the *coprimeness* is reduced. It is noted that compensator systems which have low damped complex zeros complicate this situation. This is due to the fact that the coprimeness of the solutions is compromised as well as the stability of the closed loop system. This will be reviewed later.

3. Even though the experimental set-up used in this thesis was already presented in previous works such as [Landau et al., 2005] and [Landau et al., 2011b], nowadays it presents important changes which introduce new characteristics and challenges resulting from the characteristics of the new mechanical structure.

4. There are several methods to introduce the disturbance model into the controller structure; among them, the Youla-Kučera parametrization provides useful features for stability, robustness and performance.

It is well known that in feedback controllers, the IMP could lead to an unacceptable increase of the maximum of the output sensitivity function (bringing the system close to the instability). This becomes more apparent when multiple narrow band disturbances rejection is performed. However, in the vicinity of low damped complex zeros, even single narrow band disturbance rejection can be difficult to achieve. Since the controller proposed is model based, a more accurate identified plant model is required, specially in the frequency band where disturbance rejection is performed.

Besides, even when all the information is available (plant model, disturbance model, etc.), linear control design is not a trivial task. The difficulty increases when the disturbance is unknown and considered as time-varying. Therefore the problem consists in the design of *robust adaptive control algorithms for the rejection of multiple unknown and possibly time-varying narrow band disturbances in the presence of low damped complex plant zeros.*

2.3 Literature Overview

In this section, a review of the important contributions in the literature of non-minimum phase zeros identification and feedback regulation of noise or vibrations is presented.

2.3.1 Identification of non-minimum phase zeros

Quoting the work from [Söderström and Stoica, 1988] and [Ljung, 1999], System Identification is the field of modeling dynamic systems from experimental data. This is depicted in Figure 2.4 where a dynamical system is driven by inputs $u(t)$ and disturbances $v(t)$ and where some variables are measured $y(t)$.

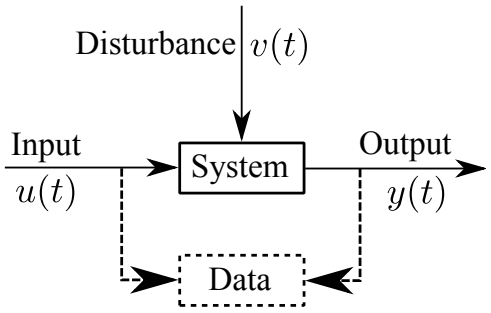

Figure 2.4: General scheme of a dynamical system where inputs, disturbances and outputs are shown.

Using the collected data, one can estimate/identify a mathematical expression who represents the relation between the inputs (controlled), disturbances (uncontrolled) and outputs (measured). The mathematical expression is known as *model*. Depending on the assumption made over the disturbances (which can be neither controlled nor measured), is the structure of the model. Since the mathematical model will represent the relation between inputs and outputs, the transfer function representation is used more often ([Ljung, 1999, Söderström and Stoica, 1988, Landau and Zito, 2005]).

In the control community, models are used often for both analysis and synthesis. Therefore the overall objective of identification for control is to deliver models suitable for control design. The works of [Gevers, 1993] and [Van Den Hof and Schrama, 1995] present an overview of this area.

One major issue in model based controller design is the bandwidth achievable by the closed loop. This is specially critical for systems that contain performance limitations as non-minimum phase zeros and time delays. This limitation increases in discrete-time since, in [Åström et al., 1984], it was proved that for different values of sampling period in many applications, unstable zeros will appear as the sample time is decreased, even though all the zeros of the continuous system model may be stable.

The standard configuration to perform a system identification is when the system is operated in open loop (no controller is considered - [Ljung, 1999],[Landau and Zito, 2005]). Nevertheless, in this research area, it was built a whole theory and techniques to identify systems who operate in closed loop. Several contributions have been made for this identification set up. In [Van Den Hof and Schrama, 1995] and [Hjalmarsson et al., 1996] it was pointed out that the closed loop experimental conditions should not be considered as a degenerate or unfavourable situation to identify dynamical systems. Provided that appropriate algorithms are used, better control models can be obtained by identification

in closed loop operation. Then in [Landau and Karimi, 1997] a unified presentation of recursive algorithms for plant model identification in closed loop was given, with some real time applications. Works such as [Gustavsson et al., 1977], [Van den Hof, 1998] and [Forssell and Ljung, 1999] represent survey papers where it is proved that the accuracy and performance of the obtained models were improved from the previous models obtained in open loop.

Recently, for more accurate identification of *restrictive* zeros (non-minimum phase or with low damping factor), [Martensson et al., 2005] presented an input design technique in order to optimize the input signal. [Mårtensson and Hjalmarsson, 2005] and [Mårtensson and Hjalmarsson, 2009] exploit the analysis of the variance of the estimated non-minimum phase zeros and deliver conclusions that using over parametrized models do not increase the variance of the zeros.

Although the previous works deal specifically with restrictive zeros, the input design technique was developed for auto-regressive models with exogenous inputs (ARX) and finite impulse response (FIR) models. Also the major conclusions for closed loop system identification of unstable poles and non-minimum phase zeros were for over parametrized models. The work presented here capitalizes on the results presented in [Landau and Karimi, 1997] and [Landau and Karimi, 1999] for closed loop identification by modifying the present controller in order to increase the system's sensitivity at the target frequencies.

2.3.2 Feedback rejection of multiple narrow band disturbances

The feedback control approach becomes the only choice when it is not possible to use a second transducer to measure the image of a disturbance. This occurs often in practice. Consider the restrictions imposed by the Bode's Sensitivity Integral ([Åström and Murray, 2008][Zhou et al., 1996]). We can only attenuate disturbances on a finite band of frequencies. Therefore, this part of the thesis is focused on the rejection of multiple time-varying sinusoidal disturbances. For a comparative analysis of feedback and feedforward disturbance rejection, readers are referred to [Elliott and Sutton, 1996].

Before presenting the review of the existing methods for narrow band disturbance rejection, we will comment about the differences about two paradigms in this area. Recently, in [Landau et al., 2011c], it was pointed out that in the classical *adaptive control* paradigm, the objective is tracking/disturbance attenuation in the presence of unknown and time varying plant model parameters. Therefore, the adaptation is done w.r.t. to variations in the parameters of the plant model. The disturbance models are assumed constant and known.

Conversely to the adaptive control paradigm, the *adaptive regulation* paradigm deals the asymptotically rejection (or attenuation) of the effect of unknown and time varying disturbances. It is assumed that the plant model parameters are known and almost invariant. A robust control design can be applied to deal with possible small variations (uncertainty) on its parameters. Then, the effort is concentrated on the disturbance model and not the process model. A remark for this paradigm is that the disturbance should be located in the frequency region where the plant model has enough gain (for robustness reasons that will be explained later).

Since the aim of this dissertation is the disturbance rejection (or attenuation), the adaptive regulation problem will be considered. The common assumption is that the disturbance is the result of a white noise or a Dirac impulse passed through

the "model of the disturbance". Several solutions have been proposed to reject its influence over the system output. One of them is the Internal Model Principle (IMP) reported in [Amara et al., 1999a], [Amara et al., 1999b], [Gouraud et al., 1997], [Hillerstrom and Sternby, 1994], [Valentinotti, 2001, Valentinotti et al., 2003], [de Callafon and Fang, 2013], [Chen and Tomizuka, 2013b], [Karimi and Emedi, 2013], [Wu and Ben Amara, 2013], [Castellanos Silva et al., 2013b]. The idea behind these methods is that the model of the disturbance is incorporated in the controller ([Bengtsson, 1977, Francis and Wonham, 1976, Johnson, 1976, Tsypkin, 1997]). Its parameters should be continuously estimated in order to be able to respond to possible changes in the disturbance's characteristics. This will lead to an indirect adaptive control algorithm ([Airimiţoaie et al., 2013], [Aranovskiy and Freidovich, 2013]). However, it has been shown in [Landau et al., 2005, Landau et al., 2011c] that direct adaptation is possible if one uses the Youla-Kučera parametrization of all stable controllers.

Another idea that has been used is to build and incorporate an adaptive observer in the controller [Ding, 2003, Marino et al., 2003, Serrani, 2006, Marino and Tomei, 2007]. However, the approach seems to be mainly focused on disturbances acting on the input of the plant. Additional hypotheses should be taken into account before applying it to disturbances on the output (the plant should have stable zeros, which is seldom the case for discrete time plant models). It can be noted that, although the Internal Model Principle is not explicitly taken into consideration in this scheme, incorporating the observer into the controller means that the internal model principle is implicitly used.

A direct approach that uses the concept of a phase-locked loop is presented in [Bodson and Douglas, 1997] and experimental results are provided in [Bodson, 2005]. It can be applied to the rejection of sinusoidal disturbances with unknown frequencies. Disturbance frequency estimation and disturbance cancellation are performed simultaneously by using a single error signal. The frequency response of the plant in the frequency range of interest is needed.

Recently in [Landau et al., 2013a], the results of an international benchmark competition on adaptive regulation of unknown and time varying narrow band disturbances have been presented. It contains the work of [Aranovskiy and Freidovich, 2013], [de Callafon and Fang, 2013], [Chen and Tomizuka, 2013b], [Karimi and Emedi, 2013], [Wu and Ben Amara, 2013], [Airimiţoaie et al., 2013] and [Castellanos Silva et al., 2013b] proving the interest and relevance about this kind of problems for the control research community. It was found also that almost all the contributions used (explicitly or not) the Internal Model Principle.

2.4 Contributions

The main objective of the thesis has been the development of adaptive algorithms for vibration attenuation in mechanical systems. The algorithms have been extensively tested on the active suspension system available at the GIPSA-Lab of the University of Grenoble.

In Part I of the dissertation, the problem of parameter uncertainty in the active vibration system is considered. The most significant contributions are:

1. Closed loop system identification of the actuator model in the presence of low damped complex poles and zeros. A modification on the closed loop identification algorithms is presented and tested on the real AVC system.

2. A performance and robust analysis is presented in a feedback regulation context.

The contributions of Part II of this thesis are:

1. Improvement of the robustness of the direct adaptive algorithm presented in [Landau et al., 2005], in order to keep the modulus of the output sensitivity function under some value.

2. Development of new feedback control methods to reject narrow band disturbances based on the IMP using the YK parametrization and an IIR Q-filter.

Experimental results are shown and confirm the results of the theoretical analysis. Although developed for an Active Vibration Control system, the algorithms are also applicable to Active Noise Control.

2.5 Dissertation Outline

In **Part I** of the thesis, parameter uncertainty due low damped complex plant zeros is treated and studied. First, **Chapter 3** presents the AVC system on which the algorithms have been tested. The experimental system, built in collaboration with the Active Noise and Vibration Control, PAULSTRA SNC (Dept. VIBRACHOC) research center, is inspired by problems encountered in the industry. A special feature of this system is the presence of low damped complex zeros due the mechanical structure. In the next two chapters, the closed-loop identification of the system model and the robustness constraints due the special characteristics are analyzed.

In **Chapter 4** the linear control problem of feedback regulation when narrow band disturbances are applied to the system is analyzed. Control objectives have been settled in order to assess how good is the performance of the controller. In this chapter, the Youla-Kučera parametrization of the RST polynomial controllers is presented. The Internal Model Principle (IMP) is applied through this parametrization. In the linear context, i.e. where both the plant and disturbance models are known, robustness constraints are settled for the application of the IMP.

Chapter 5 presents a modified version of a closed-loop identification algorithm. The modification follows the idea in the Maximum Recursive Likelihood in order to incorporate the advantages from algorithms in [Landau and Karimi, 1997] and [Landau and Karimi, 1999], considering the presence of low damped complex zeros.

In **Part II**,**Chapter 6** presents two solutions for narrow band disturbance rejection. The first one corresponds to an improved version of the direct adaptive algorithm presented in [Landau et al., 2005]. The improvements are obtained by means of the central controller design. The second solution is a mixed direct/indirect adaptive algorithm for the attenuation of multiple narrow band disturbances by means of a Q-IIR filter. The mixed procedure is based on a first step of disturbance model estimation and a second step of Q-filter updating. Both solutions are based on the Youla-Kučera parametrization. Finally, **Chapter 7** presents the simulation and real-time results for an International Benchmark example for Adaptive Regulation. The results correspond to the second solution since the results of the first solution have been already published in [Castellanos Silva et al., 2013b]. Through the Benchmark criteria, a comparative evaluation of the results presented in this chapter is done between the various contributions presented in [Landau et al., 2013a].

Conclusions and directions for future research are given in **Chapter 8**.

Part I

Parameter Uncertainty in Active Vibration Control Systems

Chapter 3

An Active Vibration Control Test bench System

This chapter gives a detailed presentation of the Active Vibration Control system used to test the adaptive algorithms proposed in this thesis (Section 3.1). The basic equations which describe such type of active vibration control system are presented in Section 3.2. The identified open loop models for both mechanical paths are given Section 3.3. Finally, concluding remarks of this chapter are given in Section 3.4.

3.1 System Description

Figures 3.1 and 3.2 show the test bench for active vibration control. It uses inertial actuators for vibration generation and compensation. The structure is representative of a number of situations encountered in practice. In Fig. 3.1 the basic control and disturbance actions are depicted.

The system is composed of a passive damper, an inertial actuator, a mechanical structure, a transducer for the residual force, a controller, a power amplifier and a shaker. The inertial actuator will create vibrational forces that will counteract the effect of vibrational disturbances introduced by the shaker. The inertial actuators use a principle similar to loudspeakers, see for example [Marcos, 2000, Landau et al., 2011b]. A general view of the system including the testing equipment is shown in Figure 3.2. The objective is to minimize the measured residual force $y(t)$.

The mechanical construction is such that the vibrations produced by the shaker, fixed to the ground, are transmitted to the upper side, on top of the passive damper. The inertial actuator is fixed to the chassis where the vibrations should be attenuated. The controller, through the power amplifier, generates electrical current in the moving coil which produces motion in order to reduce the residual force. The system input $u(t)$ is the position of the mobile part (magnet) of the inertial actuator, the output $y(t)$ is the residual force measured by a force sensor.

The disturbance is the position of the mobile part of the shaker (see Figures 3.1 and 3.2) located at the bottom of the structure (fixed to the ground). The input to the compensator system is the position of the mobile part of the inertial actuator fixed to the chassis of the structure. Since the input to the shaker and the inertial actuator is a position, both primary and secondary paths have a double differentiator behavior (since the measured output is a force).

The corresponding block diagram in closed loop operation is shown in Figure 3.3. The feedback compensator has, as input, the performance variable $y(t)$ and its output is

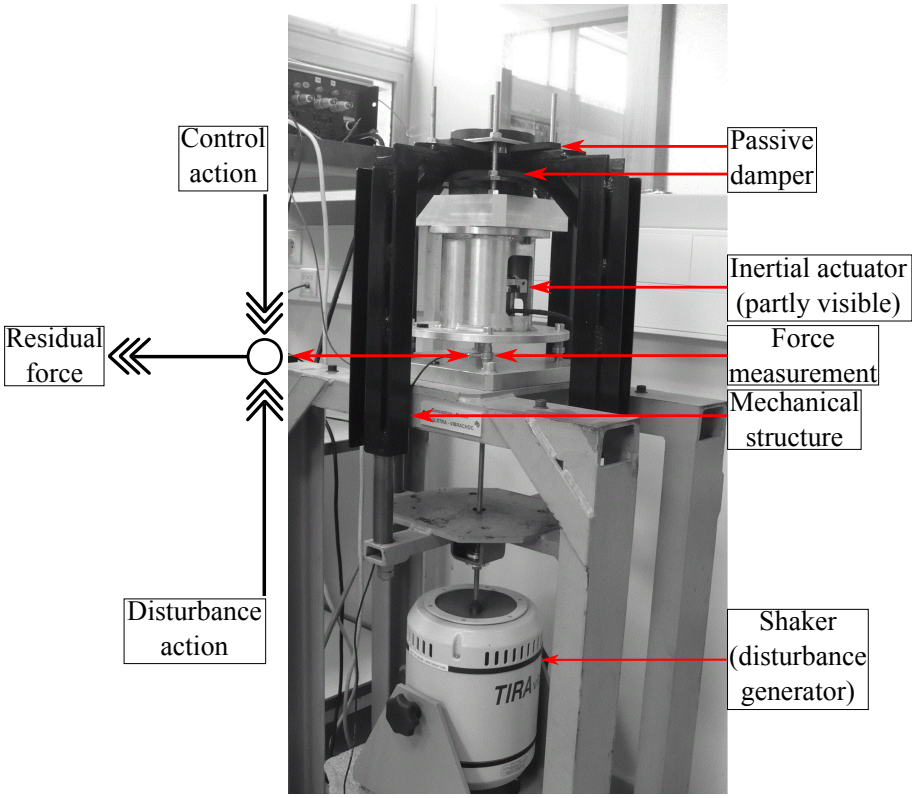

Figure 3.1: The Active Suspension System used for AVC experiments - photo.

represented by $u(t)$ as described in Subsection 2.2.1. The control signal applied to the actuator through an amplifier is

$$u(t) = -K(q^{-1}) \cdot y(t), \tag{3.1}$$

where $K(z^{-1})$ is a discrete-time transfer function who describes the controller designed. The transfer function $G(z^{-1})$ (the secondary path) characterizes the dynamics from the output of the compensator $u(t)$ to the residual force measurement (amplifier + actuator + dynamics of the mechanical system). The transfer function $D(z^{-1})$ between $\delta(t)$ and the measurement of the residual force (in open loop operation) characterizes the primary path[1].

At this stage it is important to make the following remarks, when there is no compensator nor disturbance (open loop operation):

- very reliable models for the secondary path and the primary path can be identified by applying appropriate excitation on the actuator or the shaker;
- the design of a fixed model based stabilizing feedback compensator requires the knowledge of the secondary path model only.

3.2 Basic Equations and Notations

The different blocks of the AVC system (Figure 3.3) are described in this section. The unmeasurable value of the output of the primary path (when the compensation is active) is denoted $p(t)$.

[1]In Fig. 3.2 the input to the disturbance amplifier is denoted $u_p(t)$ while for the feedback scheme (Fig. 3.3) it is $\delta(t)$, the difference arises from the fact that for the hardware scheme $u_p(t)$ is a signal generated by the computer and $\delta(t)$ is considered as the Dirac impulse used for analysis.

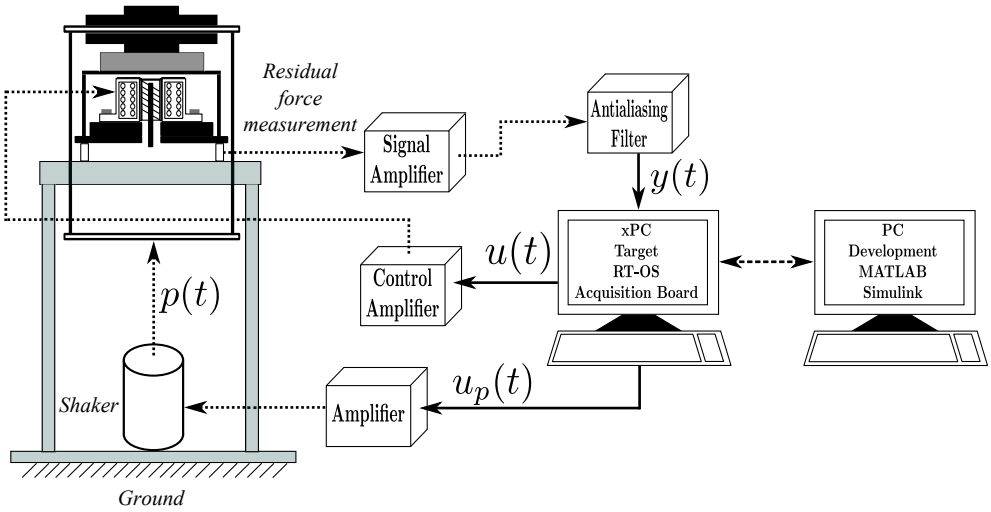

Figure 3.2: General view of the AVC system including the testing equipment.

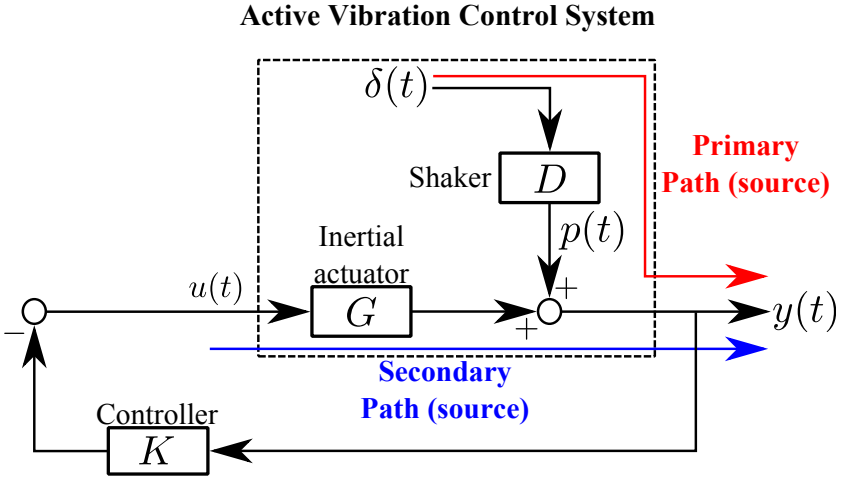

Figure 3.3: Feedback AVC with fixed feedback compensator.

The structure of the linear time-invariant discrete-time model of the plant - the secondary path - used for controller design is

$$G(z^{-1}) = \frac{z^{-d}B(z^{-1})}{A(z^{-1})} = \frac{z^{-d-1}B^*(z^{-1})}{A(z^{-1})}, \tag{3.2}$$

where

$$B(z^{-1}) = b_1 z^{-1} + ... + b_{n_B} z^{-n_B} = z^{-1}B^*(z^{-1}), \tag{3.3}$$
$$B^*(z^{-1}) = b_1 + \ldots + b_{n_B} z^{-n_B+1}, \tag{3.4}$$
$$A(z^{-1}) = 1 + a_1 z^{-1} + \ldots + a_{n_A} z^{-n_A}. \tag{3.5}$$

where $A(z^{-1})$, $B(z^{-1})$, $B^*(z^{-1})$ are polynomials in the complex variable z^{-1} and n_A, n_B and $n_B - 1$ represent their orders[2]. The identified model of the secondary path is denoted $\hat{G}$ and its numerator and denominator $\hat{B}$ and $\hat{A}$, respectively.

[2]The complex variable z^{-1} will be used to characterize the system's behavior in the frequency domain and the delay operator q^{-1} will be used for describing the system's behavior in the time domain.

Since the AVC system is focused on regulation, i.e. minimize or reject the effect of the disturbance at the output, the controller to be designed is a *RS*-type polynomial controller (or equivalently a state space controller + observer, see [Landau et al., 2011d],[Landau and Zito, 2005]).

The output of the plant $y(t)$ and the input $u(t)$ may be written as

$$y(t) = \frac{q^{-d}B(q^{-1})}{A(q^{-1})} \cdot u(t) + p(t); \tag{3.6}$$

$$S(q^{-1}) \cdot u(t) = -R(q^{-1}) \cdot y(t), \tag{3.7}$$

where q^{-1} is the delay shift operator ($x(t) = q^{-1}x(t+1)$) and $p(t)$ is the resulting additive disturbance on the output of the system. $R(z^{-1})$ and $S(z^{-1})$ are polynomials in z^{-1} having orders n_R and n_S, respectively, with the following expressions:

$$R(z^{-1}) = r_0 + r_1 z^{-1} + ... + r_{n_R} z^{-n_R} = R'(z^{-1}) \cdot H_R(z^{-1}), \tag{3.8}$$

$$S(z^{-1}) = 1 + s_1 z^{-1} + ... + s_{n_S} z^{-n_S} = S'(z^{-1}) \cdot H_S(z^{-1}), \tag{3.9}$$

where $H_R(z^{-1})$ and $H_S(z^{-1})$ are pre-specified parts of the controller (used for example to incorporate the internal model of a disturbance or to open the loop at some frequencies). According to the previous section, $K(z^{-1}) = \frac{R(z^{-1})}{S(z^{-1})}$.

We define the following sensitivity functions:

- Output Sensitivity function (the transfer function between the disturbance $p(t)$ and the output of the system $y(t)$):

$$S_{yp}(z^{-1}) = \frac{1}{1+KG} = \frac{A(z^{-1})S(z^{-1})}{A(z^{-1})S(z^{-1}) + z^{-d}B(z^{-1})R(z^{-1})}; \tag{3.10}$$

- Input Sensitivity function (the transfer function between the disturbance $p(t)$ and the input of the plant $u(t)$):

$$S_{up}(z^{-1}) = \frac{-K}{1+KG} = -\frac{A(z^{-1})R(z^{-1})}{A(z^{-1})S(z^{-1}) + z^{-d}B(z^{-1})R(z^{-1})}, \tag{3.11}$$

where

$$\begin{aligned} P(z^{-1}) &= A(z^{-1})S(z^{-1}) + z^{-d}B(z^{-1})R(z^{-1}) \\ &= A(z^{-1})S'(z^{-1})H_S(z^{-1}) + z^{-d}B(z^{-1})R'(z^{-1})H_R(z^{-1}), \end{aligned} \tag{3.12}$$

defines the poles of the closed loop (roots of $P(z^{-1})$).

In pole placement design, the polynomial $P(z^{-1})$ specifies the desired closed loop poles and the controller polynomials $R'(z^{-1})$ and $S'(z^{-1})$ are the minimal degree solutions of (3.12) where the degrees of $P(z^{-1})$, $R'(z^{-1})$ and $S'(z^{-1})$ are given by $n_P \leq n_A + n_B + n_{H_S} + n_{H_R} + d - 1$, $n_S = n_B + n_{H_R} + d - 1$ and $n_R = n_A + n_{H_S} - 1$.

3.3 Open Loop System Identification

The procedure for the identification of the primary and secondary paths will be presented in Chapter 5. Here, only the characteristics of the identified models will be presented.

The estimated orders for the secondary path are $n_A = 18$ and $n_B = 21$ and for the primary path $n_{A_p} = 13$ and $n_{B_p} = 16$. The best results, in terms of validation, have been

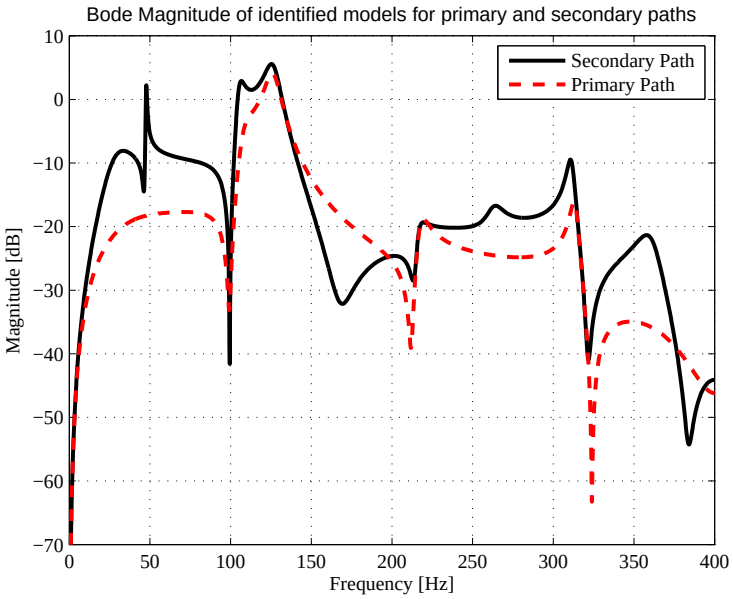

Figure 3.4: Frequency characteristics of the primary and secondary paths.

obtained with the *Recursive Extended Least Squares* method. The frequency characteristics of the secondary path is shown in Figure 3.4, where the solid line corresponds the secondary path model and the dashed line to the primary path model.

The secondary path model presents several resonant and anti-resonant modes. The most relevant resonant modes (poles) for narrow band disturbance rejection, are located at 47.64 Hz (damping of 0.008), 105.19 Hz (damping of 0.024) and 126.40 Hz (damping of 0.039). The most relevant anti-resonant modes (zeros) for narrow band disturbance rejection, are located at 46.57 Hz (damping of 0.013) and 99.45 Hz (damping of 0.0007).

3.4 Concluding Remarks

In this chapter the description of the experimental setup and the equations governing the system have been presented, as well as the characteristics of the identified models.

This will allow to assess, in the next chapter, the linear regulation problem to be solved assuming that the plant and disturbance models are known.

Chapter 4

The linear control challenge

Assuming that only one tonal vibration has to be canceled in a frequency region far from the presence of low damped complex zeros and that the models of the plant and of the disturbance are known, the design of a linear regulator is relatively straightforward, using the internal model principle.

The problem becomes much more difficult if several tonal vibrations (sinusoidal disturbances) have to be attenuated simultaneously and their frequencies may be close to those of some very low damped complex zeros of the plant.

This chapter will examine the various aspects of the design of a linear controller in the context of multiple tonal vibrations and presence of low damped complex zeros. It will also explore various controller architectures (using the Youla-Kučera Controller parametrization) in order to separate the tuning with respect to disturbance characteristic from the stabilization of the feedback loop.

4.1 Control Objectives

The tonal vibrations are located in the range between 50 and 95 Hz. The secondary path (the compensator) has a frequency characteristic covering the region between $0 f_s$ and $0.5 f_s$, where f_s is the sampling frequency (800 Hz in our case). This frequency content can be represented by the set $\Omega = \{0, \cdots, 0.5 f_s\}$ Hz. Then the set of disturbance frequencies is a subset of the frequency content represented as $\Omega_d \subseteq \Omega = \{50, \cdots, 95\}$ Hz. The subset of frequencies not contained in Ω_d is defined as $\Omega_{out} = \Omega \setminus \Omega_d$.

Assume that a tonal vibration (or narrow band disturbance) $p(t)$ is introduced into the system affecting the output $y(t)$. The effect of this disturbance is centered at a specific frequency $\omega_1 \in \Omega_d$. As mentioned in subsection 2.2.1, the IMP can be used to asymtotically reject the effects at the system's output of a narrow band disturbance.

It is important to take into account the fact that the secondary path (the actuator path) has no gain at very low frequencies and very low gain in high frequencies near $0.5 f_s$. Therefore the control system has to be designed such that the gain of the controller be very low (or zero) in these regions (preferably 0 at $0.5 f_s$). Not taking into account these constraints can lead to an undesirable stress on the actuator.

In order to assess how *good* the controller is, it is necessary to define some control objectives that have to be fulfilled. These control objectives are related to the number of tonal vibrations. There are three levels of difficulties corresponding to one, two or three tonal vibrations within the frequency range of interest (50 to 95 Hz). The control objectives for all levels are summarized in Table 4.1. Level 3 is particularly difficult in terms of tolerated amplification (at other frequencies than those of the disturbances) and

Table 4.1: Control objectives in the frequency domain.

Control Objectives	Level 1	Level 2	Level 3
Transient duration	$\leq$ 2 sec	$\leq$ 2 sec	$\leq$ 2 sec
Global attenuation	$\geq$ 30 dB*	$\geq$ 30 dB	$\geq$ 30 dB
Minimum disturbance attenuation	$\geq$ 40 dB	$\geq$ 40 dB	$\geq$ 40 dB
Maximum amplification	$\leq$ 6 dB	$\leq$ 7 dB	$\leq$ 9 dB

* For this level, the specification of 30 dB is for the range between 50 and 85 Hz, for 90 Hz is 28 dB and for 95 Hz is 24 dB.

transient requirements. A set of performance indicators has been defined for evaluating the steady state performance. Several indicators have been defined for the transient performance but the most important is the transient duration. It makes sense to examine the transient performance only if the attenuation performance is satisfactory.

Tuning capabilities: Evaluation in steady state operation after application of the disturbance once the transient settles. This indicator is evaluated in the presence of constant disturbance frequency. It is constituted from three measurements:

1. Global attenuation (GA): measured in dB and defined by

$$GA = 20 \log_{10} \frac{N^2 Y_{ol}}{N^2 Y_{cl}}, \tag{4.1}$$

where N^2Y_{ol} and N^2Y_{cl} correspond to the square of the truncated 2-norm of the measured residual force in open and closed loops, respectively, evaluated during the last 3 s of the experiment, Fig. 4.1 illustrates this measurement. The truncated 2-norm has the following expression

$$N^2T = \sum_{i=1}^{m} y(i)^2, \tag{4.2}$$

where $y(i)$ is a sample of the discrete time signal to evaluate. This quantity indicates the energy contained in the measured signal.

2. Disturbance attenuation (DA): measured in dB. It is defined as the maximum value of the difference between the estimated PSD[1] of the residual force in closed loop and in open loop as shown in Fig. 4.2 and defined by

$$DA = \min \left(PSD_{cl} - PSD_{ol} \right), \tag{4.3}$$

3. Maximum amplification (MA): measured in dB, it is defined as the maximum value of the difference between the estimated PSD of the residual force in closed loop and open loop. In this measurement, the waterbed effect is shown. It is defined by

$$MA = \max \left(PSD_{cl} - PSD_{ol} \right). \tag{4.4}$$

[1]Power Spectral Density

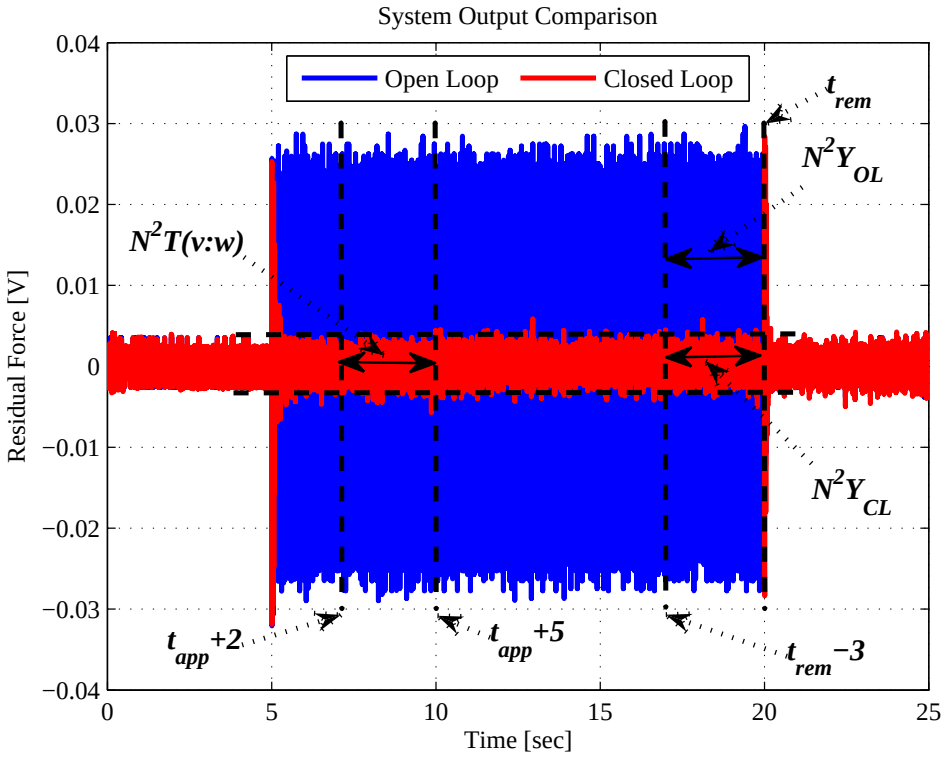

Figure 4.1: Definitions for global attenuation (GA) measurement and transient evaluation. The intervals of computation ($t_{app}+2$, $t_{app}+5$, $t_{rem}-3$, t_{rem}) are displayed.

Through these three measurements, it is possible to assess the performance of the controller in order to achieve the disturbance rejection (global and disturbance attenuations) and to analyze as well the robustness (maximum amplification).

Transient performance: will be evaluated for constant frequency.

- Transient evaluation: It is required that the transient duration, when a disturbance is applied, be smaller than 2 seconds. A performance index was establish for 100% of fulfillment (equal or less than 2 s) or 0% for a transient of 4 s. This means that 2 s after the application of a disturbance the square of the truncated 2-norm has to be equal to or smaller than 1.21 of the steady state value of the square of the truncated 2-norm of the residual force. The square of the truncated 2-norm is evaluated over an interval of 3 s both for transient and steady state. Taking into account the instant of application of the disturbance t_{app} and the instant when the disturbance is removed t_{rem}, the square of the truncated 2-norm is denoted as $N2T(v:w)$ where v and w define the interval of computation. One defines

$$\alpha = \frac{N^2T\left(t_{\text{app}}+2 : t_{\text{app}}+5\right)}{N^2T\left(t_{\text{rem}}-3 : t_{\text{rem}}\right)} = \frac{N^2T\left(t_{\text{app}}+2 : t_{\text{app}}+5\right)}{N^2Y_{CL}} \tag{4.5}$$

$$\Delta Trans = \alpha - 1.21 \quad \text{if} \quad \alpha > 1.21 \tag{4.6}$$

$$\Delta Trans = 0 \quad \text{if} \quad \alpha \leq 1.21. \tag{4.7}$$

- Square of the truncated 2-norm of the first three seconds of the closed loop test.
- Maximum value of the closed loop response defined by

$$MV = \max_{m} |y(i)| . \tag{4.8}$$

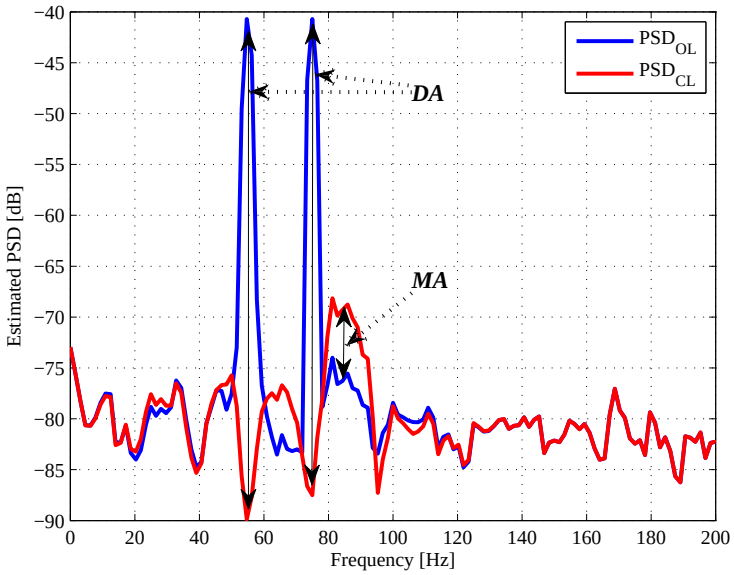

Figure 4.2: Definition of disturbance attenuation (DA) and Maximum amplification (MA).

- Mean square of the residual force of a specific time period, defined by

$$MSE = \frac{1}{m}\sum_{i=1}^{m} y(i)^2 = \frac{1}{m}N^2T, \tag{4.9}$$

where m corresponds to the number of output samples evaluated.

4.2 Controller Structure

From the previous chapter, the controller structure corresponds a RST-type polynomial controller. Since the control objective is regulation, the polynomial $T(z^{-1})$ will be not considered. From (3.8) and (3.9), the controller polynomials are recalled here

$$R(z^{-1}) = r_0 + r_1 z^{-1} + \cdots r_{n_R} z^{-n_R} = H_R(z^{-1})R'(z^{-1}) \tag{4.10}$$
$$S(z^{-1}) = 1 + s_1 z^{-1} + \cdots s_{n_S} z^{-n_S} = H_S(z^{-1})S'(z^{-1}), \tag{4.11}$$

where n_R and n_S are the degrees of the polynomials R and S respectively, and H_R and H_S represent pre-specified (fixed) parts for each polynomial. These fixed parts are used to open the loop at some frequencies or introduce the model of the disturbance.

Assuming a Pole Placement design context, the polynomials R' and S' are the minimal degree solutions from the following Bezout equation

$$\begin{aligned} P(z^{-1}) &= A(z^{-1})S(z^{-1}) + z^{-d}B(z^{-1})R(z^{-1}), \\ &= A(z^{-1})H_S(z^{-1})S'(z^{-1}) + z^{-d}B(z^{-1})H_R(z^{-1})R'(z^{-1}), \end{aligned} \tag{4.12}$$

where $P(z^{-1})$ is used to define the *desired* closed loop poles, where the degrees of $P(z^{-1})$, $R'(z^{-1})$ and $S'(z^{-1})$ are given by

$$n_P \leq n_A + n_B + d + n_{H_S} + n_{H_R} - 1,\ n_{S'} = n_B + d + n_{H_R} - 1,\ n_{R'} = n_A + n_{H_S} - 1.$$

The solution exists, providing that AH_S and BH_R are coprime, where A and B define the discrete-time plant model. Using this controller design technique, the feedback loop is represented as in Fig. 4.3 where the output of the system can be written as

$$y(t) = G(q^{-1})u(t) + p(t) = \frac{A(q^{-1})S(q^{-1})}{P(q^{-1})}p(t). \tag{4.13}$$

The unknown S' and R' can be computed by putting (4.12) into a matrix form (see also [Landau et al., 2005]). The size of the matrix equation that needs to be solved is

$$n_A + n_{H_S} + n_B + n_{H_R} + d - 1 \times n_A + n_{H_S} + n_B + n_{H_R} + d - 1.$$

Remark: the theory does not say anything about what happens if the fixed part H_S has roots close to the roots of B. If the system order is high as the active suspension system presented in the previous chapter where $n_A = 18$, $n_B = 21$ and $d = 0$, the matrix equation to solve is computer demanding.

Suppose that $p(t)$ is a deterministic disturbance, so it can be written as

$$p(t) = \frac{N_p(q^{-1})}{D_p(q^{-1})}\delta(t), \tag{4.14}$$

where $\delta(t)$ is a Dirac impulse and $N_p(z^{-1})$ and $D_p(z^{-1})$ are coprime polynomials in z^{-1}, of degrees n_{N_p}, n_{D_p}. We are interested in the rejection of narrow band disturbances and in this case, the roots of $D_p(z^{-1})$ are on the unit circle[2]. The energy of the disturbance is essentially represented by D_p. The contribution of the terms of N_p is weak, compared to the effect of D_p, so one can neglect the effect of N_p.

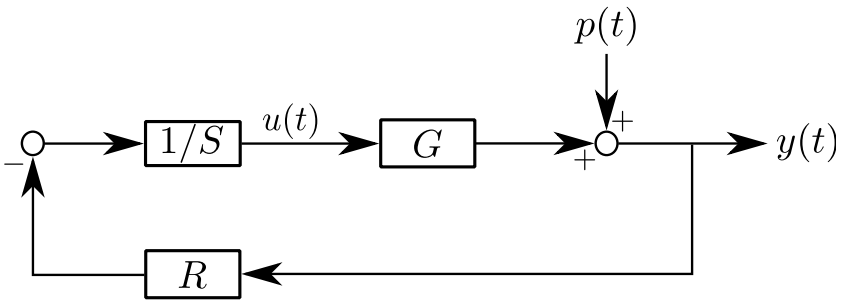

Figure 4.3: Feedback RS-type controller.

Since the objective is to cancel the effect of disturbances, it is logical to use the ***Internal Model Principle*** [Francis and Wonham, 1976]: *The effect of the disturbance given in* (4.14) *upon the output* (4.13)*, given by*

$$y(t) = \frac{A(q^{-1})S(q^{-1})}{P(q^{-1})} \cdot \frac{N_p(q^{-1})}{D_p(q^{-1})}\delta(t), \tag{4.15}$$

where $D_p(z^{-1})$ is a polynomial with the roots on the unit circle and $P(z^{-1})$ is an asymptotically stable polynomial, asymptotically converges towards zero if and only if the polynomial $S(z^{-1})$ in the RS controller has the form

$$S(z^{-1}) = D_p(z^{-1})S'(z^{-1}). \tag{4.16}$$

[2]Since the external disturbance is narrow band, the filtering effect of the primary path around the central frequency can be approximated by a gain and a phase lag which will be captured by N_p.

In other words, the pre-specified part of $S(z^{-1})$ should be chosen as $H(z^{-1}) = D_p(z^{-1})$ and the controller is computed using (4.12), where P, D_p, A, B, H_R and d are given. Through (3.7) the control signal is computed. Notice that if the disturbance model changes, the controller must be recomputed.

Recomputing the controller means, for real-time applications, a heavy computational load. An option to reduce the computation load (specially when it is required to solve such an equation at each sample time) is to use the Youla-Kučera (YK) parametrization. Another important feature is that the YK parametrization will allow to separate the problem of stabilizing the closed loop from the problem of tuning the controller with respect to the disturbance characteristics.

4.3 Narrow band disturbance rejection using the Youla Kučera parametrization

Consider the feedback control scheme depicted in 3.3. Suppose that a stabilizing controller K exist for a given plant G, which could be stable or not. It is possible to represent the set of all stabilizing controllers for the plant G, given a single stabilizing controller K and using the set of all stable Q filters. This is the so called *Youla-Kučera* (YK) Parametrization [Anderson, 1998][3]. This parametrization was introduced independently in [Kucera, 1975] and in [Youla et al., 1976].

This parametrization has two key features. First, it is assumed that one stabilizing controller is *a priori* known. Second, the plants are described using *stable transfer function fractional representations*. This representation is not restrictive because plants that could be unstable can be represented using stable transfer functions. This also allows to use notions such as coprimeness and greatest common divisor since proper rational transfer functions form an algebraic entity known as a Euclidean domain.

This parametrization can be used for multiple-input multiple-output (MIMO) systems but in this work, only single-input single-output (SISO) systems will be considered.

4.3.1 The Youla-Kučera Parametrization

Let $\mathcal{S}$ denote the set of stable proper rational transfer functions (either in continuous or discrete time). Two fractional transfer functions N, D with entries in $\mathcal{S}$ are said to be right coprime[4] if there exist transfer functions X, $Y \in \mathcal{S}$ with $XN + YD = 1$. The following theorem defines the Youla-Kučera parametrization using a right coprime factorization:

Theorem 4.3.1. *[Anderson, 1998] Let a plant $G = ND^{-1}$, with N and D coprime over $\mathcal{S}$, be stabilized by a controller (in a negative feedback loop) $K = XY^{-1}$, with X, Y coprime over $\mathcal{S}$. Then, the set of all stabilizing controllers for G is given by*

$$\mathcal{K} = \left\{ (X + DQ)(Y - NQ)^{-1} : Q \in \mathcal{S} \right\} \tag{4.17}$$

Figure 4.4 shows the block diagram using the right comprime factorization $G = ND^{-1}$ for the plant along with the controller $K = XY^{-1}$. The Q parameter is depicted explicitly. This control configuration can be particularized for different controller design techniques. The following lemma expresses the YK-parametrization in terms of the RST-digital

[3]This parametrization is also called Q-parametrization.

[4]It can be also use a left coprime factorization $G = \tilde{D}^{-1}\tilde{N}$ with they respective controller $\tilde{K} = \tilde{Y}^{-1}\tilde{X}$.

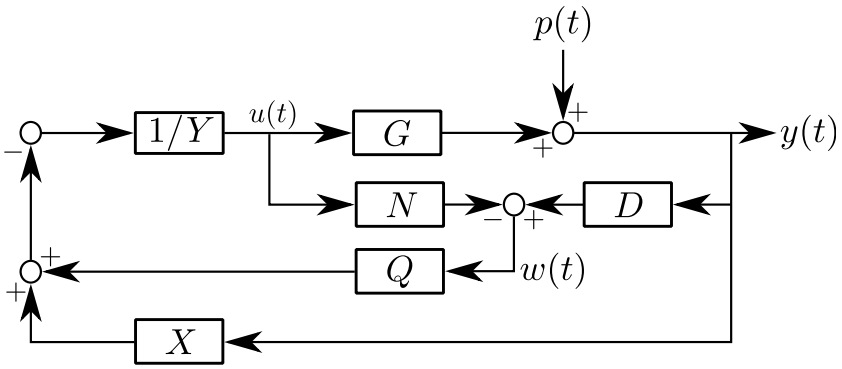

Figure 4.4: Feedback YK parametrized controller.

controllers, defined in eqs. (3.8) and (3.9), in a Pole Placement design context, assuming an infinite impulse response (IIR) filter representation of the Q parameter.

Lemma 4.3.1. *Let $ND^{-1} = z^{-d}B(z^{-1})/A(z^{-1})$ define a stable proper rational discrete time transfer function for the plant G[5]. If there are no common factors (roots) between $z^{-d}B(z^{-1})$ and $A(z^{-1})$, i.e. they are coprime, then it is possible to compute a stable transfer function $K_0(z^{-1}) = R_0(z^{-1})/S_0(z^{-1})$ such that*

$$A(z^{-1})S_0(z^{-1}) + z^{-d}BR_0(z^{-1}) = P_0(z^{-1}), \tag{4.18}$$

were

$$R_0(z^{-1}) = H_{R_0}(z^{-1})R'_0(z^{-1}),\ S_0(z^{-1}) = H_{S_0}(z^{-1})S'_0(z^{-1})$$

and $P_0(z^{-1})$ is an asymptotically stable polynomial ($P_0(z^{-1}) = 0 \rightarrow |z| < 1$). Assume that the Q parameter is represented by the following stable discrete time transfer function

$$Q(z^{-1}) = \frac{B_Q(z^{-1})}{A_Q(z^{-1})} = \frac{b_0^Q + b_1^Q z^{-1} + \cdots + b_{n_{B_Q}}^Q z^{-n_{B_Q}}}{1 + a_1^Q z^{-1} + \cdots + a_{n_{A_Q}}^Q z^{-n_{A_Q}}}. \tag{4.19}$$

Then the set of all stabilizing controllers for G is represented by

$$\mathcal{K} = \left\{ \frac{A_Q(z^{-1})R_0(z^{-1}) + A(z^{-1})B_Q(z^{-1})}{A_Q(z^{-1})S_0(z^{-1}) - z^{-d}B(z^{-1})B_Q(z^{-1})} : \frac{B_Q(z^{-1})}{A_Q(z^{-1})} \in \mathcal{S} \right\}, \tag{4.20}$$

where

$$R(z^{-1}) = A_Q(z^{-1})R_0(z^{-1}) + A(z^{-1})B_Q(z^{-1}), \tag{4.21}$$

$$S(z^{-1}) = A_Q(z^{-1})S_0(z^{-1}) - z^{-d}B(z^{-1})B_Q(z^{-1}). \tag{4.22}$$

The above lemma is particularized the case when the Q parameter is represented by a finite impulse response (FIR) filter.

Corollary 4.3.1. *Assuming the previous conditions from the Lemma 4.3.1 and using a FIR Q parameter representation ($A_Q(z^{-1}) \equiv 1$) such that*

$$Q(z^{-1}) = q_0 + q_1 z^{-1} + \cdots + q_{n_Q} z^{-n_Q}, \tag{4.23}$$

[5]In discrete time, this is particularly easy to prove since, by definition, any FIR filter is stable.

the set of all stabilizing controllers for G is represented by

$$\mathcal{K} = \left\{ \frac{R_0(z^{-1}) + A(z^{-1})Q(z^{-1})}{S_0(z^{-1}) - z^{-d}B(z^{-1})Q(z^{-1})} : Q(z^{-1}) \in \mathcal{S} \right\}, \tag{4.24}$$

where the controller polynomials are defined by

$$R(z^{-1}) = R_0(z^{-1}) + A(z^{-1})Q(z^{-1}), \tag{4.25}$$

$$S(z^{-1}) = S_0(z^{-1}) - z^{-d}B(z^{-1})Q(z^{-1}). \tag{4.26}$$

Proof. The proof can be obtained straightforwardly from Lemma 4.3.1 by making $A_Q(z^{-1}) = 1$ and $B_Q(z^{-1}) = Q(z^{-1})$. □

The following remarks can be made:

- The YK parametrization requires that the right (or left) coprime factorization should be stable, not the discrete-time model. This allows to have in the factorization either unstable poles or zeros, i.e. roots of $A(z^{-1})$ or $B(z^{-1})$ outside of the unitary circle, respectively. The right coprime factorization $N = B(z^{-1})$ and $D = A(z^{-1})$ is stable since the polynomials are represented as FIR filters, with all their poles in the origin and therefore stable.
- The YK parametrization states that the $Q(z^{-1})$ should be also a stable proper rational transfer function. In discrete time, depending on the imposed structure FIR or IIR, there are some particularities that should be considered.
- The right coprime factorization $ND^{-1} = z^{-d}B(z^{-1})/A(z^{-1})$ leads to a *disturbance observer* defined by

  $$w(t+1) = A(z^{-1})y(t+1) - z^{-d}B^*(z^{-1})u(t), \tag{4.27}$$

  which is known also as an *equation error* observer; nevertheless, this factorization is not unique and different disturbance observer configurations can be obtained, as explained in [Landau et al., 2013a].

4.3.2 Q-parametrization: IIR Case

According to Theorem 4.3.1, Q should a stable proper rational transfer function and from Lemma 4.3.1, the following remarks can be made in a Pole Placement design context:

- The polynomials $R(z^{-1})$ ans $S(z^{-1})$, preserving the fixed parts of R_0 and S_0 [Landau et al., 2011b], are defined by

  $$R(z^{-1}) = A_Q(z^{-1})R_0(z^{-1}) + A(z^{-1})H_{S_0}(z^{-1})H_{R_0}(z^{-1})B_Q(z^{-1}), \tag{4.28}$$

  $$S(z^{-1}) = A_Q(z^{-1})S_0(z^{-1}) - z^{-d}B(z^{-1})H_{S_0}(z^{-1})H_{R_0}(z^{-1})B_Q(z^{-1}). \tag{4.29}$$

- The closed loop poles, represented in $P(z^{-1})$, are modified as follows

  $$P(z^{-1}) = A_Q(z^{-1}) \left(A(z^{-1})S_0(z^{-1}) + z^{-d}B(z^{-1})R_0(z^{-1}) \right), \tag{4.30}$$

  where the need for $A_Q(z^{-1})$ to be stable becomes evident.
- From eq. (3.10), the output sensitivity function using a IIR Q filter is expressed as follows

  $$S_{yp}(z^{-1}) = \frac{A(z^{-1}) \left(A_Q(z^{-1})S_0(z^{-1}) - z^{-d}B(z^{-1})H_{S_0}(z^{-1})H_{R_0}(z^{-1})B_Q(z^{-1}) \right)}{P(z^{-1})}. \tag{4.31}$$

- From eq. (3.11), the input sensitivity function using a IIR Q filter is expressed as follows

$$S_{up}(z^{-1}) = -\frac{A(z^{-1})\left(A_Q(z^{-1})R_0(z^{-1}) + A(z^{-1})H_{S_0}(z^{-1})H_{R_0}(z^{-1})B_Q(z^{-1})\right)}{P(z^{-1})}. \tag{4.32}$$

4.3.3 Q-parametrization: FIR Case

When a FIR filter representation is considered, the following remarks are made since $A_Q(z^{-1}) \equiv 1$:

- The polynomials $R(z^{-1})$ ans $S(z^{-1})$, preserving the fixed parts of R_0 and S_0, are defined by

$$R(z^{-1}) = R_0(z^{-1}) + A(z^{-1})H_{S_0}(z^{-1})H_{R_0}(z^{-1})Q(z^{-1}), \tag{4.33}$$
$$S(z^{-1}) = S_0(z^{-1}) - z^{-d}B(z^{-1})H_{S_0}(z^{-1})H_{R_0}(z^{-1})Q(z^{-1}). \tag{4.34}$$

- For any arbitrary $Q(z^{-1})$, it is evident that

$$P(z^{-1}) = P_0(z^{-1}) = \left(A(z^{-1})S_0(z^{-1}) + z^{-d}B(z^{-1})R_0(z^{-1})\right), \tag{4.35}$$

  meaning that the YK-parametrization using a FIR filter representation for Q does not modify the closed loop poles defined in $P_0(z^{-1})$ ([Landau et al., 2005], [Valentinotti et al., 2003]). This property can be useful for stability/robustness purposes as seen in the next chapter.
- From eq. (3.10), the output sensitivity function using a FIR Q filter is expressed as follows

$$S_{yp}(z^{-1}) = \frac{A(z^{-1})\left(S_0(z^{-1}) - z^{-d}B(z^{-1})H_{S_0}(z^{-1})H_{R_0}(z^{-1})Q(z^{-1})\right)}{P_0(z^{-1})}. \tag{4.36}$$

- From eq. (3.11), the input sensitivity function using a FIR Q filter is expressed as follows

$$S_{up}(z^{-1}) = -\frac{A(z^{-1})\left(R_0(z^{-1}) + A(z^{-1})H_{S_0}(z^{-1})H_{R_0}(z^{-1})Q(z^{-1})\right)}{P_0(z^{-1})}. \tag{4.37}$$

4.3.4 Internal Model using YK-parametrizaiton

Through the YK-parametrization of the RST controllers, the Internal Model Principle (IMP) can be used to reject the effect of narrow band disturbances with a reduction in the computational load. Another important feature of this parametrization is that, as shown later, it is possible to represent the difference in performance between an optimal controller using an optimal Q_{opt} and another controller using a polynomial $\widehat{Q}$ in an equation featuring explicitly the difference between Q_{opt} and $\widehat{Q}$. This will open the path for building a direct adaptive regulation scheme.

From the IMP, through Eqs. (4.16) and (4.34) we have

$$D_p(z^{-1})S'(z^{-1}) = S'_0(z^{-1}) - z^{-d}B(z^{-1})H_{R_0}(z^{-1})Q(z^{-1}), \tag{4.38}$$

solving for S'_0, the Eq. (4.38) is rewritten

$$D_p(z^{-1})S'(z^{-1}) + z^{-d}B(z^{-1})H_{R_0}(z^{-1})Q(z^{-1}) = S'_0(z^{-1}), \tag{4.39}$$

the previous diophantine equation has an order of

$$n_{D_p} + n_B + n_{H_{R_0}} + d - 1 \times n_{D_p} + n_B + n_{H_{R_0}} + d - 1,$$

where $n_{S'} = n_B + n_{H_{R_0}} + d - 1$ and $n_Q = n_{D_p} - 1$ and the reduction obtained is of $n_A + n_{H_{S_0}}$. It is to be noted that the order of the Q-filter (n_Q) depends upon the order of the disturbance model and it does not depend on the order of the plant model. When $n_Q = n_{D_p} - 1$, the solution is minimal and unique, nevertheless it is possible to find solutions where $n_Q > n_{D_p} - 1$ which can imply an infinite number of solutions, giving freedom to tune in addition the robustness properties of the closed loop. Through the Eq. (4.39), the IM of the disturbance is introduced into the controller by means of the Q parameters. Nevertheless, some robustness constraints arise when the IMP is used and this will be discussed later on.

4.4 Robustness constraints

This section introduces some robust constraints in a feedback control approach when the Internal Model Principle is used along with the YK parametrization for narrow band disturbance rejection. A special case is the presence of low damped complex plant zeros. These constraints will set up the performance limitation/expectations to the adaptive schemes evaluated in Chapter 6. Therefore, the analysis will be done in a linear context, knowing exactly the number of narrow band disturbances as well as their frequencies. The model based control technique considered is Pole Placement; however, the results are applicable to other controls strategies.

4.4.1 Introduction

As it is well known, the introduction of the internal model for the perfect rejection of the disturbance (asymptotically) may have as an effect, to raise the maximum value of the modulus of the output sensitivity function S_{yp}. This may lead to unacceptable values of the modulus margin $\left(\Delta M = \left|S_{yp}(e^{-j\Omega})\right|^{-1}_{\max}, \text{ affecting both performance and robustness}\right)$ if the design of the central controller (polynomials R_0 and S_0) is not appropriately done.

As a consequence, a robust central control design should be considered, assuming that the model of the disturbance and its domain of variations in the frequency domain are known. The objective is that for all situations (i.e. for all possible values of the frequency of the disturbance and the corresponding Q-polynomial), an acceptable modulus margin, i.e. an acceptable value of the maximum of the output sensitivity function, is obtained. The optimal design of the central controller in this context is, in ours opinion, an open problem.

Since low damped complex zeros are often encountered in mechanical flexible structures, here an analysis of their influence for robustness and performance is done in a linear context. Since a linear controller can be considered providing the best possible achievable performance, the conclusions drawn for this chapter will set up the comparative framework for the adaptive case.

In the context of this section, it is assumed that:

- the characteristics of the narrow band disturbance acting on the system are known and they may be located anywhere on a predefined frequency region Ω_d;
- the identified dynamic model of the AVC is a reliable representation of the true plant model up to half of the sampling frequency. How to obtain such a reliable model will be described in Chapter 5.

4.4.2 Basic Equations and Notations

The output and input sensitivity functions are major indicators both of performance and robustness properties of the system. They are used to define the robustness of the closed loop system w.r.t. a specific type of uncertainty.

1. **Output sensitivity function:** it describes the behavior w.r.t. a disturbance signal $p(t)$ acting over the output $y(t)$ and is defined in (3.10). This function defines for a large extent the regulation behavior. The model uncertainty related to this function is the feedback uncertainties on the input (or output), represented by $G'(z^{-1}) = \frac{G(z^{-1})}{1+\delta(z^{-1})W_r(z^{-1})}$, where $W_r(z^{-1})$ is a stable transfer function and $\delta(z^{-1})$ is any stable transfer function having the property $\|\delta(z^{-1})\|_\infty \leq 1$. The robust stability condition for this uncertainty is

$$\left\|S_{yp}(z^{-1})W_r(z^{-1})\right\|_\infty \leq 1 \tag{4.40}$$

or equivalently

$$\left|S_{yp}(e^{-j\omega_n})\right| < \left|W_r(e^{-j\omega_n})\right|^{-1};\ \ 0 \leq \omega_n \leq \pi \tag{4.41}$$

The modulus of S_{yp} is related to the modulus margin ΔM, which is defined as the radius of the circle centered on $[-1, j0]$ (the *critical point* in the Nyquist plot) and tangent to the Nyquist plot of $H_{OL}(e^{-j\omega_n})$. This vector has the expression

$$\Delta M = |1 + H_{OL}(e^{-j\omega_n})|_{\min} = \left(|S_{yp}(e^{-j\omega_n})|_{\max}\right)^{-1} = \|S_{yp}\|_\infty^{-1}. \tag{4.42}$$

As a consequence, the reduction (or minimization) of $|S_{yp}(e^{-j\omega_n})|_{\max}$ will imply the increase (or maximization) of the modulus margin ΔM. This means that the *modulus margin* ΔM is equal to the inverse of the maximum modulus of the output sensitivity function $S_{yp}(z^{-1})$ (i.e. the inverse of the H_∞ norm of $S_{yp}(z^{-1})$).

2. **Input sensitivity function:** it assesses the impact of the disturbance $p(t)$ over the control signal introduced to the plant $u(t)$ and is defined in (3.11). Additive uncertainties are related to this function and are expressed as $G'(z^{-1}) = G(z^{-1}) + \delta(z^{-1})W_a(z^{-1})$, where $W_a(z^{-1})$ is a stable transfer function. The robust stability condition for this uncertainty is

$$\left\|S_{up}(z^{-1})W_a(z^{-1})\right\|_\infty \leq 1 \tag{4.43}$$

or equivalently

$$\left|S_{up}(e^{-j\omega_n})\right| < \left|W_a(e^{-j\omega_n})\right|^{-1};\ \ 0 \leq \omega_n \leq \pi \tag{4.44}$$

4.4.3 Robustness Constraints

Using the previous elements defined in Section 4.4.2, we will analyze the robust constraints when perfect disturbance rejection is achieved in the presence of low damped complex zeros.

Since the disturbance introduced to the system $p(t)$ is centered at a specific frequency $\omega_1 \in \Omega$, if $S(z^{-1})$ contains $D_p(z^{-1})$ as a factor, then $S(e^{-j\omega_1}) = 0$. As a consequence, the output sensitivity function, and therefore the closed-loop system, will not react to the frequency ω_1 since $S_{yp}(e^{-j\omega_1}) = 0$. This will lead to the following robust constraint for perfect disturbance rejection of narrow-band disturbances:

1. Since $S(e^{-j\omega_1}) = 0$, the modulus of the input sensitivity function is affected as follows
$$\left|S_{up}(e^{-j\omega_1})\right| = \left|\frac{A(e^{-j\omega_1})}{B(e^{-j\omega_1})}\right|, \tag{4.45}$$
meaning that the modulus of S_{up} at ω_1 is equal to the inverse of the plant model gain. By the robust stability condition for additive uncertainties expressed in Eq. (4.44), if the plant model gain at the frequency ω_1 is low, (e.g, due the presence of low damped complex zeros) the modulus of S_{up} will be high and therefore will reduce the robustness against this type of uncertainty. This also will lead to more stress on the actuator. Therefore, *perfect rejection (or in general an important attenuation) of the disturbance effect on the output should be done only in frequency regions where the system gain is large enough.*

By the Bode's Sensitivity Integral ([Zhou et al., 1996]), it is well known that the introduction of the IMP for the perfect rejection of the disturbance (asymptotically) will have as an effect to raise the maximum value of the modulus of the output sensitivity function S_{yp} (which implies the reduction of ΔM). This may lead to unacceptable values for the modulus margin if the controller design is not appropriately done, having a huge negative impact in the closed loop system performance. We can state the following restriction:

2. The introduction of the disturbance model in the controller produces a hole in S_{yp} at the disturbance frequency ω_1; this could lead also to amplifications in other frequency content in Ω (this is called also *waterbed* effect). Therefore, the effect over the modulus margin ΔM can be significant. As a consequence, by the robust stability condition defined in (4.41), the robustness against uncertainties in the input (or output) will be reduced as well as the performance. Hence, *special attention must be put in ΔM in order to minimize the effects of the IMP, once it is introduced in the controller.*

It is to be noted that the previous robustness restrictions are particularly difficult to achieve for the the following scenarios:

1. rejection of multiple narrow band disturbances (more than 2),

2. in the presence of low damped complex zeros,

3. when the frequencies of the narrow band disturbances are very close to each other.

In order to respect the previous robust restrictions, and at the same time, to fulfill the control objectives described in 4.1, it is concluded that it is necessary to minimize the modulus of S_{yp} (i.e. maximization of the modulus margin ΔM), and also that the modulus of S_{up} has to be low in high frequencies. Both conditions in the sensitivity functions have to be assured for one or multiple perturbations located in the frequency region of interest (Ω_d) with special attention in the vicinity of low damped complex zeros.

4.5 Linear Solutions

Once the control objectives have been settled, the control structure defined and the robust constraints established, two solutions are proposed for the rejection of narrow band disturbances. Each solution is characterized, according to the choice in the Q filter: FIR or IIR structure.

4.5.1 YK parametrization through Q FIR filter

If a FIR structure is chosen for the Q filter, there are two choices for the order of this polynomial. For each case, the central controller can be different (polynomials R_0 and S_0).

- When $n_Q = n_{D_p} - 1$, the solution for the diophantine equation (4.39) is minimal and unique. The Q-filter is used to introduce the IM into the controller and the robustness/stability of the closed loop is handled by the central controller. It was found that if some pairs of low damped complex poles are placed at the limits of the frequency region of interest, the waterbed effect in S_{yp} can be reduced. These complex poles are fixed and therefore it is only necessary to recompute the optimal Q for any possible disturbance and not the entire central controller. Of course, a compromise must be found between the damping of these complex poles and the attenuation achieved, especially in the vicinity of the low damped complex zeros. Also, the number of fixed complex poles is related to the number of narrow band disturbances to reject, as a consequence, the central controller should be redesigned if the number of tonal disturbances to attenuate changes.
- When $n_Q > n_{D_p} - 1$, there are an infinite number of solutions for the Eq. (4.39). It was found that the augmentation in the order of the Q-filter enhances the robustness of the controller by reducing the waterbed effect and increases the attenuation achieved. Nevertheless, the central controller is still necessary.

It is noted that a combination of both choices is possible, i.e. using an over parameterized Q-filter with a central controller using additional fixed low damped complex poles.

4.5.2 YK parametrization through a Q IIR filter

When a IIR structure is chosen for the Q filter, the Eq. (4.39) is modified as follows

$$D_p(z^{-1})S'(z^{-1}) + z^{-d}B(z^{-1})H_{R_0}(z^{-1})B_Q(z^{-1}) = S'_0(z^{-1})A_Q(z^{-1}), \tag{4.46}$$

from which it can be concluded that the order of $B_Q(z^{-1})$ depends on the order of $D_p(z^{-1})$, but nothing is said about the order of $A_Q(z^{-1})$. Actually, according to this equation, $B_Q(z^{-1})$ depends on the value of $A_Q(z^{-1})$, therefore $A_Q(z^{-1})$ should be defined first and then used it to compute $B_Q(z^{-1})$.

Among the possible choices for $A_Q(z^{-1})$, if $A_Q(z^{-1})$ is defined so its roots are located at the same frequency as the roots of $D_p(z^{-1})$, but instead of being over the unitary circle they are inside in the same radial line, the waterbed effect in $S_{yp}(z^{-1})$ can be drastically reduced. This principle is used in the notch filters. In order that $D_p(z^{-1})$ has its roots over the unitary circle, a necessary condition is that its structure should be in a mirror symmetric form, e.g. for a single narrow band disturbance $D_p(z^{-1})$ is represented as follows

$$D_p(z^{-1}) = 1 + \alpha z^{-1} + z^{-2}, \tag{4.47}$$

where $\alpha = -2\cos(2\pi\omega_1 T_s)$, ω_1 is the disturbance frequency in Hz and T_s is the sampling time. If the denominator of the Q-filter is chosen as

$$A_Q(z^{-1}) = D_p(\rho z^{-1}) = 1 + \rho\alpha z^{-1} + \rho^2 z^{-2}, \tag{4.48}$$

where $0 < \rho < 1$, the roots of $A_Q(z^{-1})$ are in the same radial line as those of $D_p(z^{-1})$ but inside of the unitary circle, and therefore stable [Nehorai, 1985]. Since $D_p(z^{-1})$ is known, a choice for $A_Q(z^{-1})$ is possible. Notice that $n_{A_Q} = n_{D_p}$.

Since the waterbed effect can be drastically reduced, the fixed low damped complex poles introduced for the FIR case are no longer necessary. Actually, this kind of selection for $A_Q(z^{-1})$ allows the rejection of multiple narrow band disturbances in a better way than the FIR case. For example, instead of having one central controller for each level, through this approach of using a IIR, it is possible to have one single central controller for all the levels. This becomes helpful in terms of implementation since the central controller can not only handle different disturbances frequencies within the range of interest, but also different number of narrow band disturbance signals.

All that can be represented graphically through the modulus of the output sensitivity function ($S_{yp}(z^{-1})$) for the both structures revised. All the controllers use the YK parametrization and the central controller is computed, using as closed loop poles, all the stable system poles along with 10 real poles for robustness. The first case corresponds to a controller using a Q FIR filter which incorporates the IM of a disturbance located at 95 Hz (close to a low damped complex zero). This is shown in Fig. 4.5, where the first case is represented with a solid line. The closed loop poles defined in $P(z^{-1})$ do not incorporate the auxiliary fixed low damped complex poles proposed in 4.3.3. As can be seen, the $\max|S_{yp}(e^{-j\omega})| = 11.4$ dB.

The second case corresponds to the same structure (YK+Q FIR filter) but the closed loop poles includes two pairs of auxiliary fixed low damped complex poles at 50 and 95 Hz. This case is represented with a dash-dotted line. The maximum value of the modulus is 8.0 dB. Finally, in the third case, the controller uses a Q-IIR filter. Since the Q filter structure requires a denominator $A_Q(z^{-1})$, the denominator is computed as proposed in (4.48) with $\rho = 0.97$. No other fixed auxiliary poles are required; this case is represented with a dashed line. The maximum value for the modulus is 5.5 dB.

The improvements of the fixed auxiliary poles are evident by reducing the maximum value of the modulus of S_{yp} (from 11.4 to 8.0 dB, 30% of reduction) and keeping the important amplifications within the frequency region of interest. This pair of fixed low damped complex poles can be used for the entire frequency region of interest. Nevertheless, the IIR filter structure shows an enhancement from the previous results with a reduction of 51.7% of the maximum value of the modulus of S_{yp}. This is achieved without using the fixed low damped complex poles from the FIR case.

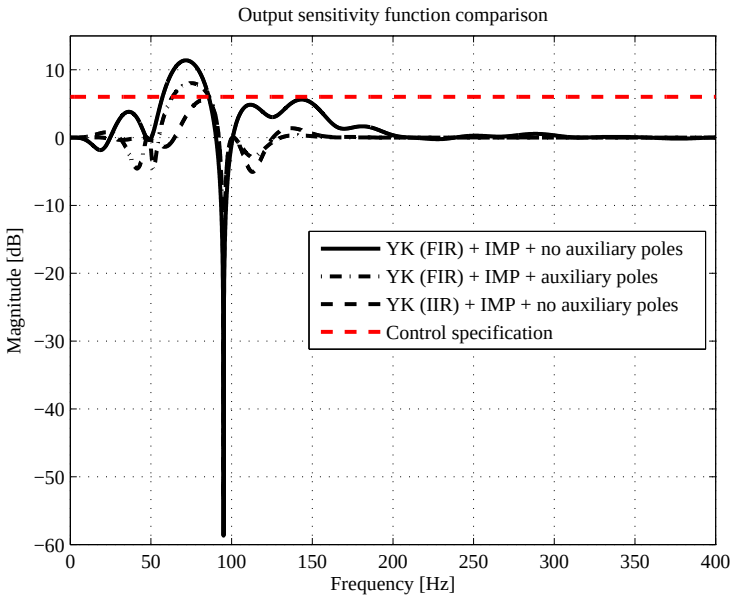

Figure 4.5: Modulus comparison of the Output sensitivity function of both structures revised. Solid line: YK parametrization - Q FIR filter without auxiliary fixed poles, dash-dot line: YK parametrization - Q FIR filter with auxiliary fixed poles, dashed line: YK parametrization - Q IIR without auxiliary poles.

4.6 Concluding Remarks

The linear design of a controller, which incorporates the IMP for total rejection of a narrow band disturbance acting on the output of the system, becomes complicated in terms of robustness and performance when low damped complex zeros are present. Also, the computational load could be significant when the plant order is high as for our system. Some advantages are obtained when the YK-parametrization is considered. Nevertheless, the presence of low damped complex zeros has to be considered and a more accurate identification of such elements can be useful for control purposes.

Chapter 5

Identification of the active vibration control system

This chapter presents the system identification of the active vibration control system. The context for such identification procedure is given in Section 5.1. In Section 5.2 the basic equations and the discrete time model representation are introduced. The open loop identification is presented in Section 5.3 and the closed loop system identification is explained in Section 5.4. Experimental results for both procedures and a comparative evaluation is done in Section 5.5 and finally the concluding remarks of this chapter are presented in Section 5.6.

5.1 Introduction

The active vibration control system, used to test the adaptive algorithms developed in this thesis, has been identified in open and closed loops. Each procedure is performed using as an excitation input a Pseudo Random Binary Signal (PRBS)[1]. In a first stage the primary and the secondary paths are identified in open loop, then the secondary path is identified in closed loop. The PRBS is generated by a bit shift register of length $N = 10$ and a frequency divider $p = 2$, applied at the input of the shaker and the inertial actuator, respectively. The sampling frequency is 800 Hz.

After the data acquisition, a complexity (order) estimation algorithm is used to determine the order of each polynomial (n_{A_p}, n_{B_p} for the primary path and n_A, n_B for the secondary path) and the delay (d_p, d) for each model. Only for simulation purposes the primary path was identified and in Section 5.3 the estimated orders are given. The details of the available algorithms for complexity estimation and generation of the PRBS signal can be found in [Landau and Zito, 2005].

The open loop identification procedure is done in the absence of controller and narrow band disturbance signal. The idea is to build an adjustable predictor (model) whose output $\widehat{y}(t)$ matches the measured output $y(t)$ as represented in the Fig. 5.1. The difference between the outputs ($\epsilon(t)$) is used to drive the *Parameter Adaptation Algorithm* to estimate the parameters of the model.

In the case of the closed loop identification, the difference lies in the presence of a controller. Therefore, the objective is to build in parallel an adjustable predictor that minimizes the differences between both closed loops, the *true* one and the *simulated* one, represented by $\epsilon_{CL}(t)$ in Fig. 5.2. For both procedures, the noise is considered as a disturbance affecting the system.

[1]This kind of signals is used as a *persistent excitation* as mentioned in [Ljung, 1999].

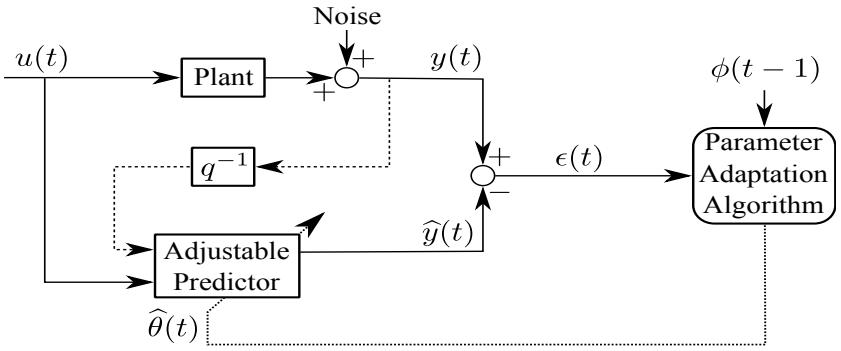

Figure 5.1: Structure of the recursive identification methods in open loop.

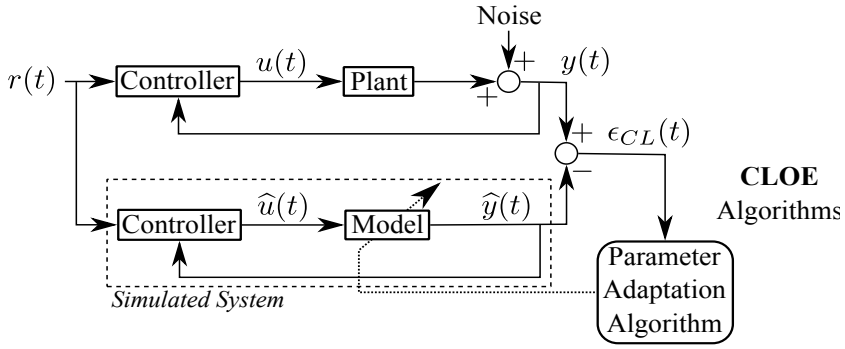

Figure 5.2: Structure of the recursive identification methods in closed loop.

The main contributions of this chapter are:

- Modification of the closed-loop identification algorithm [Landau and Karimi, 1997].
- Application on the Active Suspension System in the presence of low damped complex zeros.

5.2 Basic Equations and Notation

The structure of the *plant + noise model* considered is described by

$$y(t) = \frac{q^{-d}B(q^{-1})}{A(q^{-1})}u(t) + v(t) \tag{5.1}$$

where $u(t)$ is the plant input, $y(t)$ is the measured output and $v(t)$ is the noise. In practice, two models for the noise cover many situations:

1. $v(t)$ is a zero mean stochastic process with finite moments independent of $u(t)$, leading to the following representation:

$$y(t+1) = -A^*(q^{-1})y(t) + B^*(q^{-1})u(t-d) + v'(t+1), \tag{5.2}$$
$$= \theta^T \cdot \phi(t) + v'(t+1). \tag{5.3}$$

where $v'(t+1) = A(q^{-1})v(t+1)$ and

$$\theta = [a_1, \ldots, a_{n_A}, b_1, \ldots, b_{n_B}]^T \tag{5.4}$$

and

$$\phi(t) = [-y(t), \ldots, -y(t-n_A+1), u(t-d), \ldots, u(t-d-n_B+1)]^T. \tag{5.5}$$

2.
$$v(t) = \frac{C(q^{-1})}{A(q^{-1})}e(t)$$

where $e(t)$ is a zero mean white noise (or for technical reason defined as a martingale sequence); in this case, Eq. 5.1 is known as ARMAX model. The plant can be represented as follows:

$$y(t+1) = -A^*(q^{-1})y(t) + B^*(q^{-1})u(t-d) + C^*(q^{-1})e(t) + e(t+1) \tag{5.6}$$
$$= \theta^T \cdot \phi(t) + e(t+1). \tag{5.7}$$

where
$$\theta = [a_1, \ldots, a_{n_A}, b_1, \ldots, b_{n_B}, c_1, \ldots, c_{n_C}]^T \tag{5.8}$$

and
$$\phi(t) = [-y(t), \ldots, -y(t-n_A+1), u(t-d), \ldots, u(t-d-n_B+1), \ldots \\ \ldots, e(t), \ldots, e(t-n_C+1)]^T \tag{5.9}$$

where the monic polynomial $C(q^{-1})$ have the form:
$$C(q^{-1}) = 1 + c_1 q^{-1} + \cdots + c_{n_C} q^{-n_C} = 1 + q^{-1}C^*(q^{-1}). \tag{5.10}$$

For the identification algorithms, the estimated version of the parameter vector $\hat{\theta}(t)$ is used along with the (possibly modified) observation vector $\phi(t)$. For further details along with stability (deterministic environment) and convergence (stochastic environment) proof, see [Landau et al., 2011d]. All the identification methods (either open or closed loop) use the following *Parameter Adaptation Algorithm* (PAA):

$$\epsilon_X^0(t+1) = y(t+1) - \hat{\theta}^T(t)\phi(t) = y(t+1) - \hat{y}^0(t+1) \tag{5.11}$$
$$\epsilon_X(t+1) = \frac{\epsilon_X^0(t+1)}{1 + \Phi^T(t)F(t)\Phi(t)} \tag{5.12}$$
$$\hat{\theta}(t+1) = \hat{\theta}(t) + F(t)\Phi(t)\epsilon_X(t+1) \tag{5.13}$$
$$F(t+1) = \frac{1}{\lambda_1(t)}\left[F(t) - \frac{F(t)\Phi(t)\Phi^T(t)F(t)}{\frac{\lambda_1(t)}{\lambda_2(t)} + \Phi^T(t)F(t)\Phi(t)}\right] \tag{5.14}$$
$$0 < \lambda_1(t) \leq 1; \quad 0 \leq \lambda_2(t) < 2 \tag{5.15}$$

where X stands for open loop (OL) or closed loop (CL) and $\lambda_1(t)$ and $\lambda_2(t)$ can be chosen to obtain different variation profiles of the adaptation gain. Depending on the method, the observation vector can be $\Phi(t) = \phi(t)$ or a filtered version of $\phi(t)$.

5.3 Open Loop Identification Procedure

In this section the open loop identification procedure of the secondary path is presented; nevertheless, the remarks made for this path can be applied for the identification of the primary path.

The estimation of the complexity (order) is done using the procedure described in [Landau and Zito, 2005], assuming that the measurements are affected by non white

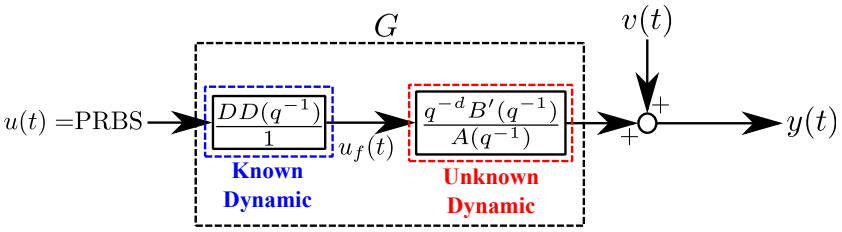

Figure 5.3: Open loop identification scheme with known and unknown dynamics.

noise[2]. The complexity estimation is consistent, meaning that one finds the exact order as the number of data tends towards infinity. Since, for controller design, the secondary path model is only necessary, the comments and procedure will be discussed w.r.t. the secondary mechanical path. Nevertheless, the same kind of remarks can be made for the primary path.

In order to concentrate all the estimation efforts to the *unknown* dynamics, the *a priori* known properties of the system should be considered. In our case, since both paths present a double differentiator behavior, this dynamic should be not estimated in the open loop identification procedure. One way to perform this is to take the input $u(t)$ and to filter this signal by the known dynamic. The resulting signal $u_f(t)$ will be used along with the measured output $y(t)$ for complexity and parameter estimation. At the end of the identification procedure, the double differentiator will be added to the model. This procedure is depicted in Fig. 5.3. Therefore, the unknown system dynamics will be estimated in $\widehat{B}'(q^{-1})$ and $\widehat{A}(q^{-1})$ for the secondary path model. The final numerator's model is expressed as $\widehat{B}(q^{-1}) = DD(q^{-1}) \cdot \widehat{B}'(q^{-1})$, where $DD(q^{-1}) = 1 - 2q^{-1} + q^{-2}$ is the double differentiator part.

The estimated orders for the secondary path model are $n_{\widehat{B}'} = 19$ and $n_{\widehat{A}} = 18$ with a plant pure time delay of $d = 0$. The estimated orders of the primary path are $n_{\widehat{A}p} = 13$ and $n_{\widehat{B}'_p} = 14$ with a plant delay of $d_p = 0$.

Several methods were used for the parameter estimation. They are classified according to the assumption made upon the noise affecting the system. Among the methods which use a system representation as in Eq. (5.2), we can mention the Output Error with Fixed Compensator (OEFC), Output Error with Filtered Observations (OEFO) and Output Error with Adaptive Filtered Observations (OEAFO). Among the methods which represent the system as in Eq. (5.6), we can mention the Recursive Extended Least Squares (RELS), Output Error With Extended Prediction Model (OEEPM) and Recursive Maximum Likelihood (RML). The validation procedure described in [Landau and Zito, 2005] is used to validate the identified models and for the comparison of the various identified models. As mentioned in Chapter 3 - Section 3.3, in the open loop identified model, it is remarked the presence of several resonance and anti-resonance modes due the presence of low damped complex poles and zeros, respectively. Because of the low damping factor of such zeros, the system has a very low gain at such frequencies, limiting the frequency content in the acquired data. A closed loop identification procedure can be applied to enhance the identified model at such frequencies, relying on the characteristics of the controller.

[2]In [Landau and Zito, 2005] a procedure is also described when is assumed that the measurements are affected by a white noise sequence; nevertheless it is not the more realistic choice.

5.4 Improving Open Loop System Identification

If a feedback controller is present, it is possible to use it to improve the model identified through a closed-loop identification scheme [Landau and Zito, 2005]. In our case, a *RST*-digital controller will be considered. Therefore

$$K = \frac{R(z^{-1})}{S(z^{-1})}, \tag{5.16}$$

and Eqs. (3.10) and (3.11) can be considered. The closed loop identification procedure is based on the *Closed Loop Output Error* methods whose principle is to find the best plant model which minimizes the prediction error $\epsilon_{CL}(t)$ between the measured output of the true closed loop system and the predicted closed loop output. The excitation signal can be added either at the control output or at the reference as is shown in Fig 5.4.

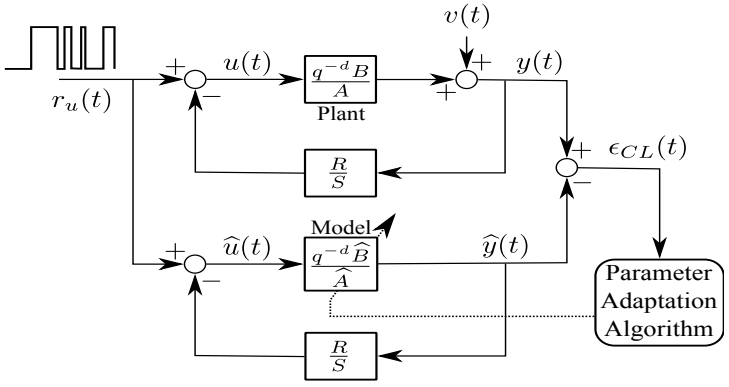

(a) Excitation superposed to control output

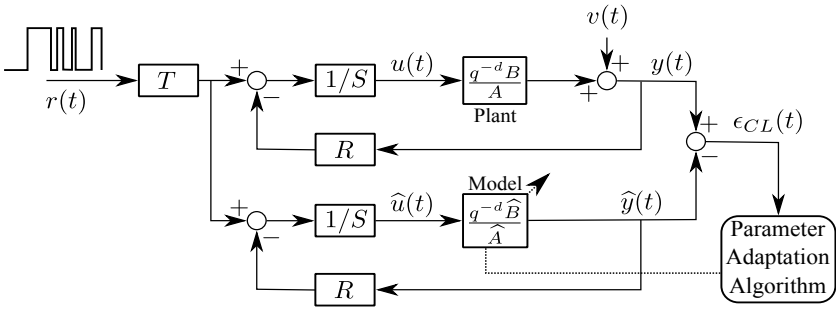

(b) Excitation superposed to the reference

Figure 5.4: Closed loop output error identification method.

An interesting aspect of such methods is that both configurations use the same algorithms but different properties for the estimated model are obtained, depending on the location of the excitation signal. For example, when the excitation signal is added to the control output, the *true* sensitivity function to approximate is the *input disturbance - output sensitivity function* described by

$$S_{yv}(z^{-1}) = \frac{z^{-d}B(z^{-1})S(z^{-1})}{P(z^{-1})}, \tag{5.17}$$

while when the excitation is added as a reference (assuming that $T(z^{-1}) = R(z^{-1})$), the approximation is done for the *complementary sensitivity function* and the *output*

sensitivity function, defined as

$$S_{yr}(z^{-1}) = \frac{z^{-d}B(z^{-1})R(z^{-1})}{P(z^{-1})}, \tag{5.18}$$

and

$$S_{yp}(z^{-1}) = \frac{A(z^{-1})S(z^{-1})}{P(z^{-1})}, \tag{5.19}$$

respectively. Therefore it was chosen to add the excitation as a reference in order to reduce the differences between the *true* and the *simulated* output sensitivity functions.

The selection in the location of the external excitation is based also on the asymptotic bias distribution. For the excitation added on the control output, the bias distribution is defined as follows

$$\widehat{\theta}^* = \arg\min_{\widehat{\theta}\in\mathbb{D}} \int_{-\pi}^{\pi} |S_{yp}|^2 \left[\left| G - \widehat{G} \right|^2 \left| \widehat{S}_{yp} \right|^2 \phi_{r_u}(\omega) + \phi_v(\omega) \right] d\omega, \tag{5.20}$$

where $r_u(t)$ is the external excitation added to the output of the controller, $\phi_{r_u}(\omega)$ and $\phi_v(\omega)$ corresponds to the spectral densities of the external excitation signal and the measurement noise, respectively and $\mathbb{D}$ is the domain of admissible parameters related to the model set. The arguments q^{-1} and $e^{-j\omega}$ have been dropped out to simplify the notation. In this equation, the spectral density of the $r_u(t)$ is shaped by the *estimated* output sensitivity function $\widehat{S}_{yp}$, but the increase of its modulus at critical frequency regions is not easy to obtain and not recommended for stability issues. Meanwhile, when the excitation is superposed to the reference, the asymptotic bias distribution is defined by

$$\widehat{\theta}^* = \arg\min_{\widehat{\theta}\in\mathbb{D}} \int_{-\pi}^{\pi} |S_{yp}|^2 \left[\left| G - \widehat{G} \right|^2 \left| \widehat{S}_{up} \right|^2 \phi_r(\omega) + \phi_v(\omega) \right] d\omega, \tag{5.21}$$

and the spectral density of $r(t)$ (the external excitation) is shaped by the *estimated* input sensitivity function $\widehat{S}_{up}$ and the estimated output sensitivity function. Shaping appropriately the sensitivity functions will allow to improve the precision of the identification in the desired frequency regions.

Thus, to improve the open loop identified model in frequency regions critical for control, two actions are proposed: *1)* design a specified controller which increases the sensitivity of the system at such frequencies and *2)* take a different initialization for a closed loop output error algorithm.

Controller design

The designed controller should increase the sensitivity of the system in the frequency regions where low damped complex zeros are located. This does not necessary mean that the controller will be *good* in terms of control performance (disturbance rejection, tracking, etc.), but only that will not destabilize the system. Meanwhile, the controller allows to obtain a better approximation in the critical regions for control purposes (close to resonant and anti-resonant modes). For such purpose, the damping of the poles located near the low damped complex zeros is increased (those around the frequencies of 50 and 100 Hz). The modulus margin is kept to the recommended value of $\Delta M = 0.5$ to assure the stability of the closed loop system.

Closed Loop Output Error Algorithms *revisited*

The key observation for these methods (according to [Landau et al., 2011d]) is that the output of the closed loop system given by (5.1), using a RST controller in a negative feedback, can be expressed as[3]

$$y(t+1) = \theta^T \varphi(t) + Av(t+1) = \theta^T \phi(t) - \left[A^* + \frac{q^{-d}B^*R}{S}\right] \epsilon_{CL}(t) + Av(t+1), \quad (5.22)$$

where

$$\varphi^T(t) = [-y(t), \cdots, -y(t-n_A+1), u(t-d), \cdots, u(t-n_B-d+1)], \quad (5.23)$$

$$u(t) = -\frac{R}{S}y(t) + \frac{R}{S}r(t), \quad (5.24)$$

$$\phi^T(t) = [-\widehat{y}(t), \cdots, -\widehat{y}(t-n_A+1), \widehat{u}(t-d), \cdots, \widehat{u}(t-n_B-d+1)], \quad (5.25)$$

$$\widehat{u}(t) = -\frac{R}{S}\widehat{y}(t) + \frac{R}{S}r(t), \quad (5.26)$$

$$\epsilon_{CL}(t+1) = y(t+1) - \widehat{y}(t+1), \quad (5.27)$$

where $r(t)$ is the external excitation added as a reference and considering that $T = R$. The parameter vector θ is defined as in (5.4), while $\widehat{\theta}$ is its corresponding estimated version. Substracting from (5.22) the output of the closed loop predictor (with fixed values) defined by

$$\widehat{y}(t+1) = -\widehat{A}^*\widehat{y}(t) + \widehat{B}^*\widehat{u}(t-d) = \widehat{\theta}^T\phi(t), \quad (5.28)$$

one obtains in the deterministic case ($v(t+1) \equiv 0$):

$$\epsilon_{CL}(t+1) = \left[\theta - \widehat{\theta}\right]^T \phi(t) - \left[A^* + \frac{q^{-d}B^*R}{S}\right] \epsilon_{CL}(t). \quad (5.29)$$

Using the following relationship

$$1 + q^{-1}\left[A^* + \frac{q^{-d}B^*R}{S}\right] = \frac{AS + q^{-d}BR}{S} = \frac{P}{S}, \quad (5.30)$$

where $P = AS + q^{-d}BR$ defines the poles of the true closed loop system, Eq. (5.29) can be rewritten as

$$\epsilon_{CL}(t+1) = \frac{S}{P}\left[\theta - \widehat{\theta}\right]^T \phi(t). \quad (5.31)$$

Note that in the linear case with known parameters, since $\phi(t)$ and $v(t)$ are uncorrelated, an optimal predictor minimizing $\mathbf{E}\{\epsilon_{CL}^2(t+1)\}$ is obtained for $\widehat{\theta} = \theta$.

Through the Eq. (5.31) several methods were build with different characteristics for stability and convergence. All the algorithms use the PAA defined in Eqs. (5.11) - (5.14). Here a summary of the various algorithms is presented.

- **Closed Loop Output Error (CLOE) Algorithm:** obtained by replacing the fixed predictor of the closed loop in (5.28) by an adjustable predictor. The sufficient condition for $\lim_{t\to\infty} \epsilon_{CL}(t+1) = 0$ together with the boundedness of $\epsilon_{CL}(t+1)$ for any initial condition for a deterministic environment is the same to assure asymptotic unbiased estimates under the richness condition. The condition is that

$$H'(z^{-1}) = \frac{S(z^{-1})}{P(z^{-1})} - \frac{\lambda_2}{2} \quad (5.32)$$

  is strictly positive real (where $\max_t\ \lambda_2(t) \leq \lambda_2 < 2$).

[3]The argument (q^{-1}) will be dropped in some of the following equations.

- **Filtered Closed Loop Output Error (F-CLOE) Algorithm:** the Eq. (5.31) can be rewritten, by multiplying both sides for $\frac{\widehat{P}S}{S\widehat{P}}$, as

$$\epsilon_{CL}(t+1) = \frac{S}{P}\frac{\widehat{P}}{S}\left[\theta - \widehat{\theta}\right]^T \frac{S}{\widehat{P}}\phi(t) = \frac{\widehat{P}}{P}\left[\theta - \widehat{\theta}\right]^T \phi_f(t) \tag{5.33}$$

where

$$\phi_f(t) = \frac{S}{\widehat{P}}\phi(t), \tag{5.34}$$

$$\widehat{P} = \widehat{A}S + q^{-d}\widehat{B}R. \tag{5.35}$$

$\widehat{P}$ is an estimation of the true closed loop poles based on an initial estimation of the plant model (for example using an open loop experiment). Neglecting the non-commutativity of time-varying operators (however an exact algorithm can be derived), the sufficient condition to assure both asymptotic stability in deterministic environment and asymptotic unbiasedness in a stochastic environment is that

$$H'(z^{-1}) = \frac{\widehat{P}(z^{-1})}{P(z^{-1})} - \frac{\lambda_2}{2} \tag{5.36}$$

is strictly positive real.

- **Adaptive Filtered Closed Loop Output Error (AF-CLOE) Algorithm:** in this algorithm the condition (5.36) is relaxed by filtering the observations $\phi(t)$ with a time-varying filter $S/\widehat{P}(t)$ where $\widehat{P}(t)$ corresponds to the current estimate of the closed loop given by $\widehat{P}(t) = \widehat{A}(t)S + q^{-d}\widehat{B}(t)R$ where $\widehat{A}(t)$ and $\widehat{B}(t)$ are the current estimates of the polynomials A and B.
- **Extended Closed Loop Output Error (X-CLOE) Algorithm:** for the systems represented by (5.6), an extended output error prediction model can be defined

$$\begin{aligned}\widehat{y}(t+1) &= -\widehat{A}^*\widehat{y}(t) + \widehat{B}^*\widehat{u}(t-d) + \widehat{H}^*\frac{\epsilon_{CL}(t)}{S} \\ &= \widehat{\theta}^T\phi(t) + \widehat{H}^*\frac{\epsilon_{CL}(t)}{S} = \widehat{\theta}_e^T\phi_e(t).\end{aligned} \tag{5.37}$$

Eq. (5.22) for the plant output becomes in this case

$$y(t+1) = \theta^T\phi(t) + H^*\frac{\epsilon_{CL}(t)}{S} - C^*\epsilon_{CL}(t) + Ce(t+1), \tag{5.38}$$

where

$$H^* = h_1 + h_2q^{-1} + \cdots + h_{n_H}q^{-n_H+1} = C^*S - A^*S - q^{-d}B^*R \tag{5.39}$$

$$H = 1 + q^{-1}H^* = 1 + CS - P \tag{5.40}$$

and substracting (5.37) from (5.38), one obtains the following expression for the closed loop prediction error (for details see [Landau and Karimi, 1999])

$$\epsilon_{CL}(t+1) = \frac{1}{C}\left[\theta_e - \widehat{\theta}_e\right]^T \phi_e(t) + e(t+1), \tag{5.41}$$

where

$$\theta_e^T = \left[\theta^T, h_1, \ldots, h_{n_H}\right] \tag{5.42}$$

$$\widehat{\theta}_e^T = \left[\widehat{\theta}^T, \widehat{h_1}, \ldots, \widehat{h}_{n_H}\right] \tag{5.43}$$

$$\phi_e^T(t) = \left[\phi^T(t), \epsilon_{CLf}(t), \ldots, \epsilon_{CLf}(t - n_H + 1)\right] \tag{5.44}$$

$$\epsilon_{CLf}(t) = \frac{1}{S}\epsilon_{CL}(t). \tag{5.45}$$

Asymptotic unbiased estimates in a stochastic environment can be obtained under the sufficient condition

$$H'(z^{-1}) = \frac{1}{C(z^{-1})} - \frac{\lambda_2}{2} \tag{5.46}$$

is strictly positive real.

The closed loop identification procedure is carried out using these algorithms. Usually good results in terms of validation are obtained with the X-CLOE algorithm, nevertheless considering the bias distribution, if the objective is to enhance the accuracy of the model in the critical frequency regions for design, F-CLOE and AF-CLOE algorithms are more suitable methods since they are not affected by the noise characteristics and they heavily weight the difference between the true plant model and estimated model in the desired frequency region. Therefore, the identification procedure has been focused on these algorithms.

For both methods, the observation vector $\phi(t)$ is filtered either by a fixed (constant) filter (F-CLOE case) or by an adaptive filter (AF-CLOE case). For F-CLOE, the filter $S/\widehat{P}$ can be calculated from the models obtained with other closed loop methods (CLOE, X-CLOE) or from an open loop identified model. For AF-CLOE, the *standard* initialization of the adaptive filter $\widehat{P}(t) = \widehat{A}(t)S + q^{-d}\widehat{B}(t)R$ at $t = 0$ is to take $\widehat{A}(0) = 1$ and $\widehat{B}(0) = 0$. Here a different initialization for AF-CLOE is proposed.

Instead of using the standard initial values, it is proposed to use an initial model as for F-CLOE. The adaptation of the filter it is not enabled until an horizon of estimation is reached. This means that for some iterations (the length of the horizon), the observations are filtered by a constant filter $S/\widehat{P}$ and once the horizon is reached, the filter is adapted with the current estimations of $\widehat{A}(t)$ and $\widehat{B}(t)$. The objective is to allow the AF-CLOE algorithm to start in the vicinity of the optimal parameters, following the idea behind the *Recursive Maximum Likelihood* algorithm. This action seeks to combine the improvements of F-CLOE and AF-CLOE methods.

5.5 Experimental Results

In this section both, identification procedure results are shown, but the emphasis is put on the closed loop identification results.

5.5.1 Open Loop Identification Results

The PRBS signal described in Section 5.1 is applied at the inertial actuator input, the residual force measurements are collected and used to identify a model. For the complexity estimation, the penalized error criterion used to chose the orders of the system shows a quite flat minimum region . This means that there is a minimum value but it is possible there are no significant differences for different order chosen. This could lead to consider

Table 5.1: Open loop identified low damped complex zeros.

Algorithm	Zero around 50 Hz Frequency (Hz)	Zero around 50 Hz Damping ($\times 10^{-3}$)	Zero around 100 Hz Frequency (Hz)	Zero around 100 Hz Damping ($\times 10^{-3}$)
OEFC	-	-	99.5	10.9
OEFO	46.1	20.3	102	3.9
OEAFO	46.7	73.5	101	0.6
RELS	46.6	13.5	99.5	0.8
OEEPM	45.8	46.2	99.7	4.0
RML	46.4	7.2	99.6	8.1

the vicinity around the minimum in order to keep the parsimony principle without losing any important dynamic.

The best compromise found between complexity and consistency for the estimated orders of the model for the secondary path corresponds to $n_{\widehat{B}'} = 19$ and $n_{\widehat{A}} = 18$ with a plant pure time delay $d = 0$. If lower orders are considered (specially for $\widehat{A}$), some identification algorithms will miss some important dynamics, mostly around low damped complex poles and zeros in low frequencies. Conversely if higher orders are used, the differences arise only in high frequencies. Since the considered disturbances are of narrow band type, high model accuracy at high frequencies is not essential for model based control, specially in a robust control framework. The estimated orders of the primary path are $n_{\widehat{A}p} = 13$ and $n_{\widehat{B}'_p} = 14$ with a plant delay of $d_p = 0$.

In terms of validation, the best result was obtained by Recursive Extended Last Squares (RELS); however a comparative analysis has been done to illustrate the differences among the several models evaluated. The comparison is done by looking at the frequency region, critical for narrow band disturbance rejection, where the low damped complex zeros are located (between 50 and 100 Hz).

The identified low damped complex zeros are listed in Table 5.1, showing their frequency along with the estimated damping. OEFC fails to identify the zero around 50 Hz, while OEFO and OEAFO show the presence of a zero near to that frequency (46.1 and 46.7 Hz, respectively). RELS, OEEPM and RML identify a zero at such a frequency but the difference is found in the damping. All the algorithms identify a zero around 100 Hz, the difference in this case is in the damping of such complex zero. The validation is based on statistical test and is coherent with the fact that RELS shows one the lowest damping factor for both zeros.

5.5.2 Closed Loop Identification Results

The same PRBS signal used for the open-loop identification was used in the closed loop identification procedure. The *RST* digital controller was calculated on the basis of the identified open-loop model from Section 5.3. The closed-loop identification scheme was implemented as in Figure 5.4(b); it was considered that $T(q^{-1}) = R(q^{-1})$ and the signal was introduced as a reference.

Four models where identified using the same orders as for the open loop model, i.e. $n_A = 18$, $n_{B'} = 19$ and $d = 0$. The considered algorithms were X-CLOE, F-CLOE

and AF-CLOE. F-CLOE uses the X-CLOE model to compute $\widehat{P}(q^{-1})$ in order to use it as filter, for AF-CLOE two different initializations were considered. The standard initialization with $\widehat{A}(q^{-1},0) = 1$, $\widehat{B}(q^{-1},0) = 0$ (denoted AF-CLOE) and a modified initialization which will be called μAF-CLOE. The μAF-CLOE uses two different filters for the observation vector $\phi(t)$. The first filter is computed as in F-CLOE using also the X-CLOE identified model, this first filter is used for an horizon of $10\,(n_A + n_{B'})$ points. Once the horizon is reached, the current estimation of the plant model parameters is used to computed the adaptive filter. Therefore one has the following identified models

$$\widehat{G}_{X-CLOE}(z^{-1}) = \frac{z^{-d}\widehat{B}_{X-CLOE}(z^{-1})}{\widehat{A}_{X-CLOE}(z^{-1})} \tag{5.47}$$

$$\widehat{G}_{F-CLOE}(z^{-1}) = \frac{z^{-d}\widehat{B}_{F-CLOE}(z^{-1})}{\widehat{A}_{F-CLOE}(z^{-1})} \tag{5.48}$$

$$\widehat{G}_{AF-CLOE}(z^{-1}) = \frac{z^{-d}\widehat{B}_{AF-CLOE}(z^{-1})}{\widehat{A}_{AF-CLOE}(z^{-1})} \tag{5.49}$$

$$\widehat{G}_{\mu AF-CLOE}(z^{-1}) = \frac{z^{-d}\widehat{B}_{\mu AF-CLOE}(z^{-1})}{\widehat{A}_{\mu AF-CLOE}(z^{-1})} \tag{5.50}$$

As for the open-loop procedure, the choice of the best model is in terms of validation. The validation procedure, explained in [Landau and Zito, 2005], includes statistical, time domain and *pole closeness* elements. The statistical part is carried out with the uncorrelation test, the pole closeness test with the *Vinnicombe* gap ([Vinnicombe, 1993]) and a visual pole chart comparison. The time domain validation is considered with the loss function.

Table 5.2 shows the validation results for each identified model. Using the input/output data along with the controller, it is possible to compare the previous open-loop identified model with the closed-loop identified models in terms of validation. The uncorrelated term ($\max RN(i)$) is used to determine where the evaluated model is valid or not. A practical limit of 0.15 for this criterion is used. The ν-gap is between 0 and 1, being 0 the best case (no distance). For the loss function, bigger means worse (bigger difference between the true closed-loop response and the simulated closed-loop response). The time domain results should be interpreted from the statistical and closeness validation and not the other way around.

The open-loop model $\widehat{G}_{OL}(z^{-1})$ (tested in a closed loop identification context) does not pass the statistical validation even though it does not present the highest ν-gap or loss function. The X-CLOE model passes the validation test but its ν-gap is over the open-loop result. The F-CLOE model improves all the previous results, obtaining the lowest ν-gap. The AF-CLOE with a standard initialization, possesses a good statistical validation (very close to the F-CLOE result), however shows the biggest ν-gap and loss function. The μAF-CLOE gets the better statistical validation with a good ν-gap and the minimum loss function. The improvements from the μAF-CLOE are reflected also in the location of the low damped complex zeros at low frequencies, which are critical for the narrow band disturbance rejection.

From the input/output data, it is possible to identify the closed-loop transfer function (plant + controller). This allows us to make a closeness comparison between the closed-loop predictor poles (computed) and the true closed-loop system poles (identified), and therefore will indicate the quality of the identified model. Figures 5.5 and 5.6 show the

Table 5.2: Validation results for the closed loop identified model

Model	$R(0)$ 10^{-6}	$\max RN(i)$ 10^{-3}	ν-gap	Loss Function 10^{-6}	Valid
$\widehat{G}_{OL}$	21.49	260.34	0.323	159.41	No
$\widehat{G}_{X-CLOE}$	12.61	141.57	0.351	112.52	Yes
$\widehat{G}_{F-CLOE}$	17.48	76.77	0.271	81.25	Yes
$\widehat{G}_{AF-CLOE}$	18.51	77.42	0.505	168.32	Yes
$\widehat{G}_{\mu AF-CLOE}$	27.86	53.26	0.279	80.40	Yes

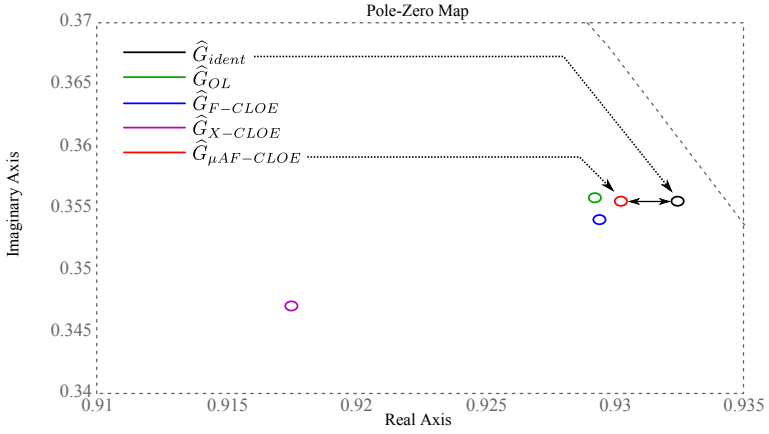

Figure 5.5: Closeness comparison for the low damped complex zero near 46.1 Hz.

location of the zero near 50 Hz and 100 Hz, respectively. In black color is indicated the identified zero using the data from $r(t)$ to $y(t)$ ($\widehat{G}_{ident}$), in green the open-loop model's zero ($\widehat{G}_{OL}$), in blue the F-CLOE model's zero ($\widehat{G}_{FCLOE}$), in violet the X-CLOE model's zero ($\widehat{G}_{XCLOE}$) and in red the zero from μAF-CLOE model ($\widehat{G}_{\mu AF-CLOE}$). The identified zero near 50 Hz with the μAF-CLOE algorithm shows the minimum distance w.r.t. the true zero. For the zero located near 100 Hz, the result from the F-CLOE was improved although the minimum distance was obtained by $\widehat{G}_{X-CLOE}$. This is also reflected in the frequency and damping of the identified zeros as shown in Table 5.3. While the X-CLOE for the zero around 100 Hz is quite close in its damping estimation, for the zero around 50 Hz it is far from the identified value. The standard initialization for AF-CLOE delivers estimations also quite far away from the identified ones in $\widehat{G}_{ident}$. The F-CLOE algorithm improves the results but the AF-CLOE with the proposed initialization and horizon delivers the closest results for both zeros.

5.6 Concluding Remarks

This chapter was focused on the identification of the model of the secondary and primary paths. One of the major objective was to improve the precision in estimation of low damped complex zeros. Modification for the initialization of a closed-loop identification algorithm presented in [Landau and Karimi, 1997] was introduced. This initialization allows to consider previous identified models as in a F-CLOE context, but incorporating the improvements of the AF-CLOE algorithm. In the presence of low damped complex zeros, the closed-loop model quality can be improved also by means of the designed

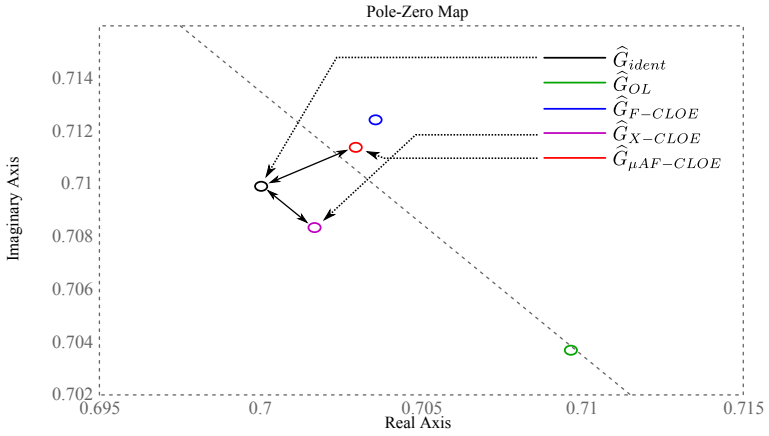

Figure 5.6: Closeness comparison for the low damped complex zero near 101 Hz.

Table 5.3: Closed loop identified low damped complex zeros.

Model	Zero around 50 Hz		Zero around 100 Hz	
	Frequency (Hz)	Damping ($\times 10^{-3}$)	Frequency (Hz)	Damping ($\times 10^{-3}$)
$\widehat{G}_{X-CLOE}$	46.1	53	101	3.7
$\widehat{G}_{F-CLOE}$	46.4	15	101	-1.6
$\widehat{G}_{AF-CLOE}$	50.2	910	99.6	38.7
$\widehat{G}_{\mu AF-CLOE}$	46.5	11.3	101	-0.2
$\widehat{G}_{ident}$	46.4	5.6	101	3.8

controller. The basic idea is to increase the closed-loop system sensitivity in the frequency regions which are critical for control purposes. Special attention was put on the low frequency content since the model will be used for narrow band disturbance rejection.

Part II

Adaptive Feedback Disturbance Compensation

Chapter 6

Robust Direct Adaptive Regulation of Unknown Narrow Band Disturbances

This chapter presents the robust direct adaptive algorithms developed for the rejection of unknown narrow band disturbances. These algorithms were developed in a feedback approach. The algorithms exploit the capabilities of a robust controller by adding adaptive features. They are based on the Youla-Kučera parametrization and the *central* robust controller is computed using Pole Placement. The Direct Adaptive algorithm for a FIR Q-filter was presented in [Landau et al., 2005]; and the case for an IIR Q-filter is presented here.

6.1 Introduction

One of the basic problem in Active Vibration Control and Active Noise Control is the *strong* attenuation of multiple narrow band disturbances[1] without measuring them. The narrow band disturbances have unknown and varying frequencies. In this context, an adaptive feedback approach, termed as *adaptive regulation* is now generally used. The feedback approach, compared to a feedforward compensation approach [Widrow and Stearns, 1985, Beranek and Ver, 1992, Fuller et al., 1997, Elliott, 2001], does not require an additional measurement highly correlated with the disturbance. This avoids the possible destabilizing positive feedback coupling between the compensator system and the measurement of the disturbance [Landau et al., 2011a] and requires less parameters.

A common assumption is that the disturbances is a white noise or a Dirac impulse passed through a filter which characterizes the model of the disturbance[2]. To be more specific, the disturbances considered can be defined as "finite band disturbances". This includes single or multiple narrow band disturbances or sinusoidal signals. For the purpose of this chapter, the disturbances are considered to be time varying, in other words, their model has time varying coefficients. This motivates the use of an adaptive regulation approach since the objective is to attenuate unknown disturbances without measuring them.

A popular methodology for this regulation problem is the design of a controller that

[1] Called *tonal* disturbances in ANC.

[2] Throughout the chapter, it is assumed that the number of multiple narrow band disturbances is known (it can be estimated from data if necessary) but not their frequency characteristics.

incorporates the model of the disturbance (internal model principle). This technique has been described in [Francis and Wonham, 1976, Bengtsson, 1977, Landau et al., 2005, Landau et al., 2011b]. The main problem, using the IMP principle, is that complete rejection of the disturbances is attempted (asymptotically) and this may have a strong influence upon the sensitivity functions outside the frequency band in which attenuation is achieved. As long as rejection of a single narrow band disturbance is considered ([Landau et al., 2005, Landau et al., 2011b]), the influence upon the output sensitivity functions does in general not pose problems. Nevertheless if low damped complex zeros are located near the disturbance frequency, even in a single narrow band disturbance context, the influence over $S_{yp}(z^{-1})$ represents a major challenge [Castellanos Silva et al., 2014]. When multiple narrow band disturbances are considered, the application of this (IMP) approach may lead to unacceptable profiles of the output sensitivity functions in terms of robustness and unacceptable amplification of the residual noise in certain frequency regions.

In this chapter, two solutions for the reduction of the waterbed effect caused by the IMP are proposed. The first is concerned by the robust central controller design. The second is obtained by changing the structure of the Q-filter from a FIR form to an IIR form. In the present framework, the hypothesis of almost constant dynamic characteristics of the AVC system is made (like in [Landau et al., 2011b]). Furthermore, the corresponding control model is supposed to be accurately identified from input/output data.

The main contributions with respect to the work presented in [Landau et al., 2005] are:

- the improvement (robustness and performance) of the direct adaptive scheme by means or a robust central controller using the Youla-Kučera parametrization, even for three unknown narrow band disturbances with time-varying frequencies in the presence of low damped complex zeros;
- the development of a new adaptive scheme, in a mixed form using an IIR Q-filter. The new scheme combines the ideas from [Landau et al., 2005] and [Chen and Tomizuka, 2012] in order to reduce the waterbed effect without the need of estimating the disturbance frequency as in [Airimitoaie and Landau, 2014] and building an indirect adaptive regulation scheme which is much more time consuming;
- the comparative evaluation in real time on the active suspension system located in GIPSA-Lab, Grenoble.

This chapter is organized as follows. In Section 6.2 the main notations and equations for the direct adaptive system are given. Section 6.3 reviews the direct adaptive algorithm and presents the proposed central controller design method, based on Pole Placement with Sensitivity function shaping. In Section 6.4 the new adaptive algorithm is developed. This algorithm uses a Q-IIR filter by means of disturbance model estimation and modifying the direct adaptive algorithm from the FIR case. Finally, in Section 6.5 the main conclusions of this chapter are given.

6.2 System Description

Consider the system description made in Section 3.1 and the equations given in Section 3.2. The basic Youla-Kučera control block diagram used is shown in Figure 6.1. The

process output is expressed as in the Eq. (4.15) and is recalled here[3]

$$y(t) = \frac{A(q^{-1})S(q^{-1})}{P(q^{-1})}p(t), \tag{6.1}$$

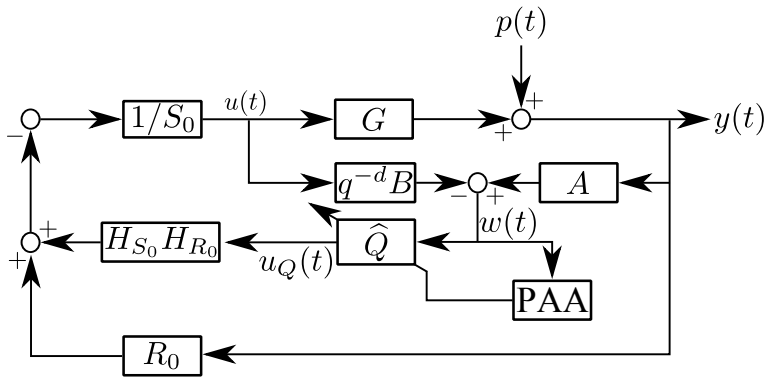

Figure 6.1: Basic scheme for direct adaptive control.

As specified in Section 6.1, the hypothesis of almost constant dynamic characteristics of the AVC system is considered (similar to [Landau et al., 2005, Landau et al., 2011b]). The right coprime factorization chosen for this application is

$$N = q^{-d}B(q^{-1}), \quad D = A(q^{-1}), \quad Y = S_0(q^{-1}), \quad X = R_0(q^{-1}). \tag{6.2}$$

The control signal is given by

$$u(t) = -R_0(q^{-1})y(t) - S_0^*(q^{-1})u(t-1) - H_{S_0}(q^{-1})H_{R_0}(q^{-1})Q(q^{-1})w(t), \tag{6.3}$$

with

$$\begin{aligned} S_0(q^{-1}) &= 1 + q^{-1}S_0^*(q^{-1}) = 1 + s_1^0 q^{-1} + \ldots + s_{n_{S_0}}^0 q^{-n_{S_0}} \\ &= H_{S_0}(q^{-1}) \cdot S_0'(q^{-1}), \end{aligned} \tag{6.4}$$

$$\begin{aligned} R_0(q^{-1}) &= r_0^0 + r_1^0 q^{-1} + \ldots + r_{n_{R_0}}^0 q^{-n_{R_0}} \\ &= H_{R_0}(q^{-1}) \cdot R_0'(q^{-1}), \end{aligned} \tag{6.5}$$

where $H_{S_0}(q^{-1})$ and $H_{R_0}(q^{-1})$ represent fixed (imposed) parts in the controller and $S_0'(q^{-1})$ and $R_0'(q^{-1})$ are computed from

$$\begin{aligned} P_0(q^{-1}) &= A(q^{-1})S_0(q^{-1}) + q^{-d}B(q^{-1})R_0(q^{-1}) \\ &= A(q^{-1})H_{S_0}(q^{-1})S_0'(q^{-1}) + q^{-d}B(q^{-1})H_{R_0}(q^{-1})R_0'(q^{-1}), \end{aligned} \tag{6.6}$$

this polynomial specifies the desired closed loop poles of the system.

[3]The complex variable z^{-1} will be used to characterize the system's behavior in the frequency domain and the delay operator q^{-1} will be used for the time domain analysis.

6.3 FIR Case

The objective of this section is to find an estimation algorithm which directly estimate the parameters of the internal model in the controller in the presence of an unknown disturbance (but known structure) without modifying the closed loop poles. Clearly, the Q-parametrization is a potential option, when a FIR filter representation is considered. The modifications of the Q polynomial will not affect the closed-loop poles. In order to build an estimation algorithm it is necessary to define an *error equation* which will reflect the difference between the optimal Q polynomial and its current estimate. A key aspect of this methodology is the use of the IMP (Section 4.2).

As seen in the subsection 4.3.4 through the Eq. (4.39), one can incorporate the internal model of the disturbance by means of the $Q(z^{-1})$ filter. Using this equation, it is possible to find an expression of the difference between the *unknown* optimal $Q(q^{-1})$ and the estimated $\widehat{Q}(q^{-1})$.

For such purpose, we recall here the definitions of the controller polynomials R and S using the Youla-Kučera parametrization (Q-parametrization) of all stable controllers ([Anderson, 1998, Tsypkin, 1997]). According to Eqs. (4.33) and (4.34), the controller polynomials have the form

$$R(z^{-1}) = R_0(z^{-1}) + A(z^{-1})H_{S_0}(z^{-1})H_{R_0}(z^{-1})Q(z^{-1}) \tag{6.7}$$

$$S(z^{-1}) = S_0(z^{-1}) - z^{-d}B(z^{-1})H_{S_0}(z^{-1})H_{R_0}(z^{-1})Q(z^{-1}), \tag{6.8}$$

where $Q(z^{-1})$ is considered as a FIR filter of the form

$$Q(z^{-1}) = q_0 + q_1 z^{-1} + \cdots + q_{n_Q} z^{-n_Q}. \tag{6.9}$$

Using the Q-parametrization, the output of the system in the presence of a disturbance can be expressed as

$$\begin{aligned} y(t) &= \frac{A(q^{-1})\left[S_0(q^{-1}) - q^{-d}B(q^{-1})H_{S_0}(q^{-1})H_{R_0}(q^{-1})Q(q^{-1})\right]}{P_0(q^{-1})} \cdot \frac{N_p(q^{-1})}{D_p(q^{-1})}\delta(t) \\ &= \frac{S_0(q^{-1}) - q^{-d}B(q^{-1})H_{S_0}(q^{-1})H_{R_0}(q^{-1})Q(q^{-1})}{P_0(q^{-1})}w(t) \end{aligned} \tag{6.10}$$

where $w(t)$ is given by (see also Fig. 6.1)

$$\begin{aligned} w(t) &= \frac{A(q^{-1})N_p(q^{-1})}{D_p(q^{-1})}\delta(t) \\ &= A(q^{-1})y(t) - q^{-d}B^*(q^{-1})u(t-1). \end{aligned} \tag{6.11}$$

In the time domain, the internal model principle can be interpreted as finding Q such that asymptotically $y(t)$ becomes zero. Assume that one has an estimation of $Q(q^{-1})$ at instant t, denoted $\widehat{Q}(q^{-1}, t)$. Denote $\epsilon^0_{FIR}(t+1)$ as the value of $y(t+1)$ obtained with $\widehat{Q}(q^{-1}, t)$. Using (6.10) one gets

$$\epsilon^0_{FIR}(t+1) = \frac{S_0(q^{-1})}{P_0(q^{-1})}w(t+1) - \frac{q^{-d}B^*(q^{-1})H_{S_0}(q^{-1})H_{R_0}(q^{-1})}{P_0(q^{-1})}\widehat{Q}(q^{-1}, t)w(t). \tag{6.12}$$

One can define now the *a posteriori* error (using $\widehat{Q}(q^{-1}, t+1)$) as

$$\epsilon_{FIR}(t+1) = \frac{S_0(q^{-1})}{P_0(q^{-1})}w(t+1) - \frac{q^{-d}B^*(q^{-1})H_{S_0}(q^{-1})H_{R_0}(q^{-1})}{P_0(q^{-1})}\widehat{Q}(q^{-1}, t+1)w(t). \tag{6.13}$$

Replacing S_0 from the last equation by (4.39), one obtains

$$\epsilon_{FIR}(t+1) = \left[Q(q^{-1}) - \widehat{Q}(q^{-1}, t+1)\right] \cdot \frac{q^{-d}B^*(q^{-1})H_{S_0}(q^{-1})H_{R_0}(q^{-1})}{P_0(q^{-1})} w(t) + \upsilon(t+1), \tag{6.14}$$

where

$$\begin{aligned} \upsilon(t+1) &= \frac{S'(q^{-1})D_p(q^{-1})}{P_0(q^{-1})} w(t+1) \\ &= \frac{S'(q^{-1})A(q^{-1})N_p(q^{-1})}{P_0(q^{-1})} \delta(t+1) \end{aligned} \tag{6.15}$$

is a signal which tends asymptotically towards zero.

Define the estimated polynomial $\widehat{Q}(q^{-1}, t)$ as $\widehat{Q}(q^{-1}, t) = \widehat{q}_0(t) + \widehat{q}_1(t)q^{-1} + \cdots + \widehat{q}_{n_Q}(t)q^{-n_Q}$ and the associated estimated parameter vector: $\widehat{\theta}(t) = \left[\widehat{q}_0(t), \widehat{q}_1(t), \cdots, \widehat{q}_{n_Q}(t)\right]^T$. Define the fixed parameter vector corresponding to the optimal value of the polynomial Q as $\theta = \left[q_0, q_1, \cdots, q_{n_Q}\right]^T$.

Denote

$$w_2(t) = \frac{q^{-d}B^*(q^{-1})H_{S_0}(q^{-1})H_{R_0}(q^{-1})}{P_0(q^{-1})} w(t) \tag{6.16}$$

and define the following observation vector

$$\phi_{FIR}^T(t) = \left[w_2(t), w_2(t-1), \cdots, w_2(t-n_Q)\right]. \tag{6.17}$$

Then Eq. (6.14) becomes

$$\epsilon_{FIR}(t+1) = \left[\theta^T - \widehat{\theta}^T(t+1)\right] \cdot \phi_{FIR}(t) + \upsilon(t+1), \tag{6.18}$$

which corresponds to an adaptation error as mentioned in [Landau et al., 2011d].

Defining

$$w_1(t+1) = \frac{S_0(q^{-1})}{P_0(q^{-1})} w(t+1), \tag{6.19}$$

and using Eqs. (6.12), (6.11) and (6.16), the *a priori* adaptation error is rewritten as

$$\epsilon_{FIR}^0(t+1) = w_1(t+1) - \widehat{\theta}^T(t)\phi_{FIR}(t), \tag{6.20}$$

the *a posteriori* adaptation error is obtained from (6.13)

$$\epsilon_{FIR}(t+1) = w_1(t+1) - \widehat{\theta}^T(t+1)\phi_{FIR}(t). \tag{6.21}$$

For the estimation of the parameters of $\widehat{Q}(q^{-1}, t)$, the PAA defined in Eqs. (5.11) to (5.14) is used. The stability proof for the algorithm under the assumption that the plant model = true plant was given in [Landau et al., 2005]. The proof for preserving the fixed parts in the YK-parametrization was given in [Landau et al., 2011b].

6.3.1 Central Controller Design

The contribution w.r.t. the previous work presented in [Landau et al., 2005] corresponds to the design of the central controller, i.e. the polynomials R_0 and S_0. The central controller plays a very important role in this approach. Its role is:

- to stabilize the system (if necessary) in the absence of disturbances,
- to ensure a small (flat) *waterbed* effect over $S_{yp}(z^{-1})$ when the IMP is incorporated to the controller through the Q-filter parameters and
- to reduce the magnitude of $S_{up}(z^{-1})$ outside of the attenuation region, when the adaptive regulation algorithm is active.

The structure of the central controller was presented in Eqs. (6.7) and (6.8) and is shown in Fig. 6.1. Since the estimation of $\widehat{Q}(z^{-1})$ is the only adaptive part in the scheme, fixed characteristics in the central controller can be imposed and preserved through the Youla-Kučera parametrization, as was shown in subsection 4.3.3. These fixed characteristics can have various purposes.

Due to the water bed effect over the output sensitivity function (S_{yp}) caused by the IMP, the central controller must shape S_{yp} in order to meet the robust and performance specifications required. The technique of pole placement with sensitivity function shaping is an option to address this problem (see details in [Landau and Zito, 2005]).

This water bed effect can be attenuated by introducing a pair of low damped complex auxiliary poles at the same or near the frequency of the narrow band disturbance which is attenuated using IMP. The damping of these fixed auxiliary complex poles has to be chosen such that the desired attenuation can be however achieved for all the frequencies within the attenuation region. Hence, this feature can be used in the central controller design to reduce the IMP waterbed effect over S_{yp}, i.e. to control the modulus margin ΔM.

Since the YK-parametrization allows the introduction of the disturbance model without modifying the closed loop poles imposed by the central controller, low damped complex *fixed* auxiliary poles can be introduced in the characteristic polynomial of the closed loop ($P(z^{-1})$), for reducing the waterbed effect within the region of attenuation. The frequency (location) and damping factor are chosen accordingly to the robustness and performance specifications.

It is recommended to have a very low magnitude of the input sensitivity function outside the frequency region (Ω_{out}) where the disturbance attenuation is done, e.g. $\left|S_{up}(e^{-j\Omega_{out}})\right| < -20$ dB. This should be done in order to not amplify the noise which may exist in these frequencies nor to reduce the robustness against possible additive uncertainties (see Section 4.4). A very efficient way to achieve this, without influencing the shape of the output sensitivity function in the attenuation region (Ω_d), is to use band stop filters (BSFs) over S_{up} (see details in [Landau and Zito, 2005, Procházka and Landau, 2003]).

6.4 IIR Case

The previous algorithm uses a FIR structure for the Q-filter. In this section, a new algorithm is developed, using an IIR structure. Controller polynomials R and S are defined, according to Eqs. (4.28)-(4.29),

$$R(z^{-1}) = A_Q(z^{-1})R_0(z^{-1}) + H_{R_0}(z^{-1})H_{S_0}(z^{-1})A(z^{-1})B_Q(z^{-1}), \tag{6.22}$$

$$S(z^{-1}) = A_Q(z^{-1})S_0(z^{-1}) - H_{R_0}(z^{-1})H_{S_0}(z^{-1})z^{-d}B(z^{-1})B_Q(z^{-1}). \tag{6.23}$$

By the Eq. (4.31), the output of the system can be written as follows

$$y(t) = \frac{A(q^{-1})\left[A_Q(q^{-1})S_0(q^{-1}) - H_{R_0}(q^{-1})H_{S_0}(q^{-1})q^{-d}B(q^{-1})B_Q(q^{-1})\right]}{P(q^{-1})}p(t), \quad (6.24)$$

$$y(t) = \frac{\left[A_Q(q^{-1})S_0(q^{-1}) - H_{R_0}(q^{-1})H_{S_0}(q^{-1})q^{-d}B(q^{-1})B_Q(q^{-1})\right]}{P(q^{-1})}w(t), \quad (6.25)$$

where the closed-loop poles are defined by

$$P(z^{-1}) = A_Q(z^{-1})\left(A(z^{-1})S_0(z^{-1}) + z^{-d}B(z^{-1})R_0(z^{-1})\right). \quad (6.26)$$

In the previous algorithm, when the disturbance model is known, it is possible to calculate the FIR Q-filter with the diophantine equation defined in (4.39). By considering an IIR structure, the diophantine equation changes to

$$D_p(z^{-1})S'(z^{-1}) + z^{-d}B(z^{-1})H_{R_0}(z^{-1})B_Q(z^{-1}) = A_Q(z^{-1})S'_0(z^{-1}) \quad (6.27)$$

where D_p, H_{R_0}, B, d and S'_0 are known and S', B_Q and A_Q are unknown. Assuming that $A_Q(z^{-1})$ is known and stable, the previous equation is solvable. As for the FIR case, the order of the $B_Q(z^{-1})$ depends on the order of the disturbance by $n_{B_Q} = n_{D_p} - 1$. The order of $A_Q(z^{-1})$ do not depend on the order of $B_Q(z^{-1})$.

Enhancing the robustness through $A_Q(z^{-1})$

It was assumed that $A_Q(z^{-1})$ should be stable since it defines auxiliary closed-loop poles. In the sequel, a discussion about the values of such polynomial is given.

As concluded in Chapter 4, the modulus of the output sensitivity function may rise to unacceptable values when the disturbance model is introduced to the controller. Since the polynomial $B_Q(z^{-1})$ performs this action, it is possible to use the polynomial $A_Q(z^{-1})$ to mitigate the waterbed effect over $S_{yp}(z^{-1})$.

By the assumption made in (4.14), the structure of $D_p(z^{-1})$ is expressed in the next equation

$$D_p(z^{-1}) = \prod_{i=1}^{n}\left(1 + \alpha_i z^{-1} + z^{-2}\right), \quad (6.28)$$

where $\alpha_i = -2\cos(2\pi\omega_i T_s)$, $\omega_i \in \Omega$, n is the number of narrow band disturbances and T_s is the sampling time. Through $B_Q(z^{-1})$, a pair of complex zeros on the unit circle are introduced in $S_{yp}(z^{-1})$ at each frequency ω_i making possible the asymptotic disturbance rejection. If a pair of complex poles is also introduced at the same frequency as the disturbance but with low damping (inside of the unitary circle and therefore stable), the waterbed effect could be minimized[4]. This can be done by means of $A_Q(z^{-1})$. This is the principle used in the notch filters [Airimiţoaie et al., 2013].

Based on the knowledge of $D_p(z^{-1})$, $A_Q(z^{-1})$ can be selected as follows ([Chen and Tomizuka, 2012])

$$A_Q(z^{-1}) = D_p(\rho z^{-1}) = \prod_{i=1}^{n}\left(1 + \rho\alpha_i z^{-1} + \rho^2 z^{-2}\right) \quad (6.29)$$

[4]Of course a compromise must be found between attenuation and amplification.

where $0 < \rho < 1$ is a positive real number smaller but close to one. Then the roots of $A_Q(z^{-1})$ are located on a circle of radius ρ. This makes $A_Q(z^{-1})$ stable and will benefit the parameter adaptation algorithm later. To see the latter point, expanding the product in (6.28), we can get

$$D_p(z^{-1}) = 1 + \alpha_1 z^{-1} + \cdots + \alpha_n z^{-n} + \cdots + \alpha_1 z^{-2n+1} + z^{-2n}, \tag{6.30}$$

where we have mapped the parameters in (6.28) to $\{\alpha_i\}_1^n$, and the new coefficient vector $[1, \alpha_1, \ldots, \alpha_n, \ldots, \alpha_1, 1]$ has a mirror symmetric form by construction. Replacing every z^{-1} with ρz^{-1}, we obtain $A_Q(z^{-1}) = D_p(\rho z^{-1})$, which is also linear in $\{\alpha_i\}_1^n$. Only these n parameters need to be later identified.

In order to build the adaptive algorithm to estimate $\widehat{B}_Q(z^{-1})$, the previous algorithm can be used if an estimation of $\widehat{A}_Q(z^{-1})$ is available. This is due to the fact that $B_Q(z^{-1})$ can be computed over the basis of $A_Q(z^{-1})$ by the Eq. (6.27). Therefore, we first develop the adaptive algorithm for estimating $\widehat{A}_Q(z^{-1})$.

Assuming that *model plant = true plant* in the frequency range where the narrow band disturbances are introduced, it is possible to get an estimation of $p(t)$, named $\widehat{p}(t)$, using the following expression

$$\widehat{p}(t) = \frac{1}{A(q^{-1})} w(t) \tag{6.31}$$

where $w(t)$ was defined in Eq. (6.11). The main idea behind this algorithm is to consider the signal $\widehat{p}(t)$ as

$$\widehat{p}(t) = \sum_{i=1}^{n} c_i \sin(\omega_i t + \beta_i) + \nu(t), \tag{6.32}$$

where $\{c_i, \omega_i, \beta_i\} \neq 0$, n is the number of narrow band disturbances and $\nu(t)$ is a noise affecting the measurement. It can be verified that, after two steps of transient $(1 - 2\cos(\omega_i)q^{-1} + q^{-2}) \cdot c_i \sin(\omega_i t + \beta_i) = 0$ [Chen and Tomizuka, 2012].

Then the objective is to find the parameter $\{\alpha\}_{i=1}^n$ that makes $D_p(q^{-1})\widehat{p}(t) = 0$. The previous product can be represented by

$$\begin{aligned} x(t) &= D_p(q^{-1})\widehat{p}(t), \\ &= \widehat{p}(t) + \alpha_1\widehat{p}(t-1) + \cdots + \alpha_n\widehat{p}(t-n) + \cdots + \alpha_1\widehat{p}(t-2n+1) + \widehat{p}(t-2n). \end{aligned} \tag{6.33}$$

The estimated product is written as follows

$$\begin{aligned} \widehat{x}(t) =& \widehat{D}_p(q^{-1})\widehat{p}(t), \\ =& \widehat{p}(t) + \widehat{\alpha}_1(t)\widehat{p}(t-1) + \cdots + \widehat{\alpha}_n(t)\widehat{p}(t-n) + \cdots \\ & \cdots + \widehat{\alpha}_1(t)\widehat{p}(t-2n+1) + \widehat{p}(t-2n). \end{aligned} \tag{6.34}$$

Assuming that an estimation of $\widehat{D_p}(q^{-1})$ is available at the instant t, the *a priori* adaptation error $\epsilon^0_{D_p}(t+1)$ is defined as

$$\begin{aligned} \epsilon^0_{D_p}(t+1) =& x(t+1) - \widehat{x}(t+1), \\ =& (\alpha_1 - \widehat{\alpha}_1(t))\left(\widehat{p}(t) + \widehat{p}(t-2n+2)\right) + \cdots + (\alpha_n - \widehat{\alpha}_n(t))\widehat{p}(t-n+1) \end{aligned} \tag{6.35}$$

Using the related parameter vector θ_{D_p} and its estimated version $\widehat{\theta}_{D_p}(t)$, with the following definitions

$$\theta_{D_p} = [\alpha_1, \cdots, \alpha_n]^T, \tag{6.36}$$

$$\widehat{\theta}_{D_p}(t) = [\widehat{\alpha}_1(t), \cdots, \widehat{\alpha}_n(t)]^T, \tag{6.37}$$

and defining the observation vector $\psi(t)$

$$\psi(t) = [\widehat{p}(t) + \widehat{p}(t-2n+2), \cdots, \widehat{p}(t-n+1)]^T, \tag{6.38}$$

then the *a priori* adaptation error is written as follows

$$\epsilon^0_{D_p}(t+1) = \left[\theta^T_{D_p} - \widehat{\theta}^T_{D_p}(t)\right] \cdot \psi(t), \tag{6.39}$$

and the *a posteriori* adaptation error using the estimation at $t+1$

$$\epsilon_{D_p}(t+1) = \left[\theta^T_{D_p} - \widehat{\theta}^T_{D_p}(t+1)\right] \cdot \psi(t), \tag{6.40}$$

which corresponds to an adaptation error according to [Landau et al., 2011d].

For implementation, since the objective is to make $x(t+1) \to 0$, the implementable *a priori* adaption error is defined as follows

$$\begin{aligned}\epsilon^0_{D_p}(t+1) &= 0 - \widehat{D_p}(q^{-1}, t)\widehat{p}(t+1) \\ &= -\widehat{\theta}^T_{D_p}(t)\psi(t) - (\widehat{p}(t+1) + \widehat{p}(t-2n+1)).\end{aligned} \tag{6.41}$$

The PAA defined in Eqs. (5.11)-(5.14) is used with $\Phi(t) = \psi(t)$, $\widehat{\theta}(t) = \widehat{\theta}_{D_p}(t)$ and $\epsilon^0(t+1) = \epsilon^0_{D_p}(t+1)$. Additional filtering can be applied on $\widehat{p}(t)$ to improve the signal-noise ratio. Since a frequency range of interest was defined, a bandpass filter can be used on $\widehat{p}(t)$.

Estimation of $B_Q(z^{-1})$

Once an estimation algorithm is developed for polynomial $\widehat{A}_Q(q^{-1})$, the next step is develop the estimation algorithm for $\widehat{B}_Q(q^{-1})$. Assuming that the estimation of $A_Q(z^{-1})$ is available and constant, we can incorporate this polynomial to the adaptation algorithm defined in Section 6.3. Using the Eqs. (6.25) and (6.26) and that an estimation of $\widehat{B}_Q(q^{-1})$ is available at the instant t, the *a priori* error is defined as the output of the closed-loop system written as follows[5]

$$\epsilon^0_{IIR}(t+1) = \frac{A_Q S_0}{A_Q P_0} w(t+1) - \frac{H_{S_0} H_{R_0} q^{-d} B^* \widehat{B}_Q(t)}{A_Q P_0} w(t). \tag{6.42}$$

One can define now the *a posteriori* error (using $\widehat{B}_Q(q^{-1}, t+1)$) as

$$\epsilon_{IIR}(t+1) = \frac{A_Q S_0}{A_Q P_0} w(t+1) - \frac{H_{S_0} H_{R_0} q^{-d} B^* \widehat{B}_Q(t+1)}{A_Q P_0} w(t). \tag{6.43}$$

Substituting the (6.27) in (6.42)

$$\begin{aligned}\epsilon^0_{IIR}(t+1) &= \frac{\left[D_p S' H_{S_0} + H_{S_0} H_{R_0} q^{-d} B B_Q\right]}{A_Q P_0} w(t+1) - \frac{H_{S_0} H_{R_0} q^{-d} B^* \widehat{B}_Q(t)}{A_Q P_0} w(t), \\ &= \varrho(t+1) + \frac{H_{S_0} H_{R_0} q^{-d} B^* B_Q}{A_Q P_0} w(t) - \frac{H_{S_0} H_{R_0} q^{-d} B^* \widehat{B}_Q(t)}{A_Q P_0} w(t), \\ &= \varrho(t+1) + \left[B_Q - \widehat{B}_Q(t)\right] \frac{H_{S_0} H_{R_0} q^{-d} B^*}{A_Q P_0} w(t),\end{aligned} \tag{6.44}$$

[5]The argument (q^{-1}) will be dropped in some of the following equations.

where $\varrho(t+1)$ is defined by

$$\begin{aligned}\varrho(t+1) &= \frac{D_p S' H_{S_0}}{A_Q P_0} \cdot \frac{AN_p}{D_p}\delta(t+1), \\ &= \frac{S' H_{S_0} AN_p}{A_Q P_0}\delta(t+1)\end{aligned} \tag{6.45}$$

which tends asymptotically towards zero since both A_Q and P_0 are stable polynomials.

Then the *a posteriori* error is defined as the value of $y(t+1)$ obtained with $\widehat{B}_Q(q^{-1}, t+1)$ as follows

$$\epsilon_{IIR}(t+1) = \left[B_Q - \widehat{B}_Q(t+1)\right] \cdot \frac{H_{S_0} H_{R_0} q^{-d} B^*}{A_Q P_0} w(t) + \varrho(t+1). \tag{6.46}$$

Define the estimated polynomial $\widehat{B}_Q(q^{-1}, t) = \widehat{b}_0^Q(t) + \widehat{b}_1^Q(t)q^{-1} + \cdots + \widehat{b}_{n_{B_Q}}^Q q^{-n_{B_Q}}$ and the associated estimated parameter vector: $\widehat{\theta}_{IIR}(t) = \left[\widehat{b}_0^Q(t), \widehat{b}_1^Q(t), \cdots, \widehat{b}_{n_{B_Q}}^Q(t)\right]^T$. Define the fixed parameter vector corresponding to the optimal value of the polynomial B_Q as $\theta_{IIR} = \left[b_0^Q, b_1^Q, \cdots, bn_{B_Q}^Q\right]^T$.

Denote

$$w_2^f(t) = \frac{1}{A_Q} \cdot \frac{H_{S_0} H_{R_0} q^{-d} B^*}{P_0} w(t) \tag{6.47}$$

and define the following observation vector

$$\phi_{IIR}^T(t) = \left[w_2^f(t), w_2^f(t-1), \cdots, w_2^f(t-n_Q)\right]. \tag{6.48}$$

Then, Eq. (6.46) becomes

$$\epsilon_{IIR}(t+1) = \left[\theta_{IIR}^T - \widehat{\theta}_{IIR}^T(t+1)\right] \cdot \phi_{IIR}(t) + \varrho(t+1), \tag{6.49}$$

which also corresponds to an adaptation error according to [Landau et al., 2011d].

From Eq. (6.42), one obtains the *a priori* adaptation error

$$\epsilon_{IIR}^0(t+1) = w_1(t+1) - \widehat{\theta}_{IIR}^T(t)\phi_{IIR}(t) \tag{6.50}$$

with $w_1(t+1)$ defined as in (6.19) (since $A_Q(q^{-1})$ is considered as constant). The *a posteriori* adaptation error is obtained from (6.43)

$$\epsilon_{IIR}(t+1) = w_1(t+1) - \widehat{\theta}_{IIR}^T(t+1)\phi_{IIR}(t). \tag{6.51}$$

Comparing with the previous algorithm, in order to implement the estimation of B_Q, the difference is on the observation vector $\phi_{IIR}(t)$ which basically consist in filtering the signal $w_2(t)$ defined in Eq. (6.16) by the filter $\frac{1}{A_Q(q^{-1})}$.

The following procedure is applied at each sampling time for adaptive operation:

1. Get the measured output $y(t+1)$ and the applied control $u(t)$ to compute $w(t+1)$ using (6.11).
2. Obtain the filtered signal $\widehat{p}(t+1)$ from (6.31).
3. Compute the implementable *a priori* adaptation error with the Eq. (6.41).

4. Estimate $\widehat{A}_Q(q^{-1})$ using the PAA.
5. Compute $w_2^f(t)$ with Eq. (6.47).
6. Compute $w_1(t+1)$ with Eq. (6.19).
7. Put the filtered signal $w_2^f(t)$ in the observation vector, as in Eq. (6.48).
8. Compute the *a priori* adaptation error defined in Eq. (6.50).
9. Estimate the B_Q polynomial using the parametric adaptation algorithm (5.11) - (5.14).
10. Compute and apply the control (see Fig. 6.1):

$$S_0 u(t) = -R_0 y(t+1) - H_{S_0} H_{R_0} \widehat{B}_Q(t) w(t+1) - A_Q^* u_Q(t). \tag{6.52}$$

6.4.1 Stability Considerations

The stability analysis of the algorithm for adapting the notch filters has been done in [Stoica and Nehorai, 1988] and will not be recalled here.

If $\widehat{A}_Q(q^{-1})$ is constant, the proof from [Landau et al., 2005] remains valid. However, we have not studied the stability when the estimation of A_Q is combined with estimations of B_Q. A complete stability analysis of the full adaptive control scheme remains to be done and will be the subject of a future research.

6.5 Concluding Remarks

In this chapter two adaptive algorithms for the rejection of multiple unknown/time-varying narrow band disturbances have been developed. It was assumed that only the structure of the disturbance model is known (number of model parameters), but not its frequency characteristics.

The first algorithm improves the robustness from the algorithm presented in [Landau et al., 2005] by means of the central controller. This is due to the presence of complex zeros with a very low damping factor. The improvements are based on the fact that the algorithm uses the YK-parametrization with a Q-FIR filter, allowing the preserve the *desired* closed loop poles. The waterbed effect produced by the IMP was reduced for one to multiple (3) narrow band disturbances. Also through the fixed parts of the central controller, some band stop filters (BSF) can be added to shape the sensitivity functions in frequency regions critical for control.

The second algorithm has been developed to enhance further the results obtained from the first algorithm. By changing the structure of the Q-filter, using an IIR filter, it was possible to reduce the complexity of the central controller, regardless the number of narrow band disturbances. The main feature is the selection of the denominator $A_Q(z^{-1})$, which allows to reduce further the waterbed effect in S_{yp}. Unlike the work presented in [Airimitoaie and Landau, 2014], the estimation of the frequency or the solution of matrix equations is not necessary.

Chapter 7

Comparative Evaluation of the Proposed Algorithms

The present chapter shows the results of the several experiments carried out on the Active Vibration Control System presented in the Chapter 3. Multiple narrow band signals with unknown and possibly time-varying frequencies are considered. The difficulty is increased by the fact that the compensator system (the plant) has several resonant and anti-resonant modes in the band frequency of interest for multiple narrow band disturbances rejection. The comparison has been done in the context of an international benchmark competition where control specifications and performance index were defined.

7.1 Introduction

The strong attenuation of unknown multiple narrow-band disturbances is one of the basic problems in AVC and ANC. One solution uses a feedback approach. In Chapter 4, we showed the difficulty to achieve total rejection of multiple narrow band disturbances, due the waterbed effect over the output sensitivity function. The difficulty is increased when low damped complex plant zeros are located close to or at the frequency of the disturbance, because this leads to increase the modulus of $S_{up}(z^{-1})$, reducing the robustness of the system against additive uncertainties and noise.

In this context, an International Benchmark Competition was proposed in [Landau et al., 2013a]. Seven teams from around the world decided to participate and present their solutions for this kind of problem. The results were published in a special issue in [Landau et al., 2013a] and as an invited session in [Landau et al., 2013b].

The improved solution, based on the algorithm from [Landau et al., 2005], presented in Section 6.3, was tested in this international competition as well as the new algorithm presented in 6.4 (the new algorithm has not been considered in the benchmark competition). This new algorithm will be compared also according to the benchmark specifications in this chapter.

7.2 International Benchmark in Adaptive Regulation

Using the Active Vibration Control system described in Chapter 3, an International Benchmark Competition was proposed. The competition context was to perform an adaptive feedback regulation when multiple unknown/time varying narrow band disturbances are introduced into the system.

Industry needs to know the *state of the art* in the field, based on a solid experimental

verification on a benchmark. The objective of the proposed benchmark was to evaluate, on an experimental basis, the available techniques for adaptive regulation in the presence of unknown/time varying multiple narrow band disturbances. Active vibration control constitutes an excellent example of a field where this situation occurs. Similar situations also occur in disc drive control and active noise control. Solutions for the problem of active vibration control can be extrapolated to the control of disc drives and active noise control (see for example the applications described in [Landau et al., 2011c]). The benchmark has allowed to test various approaches in the specific context of an active vibration control system which was used as a test bed.

The scientific objective of the benchmark was to evaluate current available procedures for adaptive regulation which may be applied in the presence of unknown/time varying multiple narrow band disturbances. Specifically, the benchmark was focused in testing: *1)* performance, *2)* robustness and *3)* complexity.

The test bed is representative of many situations encountered in practice and, in particular, of light weighted mechanical structures featuring strong resonance and anti-resonance behavior and impacted by vibration sources of different frequencies.

For the comparative evaluation, control specifications along with various criteria for performance, robustness and complexity have been defined. They can be found in Appendix A. Here a summary of the most important criteria is presented. The control specifications can be summarized in Table A.1.

1. Steady State Performance (Tuning capabilities)

   - Global criterion for steady state performance for one level (J_{SS_k}): defined in Eq. A.4, performs the average of the mean of three tuning capabilities measurements: global attenuation (GA, defined in Eq. (4.1)), disturbance attenuation (DA, defined in Eq. (4.3)) and maximum amplification (MA, defined in Eq. (4.4)). In general, "lower values" means better performance.
   - Benchmark Satisfaction Index for steady state performance (BSI_k): defined in Eq. (A.5), indicates the fulfillment of the benchmark specifications related to the tuning capabilities using a percentage. A 100% in the BSI_k means total fulfillment of the benchmark specifications. It is one of the most important index.

2. Robustness with respect to model uncertainties

   - Normalized Performance Loss (NPL): defined in Eq. (A.7), relates the difference between the BSI_k in simulation and the BSI_k in real-time for each level. "Lower values" means more robustness against differences between the plant model and the real system.

3. Transient Performance

   - Benchmark Satisfaction Index for the transient evaluation in simple step (BSI_{Trans_k}): defined in Eq. (A.9), performs an evaluation of the fulfillment of the benchmark specification for a transient duration equal to or less than 2 sec. A 100% in the BSI_{Trans_k} means total fulfillment of the benchmark specification.
   - Average global criterion for transient performance for one level (J_{TRAV_k}): defined in Eq. (A.13), performs an average of three global criteria for the

transient performance in simple step test (J_{TR_k}), step changes in frequencies test (J_{STR_k}) and chirp test (J_{chirp_k}).

4. Evaluation of the complexity
   - Global criterion for complexity comparison (ΔTET_k): defined in Eq. (A.17), performs an average of three criteria indicators for simple step test ($\Delta TET_{Simple,k}$), step changes in frequency test ($\Delta TET_{Step,k}$) and chirp test ($\Delta TET_{Chirp,k}$).

5. Performance robustness with respect to a different experimental protocol test
   - Using BSI_k and BSI_{Trans_k}, the performance robustness with respect to changes in the protocol test is evaluated.

7.3 Results for multiple narrow band disturbances rejection

This section presents the results obtained in simulation and for real-time experiments of the algorithm developed in Sections 6.4. The results for the algorithm developed in Section 6.3 are reproduced from [Castellanos Silva et al., 2013b]. An evaluative comparison is done between the results presented in [Landau et al., 2013a] and the ones in this section.

The eight participants are listed here:

- [Aranovskiy and Freidovich, 2013], denoted as AF.
- [de Callafon and Fang, 2013], denoted as CF.
- [Karimi and Emedi, 2013], denoted as KE.
- [Wu and Ben Amara, 2013], denoted as WB.
- [Chen and Tomizuka, 2013b], denoted as CT.
- [Airimiţoaie et al., 2013], denoted as ACL.
- [Castellanos Silva et al., 2013b], denoted as YK-FIR (Section 6.3).
- Algorithm from Section 6.4, denoted as YK-IIR.

From the previous list, the contributions from [Aranovskiy and Freidovich, 2013], [Chen and Tomizuka, 2013b] and [Airimiţoaie et al., 2013] use (or can use) an IIR filter structure for their control configurations (the Q-filter). The new algorithm presented here takes ideas from [Chen and Tomizuka, 2013b]. Nevertheless, even with a FIR structure, good results were obtained as in [Wu and Ben Amara, 2013] and [Castellanos Silva et al., 2013b].

Simulation Results

Using the simulator provided by the organizers of the international benchmark, the three protocols were tested for the YK-FIR and YK-IIR algorithms. The results for the three levels are displayed.

YK-FIR Algorithm

The results of the YK-FIR algorithms in the *Simple Step* Test (Protocol 1) are shown in Table 7.1. From these results, we can see the good performance of this algorithm, specially at Level 3. At Level 1, the global attenuation (GA), disturbance attenuation (DA) and transient duration (TD) specifications are fulfilled for almost all the frequencies.

The exception is the case of 95 Hz, where both global and disturbance attenuations are under the specified value. The maximum amplification (MA) shows, for all the cases, results over the benchmark specification with a maximum of 7.8 dB for the case of 70 Hz, w.r.t. the open loop response. Level 2 presents good results in terms of GA and TD. The DA is fulfilled for all the cases except for 70-95 Hz, where the attenuation achieved for 95 Hz was 37.3 dB. For MA, the results are slightly over the benchmark specification. Finally, the results for Level 3 are good in terms of GA and TD (fulfillment for all the cases). Only for one frequency, in the case where the disturbances are located at 65-80-95 Hz, the DA achieved is under the specified value (37.9 dB). However, at this level the MA for all the cases is under the benchmark specification.

Table 7.1: Simulation results for YK-FIR Algorihtm - Simple Step Test.

	Frequency (Hz)	**GA (dB)**	**DA (dB)**	**MA (dB@Hz)**	**N^2T ($\times 10^{-3}$)**	**N^2R ($\times 10^{-3}$)**	**MV ($\times 10^{-3}$)**	**TD (%)**
Level 1	**50**	34.2	44.4	7.2@67.2	14.5	3.8	17.7	100
	55	32.8	46.8	6.7@78.1	10.2	4.4	19.9	100
	60	32.3	46.9	6.8@82.8	10.2	4.7	20.1	100
	65	32.8	48.4	7.0@50.0	9.3	4.5	19.9	100
	70	33.3	50.0	7.8@53.1	8.3	4.3	19.9	100
	75	34.0	51.9	7.3@53.1	7.9	4.0	19.8	100
	80	34.6	51.6	7.7@93.8	8.2	3.8	21.8	100
	85	34.4	52.3	6.7@64.1	9.8	3.7	23.9	100
	90	31.9	45.0	7.5@68.8	13.3	4.0	26.8	100
	95	23.9	35.7	6.2@87.5	20.8	4.6	29.1	100
Level 2	**50-70**	39.2	41.8-47.5	6.1@79.7	25.0	4.3	29.4	100
	55-75	38.4	48.3-47.7	7.7@87.5	23.4	4.8	34.7	100
	60-80	39.4	50.1-49.3	7.9@50.0	19.4	4.2	34.2	100
	65-85	39.8	49.1-51.0	7.2@53.1	18.3	3.9	36.6	100
	70-90	38.5	51.5-42.6	7.6@59.4	27.3	4.2	40.6	100
	75-95	36.5	54.0-37.3	6.0@87.5	35.6	4.1	44.5	100
Level 3	**50-65-80**	42.8	43.9-44.9-41.3	7.7@87.5	136.0	4.2	72.5	100
	55-70-85	43.0	48.8-49.6-46.8	7.6@76.6	352.3	4.1	133.4	100
	60-75-90	42.0	47.7-49.7-42.4	8.5@51.5	655.8	4.4	209.2	100
	65-80-95	40.9	44.5-42.3-37.9	7.9@73.4	1615.7	4.1	295.9	100

For the *Step Changes in Frequencies* Test (Protocol 2), the results are summarized in Table 7.2 for the three levels. According to the level, a number of sequences was established. Each sequence is based on a central disturbance frequency, where changes of $\pm$ 10 Hz (for Level 1) or $\pm$ 5 Hz (for levels 2 and 3), occurs each 3 sec. In this test are evaluated four steps, i.e. four changes in the disturbance frequency. The sequences are defined here, the frequency values are indicated in Hz:

a) Level 1

- Sequence 1, Steps: $60 \rightarrow 70,\ 70 \rightarrow 60,\ 60 \rightarrow 50,\ 50 \rightarrow 60$
- Sequence 2, Steps: $75 \rightarrow 85,\ 85 \rightarrow 75,\ 75 \rightarrow 65,\ 65 \rightarrow 75$

- Sequence 3, Steps: $85 \rightarrow 95,\ 95 \rightarrow 85,\ 85 \rightarrow 75,\ 75 \rightarrow 85$

b) Level 2

- Sequence 1, Steps: $[55, 75] \rightarrow [60, 80]$, $[60, 80] \rightarrow [55, 75]$, $[55, 75] \rightarrow [50, 70]$, $[50, 70] \rightarrow [55, 75]$
- Sequence 2, Steps: $[70, 90] \rightarrow [75, 95]$, $[75, 95] \rightarrow [70, 90]$, $[70, 90] \rightarrow [65, 85]$, $[65, 85] \rightarrow [70, 90]$

c) Level 3

- Sequence 1, Steps: $[55, 70, 85] \rightarrow [60, 75, 90]$, $[60, 75, 90] \rightarrow [55, 70, 85]$, $[55, 70, 85] \rightarrow [50, 65, 80]$, $[50, 65, 80] \rightarrow [55, 70, 85]$
- Sequence 2, Steps: $[60, 75, 90] \rightarrow [65, 80, 95]$, $[65, 80, 95] \rightarrow [60, 75, 90]$, $[60, 75, 90] \rightarrow [55, 70, 85]$, $[55, 70, 85] \rightarrow [60, 75, 90]$

The results of the *Chirp* Test (Protocol 3), are shown in Table 7.3. The symbols $\nearrow$ and $\searrow$ are used to specify the chirp period (**up** and **down**). The maximum value during the chirp is under the specification for all the levels.

Table 7.2: Simulation results for the YK-FIR algorithm - Step Changes in Frequency.

Level	**Step**	**Sequence 1**		**Sequence 2**		**Sequence 3**	
		N^2T ($\times 10^{-3}$)	**MV** ($\times 10^{-3}$)	**N^2T** ($\times 10^{-3}$)	**MV** ($\times 10^{-3}$)	**N^2T** ($\times 10^{-3}$)	**MV** ($\times 10^{-3}$)
1	**1**	17.1	22.2	16.7	15.7	39.3	23.8
	2	17.0	16.1	15.4	18.6	32.9	28.1
	3	46.2	18.7	14.2	15.1	15.5	21.1
	4	41.8	30.7	14.3	17.1	16.3	15.8
2	**1**	38.3	34.7	60.1	30.9	-	-
	2	36.2	30.4	66.7	40.3	-	-
	3	78.0	35.5	39.5	34.6	-	-
	4	70.1	39.1	39.4	29.4	-	-
3	**1**	154.7	52.5	180.2	51.5	-	-
	2	141.2	56.7	166.4	78.2	-	-
	3	253.5	62.5	136.2	56.0	-	-
	4	147.7	63.8	144.9	51.9	-	-

Table 7.3: Simulation results for the YK-FIR algorithm - Chirp Test.

Level	**MSE** ($\times 10^{-6}$)		**MV** ($\times 10^{-3}$)	
	$\nearrow$	$\searrow$	$\nearrow$	$\searrow$
1	14.5	14	13.9	14.9
2	42.5	42.1	19.4	19.9
3	93.1	87.6	39.4	42.3

YK-IIR Algorithm

From these results, the improvements of the YK-IIR algorithms are shown. In Protocol 1, at Level 1, the global attenuation, disturbance attenuation and transient duration specifications are fulfilled. The maximum amplification is achieved in almost all the cases, where the maximum value (the worst case) is at 75 Hz with an amplification of 7.0 dB w.r.t. the open loop response. Level 2 presents also good results, since only one case (at 50-70 Hz) shows a maximum amplification over the specified value. Finally, in Level 3, one sees the enhancements of this algorithm since all the tuning capabilities (GA, DA and MA) are fulfilled. Nevertheless, the transient duration for the last case (at 65-80-95 Hz) shows a fulfillment of 70% of this criterion.

Table 7.4: Simulation results for YK-IIR Algorithm - Simple Step Test.

	Frequency (Hz)	**GA (dB)**	**DA (dB)**	**MA (dB@Hz)**	**N^2T ($\times 10^{-3}$)**	**N^2R ($\times 10^{-3}$)**	**MV ($\times 10^{-3}$)**	**TD (%)**
Level 1	**50**	35.8	40.5	6.2@57.8	76.4	3.6	24.1	100
	55	35.4	44.8	4.6@48.5	55.5	3.7	35.2	100
	60	35.3	45.2	4.8@51.6	45.3	3.6	34.3	100
	65	34.9	49.7	5.4@54.7	40.7	3.7	33.8	100
	70	34.8	51.9	5.2@64.1	31.0	3.8	25.4	100
	75	34.8	48.5	7.0@68.8	21.4	3.8	21.9	100
	80	35.0	46.5	5.0@71.9	15.9	3.7	22.3	100
	85	34.5	44.4	3.9@75.0	15.9	3.7	22.3	100
	90	33.3	42.7	4.1@79.7	19.1	3.8	25.9	100
	95	29.5	38.4	5.4@85.9	21.0	4.2	32.9	100
Level 2	**50-70**	41.2	43.5-50.3	7.2@59.4	71.7	3.7	31.3	100
	55-75	40.9	47.6-49.5	6.1@67.2	51.6	3.8	31.9	100
	60-80	41.1	44.1-45.3	6.0@71.9	33.3	3.7	35.8	100
	65-85	40.6	45.8-44.2	5.9@75.0	28.9	3.8	38.2	100
	70-90	39.6	50.6-40.7	5.5@78.1	41.1	4.0	41.7	100
	75-95	37.9	50.0-43.0	6.0@87.5	50.4	4.2	45.8	100
Level 3	**50-65-80**	44.5	42.2-42.3-45.3	8.2@54.7	167.7	3.8	60.0	100
	55-70-85	43.7	45.5-45.4-43.4	6.6@64.1	138.6	4.0	71.4	100
	60-75-90	43.0	45.4-47.2-40.7	6.2@82.8	127.5	4.1	54.1	100
	65-80-95	42.5	45.7-42.3-43.4	6.4@89.1	125.8	4.0	61.4	70.80

For Protocol 2, the results are summarized in Table 7.5 for the three levels. The results of Protocol 3 are shown in Table 7.6. The symbols $\nearrow$ and $\searrow$ are used to specify the chirp period (**up** and **down**). The maximum value during the chirp is under the specification for all the levels.

Real-time Results

Using the xPC Target environment from MATLAB, the three protocols have been tested on the AVC system using the YK-FIR and YK-IIR algorithms, proposed in Sections 6.3 and 6.4, respectively. The results for the three levels are displayed.

Table 7.5: Simulation results for the YK-IIR algorithm - Step Changes in Frequency.

Level	Step	Sequence 1		Sequence 2		Sequence 3	
		$\mathbf{N^2T}$ ($\times\mathbf{10^{-3}}$)	MV ($\times\mathbf{10^{-3}}$)	$\mathbf{N^2T}$ ($\times\mathbf{10^{-3}}$)	MV ($\times\mathbf{10^{-3}}$)	$\mathbf{N^2T}$ ($\times\mathbf{10^{-3}}$)	MV ($\times\mathbf{10^{-3}}$)
1	**1**	19.5	23.1	19.4	24.2	41.6	23.9
	2	17.8	22.8	24.3	27.8	61.3	28.9
	3	24.6	26.0	18.6	25.5	22.2	25.6
	4	39.5	33.5	20.1	24.5	21.1	24.4
2	**1**	44.0	34.4	68.1	35.4	-	-
	2	40.6	32.7	86.1	37.9	-	-
	3	54.0	37.9	56.9	37.0	-	-
	4	60.8	41.7	50.0	34.9	-	-
3	**1**	128.7	68.4	170.3	59.1	-	-
	2	164.5	66.8	233.1	59.3	-	-
	3	105.5	61.0	123.7	63.7	-	-
	4	152.6	69.0	131.7	68.4	-	-

Table 7.6: Simulation results for the YK-IIR algorithm - Chirp Test.

Level	MSE ($\times\mathbf{10^{-6}}$)		MV ($\times\mathbf{10^{-3}}$)	
	↗	↘	↗	↘
1	6.0	8.0	8.8	12.0
2	29.1	49.6	17.4	25.0
3	37.9	58.2	20.0	32.3

YK-FIR Algorithm

Passing from simulation to real-time experiments, one notices a difference between the simulation and real-time results. For instance, in Table 7.7 at Level 1, GA for 75 and 85 Hz is below the specified value. DA for the frequency limits, 50 and 95 Hz, does not achieve the benchmark specification. Regarding to MA, all the cases are over the benchmark limit, with a maximum of 10.7 dB for the case of 85 Hz. The TD at 95 Hz achieves 64.6%. For Level 2, GA is fulfilled for all the cases. Instead, DA is achieved for all the cases, except at the vicinity of the low damped complex zeros, around 50 and 95 Hz. Here the MA shows a maximum value of 11.9 dB for the case of $[55, 75]$ Hz and the TD specification achieves only 90.1%. Finally, in the most important level (3), the YK-FIR algorithm in general fulfills all the benchmark specifications with some exceptions for DA. It is noted that for this level, the MA over pass slightly the specified value with a maximum of 9.4 dB for the case of $[50, 65, 80]$ HZ.

Results from Protocols 2 and 3 are summarized in Table 7.8 and Table 7.9, respectively. The maximum value during the chirp is under the specification for all the levels. As for the simulation results, the main analysis of these results is done with the help of the evaluation criteria.

Table 7.7: Real-time results for the YK-FIR algorihtm - Simple Step Test.

	Frequency (Hz)	**GA (dB)**	**DA (dB)**	**MA (dB@Hz)**	**N^2T ($\times 10^{-3}$)**	**N^2R ($\times 10^{-3}$)**	**MV ($\times 10^{-3}$)**	**TD (%)**
Level 1	**50**	34.6	38.5	9.8@65.6	14.5	4.9	13.9	100
	55	34.6	50.5	9.5@118.8	13.3	4.9	20.0	100
	60	33.3	49.5	8.2@79.7	14.7	5.2	21.2	100
	65	32.8	50.0	9.7@90.6	14.2	4.5	20.5	100
	70	30.5	47.9	9.0@89.1	14.7	4.9	23.0	100
	75	29.5	45.2	8.9@50.0	11.2	4.9	19.3	100
	80	30.3	48.7	8.5@95.3	8.1	4.2	21.1	100
	85	28.5	45.9	10.7@57.8	10.1	6.9	25.1	100
	90	28.0	42.7	8.2@73.4	17.1	6.9	25.1	100
	95	24.6	34.6	9.1@82.8	50.1	8.3	32.4	64.6
Level 2	**50-70**	34.4	33.6-42.9	8.3@59.4	32.1	9.4	29.0	100
	55-75	33.3	44.9-44.2	11.9@115.6	32.5	8.0	30.2	90.1
	60-80	33.4	45.6-41.7	8.8@118.8	31.4	7.1	29.0	100
	65-85	31.7	40.0-43.7	8.0@106.3	22.8	7.6	31.4	100
	70-90	32.9	41.4-38.6	7.5@59.4	21.4	6.0	33.9	100
	75-95	31.0	48.9-34.7	7.1@87.5	28.3	6.7	38.4	100
Level 3	**50-65-80**	41.7	38.4-46.9-42.4	9.4@117.2	250.8	6.2	81.9	100
	55-70-85	40.6	44.8-45.0-38.3	8.8@76.6	357.5	5.7	143.2	100
	60-75-90	37.7	44.7-46.4-43.9	6.7@82.2	338.8	7.2	139.5	100
	65-80-95	38.6	46.6-41.1-38.7	9.2@54.7	561.6	5.6	141.1	100

Table 7.8: Real-time results for the YK-FIR algorithm - Step Changes in Frequency.

		Sequence 1		**Sequence 2**		**Sequence 3**	
Level	**Step**	**N^2T ($\times 10^{-3}$)**	**MV ($\times 10^{-3}$)**	**N^2T ($\times 10^{-3}$)**	**MV ($\times 10^{-3}$)**	**N^2T ($\times 10^{-3}$)**	**MV ($\times 10^{-3}$)**
1	**1**	16.8	21.2	16.0	15.1	40.8	16.8
	2	16.8	19.3	15.5	18.7	30.7	23.7
	3	69.2	20.1	14.6	18.0	15.2	19.1
	4	46.1	33.4	14.2	18.7	16.0	14.3
2	**1**	38.6	35.2	66.5	32.7	-	-
	2	38.5	31.0	60.0	33.8	-	-
	3	117.3	40.1	42.6	35.2	-	-
	4	69.2	43.3	43.0	28.6	-	-
3	**1**	114.5	57.7	213.0	56.5	-	-
	2	186.3	61.2	181.0	68.5	-	-
	3	251.5	75.9	128.8	58.7	-	-
	4	224.6	67.5	150.0	54.0	-	-

Table 7.9: Real-time results for the YK-FIR algorithm - Chirp Test.

Level	**MSE** ($\times 10^{-6}$) ↗	**MSE** ($\times 10^{-6}$) ↘	**MV** ($\times 10^{-3}$) ↗	**MV** ($\times 10^{-3}$) ↘
1	13.7	13.9	15.0	15.0
2	41.3	42.4	21.6	21.2
3	93.1	90.8	41.7	37.9

YK-IIR Algorithm

Table 7.10: Real-time results for the YK-IIR algorihtm - Simple Step Test.

	Frequency (Hz)	**GA (dB)**	**DA (dB)**	**MA (dB@Hz)**	**N²T** ($\times 10^{-3}$)	**N²R** ($\times 10^{-3}$)	**MV** ($\times 10^{-3}$)	**TD (%)**
Level 1	**50**	34.5	40.3	9.3@62.5	111.3	6.8	30.7	92.2
	55	33.1	45.4	8.2@50.0	47.6	5.8	29.4	100
	60	33.3	45.6	6.8@125.0	27.5	5.1	20.9	100
	65	31.8	45.4	9.1@56.3	15.2	5.2	19.6	100
	70	29.9	45.6	8.1@131.3	13.6	5.6	20.8	100
	75	30.3	47.9	8.6@70.3	19.8	5.0	18.4	100
	80	29.5	48.6	7.7@6.3	13.4	5.3	20.9	100
	85	29.5	43.6	6.3@117.2	21.3	5.2	23.3	100
	90	29.1	43.7	7.5@117.2	18.1	5.0	23.4	100
	95	27.1	39.0	6.8@375.0	20.9	4.8	28.1	100
Level 2	**50-70**	38.2	40.9-43.9	10.3@64.1	99.3	6.8	30.9	100
	55-75	35.9	46.1-47.2	11.9@60.9	52.9	6.9	30.5	100
	60-80	37.8	45.6-45.9	7.9@70.3	38.0	5.1	34.2	100
	65-85	35.2	42.9-42.9	7.9@212.5	28.9	6.2	35.7	100
	70-90	36.1	43.7-44.9	10.0@115.6	42.8	5.2	39.3	100
	75-95	35.0	44.9-40.0	9.9@128.1	51.3	5.4	44.2	100
Level 3	**50-65-80**	40.1	38.3-39.7-43.7	8.9@125.0	151.5	7.2	50.2	100
	55-70-85	40.1	45.2-45.1-42.7	7.8@78.1	103.0	6.0	57.6	100
	60-75-90	38.7	45.2-42.2-43.3	10.8@78.1	105.3	6.4	79.7	100
	65-80-95	38.8	43.9-41.7-40.5	10.2@85.9	119.2	5.8	63.6	80.9

For the YK-IIR algorithm, there are also some differences passing from simulation to real-time experiments. For Level 1 at Table 7.10 for example, even though GA is fulfilled for all the cases, the MA shows values with a maximum in 9.3 dB (for a 50 Hz disturbance). Nevertheless, comparing with the previous result for YK-FIR, there is a reduction of 13% in this specification. The differences are also reflected in TD, since in the same case the fulfillment is of 92%. Level 2 presents also some differences, MA exceeds the specified value in all the cases with a maximum of 11.9 dB (for a 55-75 Hz disturbances), it is noticed that is the same maximum valued was achieved by the YK-FIR algorithm. But at Level 3, only two cases are over the limit in the MA (same as

YK-FIR algorithm), while the DA is not fulfilled only for the first case (50-65-80 Hz). For MA the maximum value obtained was 10.8, meaning that YK-FIR algorithm has a better performance w.r.t. this specification. TD for the last case (65-80-95 Hz) shows a fulfillment of 80.9%, due to the proximity of the low damped complex zeros.

Results from Protocols 2 and 3 are summarized in Table 7.11 and Table 7.12, respectively. The maximum value during the chirp is under the specification for all the levels. As for the simulation results, the main analysis of these results is done with the help of the evaluation criteria.

Table 7.11: Real-time results for the YK-IIR algorithm - Step Changes in Frequency.

Level	**Step**	**Sequence 1**		**Sequence 2**		**Sequence 3**	
		$\mathbf{N^2T}$ $(\times\mathbf{10^{-3}})$	**MV** $(\times\mathbf{10^{-3}})$	$\mathbf{N^2T}$ $(\times\mathbf{10^{-3}})$	**MV** $(\times\mathbf{10^{-3}})$	$\mathbf{N^2T}$ $(\times\mathbf{10^{-3}})$	**MV** $(\times\mathbf{10^{-3}})$
1	**1**	23.3	23.2	18.2	23.2	33.4	18.5
	2	22.2	25.7	21.3	23.4	57.7	26.8
	3	50.5	23.2	20.3	24.4	21.1	24.4
	4	48.0	36.8	19.8	22.0	19.3	20.1
2	**1**	47.6	37.9	66.6	40.6	-	-
	2	48.7	35.7	79.2	38.1	-	-
	3	65.0	37.9	59.3	35.4	-	-
	4	70.5	45.5	49.5	33.2	-	-
3	**1**	102.3	66.0	167.8	59.0	-	-
	2	145.6	68.8	237.7	60.2	-	-
	3	168.8	63.5	146.1	67.6	-	-
	4	125.9	65.2	143.5	66.0	-	-

Table 7.12: Real-time results - Chirp Test.

Level	**MSE** $(\times\mathbf{10^{-6}})$		**MV** $(\times\mathbf{10^{-3}})$	
	↗	↘	↗	↘
1	7.9	9.5	14.6	12.4
2	26.2	50.3	17.4	25.5
3	34.6	53.5	20.7	34.5

7.4 Comparative Evaluation

Using the evaluation criteria defined in A.1.2, a comparative evaluation of the performance, robustness and complexity of both algorithms is done. The results published in [Landau et al., 2013a] have been used to evaluate the FIR and IIR designs proposed in this thesis. The corresponding results for these algorithms are highlighted in **bold**, while the best results are highlighted in *italic*.

Performance Comparison

For the eight participants, the performance comparison in steady state is performed by means of the Benchmark Satisfaction Index defined in Eq. (A.5) and the Global criterion of steady state performance for each level (Eq. (A.4)). The simulation results are summarized in Table 7.13 and the real-time results in Table 7.14. The BSI concerning all the levels and contributors for simulation and real-time results is represented graphically in Fig. 7.1. Although in general, low values of J_{SS_k} indicate an "average" good performance, the BSI_k allows a better characterization of the performance w.r.t. the various benchmark specifications. The simulation results are relevant to indicate the capabilities of a design method to meet the benchmark specifications. It is also important to recall that the Level 3 of the benchmark is the most important.

Table 7.13: Benchmark Satisfaction Index for simulation results.

Participant	**LEVEL 1**		**LEVEL 2**		**LEVEL 3**	
	J_{SS_1}	BSI_1	J_{SS_2}	BSI_2	J_{SS_3}	BSI_3
AF	0.87	86.94%	1.77	76.33%	0.84	90.65%
CF	2.12	89.21%	5.02	72.89%	17.14	51.74%
KE	1.33	91.92%	3.42	76.13%	-	-
WB	0.11	98.31%	0.13	98.48%	0.18	98.01%
CT	*0.00*	*100.00%*	*0.00*	*100.00%*	*0.04*	*99.78%*
ACL	0.08	98.69%	0.11	98.38%	0.11	99.44%
YK-FIR	**0.50**	**93.30%**	**0.29**	**97.29%**	**0.17**	**99.13%**
YK-IIR	***0.09***	***99.07%***	***0.01***	***99.84%***	***0.00***	***100%***

The algorithm YK-IIR practically meets all the benchmark specifications for all the levels, according to the results in Table 7.13. The design method from [Chen and Tomizuka, 2013b] (denoted CT) shows an equivalent performance. The YK-FIR has a close performance, specially at the Level 3. Looking at Table 7.14, it is noticed that there are some differences between the simulation results and the real-time results. However, the YK-IIR algorithm remains among the best design methods. Through the real-time results, more exactly the difference between simulation and real-time results, one can characterize the robustness in performance w.r.t. uncertainties on design model and noise model.

The loss in performance is due the presence of uncertainties on the plant model and the noise used for simulations. The uncertainties mostly come from the difficulty of correctly identifying very low damped complex zeros. Nevertheless, with the procedure developed in Chapter 5 and with a more realistic noise sample, the performance loss was reduced but in order to be able to compare with the results in [Landau et al., 2013a] the same noise sample was used. To assess the performance loss, the *Normalized Performance Loss* and its global index are used. They are defined in Eqs. (A.6) and (A.7), respectively. Table 7.15 shows the results for this comparison. The YK-FIR algorithm has the second best result for Level 1, the best result for Levels 2 and 3. While, the YK-IIR obtains the best (lower) performance loss for Level 1, the third best result for Level 2 and the second best result for Level 3. With respect to global results, the YK-FIR is the best design method (7.62% of performance loss) and the YK-IIR is the second best design

Table 7.14: Benchmark Satisfaction Index for real-time results.

Participant	LEVEL 1		LEVEL 2		LEVEL 3	
	J_{SS_1}	BSI_1	J_{SS_2}	BSI_2	J_{SS_3}	BSI_3
AF	1.20	80.22%	2.04	73.58%	1.41	84.89%
CF	6.74	49.37%	11.01	29.08%	31.47	8.40%
KE	2.17	72.89%	7.43	44.33%	-	-
WB	1.31	83.83%	1.35	84.69%	1.34	91.00%
CT	*1.00*	*86.63%*	1.37	*86.65%*	1.45	92.52%
ACL	1.23	81.11%	*0.94*	*88.51%*	1.58	90.64%
YK-FIR	**1.35**	**80.87%**	**1.20**	***89.56%***	***0.43***	***97.56%***
YK-IIR	***0.68***	***89.37%***	***0.88***	***87.38%***	***0.42***	***96.39%***

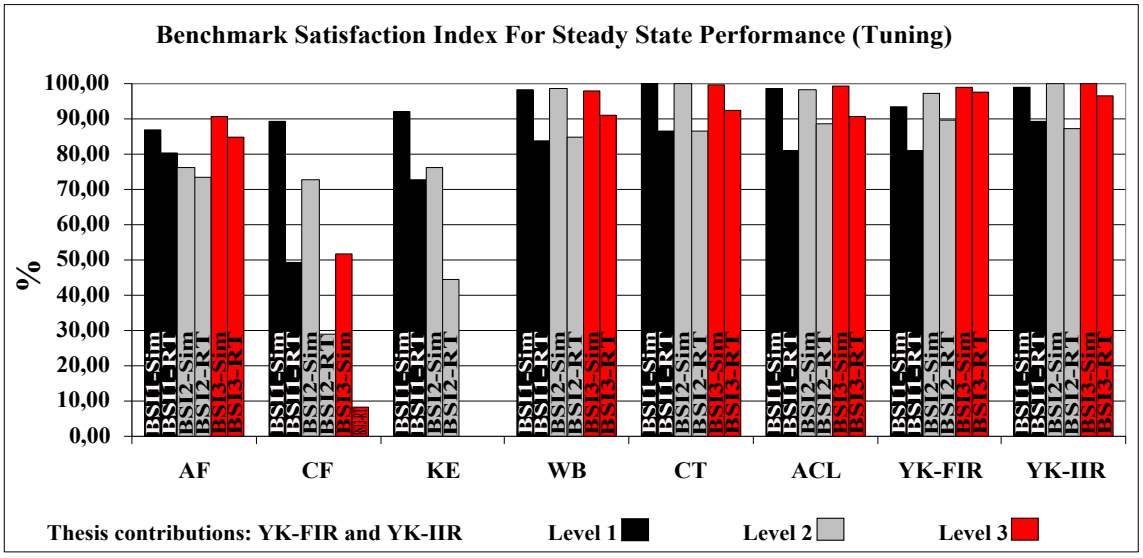

Figure 7.1: Benchmark Satisfaction Index (BSI) for all levels for simulation and real-time results.

method (8.63% of performance loss). This is graphically represented in Fig. 7.2. The contributions denoted as AF and CF are not taken into account since they have used different controllers for simulation and real-time.

The transient performance is evaluated for the three protocols. The Simple Step Test is evaluated through two criteria, transient duration evaluation and transient performance. Step Changes in Frequency Test and Chirp Test are evaluated only through the transient performance. The transient duration evaluation, defined in Eqs. (4.5) - (4.7), is evaluated using the global criterion (Eq. (A.8)) and the Benchmark Satisfaction Index for the transient evaluation, defined in (A.5). Through these criteria, the transient duration of the various design methods have been evaluated. The results are summarized in Table 7.16. The YK-IIR algorithm fulfills, both in simulation (Sim) and real-time (RT), the specification for Levels 1 and 2. Level 3 shows a little decrease in the performance but is still above 90% for simulation and real-time. Conversely, the YK-FIR algorithm has a better transient evaluation at Level 3, while the first two levels are above 95% (real-time results).

Table 7.15: Normalized Performance Loss for all the contributors.

Participant	NPL_1	NPL_2	NLP_3	NPL
AF	7.73%*	3.61%*	6.35%*	5.90%*
CF	44.66%*	60.11%*	83.77%*	62.85%*
KE	20.70%	41.77%	-	31.24%
WB	14.73%	14.01%	7.16%	11.96%
CT	13.37%	13.35%	7.28%	11.33%
ACL	17.81%	10.03%	8.85%	12.23%
YK-FIR	**13.32%**	***7.95%***	***1.58%***	***7.62%***
YK-IIR	***9.79%***	**12.48%**	**3.61%**	**8.63%**

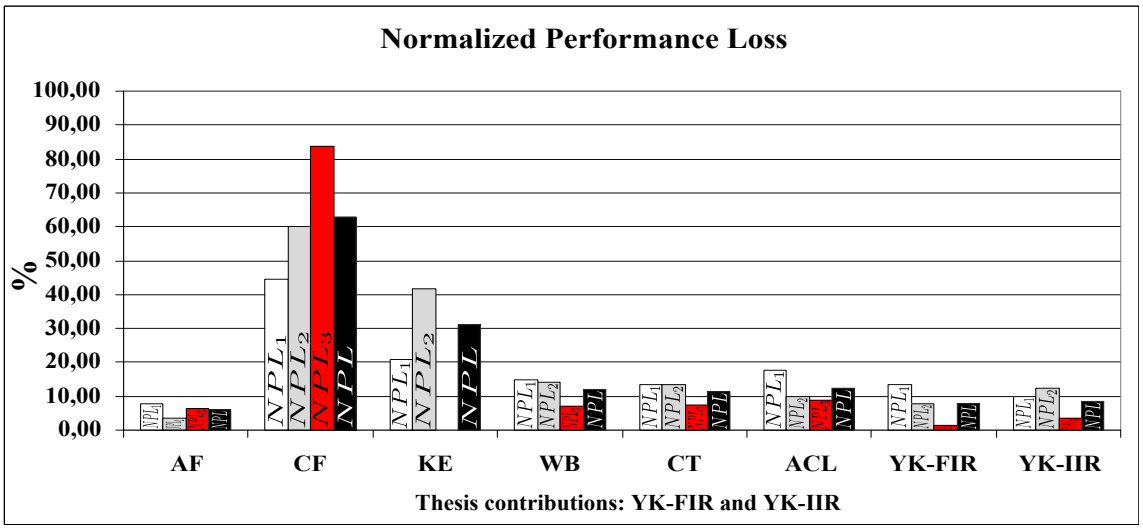

Figure 7.2: Normalized Performance Loss (NPL) for all levels (smaller = better).

Table 7.16: Benchmark Satisfaction Index for Transient Performance (for simple step test).

Index / Participant	$\mathbf{BSI_{Trans_1}}$		$\mathbf{BSI_{Trans_2}}$		$\mathbf{BSI_{Trans_3}}$	
	Sim	RT	Sim	RT	Sim	RT
AF	100%	100%	100%	100%	100%	100%
CF	100%	100%	100%	100%	100%	92.35%
KE	100%	97.69%	100%	91.79%	-	-
WB	100%	99.86%	94.85%	100%	100%	92.40%
CT	100%	100%	100%	100%	100%	100%
ACL	100%	99.17%	83.33%	100%	100%	100%
YK-FIR	**100%**	**96.45%**	**100%**	**95.74%**	**100%**	**100%**
YK-IIR	**100%**	**99.20%**	**100%**	**100%**	**92.74%**	**95.23%**

For the transient performance, the *Average global criterion for transient performance (one level)*, defined in Eq. (A.13), is used. The results are shown in Table 7.17 and graphically represented in Fig. 7.3. In this criterion, "lower values" means a better

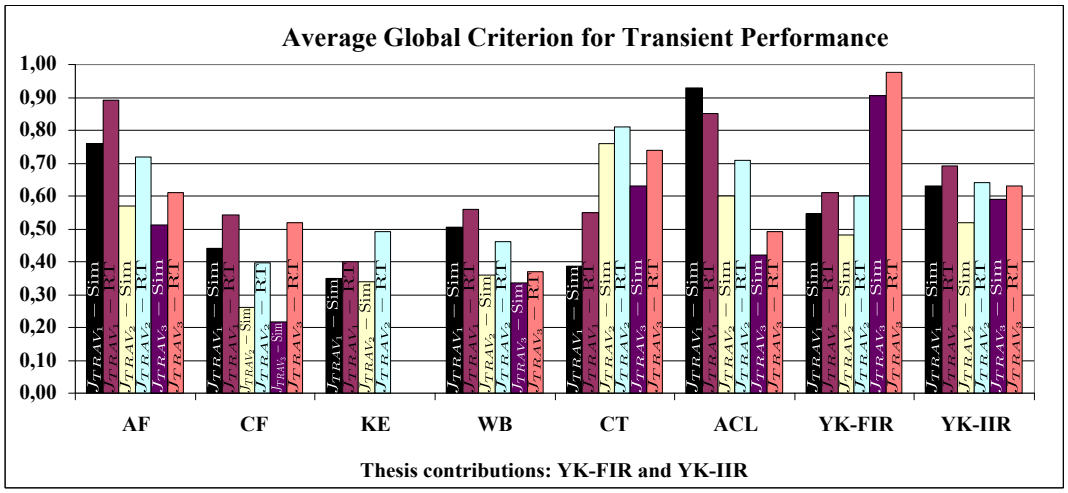

Figure 7.3: Average global criterion for transient performance (J_{TRAV}) for all levels (smaller = better).

performance. For levels 1 and 2, both algorithms, YK-FIR and YK-IIR, present almost the same performance along with WB and CF. In the third level, it is noticed that YK-IIR presents a better performance than the YK-FIR. This is due to the initial value of the adaptation gain. In general, the YK-IIR algorithm shows a good transient performance for all the levels.

Table 7.17: Average global criterion for transient performance.

Participant	$\mathbf{J_{TRAV_1}}$		$\mathbf{J_{TRAV_2}}$		$\mathbf{J_{TRAV_3}}$	
	Sim	**RT**	**Sim**	**RT**	**Sim**	**RT**
AF	0.76	0.89	0.57	0.72	0.51	0.61
CF	0.44	0.54	*0.26*	*0.40*	*0.22*	0.52
KE	*0.35*	*0.40*	0.34	0.49	-	-
WB	0.50	0.56	0.36	0.46	0.34	*0.37*
CT	0.39	0.55	0.76	0.81	0.63	0.74
ACL	0.93	0.85	0.60	0.71	0.42	0.49
YK-FIR	**0.55**	**0.61**	**0.48**	**0.60**	**0.90**	**0.98**
YK-IIR	**0.63**	**0.69**	**0.52**	**0.64**	**0.59**	**0.63**

Evaluation of the Complexity

The complexity is evaluated through the Task Execution Time (TET) from the xPC Target environment. A criterion for each test was defined in Eqs. (A.14) - (A.16). A global criterion for each level was defined in Eq. (A.17). The obtained results, measured in microseconds (μsec), are summarized in Table 7.18. The lower values (lower complexity) are highlighted. As expected, the YK-IIR algorithm presents a higher computation time and therefore, a higher complexity than the one obtained with the YK-FIR algorithm. This is due to the incorporation of the estimation of $A_Q(z^{-1})$. Nevertheless, the average computation time does not pass the 50 μsec, showing a very good balance between

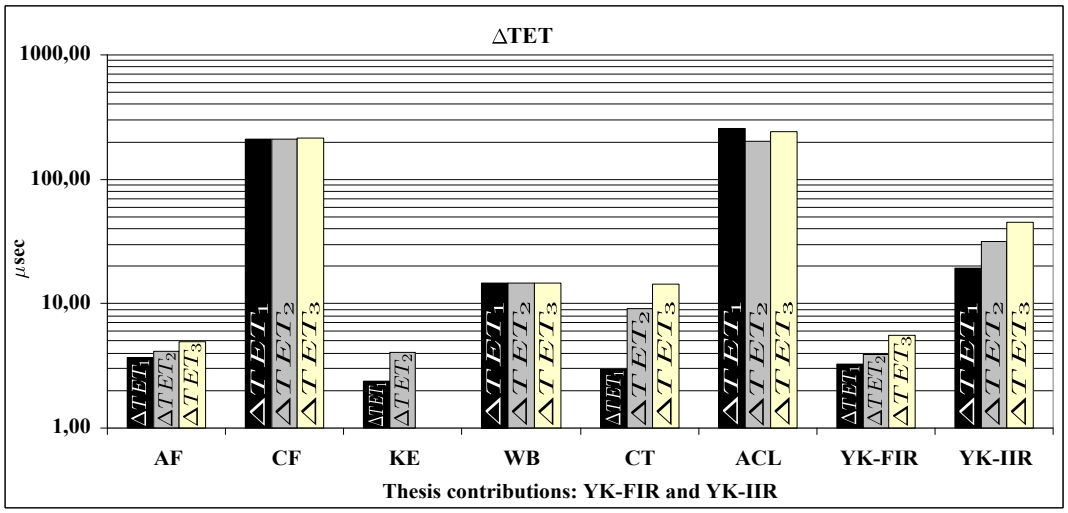

Figure 7.4: The controller average task execution time (ΔTET).

performance (represented in the BSI_k) and complexity. The results are represented graphically in Fig. 7.4.

Table 7.18: Task Execution Time.

Participant	ΔTET		
	L1	**L2**	**L3**
AF	3.71	4.18	*4.92*
CF	210.68	209.90	212.62
KE	*2.37*	4.08	-
WB	14.73	14.65	14.74
CT	2.96	9.11	14.27
ACL	254.24	203.83	241.22
YK-FIR	**3.26**	***3.90***	**5.60**
YK-IIR	**19.42**	**31.63**	**44.95**

Performance robustness with respect to a different experimental protocol test

In order to answer the question of what happens if the experimental protocols are changed, but maintaining the range of operation in the frequency domain, a new protocol for simple step test and step changes in frequency test was proposed. The (central) disturbance frequencies have been changed in terms of separation (in Hz) between disturbances and by considering non integer values. The disturbance frequencies for Level 2 are 61.5 Hz and 71.5 Hz and for Level 3, they are 61.5 Hz, 71.5 Hz and 81.5 Hz. Around these frequencies, variations of $\pm$ 5 Hz were considered for the sequences in the step changes in frequency test. For the YK-FIR algorithm, the simulation and real-time results are displayed in Table 7.19 and Table 7.20 for simple step and step frequency changes test, respectively. Tables 7.21 and 7.22 summarize the results for the YK-IIR algorithm.

Table 7.19: Simple Step Test - New Protocol Results for the YK-FIR algorithm.

Level		**GA (dB)**	**DA (dB)**	**MA (dB@Hz)**	**N^2T ($\times 10^{-3}$)**	**N^2R ($\times 10^{-3}$)**	**MV ($\times 10^{-3}$)**	**TD (%)**
2	Sim	36.2	42.8-43.0	10.0@85.9	32.0	4.1	35.7	100%
	RT	36.7	44.8-45.0	12.6@51.6	45.7	6.7	36.0	100%
3	Sim	41.9	45.8-47.1-45.9	12.4@50.0	81.5	5.3	76.1	100%
	RT	37.3	40.1-41.3-40.6	20.1@51.6	151.6	8.2	74.6	100%

Table 7.20: Step Changes in Frequency - New Protocol Results for the YK-FIR algorihtm.

Level	**Frequency (Hz)**	**N^2T ($\times 10^{-3}$)**		**MV ($\times 10^{-3}$)**	
		Sim	RT	Sim	RT
2	$[\mathbf{61.5}, \mathbf{71.5}] \rightarrow [\mathbf{66.5}, \mathbf{76.5}]$	76.1	69.8	22.9	27.8
	$[\mathbf{66.5}, \mathbf{76.5}] \rightarrow [\mathbf{61.5}, \mathbf{71.5}]$	59.1	68.7	27.2	31.5
	$[\mathbf{61.5}, \mathbf{71.5}] \rightarrow [\mathbf{56.5}, \mathbf{66.5}]$	45.8	47.7	25.7	27.8
	$[\mathbf{56.5}, \mathbf{66.5}] \rightarrow [\mathbf{61.5}, \mathbf{71.5}]$	45.7	47.7	20.9	25.3
3	$[\mathbf{61.5}, \mathbf{71.5}, \mathbf{81.5}] \rightarrow [\mathbf{66.5}, \mathbf{76.5}, \mathbf{86.5}]$	182.2	166.8	42.1	47.9
	$[\mathbf{66.5}, \mathbf{76.5}, \mathbf{86.5}] \rightarrow [\mathbf{61.5}, \mathbf{71.5}, \mathbf{81.5}]$	102.8	157.3	40.7	58.9
	$[\mathbf{61.5}, \mathbf{71.5}, \mathbf{81.5}] \rightarrow [\mathbf{56.5}, \mathbf{66.5}, \mathbf{76.5}]$	146.7	141.2	42.6	39.3
	$[\mathbf{56.5}, \mathbf{66.5}, \mathbf{76.5}] \rightarrow [\mathbf{61.5}, \mathbf{71.5}, \mathbf{81.5}]$	109.3	109.0	40.2	45.3

Table 7.21: Simple Step Test - New Protocol Results for the YK-IIR algorithm.

Level		**GA (dB)**	**DA (dB)**	**MA (dB@Hz)**	**N^2T ($\times 10^{-3}$)**	**N^2R ($\times 10^{-3}$)**	**MV ($\times 10^{-3}$)**	**TD (%)**
2	Sim	40.7	43.8-47.1	3.9@54.7	90.2	3.8	43.6	100%
	RT	37.0	41.0-40.4	8.0@135.9	59.9	5.7	31.7	100%
3	Sim	43.8	40.7-40.8-42.7	5.8@76.6	459.9	4.0	111.4	100%
	RT	39.2	36.9-35.4-41.2	5.6@65.6	214.6	6.2	66.1	100%

Through these new results, using the previous criteria, the Benchmark Satisfaction Index in this new test protocol is computed. The results are summarized in Table 7.23. With respect to the simulation results, the design methods denoted by CT, ACL and YK-IIR show the best performance index, while the YK-FIR shows lower values for this criterion w.r.t. previous results. The main drawback for the YK-FIR algorithm in this new test protocol is the maximum amplification, achieving 20.1 dB in the real-time experiment. This is highly penalized in the BSI_k as is shown in Table 7.23. However, when the real-time results are evaluated, the improvements of YK-IIR are evident by reaching a BSI for Level 2 of 95.24% while for Level 3, one obtains 95.72% of satisfaction, which are the highest values. This comparison is shown in Fig. 7.5.

Table 7.24 gives the BSI_{trans} for the case of the new protocol. The YK-IIR algorithm

Table 7.22: Step Changes in Frequency - New Protocol Results for the YK-IIR algorihtm.

Level	Frequency (Hz)	$\mathbf{N^2T}$ ($\times\mathbf{10^{-3}}$)		MV ($\times\mathbf{10^{-3}}$)	
		Sim	RT	Sim	RT
2	$[\mathbf{61.5}, \mathbf{71.5}] \rightarrow [\mathbf{66.5}, \mathbf{76.5}]$	55.8	47.5	38.2	35.5
	$[\mathbf{66.5}, \mathbf{76.5}] \rightarrow [\mathbf{61.5}, \mathbf{71.5}]$	53.0	64.3	41.3	40.5
	$[\mathbf{61.5}, \mathbf{71.5}] \rightarrow [\mathbf{56.5}, \mathbf{66.5}]$	52.9	62.1	38.9	41.6
	$[\mathbf{56.5}, \mathbf{66.5}] \rightarrow [\mathbf{61.5}, \mathbf{71.5}]$	57.0	54.1	40.3	41.6
3	$[\mathbf{61.5}, \mathbf{71.5}, \mathbf{81.5}] \rightarrow [\mathbf{66.5}, \mathbf{76.5}, \mathbf{86.5}]$	170.0	158.9	66.7	62.5
	$[\mathbf{66.5}, \mathbf{76.5}, \mathbf{86.5}] \rightarrow [\mathbf{61.5}, \mathbf{71.5}, \mathbf{81.5}]$	189.0	204.9	82.0	76.0
	$[\mathbf{61.5}, \mathbf{71.5}, \mathbf{81.5}] \rightarrow [\mathbf{56.5}, \mathbf{66.5}, \mathbf{76.5}]$	162.6	199.8	62.2	62.5
	$[\mathbf{56.5}, \mathbf{66.5}, \mathbf{76.5}] \rightarrow [\mathbf{61.5}, \mathbf{71.5}, \mathbf{81.5}]$	195.1	197.4	72.9	67.4

Table 7.23: Benchmark Satisfaction Index for the new protocol.

Participant	**LEVEL 2**				**LEVEL 3**			
	Simulation		**Real Time**		**Simulation**		**Real Time**	
	J_{SS_2}	BSI_2	J_{SS_2}	BSI_2	J_{SS_3}	BSI_3	J_{SS_3}	BSI_3
AF	4.55	57.78%	8.52	44.65%	5.26	61.62%	15.55	20.92%
CF	3.33	79.95%	16.75	14.55%	5.56	65.68%	16.14	5.13%
KE	5.39	68.76%	17.99	11.89%	-	-	-	-
WB	0.74	89.48%	1.68	76.00%	3.88	62.90%	33.79	0.00%
CT	*0.00*	*100%*	0.94	86.63%	0.81	95.96%	*0.70*	*95.05%*
ACL	*0.00*	*100%*	0.86	87.71%	*0.00*	*100%*	*0.69*	*92.30%*
YK-FIR	**1.01**	**85.57%**	**1.85**	**73.52%**	**1.14**	**87.30%**	**3.69**	**66.67%**
YK-IIR	***0.00***	***100%***	***0.33***	***95.24%***	***0.00***	***100%***	***0.86***	***95.72%***

does not show any change, passing from simulation to real-time. The fulfillment of the benchmark specification in this new protocol was achieved. Considering the previous results, the following remarks are made:

- The YK-IIR algorithm has shown one of the most robust performance with respect to a different experimental protocol test.
- The robustness of the scheme, based on the central controller and the selection of $A_Q(z^{-1})$, improves the results already obtained with the algorithm from Section 6.3. This can be verified through the comparison of Tables 7.15 and 7.23, where the YK-IIR algorithm shows one of the lowest performance loss (NPL) and one of the best Benchmark Satisfaction Index (BSI) in a different experimental protocol test.
- The complexity of the proposed YK-IIR algorithm is higher than the one of YK-FIR (Section 6.3). Nevertheless, compared with other design methods, the complexity of the proposed YK-IIR scheme can be considered as reasonable for implementation purposes.
- The transient performance is linked to the estimation of $A_Q(z^{-1})$. Faster estimations deliver faster transient behaviors.

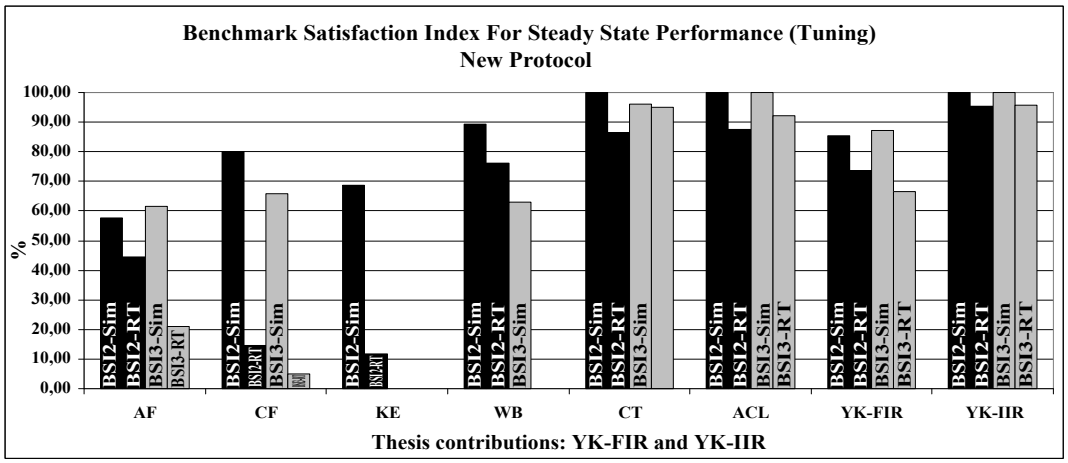

Figure 7.5: Comparison of the BSI for the new protocol.

- Despite the results, the algorithm given in Section 6.3 should not be considered obsolete. This scheme is easier and faster to implement and the stability is demonstrated. Also, it was shown that augmenting the number of parameters in the Q FIR filter would help to increase the robustness and performance of the adaptive controller.

Table 7.24: Benchmark Satisfaction Index for Transient Performance (for simple step test) in the new protocol.

Index / Participant	$\mathbf{BSI_{Trans_2}}$		$\mathbf{BSI_{Trans_3}}$	
	Simulation	Real Time	Simulation	Real Time
AF	100%	100%	100%	100%
CF	100%	100%	100%	100%
KE	100%	78.53%	-	-
WB	83.02%	100%	100%	100%
CT	100%	100%	0%	100%
ACL	100%	100%	100%	100%
YK-FIR	**100%**	**100%**	**100%**	**100%**
YK-IIR	**100%**	**100%**	**100%**	**100%**

7.5 Concluding Remarks

In this chapter, a comparative evaluation of the algorithms developed in Sections 6.3 and 6.4 was made. The evaluation has been done using the protocols, measurements and criteria of an international benchmark competition in adaptive regulation. The results show that the proposed algorithms have a good balance between performance, complexity and robustness.

During the international competition, the algorithm given in Section 6.3 (denoted YK-FIR) with the improved central controller design was tested and compared with different design methods. The enhancements allow to achieve one of the best performances with lower complexity and a good robustness against differences between the simulator and the

real system (uncertainties). The main drawback for this approach is that the waterbed effect becomes very difficult to minimize when the disturbance frequencies are close to each other (as proposed in the new test protocol).

Comparatively, the algorithm from Section 6.4, has proved that it can improve what was done by the YK-FIR algorithm in terms of robustness and performance. Nevertheless, the downside is the complexity (computation time) of in the scheme.

Chapter 8

Conclusions and Future Work

8.1 Overall Conclusions

The conclusions of this work have been classified according to each part of the thesis.

Parameter Uncertainty in Active Vibration Control Systems

The main concern of this part was the understanding of the influence of low damped complex zeros for active vibration control. The relevance of such zeros is due to the fact that they are often found in the mechanical structures of active vibration control systems.

For control purposes, it was shown that, even in a linear context, the presence of such zeros increases the difficulty for perfect rejection of narrow band disturbances through a feedback approach. Important robust constraints were derived from the analysis of the closed loop system. It was concluded that there is a link between the maximum value of the output sensitivity function and the reduction of the coprimeness between the plant zeros and the disturbance poles. In a Youla-Kučera parameterized controller, some improvements can be obtained, according to the selection of the Q-filter. Using a FIR filter, the undesirable effects of close location of low damped complex zeros and disturbances in the frequency domain can be attenuated either by means of the central controller or by increasing the number of parameters in the Q-filter. When a IIR filter is considered, the appropriated selection of the denominator further enhance the attenuation of such undesirable effects.

Concerning the system identification, it was shown that a closed loop identification procedure improves the estimation of the frequency and damping of low damped complex zeros. The improvements have been obtained by means of the redesigned controller, which enhance the output sensitivity function around the frequency regions critic for control, and a modified closed loop identification algorithm. The modification consisted in a initialization that allows to combine the advantages of algorithms such as F-CLOE and AF-CLOE. The results have shown that with this modification along with the controller, the closed loop model improves the open loop identified model, specially in frequency regions critical for control purposes.

Adaptive Feedback Disturbance Compensation

The focus of this part was to develop adaptive algorithms for feedback regulation of narrow band disturbances. The adaptive algorithms are based on the Internal Model Principle and the Youla-Kučera parametrization. Two solutions have been proposed, tested and evaluated. The first one is based on a previous work. The difference lies in the ***new***

design of the central controller. It was shown that the appropriately selection of the closed loop poles can improve the robustness of the control scheme in the presence of low damped complex zeros. With the proposed design, the modulus margin was controlled for the entire frequency region of interest, allowing total rejection along with a robust behavior.

The second algorithm has been developed with the aim of improving the previous results and avoiding a specific selection of the closed loop poles for the central controller. An IIR Q-filter is used for the development. In a first stage, the disturbance model is estimated and then, used for the computation of the denominator of the IIR filter. This allows to introduce a pair of stable complex poles at the same frequency as that of the disturbance. This drastically reduces the waterbed effect of the IMP over the output sensitivity function. The IMP is incorporated by means of the numerator of the IIR filter. Unlike other indirect adaptive approaches, neither frequency estimation is required nor the solution of matrix equations. The result is a mixed direct/indirect adaptive algorithm. The results have shown that this algorithm obtains better performance and robustness results with a slightly increase in the computational load. In addition it needs sensible less computer power that the indirect approach, e.g. [Airimiţoaie et al., 2013].

8.2 Future Work and Prospect

The main objective of this thesis was to develop and test Active Vibration Control algorithms; however, these algorithms are also applicable to Active Noise Control. Considering that in sound applications, the sampling frequency is around $20,000$ Hz, these algorithms should be implemented in a fast-array way, which requires a specific implementation work.

For the development of the algorithms, it was assumed that the *plant model = true model*, and that possible little variations in the plant parameters are handled by the robust central controller. There are however situations where the characteristics of the compensator system may change in time and procedure for simultaneously adaptation with respect to disturbance and plant variations should be developed.

Even though in this work the adaptive feedforward compensation problem is not addressed, it would be interesting to deduce the conditions and to develop algorithms that allow an integration between an adaptive feedback scheme and an adaptive feedforward. This would allow to reject time-varying broad band and narrow band disturbances simultaneously.

Appendix A

Benchmark Critera for Chapter 7

A.1 International Benchmark in Adaptive Regulation - Criteria for comparison

A.1.1 Control specifications

As mentioned in Chapter 4, the narrow band disturbances are located in the range from 50 to 95 Hz. There are three levels of difficulty corresponding to one, two or three unknown time varying narrow band disturbances:

- *Level 1:* Rejection of a single time varying sinusoidal disturbance within 50 and 95 Hz.
- *Level 2:* Rejection of two time varying sinusoidal disturbances within 50 and 95 Hz.
- *Level 3:* Rejection of three time varying sinusoidal disturbances within 50 and 95 Hz.

The control objectives for all levels are summarized in Table A.1. Level 3 is particularly difficult in terms of tolerated amplification (at other frequencies than those of the disturbances) and transient requirements. The difference w.r.t. the control objectives settled in Section 4.1 is that the frequency of the disturbances is considered unknown and possibly time-varying. The measurements defined in Eqs. (4.1) through (4.9) are used in this chapter. Also, the transient performance in a time-varying frequency context will be evaluated.

In order to test the required performances, 3 protocols have been defined:

- **Protocol 1.** Tuning capabilities: Evaluation in steady state operation after application of the disturbance once the adaptation settles. *This is the most*

Table A.1: Control specifications in the frequency domain.

Control specifications	Level 1	Level 2	Level 3
Transient duration	≤ 2 s	≤ 2 s	≤ 2 s
Global attenuation	≥ 30 dB	≥ 30 dB	≥ 30 dB
Minimum disturbance attenuation	≥ 40 dB	≥ 40 dB	≥ 40 dB
Maximum amplification	≤ 6 dB	≤ 7 dB	≤ 9 dB
Chirp speed	10 Hz/s	6.25 Hz/s	3 Hz/s
Maximum value during chirp	≤ 0.1 V	≤ 0.1 V	≤ 0.1 V

important aspect of the benchmark. Test 1: The steady state performance in the time domain is evaluated by measuring the truncated 2-norm of the residual force which is compared with the value of the residual in open loop (providing a measure of the global attenuation). Test 2: Power spectral density performances. For constant frequency disturbances, once the adaptation transient is settled, the performance with respect to the open loop is evaluated as follows:
  - Attenuation of the disturbance (w.r.t. the open loop) should be larger than the specified value.
  - Amplification at other frequencies (w.r.t. the open loop) should be less than the specified value.
- **Protocol 2.** Transient performance in the presence of disturbances. The frequencies of the disturbances around specified central values are changed by $\pm$ 5 Hz. An upper bound for the duration of the adaptation transient is imposed (2 sec). However, it was not possible to define a reliable test for measuring the duration of the transient for Test 2. The quantities which have been measured for the purpose of performance evaluation are:
  - the truncated 2-norm of the residual force over a time horizon;
  - the maximum value of the residual force during transient.
- **Protocol 3.** Chirp changes in frequency. Linear time varying frequency changes between two situations are considered. The maximum value of the residual force during the chirp has been measured as well as the mean square value of the residual force. The loop is closed before the disturbances are applied for all the above tests.

Supplementary test:
- The operation of the system should remain stable for all the levels when one, two or three sinusoidal disturbances are applied simultaneously.
- The operation of the loop should remain stable if the disturbance is applied simultaneously with the closing of the loop.

A.1.2 Evaluation Criteria

The results of each group will be evaluated with respect to the benchmark specifications. However, for some performance indices no bounds have been set in the benchmark and the comparison will be done between the various indices obtained. To summarize, two types of criteria will be considered:
- criteria for taking into account the fact that not all the specifications have been satisfied (when applicable),
- normalized quantitative criteria for comparison of performance indices for which benchmark specifications were not available.

Evaluation of the performances will be done for both simulation and real-time results. The simulation results give us information upon the potential of the design method under the assumption: *design model = true plant model.* The real-time results tell us in addition what is the robustness of the design with respect to plant model uncertainties and real noise. These criteria are given in the sequel.

Steady State Performance (Tuning capabilities)

As mentioned earlier, these are the most important performances. Only if a good tuning for the attenuation of the disturbance can be achieved, it makes sense to examine the

transient performance of a given scheme. For the steady state performance, which is evaluated only in the *simple step test*, the variable k, with $k = 1, \ldots, 3$, will indicate the *level* of the benchmark. In several criteria, the mean of certain variables will be considered. The number of distinct experiments, M, is used to compute the mean. This number depends upon the level of the benchmark as follows:

$$\begin{aligned} M &= 10, \quad \text{if} \quad k = 1 \\ M &= 6, \quad \text{if} \quad k = 2 \\ M &= 4, \quad \text{if} \quad k = 3 \end{aligned}$$

The performances can be evaluated with respect to the benchmark specifications. The benchmark specifications will be in the form: XXB, where XX will denote the evaluated variable and B will indicate the benchmark specification. ΔXX will represent the error with respect to the benchmark specification.

Global Attenuation - GA

The benchmark specification corresponds to $GAB_k = 30$ dB, for all the levels and frequencies, except for 90 Hz and 95 Hz at $k = 1$, for which GAB_1 is 28 dB and 24 dB respectively.

Error:

$$\begin{aligned} \Delta GA_i &= GAB_k - GA_i \quad \text{if} \quad GA_i < GAB_k \\ \Delta GA_i &= 0 \quad \text{if} \quad GA_i \geq GAB_k \end{aligned}$$

with $i = 1, \ldots, M$.

Global Attenuation Criterion

$$J_{\Delta GA_k} = \frac{1}{M} \sum_{j=1}^{M} \Delta GA_i \tag{A.1}$$

Disturbance Attenuation - DA

The benchmark specification corresponds to $DAB = 40$ dB, for all the levels and frequencies.

Error:

$$\begin{aligned} \Delta DA_{ij} &= DAB - DA_{ij} \quad \text{if} \quad DA_{ij} < DAB \\ \Delta DA_{ij} &= 0 \quad \text{if} \quad DA_{ij} \geq DAB \end{aligned}$$

with $i = 1, \ldots, M$ and $j = 1, \ldots, j_{max}$, where $j_{max} = k$.

Disturbance Attenuation Criterion

$$J_{\Delta DA_k} = \frac{1}{M} \sum_{i=1}^{M} \sum_{j=1}^{j_{max}} \Delta DA_{ij} \tag{A.2}$$

Maximum Amplification - MA

The benchmark specifications depend on the level, and are defined as

$$\begin{aligned} MAB_k &= 6 \text{ dB}, \quad \text{if} \quad k = 1 \\ MAB_k &= 7 \text{ dB}, \quad \text{if} \quad k = 2 \\ MAB_k &= 9 \text{ dB}, \quad \text{if} \quad k = 3 \end{aligned}$$

Error:

$$\begin{aligned} \Delta MA_i &= MA_i - MAB_k, \quad \text{if} \quad MA_i > MAB_k \\ \Delta MA_i &= 0, \quad \text{if} \quad MA_i \leq MAB_k \end{aligned}$$

with $i = 1, \ldots, M$.

Maximum Amplification Criterion

$$J_{\Delta MA_k} = \frac{1}{M} \sum_{i=1}^{M} \Delta MA_i \tag{A.3}$$

Global criterion of steady state performance for one level

$$J_{SS_k} = \frac{1}{3}[J_{\Delta GA_k} + J_{\Delta DA_k} + J_{\Delta MA_k}] \tag{A.4}$$

Benchmark Satisfaction Index (BSI) for Steady State Performance

Following the procedure for the *robust digital control benchmark* [Landau et al., 1995], a *Benchmark Satisfaction Index* can be defined. The BSI is a performance index computed from the *average* criteria $J_{\Delta GA_k}$, $J_{\Delta DA_k}$ and $J_{\Delta MA_k}$. The *Benchmark Satisfaction Index* is 100%, if these quantities are "0" (full satisfaction of the benchmark specifications) and it is 0% if the corresponding quantities are half of the specifications for GA, and DA or twice the specifications for MA. The corresponding reference error quantities are summarized below:

$$\begin{aligned} \Delta GA_{index} &= 15, \\ \Delta DA_{index} &= 20, \\ \Delta MA_{index,1} &= 6, \quad \text{if} \quad k = 1, \\ \Delta MA_{index,2} &= 7, \quad \text{if} \quad k = 2, \\ \Delta MA_{index,3} &= 9, \quad \text{if} \quad k = 3. \end{aligned}$$

The computation formulas are

$$\begin{aligned} GA_{index,k} &= \left(\frac{\Delta GA_{index} - J_{\Delta GA_k}}{\Delta GA_{index}} \right) 100\% \\ DA_{index,k} &= \left(\frac{\Delta DA_{index} - J_{\Delta DA_k}}{\Delta DA_{index}} \right) 100\% \\ MA_{index,k} &= \left(\frac{\Delta MA_{index,k} - J_{\Delta MA_k}}{\Delta MA_{index,k}} \right) 100\%. \end{aligned}$$

Then, the *Benchmark Satisfaction Index* (BSI), is defined as

$$BSI_k = \frac{GA_{index,k} + DA_{index,k} + MA_{index,k}}{3} \tag{A.5}$$

Robustness with respect to model uncertainties

As mentioned earlier, there are uncertainties on the plant model used for design. These uncertainties come mostly from the difficulty of correctly identifying very low damped complex zeros. The identification results concerning the low damped complex zeros are influenced by the level of noise. When carrying out the test for the benchmark competition, the noise was different in the simulator with respect to the real system. This sample of the noise has been used for the simulations of the proposed algorithm from Section 6.4, in order to be able to compare the simulation results, however, a more realistic noise sample is available for simulation purposes. An important point is to assess the robustness in performance for those which use the same controller in simulation and in real time. This will be done by defining the *Normalized Performance Loss* (NPL).

For each level one defines the *Normalized Performance Loss* as:

$$NPL_k = \left(\frac{BSI_{ksim} - BSI_{kRT}}{BSI_{ksim}}\right) 100\% \tag{A.6}$$

and the global NPL is given by

$$NPL = \frac{1}{N}\sum_{k=1}^{N} NPL_k \tag{A.7}$$

where $N = 3$ for all the participants except for Karimi *et al.* (KE), who provided only solutions for levels 1 and 2; for them, $N = 2$.

Transient Performance

Transient performances will be evaluated for

- Simple Step Test (application of the disturbance).
- Step Changes in the frequencies.
- Chirp Changes in the frequencies.

We will consider first the case of the *simple step test*.

Simple Step Test

The transient evaluation for the simple step test was defined in Section 4.1 through Eqs. 4.5 - (4.7). For each experiment a $\Delta Trans_i$ has been computed with $i = 1, \ldots, M$. The global criterion for the transient evaluation is defined as

$$J_{\Delta Trans_k} = \frac{1}{M}\sum_{i=1}^{M} \Delta Trans_i, \tag{A.8}$$

and the Benchmark Satisfaction Index for the transient evaluation is defined as

$$BSI_{Trans_k} = \left(\frac{1.21 - J_{\Delta Trans_k}}{1.21}\right) 100\% \qquad k = 1, \ldots, 3 \tag{A.9}$$

where M is given by

$$\begin{aligned} M &= 10, \quad \text{if} \quad k = 1 \\ M &= 6, \quad \text{if} \quad k = 2 \\ M &= 4, \quad \text{if} \quad k = 3 \end{aligned}$$

The transient performances have been further investigated in order to compare the various approaches. Simple step test, step changes in frequencies and chirp tests have been considered. Two quantities have been defined.

- The truncated 2-norm of residual force N^2T.
- Maximum value during transient MV.

Note: In order to introduce the "normalized" criteria (maximum value = 1), one has to define for these 2 quantities the $(Max)_{\max}$ within the results provided by all the participants. These quantities will be called $(J^U_{NT_k})_{\max}$, $(J^U_{MV_k})_{\max}$, where "U" stands for *un-normalized*.

$$J^U_{NT_k} = \frac{1}{M}\sum_{i=1}^{M} N^2T(i), \qquad J^U_{MV_k} = \frac{1}{M}\sum_{i=1}^{M} MV(i)$$
$$J_{NT_k} = \frac{J^U_{NT_k}}{(J^U_{NT_k})_{\max}}, \qquad J_{MV_k} = \frac{J^U_{MV_k}}{(J^U_{MV_k})_{\max}}$$

where M is given by

$$M = 10, \quad \text{if} \quad k = 1$$
$$M = 6, \quad \text{if} \quad k = 2$$
$$M = 4, \quad \text{if} \quad k = 3$$

Global criterion for transient evaluation for simple step test

$$J_{TR_k} = \frac{1}{2}\left[J_{NT_k} + J_{MV_k}\right] \tag{A.10}$$

Step Changes in Frequencies Test

Only the truncated 2-norm of the residual force and the maximum value during transient will be considered (case similar to the simple step test). The corresponding criteria are given below.

$$J^U_{SNT_k} = \frac{1}{M}\sum_{i=1}^{M} N^2T_i, \qquad J^U_{SMV_k} = \frac{1}{M}\sum_{i=1}^{M} MV_i$$
$$J_{SNT_k} = \frac{J^U_{SNT_k}}{(J^U_{SNT_k})_{\max}}, \qquad J_{SMV_k} = \frac{J^U_{SMV_k}}{(J^U_{SMV_k})_{\max}}$$

where M is given by

$$M = 12, \quad \text{if} \quad k = 1$$
$$M = 8, \quad \text{if} \quad k = 2$$
$$M = 8, \quad \text{if} \quad k = 3$$

Global criterion for transient performance evaluation - step changes in frequencies

$$J_{STR_k} = \frac{1}{2}\left[J_{SNT_k} + J_{SMV_k}\right] \tag{A.11}$$

Chirp Test

As for the Step Frequencies Changes , the maximum values among all the participants will be used to normalize the results. For each level, two measurements have been done for:

- Mean Square of the residual force (MSE),
- Maximum Value of the residual force (MV),

during the periods of application of the chirp. They are denoted by **up** when the frequencies increase and **down** when the frequencies decrease.
One defines the criterion for the mean square error (for each level) for all the levels ($k = 1, \ldots, 3$) as follows[1]

$$J^U_{MSE_k} = \frac{1}{2}\left[MSE_{up} + MSE_{down}\right]$$
$$J_{MSE_k} = \frac{J^U_{MSE_k}}{(J^U_{MSE_k})_{\max}}$$

The benchmark specifications for the *maximum value* were far too conservative. However, a comparison between the various approaches has to be done. For the maximum value, one defines the criterion

$$J^U_{MV_k} = \frac{1}{2}\left[MV_{up} + MV_{down}\right]$$
$$J_{MV_k} = \frac{J^U_{MV_k}}{(J^U_{MV_k})_{\max}}$$

Global criterion for chirp disturbance

$$J_{chirp_k} = \frac{1}{2}\left[J_{MSE_k} + J_{MV_k}\right] \tag{A.12}$$

Average Global criterion for transient performance (one level)

An average global criterion for the transient performance is defined for each level as:

$$J_{TRAV_k} = \frac{1}{3}[J_{TR_k} + J_{STR_k} + J_{chirp_k}] \tag{A.13}$$

Evaluation of the complexity

For complexity evaluation, the measure of the *Task Execution Time* (TET) in the xPC Target environment will be used. This is the time required to perform all the calculations on the host target PC for each method. Such process has to be done on each sample time. The more complex is the approach, the bigger is the TET. One can argue that the TET depends also on the programming of the algorithm. However this will may change the TET by a factor of 2 to 4 but not by an order of magnitude. The xPC Target MATLAB environment delivers an *average* of the TET ($ATET$). It is however interesting to assess the TET specifically associated to the controller by subtracting from the measured TET in closed loop operation, the average TET in open loop operation.

[1]The results are exactly the same for the normalized values J_{MSE_k}if one uses N^2T instead of MSE.

To compare the complexity between all the approaches, the following criteria are defined.

$$\Delta TET_{Simple,k} = ATET_{Simple,k} - ATET_{OL_{Simple,k}}, \tag{A.14}$$

$$\Delta TET_{Step,k} = ATET_{Step,k} - ATET_{OL_{Step,k}}, \tag{A.15}$$

$$\Delta TET_{Chirp,k} = ATET_{Chirp,k} - ATET_{OL_{Chirp,k}}, \tag{A.16}$$

where $k = 1, \ldots, 3$. The symbols *Simple, Step* and *Chirp* are associated respectively to Simple Step Test (application of the disturbance), Step Changes in Frequency and Chirp Changes in Frequency.

The global ΔTET_k for one level is defined as the average of the above computed quantities:

$$\Delta TET_k = \frac{1}{3}\left(\Delta TET_{Simple,k} + \Delta TET_{Step,k} + \Delta TET_{Chirp,k}\right) \tag{A.17}$$

where $k = 1, \ldots, 3$.

Performance robustness with respect to a different experimental protocol test

The benchmark specifications have been measured under pre-specified experimental protocols in terms of: 1) values of frequencies, 2) difference in frequency between two neighbor disturbances, 3) time of application of the disturbances and 4) magnitude of the step changes in frequencies. An obvious question is: what happens if the experimental protocols are changed (but maintaining the range of operation in the frequency domain)? Since the algorithm is adaptive, these changes should not have too much influence upon the results.

Only two tests have been conducted for each participant, *Simple Step Test* and *Step Changes in Frequency Test*. Only the Levels 2 and 3 of the benchmark are considered. In the original protocol, the separation (in Hz) between the sinusoidal disturbances was 20 Hz for Level 2 and 15 Hz for Level 3. For this *new* protocol, 10 Hz of separation is considered both for Level 2 and 3. The (central) frequencies chosen (expressed in Hz) are in addition non integers[2] with the following values:

- 61.5 Hz − 71.5 Hz for Level 2.
- 61.5 Hz − 71.5 Hz − 81.5 Hz for Level 3.

For *Simple Step Test*, only the central frequencies are applied while for *Step Changes in Frequencies Test*, variations of $+/-$ 5 Hz of the central frequencies are considered (as in the benchmark protocol, in order to compare transient results).

The application time of the first disturbance was changed from 5 seconds to 3.75 seconds for both tests, but the duration of the steps in frequencies was kept at 3 seconds, in order to be able to compare the new transient results with the previous results. The previous measurements defined in Section 4.1 and the criteria from A.1.2 have been used.

For more details, the reader is encouraged to see `http://www.gipsa-lab.grenoble-inp.fr/~ioandore.landau/benchmark_adaptive_regulation/index.html`.

[2]In the benchmark protocols, only integer values have been considered.

Appendix B

Direct Adaptive Rejection of Unknown Time-varying Narrow Band Disturbances applied to a Benchmark Problem

Authors: Abraham Castellanos Silva, Ioan Doré Landau and Tudor-Bogdan Airimiţoaie
Journal: European Journal of Control 19(4) (2013) 326–336
Type of submission: Regular paper

European Journal of Control 19 (2013) 326–336

Contents lists available at SciVerse ScienceDirect

European Journal of Control

journal homepage: www.elsevier.com/locate/ejcon

Direct adaptive rejection of unknown time-varying narrow band disturbances applied to a benchmark problem

Abraham Castellanos Silva [a], Ioan Doré Landau [a,*], Tudor-Bogdan Airimiţoaie [a,b]

[a] Control system department of GIPSA-lab, St. Martin d'Héres, 38402, France
[b] Faculty of Automatic Control and Computers, University "Politehnica" of Bucharest, Bucharest 060042, Romania

ARTICLE INFO

Article history:
Received 27 December 2012
Accepted 5 May 2013
Recommended by A. Karimi/D.W. Clarke
Available online 9 May 2013

Keywords:
Adaptive regulation
Active vibration control
Inertial actuators
Multiple narrow band disturbances
Youla–Kučera parametrization
Internal model principle

ABSTRACT

The paper presents a direct adaptive algorithm for the rejection of unknown time-varying narrow band disturbances, applied to an adaptive regulation benchmark. The objective is to minimize the residual force by applying an appropriate control signal on the inertial actuator in the presence of multiple and/or unknown time-varying disturbances. The direct adaptive control algorithm is based on the internal model principle (IMP) and uses the Youla–Kučera (YK) parametrization. A direct feedback adaptive regulation is proposed and evaluated both in simulation and real-time. The robustness is improved by shaping the sensitivity functions of the system through band stop filters (BSF).

1. Introduction

The problem posed by this benchmark [15] is the attenuation (rejection) of multiple narrow band disturbances of unknown and time-varying frequencies without measuring them. The energy of these disturbances (or vibrations) is concentrated in narrow bands around some unknown frequencies and could be modelled as a white noise or a Dirac impulse passed through a *model of the disturbance*. While, in general, one can assume a certain structure for such *model of disturbance*, its parameters are unknown and may be time-varying. The need of an adaptive approach arises.

A *feedback* approach can provide disturbance rejection (at least asymptotically), using the measurement of the residual force (acceleration) as in [1,2,17]. In this benchmark as well as in many other applications one can consider that a model of the compensator system (which includes the actuator providing disturbance compensation capabilities) is available (obtained in general by system identification). This model is in general time invariant even if one has to consider that uncertainties in the model may be present in certain frequency regions. The approach which is proposed for solving the benchmark problem belongs to the class of solutions using the internal model principle (IMP) [1,2,5,9–12,17,23,24]. Other related references are [6,7,4,20,21,8]. Since the model of the disturbance is considered unknown, an adaptive configuration has to be considered. *Direct* or *indirect* adaptive regulation schemes can be built.

Through the use of the Youla–Kučera (YK) parametrization of the controller and the Internal Model Principle (IMP) a direct adaptive regulation scheme can be built. Direct adaptive schemes are simpler and require less computational time than indirect schemes. They provide in general excellent adaptation transients and stability proofs are available for realistic operational conditions [17]. This approach has been successfully used in a number of applications [17,16,13], and therefore has been considered to be applied to the benchmark.

The YK parametrization (known also as the Q-parametrization) allows to insert and adjust the internal model of the disturbance into the controller by adjusting the parameters of the polynomial $\hat{Q}(z^{-1})$ (see Fig. 1). This is done without recomputing the *central controller* ($R_0(z^{-1})$ and $S_0(z^{-1})$ in Fig. 1 remain unchanged). The number of parameters to be directly adapted is roughly equal to the number of parameters in the denominator of the disturbance model. This means that the size of the adaptation algorithm will depend upon the complexity of the disturbance model and not upon the complexity of the plant model. It is also important to remind that feedback compensation of the disturbances can be done only in the frequencies region where the plant (the compensator system) has enough gain [16].

* Corresponding author.
E-mail addresses: abraham.castellanos-silva@gipsa-lab.grenoble-inp.fr (A. Castellanos Silva), ioan-dore.landau@gipsa-lab.grenoble-inp.fr (I.D. Landau), tudor-bogdan.airimitoaie@gipsa-lab.grenoble-inp.fr (T.-B. Airimiţoaie).

0947-3580/$ - see front matter © 2013 European Control Association. Published by Elsevier Ltd. All rights reserved.
http://dx.doi.org/10.1016/j.ejcon.2013.05.012

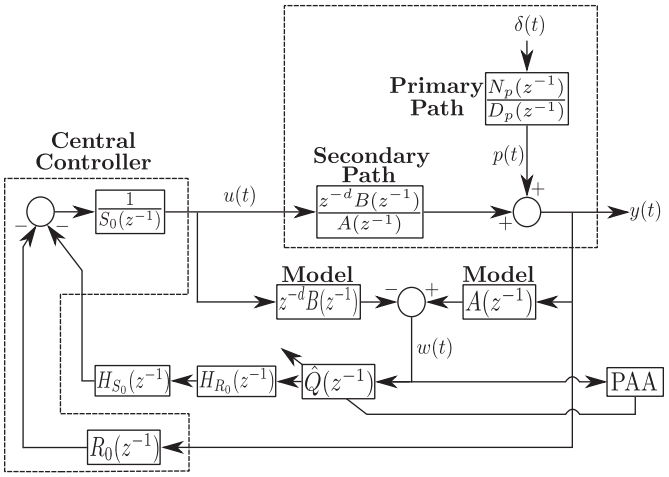

Fig. 1. Direct adaptive regulation scheme for rejection of unknown disturbances.

The major problem encountered with this approach is the design of the central controller such that for any internal model of the disturbances (i.e. for all possible values of the frequencies of the disturbances) within the range of frequencies considered, good robustness of the system (modulus margin, delay margin, low magnitude of input sensitivity function outside the region of compensation) is assured as well as a low amplification at other frequencies than those of the disturbances (one need to get a flat "water bed" effect). The problem becomes even more difficult when there are several narrow band disturbances to be compensated simultaneously which is the case for levels 2 and 3 of the benchmark. One of the main original contributions of this paper is a methodology for the design of the central controller for the case of multiple narrow band disturbances in order to allow satisfaction of benchmark specifications in adaptive operation. It is important to underline that even in the linear case with constant parameters, the design of the central controller is difficult in the case of the benchmark as a consequence of the presence of two pairs of very low damped zeros in the plant model very near to the border of the frequency region where disturbance compensation has to be achieved.

The paper is organized as follows. Section 2 presents the general plant and controller structure in the context of the YK parametrization. The direct adaptive algorithm is presented in Section 3. Section 4 discusses the design of the central controller. Simulation results are presented in Section 5, while experimental results for this methodology are given in Section 6. Concluding remarks are presented in Section 7.

2. Plant representation and controller structure

The structure of the LTI discrete time model of the plant (the compensator system), also called *secondary path*, used for controller design is

$$G(z^{-1}) = \frac{z^{-d}B(z^{-1})}{A(z^{-1})} = \frac{z^{-d-1}B^*(z^{-1})}{A(z^{-1})}, \tag{1}$$

where

$$A(z^{-1}) = 1 + a_1 z^{-1} + \cdots + a_{n_A} z^{-n_A}, \tag{2}$$

$$B(z^{-1}) = b_1 z^{-1} + \cdots + b_{n_B} z^{-n_B} = z^{-1} B^*, \tag{3}$$

$$B^* = b_1 + \cdots + b_{n_B} z^{-n_B+1}, \tag{4}$$

and d is the plant pure time delay in number of sampling periods.[1]

Without considering a reference signal, the output of the plant $y(t)$ and the input $u(t)$ may be written as (see Fig. 1)

$$y(t) = \frac{q^{-d}B(q^{-1})}{A(q^{-1})} \cdot u(t) + p(t), \tag{5}$$

$$S(q^{-1}) \cdot u(t) = -R(q^{-1}) \cdot y(t). \tag{6}$$

In (5), $p(t)$ is the effect of the disturbances on the measured output[2] and $R_0(z^{-1})$, $S_0(z^{-1})$ are polynomials in z^{-1} having the following expressions[3]:

$$S_0 = 1 + s_1^0 z^{-1} + \ldots + s_{n_{S_0}}^0 z^{-n_{S_0}} = S'_0(z^{-1}) \cdot H_{S_0}(z^{-1}), \tag{7}$$

$$R_0 = r_0 + r_1^0 z^{-1} + \ldots + r_{n_{R_0}}^0 z^{-n_{R_0}} = R'_0(z^{-1}) \cdot H_{R_0}(z^{-1}), \tag{8}$$

where $H_{S_0}(q^{-1})$ and $H_{R_0}(q^{-1})$ represent pre-specified parts of the controller (used for example to incorporate the internal model of a disturbance or to open the loop at certain frequencies) and $S'_0(q^{-1})$ and $R'_0(q^{-1})$ are computed.

We define the output sensitivity function (the transfer function between the disturbance $p(t)$ and the output of the system $y(t)$) as

$$S_{yp}(z^{-1}) = \frac{A(z^{-1})S(z^{-1})}{P(z^{-1})} \tag{9}$$

and the input sensitivity function (the transfer function between the disturbance $p(t)$ and the control input $u(t)$) as

$$S_{up}(z^{-1}) = -\frac{A(z^{-1})R(z^{-1})}{P(z^{-1})}, \tag{10}$$

where

$$P(z^{-1}) = A(z^{-1})S_0(z^{-1}) + z^{-d}B(z^{-1})R_0(z^{-1}), \tag{11}$$

the characteristic polynomial, specifies the desired closed loop poles of the system[4] (see also [19]). It is important to remark that one should only reject disturbances located in frequency regions where the plant model has enough gain. This can be seen by looking at Eq. (9) and noticing that perfect rejection at a certain frequency, ω_0, is obtained *iff* $S(e^{-j\omega_0}) = 0$. But from Eq. (10) one can see that the modulus of the input sensitivity function at this frequency is given by

$$|S_{up}(e^{-j\omega_0})| = \left|\frac{A(e^{-j\omega_0})}{B(e^{-j\omega_0})}\right|.$$

The modulus of the input sensitivity function at this frequency is equal to the inverse of the plant gain at this frequency. Therefore, low plant gain will imply that the robustness *vs* additive plant model uncertainties is reduced and the stress on the actuator will become important. Furthermore, it can be observed that serious problems will occur if $B(z^{-1})$ has complex zeros close to the unit circle at frequencies where an important attenuation of disturbances is introduced. It is mandatory to avoid attenuation of disturbances at these frequencies [16].

In this paper, the Youla–Kučera parametrization [3,23] is used. Supposing a finite impulse response (FIR) representation of the

[1] The complex variable z^{-1} will be used to characterize the system's behaviour in the frequency domain and the delay operator q^{-1} will be used for the time domain analysis.

[2] The disturbance passes through a so called *primary path* which is represented in this figure, and $p(t)$ is its output.

[3] The argument (z^{-1}) will be omitted in some of the following equations to make them more compact.

[4] It is assumed that a reliable model identification is achieved and therefore the estimated model is assumed to be equal to the true model.

adaptive Q filter

$$Q(z^{-1}) = q_o + q_1 z^{-1} + \cdots + q_{n_Q} z^{-n_Q} \tag{12}$$

the equivalent controller's polynomials become

$$R = R_0 + AQH_{S_0}H_{R_0}, \tag{13}$$

$$S = S_0 - z^{-d}BQH_{S_0}H_{R_0}. \tag{14}$$

where R_0 and S_0 define the central controller (Fig. 1) which verifies the desired specifications in the absence of the disturbance. The characteristic polynomial of the closed loop becomes (as in (11)):

$$P = AS_0 + z^{-d}BR_0. \tag{15}$$

3. Direct adaptive regulation for disturbance rejection

This section presents the direct adaptive control algorithm [17,16] that will be used for the benchmark problem. A key aspect of this methodology is the use of the IMP. It is supposed that $p(t)$ is a deterministic disturbance given by

$$p(t) = \frac{N_p(q^{-1})}{D_p(q^{-1})} \cdot \delta(t), \tag{16}$$

where $\delta(t)$ is a Dirac impulse and N_p, D_p are coprime polynomials of degrees n_{N_p} and n_{D_p}, respectively.[5] In the case of stationary narrow-band disturbances, the roots of $D_p(z^{-1})$ are on the unit circle and the contribution of the terms of N_p can be neglected.

Internal model principle: The effect of the disturbance given in (16) upon the output

$$y(t) = \frac{A(q^{-1})S(q^{-1})}{P(q^{-1})} \cdot \frac{N_p(q^{-1})}{D_p(q^{-1})} \cdot \delta(t), \tag{17}$$

where $D_p(z^{-1})$ is a polynomial with roots on the unit circle and $P(z^{-1})$ is an asymptotically stable polynomial, converges asymptotically towards zero *iff* the polynomial $S(z^{-1})$ in the *RS* controller has the form

$$S(z^{-1}) = H_S(z^{-1})S'(z^{-1}). \tag{18}$$

Thus, the pre-specified part of $S(z^{-1})$ should be chosen as

$$H_S(z^{-1}) = D_p(z^{-1})H_{S_0}(z^{-1})$$

and the controller is computed solving

$$P = AD_pH_{S_0}S' + z^{-d}BH_{R_0}R', \tag{19}$$

where P, D_p, A, B, H_{R_0}, H_{S_0} and d are given.[6]

To compute $Q(z^{-1})$ in order that the polynomial $S(z^{-1})$ given by (14) incorporates the internal model of the disturbance (18), one has to solve the diophantine equation (taking into account Eq. (7))

$$S'D_p + z^{-d}BH_{R_0}Q = S'_0, \tag{20}$$

where D_p, d, B, S'_0, and H_{R_0} are known and S' and Q are unknown. Eq. (20) has a unique solution for S' and Q with: $n_{S'_0} \le n_{D_p} + n_B + d + n_{H_{R_0}} - 1$, $n_{S'} = n_B + d + n_{H_{R_0}} - 1$, $n_Q = n_{D_p} - 1$. One sees that the order n_Q of the polynomial Q depends upon the structure of the disturbance model. The use of the Youla–Kučera parametrization, with Q given in (12), is interesting because it allows to maintain the closed loop poles as given by the central controller but at the same time introduces the parameters of the internal model into the controller. The development of the parametric adaptation algorithm (PAA) requires first to find an *error equation* (see also [23,17,16]). Using the Q-parametrization, the output of the system in the presence of a disturbance can be expressed as

$$y(t) = \frac{A[S_0 - q^{-d}BH_{S_0}H_{R_0}Q]}{P} \cdot \frac{N_p}{D_p} \cdot \delta(t)$$
$$= \frac{S_0 - q^{-d}BH_{S_0}H_{R_0}Q}{P} \cdot w(t), \tag{21}$$

where $w(t)$ is given by (see also Fig. 1)

$$w(t) = \frac{AN_p}{D_p} \cdot \delta(t) = A \cdot y(t) - q^{-d} \cdot B \cdot u(t). \tag{22}$$

Taking into consideration that the adaptation of Q is done in order to obtain an output $y(t)$ which tends asymptotically to zero, one can define $\varepsilon^0(t+1)$ as the value of $y(t+1)$ obtained with $\hat{Q}(t, q^{-1})$ (the estimate of Q at time t, written also $\hat{Q}(t)$):

$$\varepsilon^0(t+1) = \frac{S_0}{P} \cdot w(t+1) - \hat{Q}(t)\frac{q^{-d}B^*H_{S_0}H_{R_0}}{P} \cdot w(t). \tag{23}$$

Similarly, the *a posteriori* error becomes (using $\hat{Q}(t+1)$)

$$\varepsilon(t+1) = \frac{S_0}{P} \cdot w(t+1) - \hat{Q}(t+1)\frac{q^{-d}B^*H_{S_0}H_{R_0}}{P} \cdot w(t). \tag{24}$$

Replacing S_0 by Eq. (7) and S'_0 by Eq. (20) one obtains

$$\varepsilon(t+1) = [Q - \hat{Q}(t+1)] \cdot \frac{q^{-d}B^*H_{S_0}H_{R_0}}{P} \cdot w(t) + v(t+1), \tag{25}$$

where

$$v(t) = \frac{S'D_pH_{S_0}}{P} \cdot w(t) = \frac{S'H_{S_0}AN_p}{P} \cdot \delta(t) \tag{26}$$

is a signal which tends asymptotically towards zero.

Define the estimated polynomial $\hat{Q}(t, q^{-1}) = \hat{q}_0(t) + \hat{q}_1(t)q^{-1} + \ldots + \hat{q}_{n_Q}(t)q^{-n_Q}$ and the associated estimated parameter vector $\hat{\theta}(t) = [\hat{q}_0(t)\hat{q}_1(t)\ldots\hat{q}_{n_Q}(t)]^T$. Define the fixed parameter vector corresponding to the optimal value of the polynomial Q as: $\theta = [q_0 q_1 \ldots q_{n_Q}]^T$.

Denote

$$w_2(t) = \frac{q^{-d}B^*H_{S_0}H_{R_0}}{P} \cdot w(t) \tag{27}$$

and define the following observation vector:

$$\phi^T(t) = [w_2(t)w_2(t-1)\ldots w_2(t-n_Q)]. \tag{28}$$

Eq. (25) becomes

$$\varepsilon(t+1) = [\theta^T - \hat{\theta}^T(t+1)] \cdot \phi(t) + v(t+1). \tag{29}$$

One can remark that $\varepsilon(t+1)$ corresponds to an adaptation error [14].

From Eq. (23), one obtains the *a priori* adaptation error

$$\varepsilon^0(t+1) = w_1(t+1) - \hat{\theta}^T(t)\phi(t), \tag{30}$$

with

$$w_1(t+1) = \frac{S_0(q^{-1})}{P(q^{-1})} \cdot w(t+1), \tag{31}$$

$$w(t+1) = A(q^{-1}) \cdot y(t+1) - q^{-d}B^*(q^{-1}) \cdot u(t), \tag{32}$$

where $B(q^{-1})u(t+1) = B^*(q^{-1})u(t)$.

The *a posteriori* adaptation error is obtained from (24):

$$\varepsilon(t+1) = w_1(t+1) - \hat{\theta}^T(t+1)\phi(t). \tag{33}$$

For the estimation of the parameters of $\hat{Q}(t, q^{-1})$ the following PAA is used [14]:

$$\hat{\theta}(t+1) = \hat{\theta}(t) + F(t)\phi(t)\varepsilon(t+1), \tag{34}$$

$$\varepsilon(t+1) = \frac{\varepsilon^0(t+1)}{1 + \phi^T(t)F(t)\phi(t)}, \tag{35}$$

[5] Throughout the paper, n_X denotes the degree of the polynomial X.

[6] Of course, it is assumed that D_p and B do not have common factors.

$$\varepsilon^0(t+1) = w_1(t+1) - \hat{\theta}^T(t)\phi(t), \tag{36}$$

$$F(t+1) = \frac{1}{\lambda_1(t)}\left[F(t) - \frac{F(t)\phi(t)\phi^T(t)F(t)}{\frac{\lambda_1(t)}{\lambda_2(t)} + \phi^T(t)F(t)\phi(t)}\right], \tag{37}$$

$$1 \geq \lambda_1(t) > 0, \quad 0 \leq \lambda_2(t) < 2, \tag{38}$$

where $\lambda_1(t)$, $\lambda_2(t)$ allow to obtain various profiles for the evolution of the adaptation gain $F(t)$ (for details see [14,19]).

4. Central controller design

The central controller plays a very important role in this approach. Its role is to stabilize the system in the absence of disturbances, to ensure a small (flat) "water bed" effect when the internal model of the disturbance is incorporated to the controller through the Q-filter parameters and a reduced magnitude of the input sensitivity function outside the attenuation region, when the adaptive regulation algorithm is active. The structure of the central controller was presented in Eqs. (7) and (8) and is indicated in Fig. 1. Since the estimation of $\hat{Q}(z^{-1})$ is the only adaptive part in the scheme, fixed characteristics in the central controller can be imposed and preserved through the Youla–Kučera parametrization, as was shown in Section 3. These fixed characteristics can have various purposes.

Due to the *water bed* effect on the Bode integral of the output sensitivity function (S_{yp}) caused by the IMP, the central controller must shape S_{yp} in order to meet the benchmark specifications. The technique of pole placement with sensitivity function shaping is an option to address this problem (see details in [19]). This *water bed* effect can be attenuated by introducing a pair of low-damped complex auxiliary poles at the same or near the frequency of the narrow band disturbance which is attenuated using IMP. The damping of this fixed auxiliary complex pole has to be chosen such that the desired attenuation can be however achieved for all the frequencies within the attenuation region. Hence, this feature can be used in the central controller design for attenuating the IMP "water bed" effects over S_{yp} (i.e. controlling the maximum of the modulus of S_{yp}).

The Youla–Kučera parametrization allows the introduction of the disturbance model without modifying the closed loop poles imposed by the central controller. With this in mind, low-damped complex *fixed* auxiliary poles can be introduced in the characteristic polynomial of the closed loop ($P(z^{-1})$), for reducing the water bed effect within the region of attenuation. The frequency (position) and damping factor are chosen accordingly to the benchmark specifications for each level (one, two or three sinusoids) in order to obtain a flat *water bed* effect.

Since in the benchmark specifications the frequency region of interest is from 50 to 95 Hz, an analysis of the secondary path in this region is necessary. The secondary path model has two pairs of low-damped complex zeros near the limits of the frequency region considered. These zeros are located at 45.64 and 98.5 Hz. The effect of the zeros at 98.5 Hz, over the magnitude of the frequency response, produces an attenuation close to −27 dB meanwhile the zeros at 45.65 Hz introduce an attenuation around −15 dB, as is shown in Fig. 2, where a zoom of the frequency characteristic of the magnitude of the secondary path gain from 40 to 105 Hz is shown. Near to these zeros, the system has two pairs of low-damped complex poles at 47.36 and 101.92 Hz. It was found that the introduction of two pairs of complex auxiliary poles at 50 and 95 Hz allows to achieve the desired objectives on the shaping of the output sensitivity function. These poles are used for all the benchmark levels. Since the damping factor of these auxiliary poles influences both the disturbance attenuation and the maximum amplification, a compromise has to be found.

In Fig. 3 the result of adding these auxiliary poles is shown. In this case the internal model of a sinusoidal perturbation at 50 Hz is added to the controller. The figure shows the modulus of the output sensitivity function for the cases where the central controller is designed with or without using these auxiliary poles. Important amplifications arise when these auxiliary poles are not present. This proves the usefulness of such auxiliary poles in order to meet the benchmark specifications. Since for the level 2 and 3 the number of sinusoidal perturbations increases, the number of auxiliary poles also should increase. Thus for level 2, the central controller incorporates a third pair of complex auxiliary poles located at 70 Hz, while the central controller for level 3 includes a

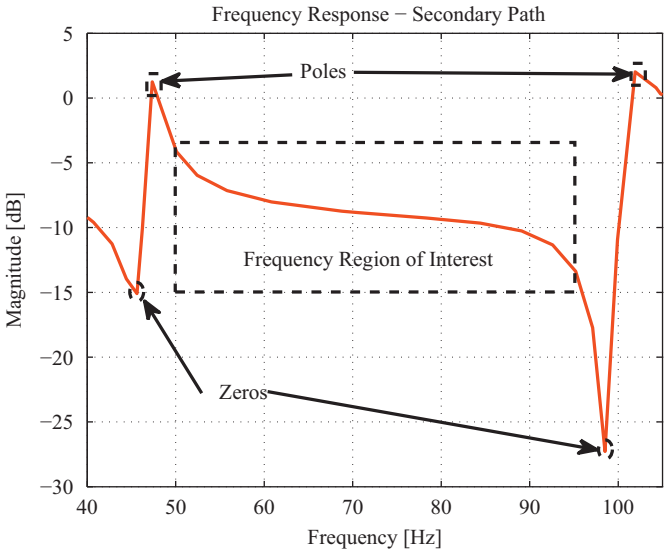

Fig. 2. Zoom at the magnitude of the frequency response of the secondary path, between 40 and 105 Hz.

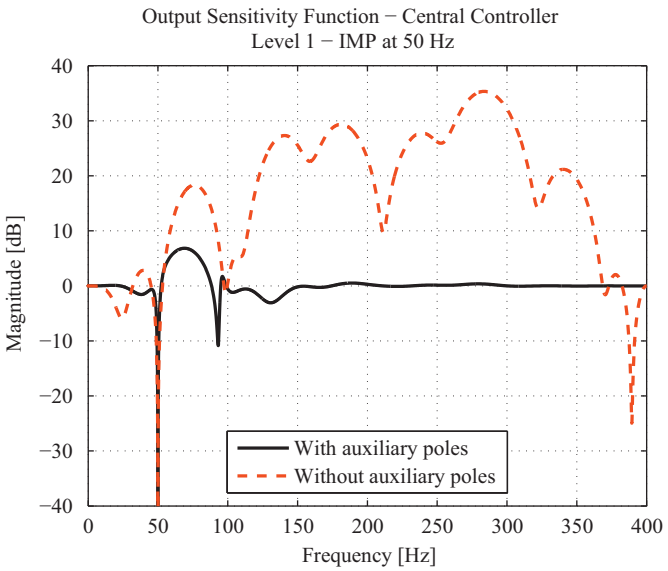

Fig. 3. Output sensitivity function comparison between central controllers for a single sinusoidal rejection, using auxiliary poles (solid line) and without auxiliary poles (dashed line).

Table 1
Simulation results—Simple Step Test.

LEVEL 1							
Frequency (Hz)	**GA (dB)**	**DA (dB)**	**MA (dB@Hz)**	**N^2T ($\times 10^{-3}$)**	**N^2R ($\times 10^{-3}$)**	**MV ($\times 10^{-3}$)**	**TD (ratio)**
50	34.17	44.43	7.21@67.18	14.48	3.75	17.68	1.108
55	32.78	46.84	6.66@78.12	10.15	4.43	19.90	1.078
60	32.30	46.94	6.76@82.81	10.23	4.69	20.14	1.069
65	32.77	48.38	6.95@50.00	9.30	4.51	19.90	1.066
70	33.29	50.04	7.84@53.13	8.31	4.30	19.94	1.069
75	34.01	51.90	7.31@53.13	7.92	4.05	19.82	1.078
80	34.57	51.56	7.65@93.75	8.16	3.75	21.75	1.094
85	34.39	52.29	6.70@64.06	9.75	3.70	23.90	1.110
90	31.94	44.98	7.46@68.75	13.33	4.04	26.84	1.105
95	23.87	35.70	6.17@87.50	20.76	4.55	29.12	1.063
LEVEL 2							
Frequency (Hz)	**GA (dB)**	**DA (dB)–(dB)**	**MA (dB@Hz)**	**N^2T ($\times 10^{-3}$)**	**N^2R ($\times 10^{-3}$)**	**MV ($\times 10^{-3}$)**	**TD (ratio)**
50–70	39.16	41.81–47.49	6.11@79.69	25.035	4.258	29.441	1.057
55–75	38.35	48.33–47.66	7.74@87.50	23.40	4.75	34.73	1.055
60–80	39.42	50.14–49.26	7.87@50.00	19.40	4.17	34.19	1.110
65–85	39.83	49.13–51.04	7.24@53.13	18.27	3.94	36.55	1.121
70–90	38.45	51.49–42.59	7.61@59.37	27.33	4.24	40.64	1.084
75–95	36.47	54.02–37.28	6.06@87.50	35.62	4.06	44.51	1.062
LEVEL 3							
Frequency (Hz)	**GA (dB)**	**DA (dB)-(dB)-(dB)**	**MA (dB@Hz)**	**N^2T ($\times 10^{-3}$)**	**N^2R ($\times 10^{-3}$)**	**MV ($\times 10^{-3}$)**	**TD (ratio)**
50–65–80	42.75	43.94–44.86–41.27	7.66@87.50	135.97	4.24	72.54	1.105
55–70–85	42.98	48.84–49.55–46.81	7.57@76.56	352.26	4.10	133.43	1.113
60–75–90	41.98	47.67–49.70–42.43	8.46@51.56	655.83	4.37	209.18	1.115
65–80–95	40.93	44.53–42.34–37.92	7.92@73.43	1615.70	4.14	295.94	1.151

third and a fourth pair of complex auxiliary poles located at 70 and 80 Hz. The differences between the central controllers for the various levels concern the damping factors of the auxiliary poles. They are chosen for each level in order to make a compromise between the disturbance attenuation and the maximum amplification.

Since there may exist uncertainties in the model of the secondary path outside the attenuation region and that also we do not want to amplify noise which may exist outside the frequency region where disturbance attenuation is done, one has to get a very low magnitude of the input sensitivity function in these regions.

A very efficient way to achieve this, without influencing the shape of the output sensitivity function in the attenuation region, is to use band stop filters (BSFs) over S_{up} (see details in [19,22]). The structure of a BSF, according to [19], can be described as

$$\frac{N_{BSF}(z^{-1})}{D_{BSF}(z^{-1})} = \frac{1+\beta_1 z^{-1}+\beta_2 z^{-2}}{1+\alpha_1 z^{-1}+\alpha_2 z^{-2}}. \tag{39}$$

In order to incorporate the BSF in the central controller, the BSF transfer function numerator ($N_{BSF}(z^{-1})$) is included in the pre-specified part of the central controller's polynomial $R_0(z^{-1})$, while the BSF transfer function denominator ($D_{BSF}(z^{-1})$) defines additional closed loop poles introduced in ($P(z^{-1})$). The equation of the input sensitivity function (Eq. (10)) becomes

$$S_{up} = -\frac{AR}{P} = -\frac{A(R_0 + AQH_{S_0}H_{R_0})N_{BSF}}{(AS_0 + z^{-d}BR_0)D_{BSF}} \tag{40}$$

Fig. 4 shows a comparison of the modulus of S_{up} obtained with two central controllers. In both controllers the internal model of the disturbance at 50 Hz is added. The first one corresponds to the central controller designed to shape S_{yp} (see Fig. 3). It does not incorporate BSFs for shaping S_{up}. The second one in Fig. 4, besides the auxiliary poles, incorporates three BSFs in the region between 110 and 170 Hz. The difference in the modulus of S_{up} is significant.

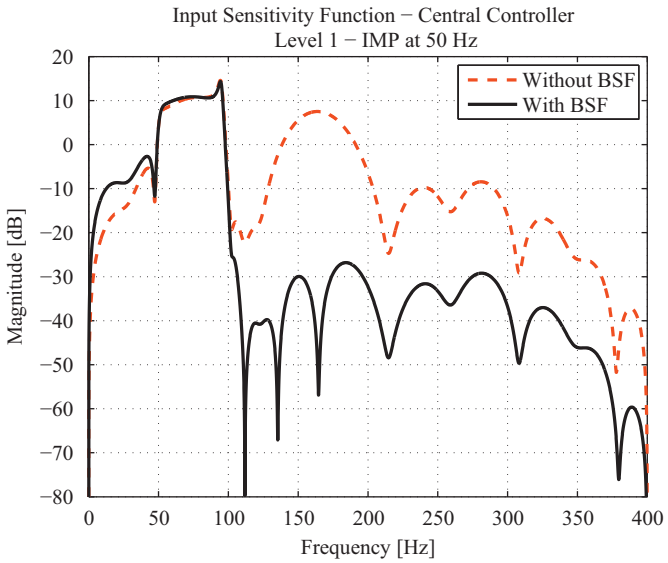

Fig. 4. Input sensitivity function comparison between central controllers for a single sinusoidal rejection, using BSFs (solid line) and without BSFs (dashed line).

It reduces the modulus of S_{up} by 20–30 dB in the frequency region above 100 Hz.

5. Simulation results

According to [15], the benchmark's specifications consider three levels in terms of the number of narrow band disturbances to be rejected (attenuated). For each level, three types of tests were designed for which performance specifications have to be achieved.

Table 2
Simulation results – Level 1 – Step Frequency Changes Test.

Frequency (**Hz**)	$\mathbf{N^2T}$ ($\times 10^{-3}$)	**MV** ($\times 10^{-3}$)
SEQUENCE-1		
60→70	17.13	22.15
70→60	16.95	16.10
60→50	46.21	18.72
50→60	41.76	30.72
SEQUENCE-2		
75→85	16.74	15.66
85→75	15.42	18.57
75→65	14.18	15.09
65→75	14.25	17.14
SEQUENCE-3		
85→95	39.32	23.84
95→85	32.88	28.05
85→75	15.45	21.13
75→85	16.31	15.77

Table 3
Simulation results – Level 1 – Chirp Test.

	Error-mean square value	**Error-maximum value**
↗	14.50 × 10−6	13.97×10^{-3}
↘	14 × 10−6	14.86×10^{-3}

The first series of tests, called *Simple Step Test*, deals with global attenuation (GA in dB), disturbance attenuation (DA in dB) and maximum amplification (MA in dB) outside the attenuation frequencies (these quantities are evaluated, in the frequency domain, once the adaptation has settled), while the maximum value (MV in Volts) during transient, a measure of the square of the truncated two norm during transient (N^2T), and after settling of the adaptation (N^2R) are evaluated in time domain. The transient duration is evaluated for the simple step test. It should be less than 2 s. Since the disturbance is applied at $t=5$ s, the transient duration of 2 s is considered to be achieved if the ratio $N^2T(7:10)/N^2T(17:20)$ (the square of the truncated norms between 7 and 10 s over the square of the truncated two norm between 17 and 20 s) is smaller than equal to 1.21 [18]. The second series of tests (called *Step Frequency Changes Test*) evaluate the performances of the algorithm for step changes in the frequency of the disturbances, while the last test (called *Chirp Test*) evaluates the rejection of chirp disturbances. In both tests only evaluations in time domain are done, adding to the *Chirp Test* the measurement of the mean-square value of the error during the chirp (for more details about the measurements and performance index see [18]).

5.1. Level 1 results

Table 1 shows the results obtained in the presence of one sinusoidal disturbance with constant frequency (Simple Step Test). The benchmark specifications for global attenuation and disturbance attenuation[7] are achieved at all frequencies. The maximum amplifications obtained are slightly over the limit (6 dB), while the transient duration ratio is lower than 1.21 for all the cases. Table 2 summarizes the results obtained when the disturbance frequency changes (Step Frequency Changes Test).

The results for the Chirp Test are shown in Table 3. The two periods of chirp are indicated as ↗ (for increasing frequency) and ↘ (for decreasing frequency). The benchmark requirement is that the maximum value of the residual force (output of the system) is not greater than 0.1 V. One can see that the benchmark specifications are satisfied.

[7] At 95 Hz the disturbance attenuation is marginally below the benchmark specification for the three levels.

5.2. Level 2 results

The difficulty is increased for Level 2 by introducing two simultaneous narrow-band disturbances. The results are shown in Table 1. The specifications for both GA and DA have been satisfied. The maximum amplification is in some cases marginally over the limit (7 dB for this level). For step changes frequency test, the results are given in Table 4. The chirp requirement is also fulfilled for this level (Table 5).

5.3. Level 3 results

The third level considers three narrow band disturbances and is on this level where the advantages of the approach used for the central

Table 4
Simulation results – Level 2 – Step Frequency Changes Test.

Frequency (**Hz**)	$\mathbf{N^2T}$ ($\times 10^{-3}$)	**MV** ($\times 10^{-3}$)s
SEQUENCE-1		
[55, 75]→[60, 80]	38.33	34.67
[60, 80]→[55, 75]	36.20	30.36
[55, 75]→[50, 70]	78.02	35.47
[50, 70]→[55, 75]	70.11	39.08
SEQUENCE-2		
[70, 90]→[75, 95]	60.99	30.85
[75, 95]→[70, 90]	66.67	40.34
[70, 90]→[65, 85]	39.50	34.57
[65, 85]→[70, 90]	39.36	29.37

Table 5
Simulation results – Level 2 – Chirp Test.

	Error-mean square value	**Error-maximum value**
↗	42.47×10^{-6}	19.44×10^{-3}
↘	42.10×10^{-6}	19.86×10^{-3}

Table 6
Simulation results – Level 3 – Step Frequency Changes Test.

Frequency (**Hz**)	$\mathbf{N^2T}$ ($\times 10^{-3}$)	**MV** ($\times 10^{-3}$)
SEQUENCE-1		
[55, 70, 85]→[60, 75, 90]	154.68	52.49
[60, 75, 90]→[55, 70, 85]	141.20	56.72
[55, 70, 85]→[50, 65, 80]	253.53	62.49
[50, 65, 80]→[55, 70, 85]	147.72	63.84
SEQUENCE-2		
[60, 75, 90]→[65, 80, 95]	180.21	51.51
[65, 80, 95]→[60, 75, 90]	166.43	78.22
[60, 75, 90]→[55, 70, 85]	136.18	56.03
[55, 70, 85]→[60, 75, 90]	144.88	51.90

Table 7
Simulation results – Level 3 – Chirp Test.

	Error-mean square value	**Error-maximum value**
↗	93.11×10^{-6}	39.4×10^{-3}
↘	87.62×10^{-6}	42.3×10^{-3}

Table 8
Experimental results—Simple Step Test.

LEVEL 1							
Frequency (Hz)	**GA (dB)**	**DA (dB)**	**MA (dB@Hz)**	**N^2T ($\times 10^{-3}$)**	**N^2R ($\times 10^{-3}$)**	**MV ($\times 10^{-3}$)**	**TD (ratio)**
50	34.60	38.49	9.83@65.63	14.478	4.88	13.86	0.941
55	34.54	50.45	9.48@118.75	13.32	4.94	19.97	0.990
60	33.34	49.49	8.23@79.69	14.72	5.16	21.19	0.945
65	32.78	50.04	9.65@90.63	14.17	4.53	20.50	1.125
70	30.54	47.90	9.01@89.06	14.73	4.87	22.96	0.905
75	29.53	45.54	8.90@50.00	11.20	4.86	19.28	0.869
80	30.28	48.72	8.49@95.31	8.14	4.17	21.14	0.964
85	28.47	45.94	10.66@57.81	10.05	6.90	25.14	0.959
90	28.02	42.65	8.24@73.44	17.08	6.94	25.11	1.089
95	24.63	34.55	9.06@82.81	50.09	8.33	32.44	1.638
LEVEL 2							
Frequency (Hz)	**GA (dB)**	**DA (dB)–(dB)**	**MA (dB@Hz)**	**N^2T ($\times 10^{-3}$)**	**N^2R ($\times 10^{-3}$)**	**MV ($\times 10^{-3}$)**	**TD (ratio)**
50–70	34.42	33.58–42.90	8.32@59.38	32.10	9.35	29.02	0.911
55–75	33.27	44.90–44.18	11.85@115.63	32.49	8.04	30.23	1.518
60–80	33.42	45.59–41.70	7.78@118.75	31.35	7.08	28.99	0.943
65–85	31.72	40.01–43.66	8.02@106.25	22.75	7.62	31.44	1.019
70–90	32.91	41.43–38.63	7.52@59.38	21.38	6.05	33.90	1.112
75–95	31.04	48.89–34.66	7.09@87.50	28.33	6.65	38.40	0.998
LEVEL 3							
Frequency (Hz)	**GA (dB)**	**DA (dB)–(dB)–(dB)**	**MA (dB@Hz)**	**N^2T ($\times 10^{-3}$)**	**N^2R ($\times 10^{-3}$)**	**MV ($\times 10^{-3}$)**	**TD (ratio)**
50–65–80	41.69	38.39–46.91–42.44	9.41@117.19	250.83	6.24	81.94	0.997
55–70–85	40.62	44.75–45.01–38.31	8.81@76.56	357.51	5.71	143.23	0.957
60–75–90	37.67	44.71–46.38–43.92	6.68@82.21	338.79	7.22	139.54	0.999
65–80–95	38.59	43.64–41.07–38.73	9.16@54.69	561.64	5.59	141.08	1.112

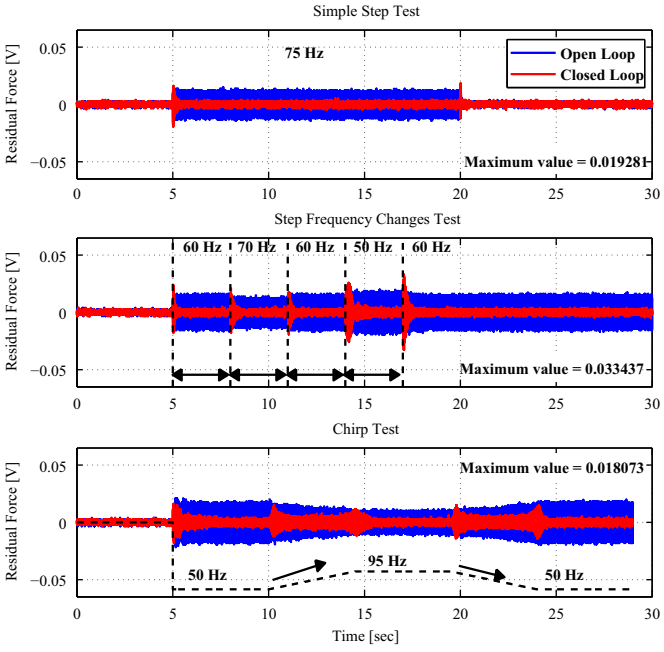

Fig. 5. Time response comparison between open and closed loop response. Simple Step Test (top), Step Frequency Changes Test (middle) and Chirp Test (bottom).

controller design show up. Generally speaking, all the benchmark specifications were satisfied, as can be seen from Tables 1, 6 and 7.

6. Experimental results

In this section, real-time results are presented. The same central controllers and adaptation gains used in simulation have been considered for real-time experiments. Through bar graphics a comparison between the simulation and the experimental results is done also in this section.

Table 9
Experimental results – Level 1 – Step Frequency Changes Test.

Frequency (Hz)	**N^2T ($\times 10^{-3}$)**	**MV ($\times 10^{-3}$)**
SEQUENCE-1		
60→70	16.79	21.18
70→60	16.80	19.26
60→50	69.22	20.09
50→60	46.05	33.44
SEQUENCE-2		
75→85	15.96	15.06
85→75	15.53	18.73
75→65	14.55	18.03
65→75	14.22	18.73
SEQUENCE-3		
85→95	40.82	16.80
95→85	30.73	23.65
85→75	15.23	19.98
75→85	16.04	14.34

6.1. Level 1 results

Table 8 presents the simple step test results. An example of this is shown in Fig. 5 which presents the time response of simple step test (top), step frequency changes (middle — sequence 1) and chirp test (bottom), and Fig. 6 where the PSD comparison is done for the simple step at 75 Hz. In the figure the solid line indicates the closed loop result while the dashed the open loop result. The *water bed* effect is depicted in the PSD comparison near the limits of the frequency region of interest. Table 9 gives

Table 10
Experimental results – Level 1 – Chirp Test.

	Error-mean square value	Error-maximum value
↗	13.74×10^{-6}	15.02×10^{-3}
↘	13.94×10^{-6}	15.02×10^{-3}

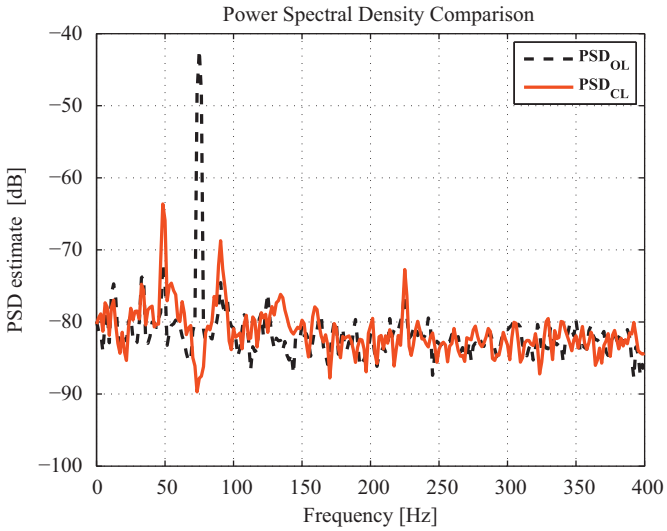

Fig. 6. Disturbance attenuation comparison between open loop (dashed line) and closed loop (solid line) for Simple Step-Level 1, disturbances at 75 Hz.

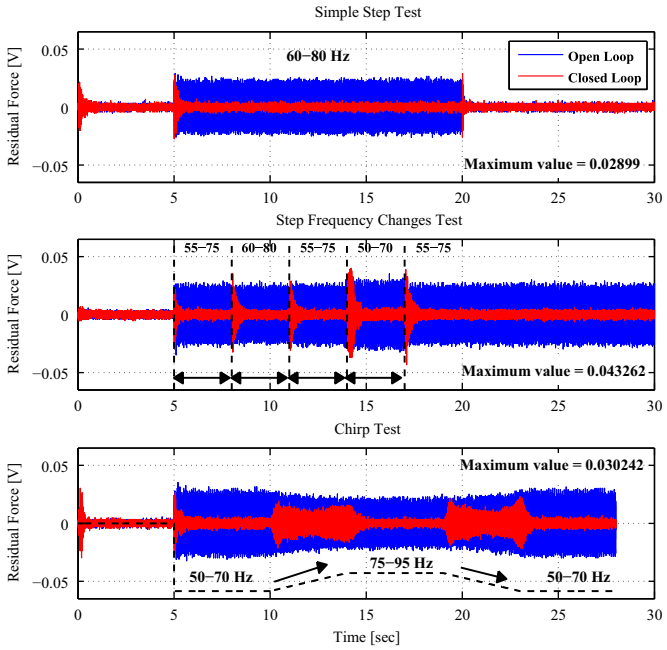

Fig. 7. Time response comparison between open and closed loop response. Simple Step Test (top), Step Frequency Changes Test (middle) and Chirp Test (bottom).

the results for step frequency changes and Table 10 gives the results for the chirp test. The results in simulation and in real-time are quite close with the exception of the maximum amplification. The differences concerning maximum amplification can be explained by the fact that the level of noise in the simulator over 100 Hz is much lower than the level of noise in the real system.

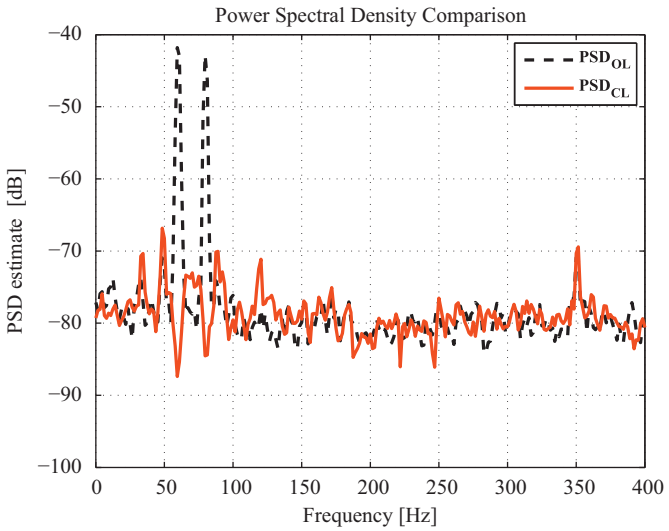

Fig. 8. Disturbance attenuation comparison between open loop (dashed line) and closed loop (solid line) for Simple Step-Level 2, disturbances at [60–80] Hz.

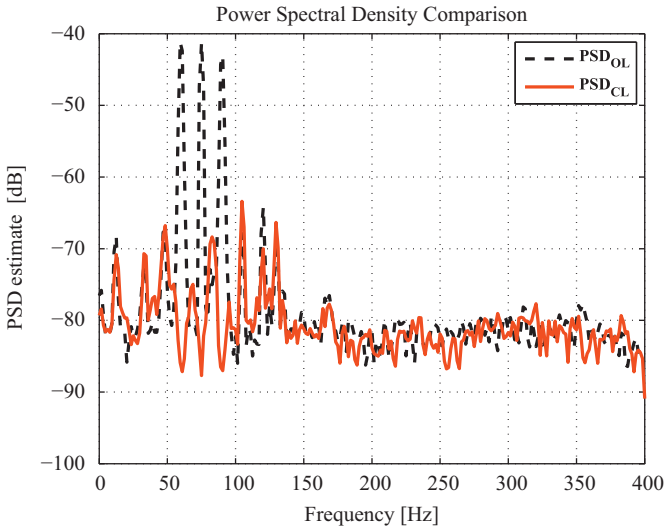

Fig. 9. Disturbance attenuation comparison between open loop (dashed line) and closed loop (solid line) for Simple Step-Level 3, disturbances at [60, 75, 90] Hz.

6.2. Level 2 results

The results for level 2 are summarized in Tables 8, 11 and 12. The results in real-time experiments are close to those obtained in simulation. The time response of the system for this level is depicted in Fig. 7, where the three tests are plotted. The PSD comparison in Fig. 8 shows the attenuations introduced as well as the low magnitude of the *water bed* effect as a consequence of the design proposed for the central controller.

6.3. Level 3 results

Finally, the most difficult level shows that the direct adaptive algorithm achieves most of the benchmark specifications. This is illustrated in Tables 8, 13 and 14. In the frequency domain,

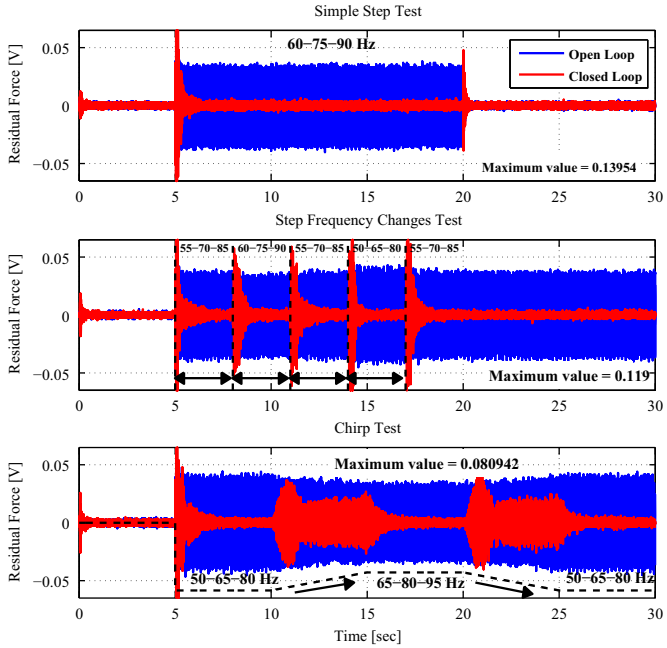

Fig. 10. Time response comparison between open and closed loop response. Simple Step Test (top), Step Frequency Changes Test (middle) and Chirp Test (bottom).

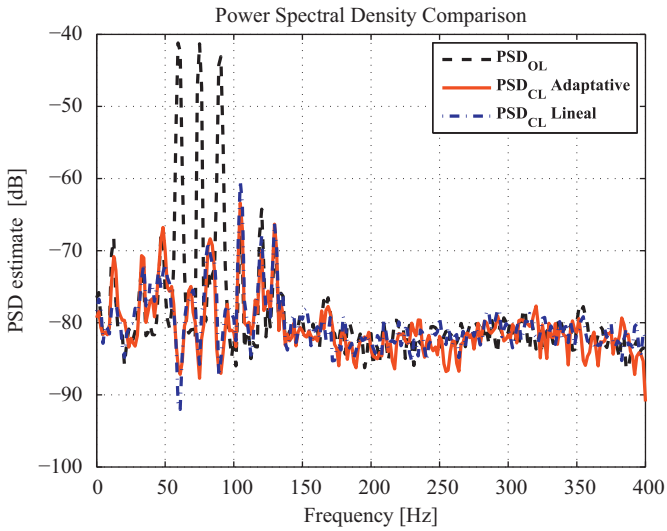

Fig. 11. Attenuation comparison between a *tuned* linear controller and the direct adaptive algorithm proposed.

a comparison of disturbance attenuation (**DA**) obtained in real-time is shown in Fig. 9. The case corresponds to the Simple Step Test – Level 3 at 60–75–90 Hz. The attenuations for the three frequencies exceed the 40 dB and the maximum amplification is located in the frequency region of interest and do not pass the benchmark limit.

Fig. 10 shows the time response for Simple Step Test, Step Frequency Changes Test and Chirp Test for the Level 3. In the top of the figure the Simple Step Test experimental response of the system is depicted (for the same case analyzed in Fig. 9). In the middle the Step Frequency Changes Test (Sequence 1) result

Table 11
Experimental results – Level 2 – Step Frequency Changes Test.

Frequency (Hz)	$\mathbf{N^2T}$ ($\times 10^{-3}$)	**MV** ($\times 10^{-3}$)s
SEQUENCE-1		
[55, 75]→[60, 80]	38.58	35.17
[60, 80]→[55, 75]	38.51	31.01
[55, 75]→[50, 70]	117.28	40.08
[50, 70]→[55, 75]	69.19	43.27
SEQUENCE-2		
[70, 90]→[75, 95]	66.52	32.70
[75, 95]→[70, 90]	60.01	33.83
[70, 90]→[65, 85]	42.56	35.15
[65, 85]→[70, 90]	42.95	28.58

Table 12
Experimental results – Level 2 – Chirp Test.

	Error-mean square value	Error-maximum value
↗	41.28×10^{-6}	21.62×10^{-3}
↘	42.38×10^{-6}	21.23×10^{-3}

Table 13
Experimental results – Level 3 – Step Frequency Changes Test.

Frequency (Hz)	$\mathbf{N^2T}$ ($\times 10^{-3}$)	**MV** ($\times 10^{-3}$)
SEQUENCE-1		
[55, 70, 85]→[60, 75, 90]	141.48	57.73
[60, 75, 90]→[55, 70, 85]	186.33	61.15
[55, 70, 85]→[50, 65, 80]	251.47	75.85
[50, 65, 80]→[55, 70, 85]	224.61	67.53
SEQUENCE-2		
[60, 75, 90]→[65, 80, 95]	212.98	56.48
[65, 80, 95]→[60, 75, 90]	181.00	68.52
[60, 75, 90]→[55, 70, 85]	128.80	58.72
[55, 70, 85]→[60, 75, 90]	150.02	54.03

is presented and in the bottom the Chirp Test result is shown. In each case the maximum value obtained in the entire test is depicted.[8]

The adaptation gains $(\lambda_1(t), \lambda_2(t))$ used both for simulation and real-time were the same. For Level 1 and 2 a constant trace was used, while for Level 3 a gain adjustment through a variable forgetting factor was considered.

6.4. Tuned linear controller comparison

A comparison between a *tuned* linear controller and the direct adaptive scheme proposed has been done on the real system. The *tuned* linear controller will give the maximum achievable performance for the adaptive scheme. The linear controller is based on the central controller configuration described in Section 4 and includes the internal model of the disturbance for 60–75–90 Hz case. Fig. 11 presents the attenuation achieved by both controllers

[8] The value of the figure for the Chirp Test do not corresponds to the one in Table 14 since in the benchmark specification the maximum value constraint is evaluated during the chirp application.

in real-time. Since the linear controller gives the maximum achievable performance (for a given central controller), one can conclude that the direct adaptive regulation approaches the maximum achievable performance.

6.5. Further comparison between simulation and experimental results

Fig. 12 shows a performance comparison between the results in simulation and the experimental ones for level 1. Four measurements have been taken into account: Global attenuation (DA), disturbance attenuation (DA), maximum amplification (MA) and transient duration (TD). In all the cases the benchmark specifications are indicated. Fig. 13 presents the same comparison for the Level 2. For levels 1 and 2 the results in real-time are in general faster (lower ratio in TD), but the simulations presents bigger attenuations (DA) and lower amplifications (MA).

In Fig. 14 the results for Level 3 are presented. The results in simulation and in real-time are very close and in almost all the cases the benchmark specifications were fulfilled.

Table 14
Experimental results – Level 3 – Chirp Test.

	Error-mean square value	Error-maximum value
↗	93.08×10^{-6}	41.7×10^{-3}
↘	90.76×10^{-6}	37.9×10^{-3}

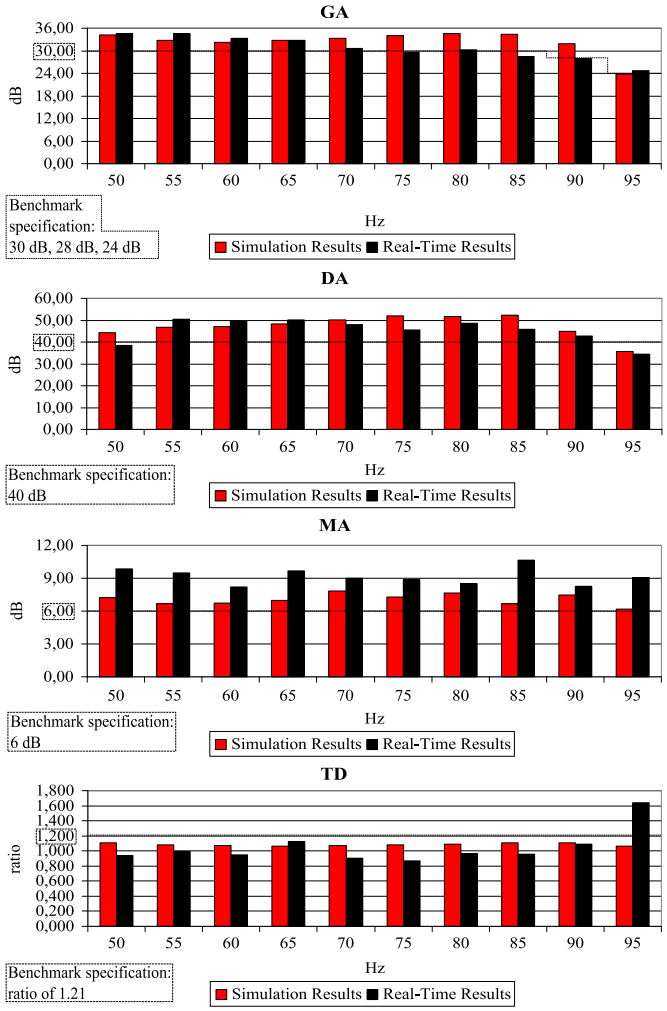

Fig. 12. Performance comparison between the simulation and experimental results for Simple Step Level 1.

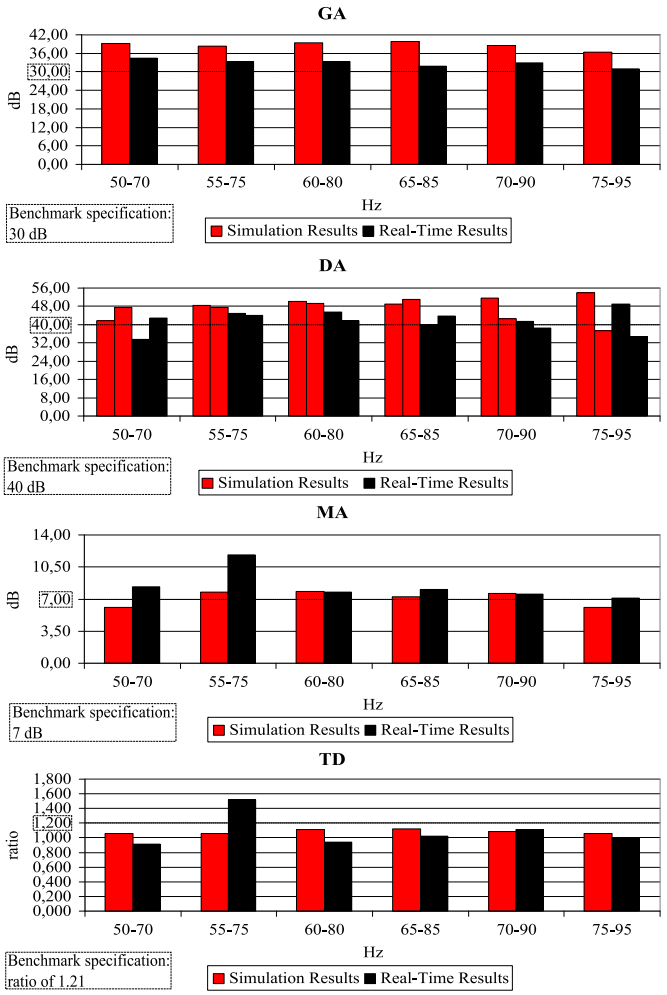

Fig. 13. Performance comparison between the simulation and experimental results for Simple Step Level 2.

7. Concluding remarks

The benchmark performances have been achieved to a large extent. The computational complexity of the proposed algorithm is very low. Good coherence has been found between the simulation and real-time results, since the same central controllers and adaptation gains were used in both situations. This shows the robustness of the scheme with respect to the uncertainties of the identified model of the plant and unmodeled noise. The maximum level of the *water bed* effect over the modulus of the output sensitivity function was kept at a very acceptable value using the design technique proposed for the central controller.

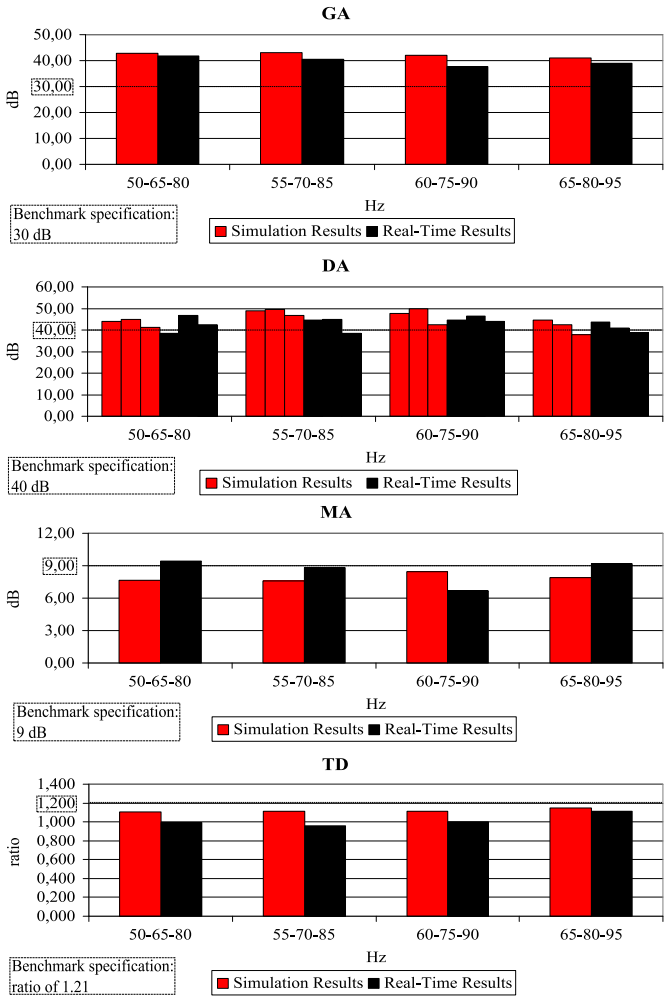

Fig. 14. Performance comparison between the simulation and experimental results for Simple Step Level 3.

References

[1] F. Ben Amara, P.T. Kabamba, A.G. Ulsoy, Adaptive sinusoidal disturbance rejection in linear discrete-time systems - part I: theory, Journal of Dynamic Systems Measurement and Control 121 (1999) 648–654.

[2] F. Ben Amara, P.T. Kabamba, A.G. Ulsoy, Adaptive sinusoidal disturbance rejection in linear discrete-time systems - Part II: experiments, Journal of Dynamic Systems Measurement and Control 121 (1999) 655–659.

[3] B.D.O. Anderson, From Youla-Kucera to identification, adaptive and nonlinear control, Automatica 34 (1998) 1485–1506.

[4] S.V. Aranovskii, A.A. Bobtsov, A.A. Pyrkin, Adaptive observer of an unknown sinusoidal output disturbance for linear plants, Automation and Remote Control 70 (11) (2009) 1862–1870.

[5] G. Bengtsson, Output regulation and internal models – a frequency domain approach, Automatica 13 (4) (1977) 333–345.

[6] A.A. Bobtsov, Output control algorithm with the compensation of biased harmonic disturbances, Automation and Remote Control 69 (8) (2008) 1289–1296.

[7] A.A. Bobtsov, S.A. Kolyubin, A.S. Kremlev, A.A. Pyrkin, An iterative algorithm of adaptive output control with complete compensation for unknown sinusoidal disturbance, Automation and Remote Control 73 (8) (2012) 1327–1336.

[8] F. Celani, Output regulation for the TORA benchmark via rotational position feedback, Automatica 47 (3) (2011) 584–590.

[9] B.A. Francis, W.M. Wonham, The internal model principle of control theory, Automatica 12 (5) (1976) 457–465.

[10] T. Gouraud, M. Gugliemi, F. Auger, Design of robust and frequency adaptive controllers for harmonic disturbance rejection in a single-phase power network, in: Proceedings of the European Control Conference, Bruxelles, 1997.

[11] G. Hillerstrom, J. Sternby, Rejection of periodic disturbances with unknown period - a frequency domain approach, in: Proceedings of American Control Conference, Baltimore, 1994, pp. 1626–1631.

[12] C.D. Johnson, Theory of disturbance-accommodating controllers, in: C.T. Leondes (Ed.), Control and Dynamical Systems, vol. 12, 1976, pp. 387–489.

[13] I.D. Landau, M. Alma, A. Constantinescu, J.J. Martinez, M. Noë, Adaptive regulation—rejection of unknown multiple narrow band disturbances (a review on algorithms and applications), Control Engineering Practice 19 (10) (2011) 1168–1181.

[14] I.D. Landau, R. Lozano, M. M'Saad, A. Karimi, Adaptive Control, 2nd ed., Springer, London, 2011.

[15] I.D. Landau, T.B. Airimitoaie, A. Castellanos Silva, G. Buche, Benchmark on adaptive regulation. ⟨http://www.gipsa-lab.grenoble-inp.fr/ioandore.landau/benchmark_adaptive_regulation/⟩.

[16] I.D. Landau, M. Alma, J.J. Martinez, G. Buche, Adaptive suppression of multiple time-varying unknown vibrations using an inertial actuator, IEEE Transactions on Control Systems Technology 19 (November (6)) (2011) 1327–1338.

[17] I.D. Landau, A. Constantinescu, D. Rey, Adaptive narrow band disturbance rejection applied to an active suspension - an internal model principle approach, Automatica 41 (4) (2005) 563–574.

[18] I.D. Landau, A. Castellanos Silva, T.B. Airimiţoaie, G. Buche, M. Noë, Benchmark on adaptive regulation - rejection of unknown/time-varying multiple narrow band disturbances, European Journal of Control, Synthesis paper (Special Issue), 2013.

[19] I.D. Landau, G. Zito, Digital Control Systems - Design, Identification and Implementation, Springer, London, 2005.

[20] R. Marino, G.L. Santosuosso, Regulation of linear systems with unknown exosystems of uncertain order, IEEE Transactions on Automatic Control 52 (2) (2007) 352–359.

[21] R. Marino, G.L. Santosuosso, P. Tomei, Output feedback stabilization of linear systems with unknown additive output sinusoidal disturbances, European Journal of Control 14 (2) (2008).

[22] H. Procházka, I.D. Landau, Pole placement with sensitivity function shaping using 2nd order digital notch filters, Automatica 39 (6) (2003) 1103–1107.

[23] Y.Z. Tsypkin, Stochastic discrete systems with internal models, Journal of Automation and Information Sciences 29 (4&5) (1997) 156–161.

[24] S. Valentinotti, Adaptive Rejection of Unstable Disturbances: Application to a Fed-Batch Fermentation, Thèse de doctorat, École Polytechnique Fédérale de Lausanne, April 2001.

Appendix C

Indirect Adaptive Regulation Strategy for the Attenuation of Time Varying Narrow-band Disturbances applied to a Benchmark Problem

Authors: Tudor-Bogdan Airimiţoaie, Abraham Castellanos Silva and Ioan Doré Landau
Journal: European Journal of Control 19(4) (2013) 313–325
Type of submission: Regular paper

European Journal of Control 19 (2013) 313–325

Contents lists available at SciVerse ScienceDirect

European Journal of Control

journal homepage: www.elsevier.com/locate/ejcon

Indirect adaptive regulation strategy for the attenuation of time varying narrow-band disturbances applied to a benchmark problem

Tudor-Bogdan Airimiţoaie [a,b], Abraham Castellanos Silva [a], Ioan Doré Landau [a,*]

[a] Control systems department of GIPSA-lab, St. Martin d'Héres, 38402, France
[b] Faculty of Automatic Control and Computers, University "Politehnica" of Bucharest, Bucharest 060042, Romania

ARTICLE INFO

Article history:
Received 8 January 2013
Accepted 5 May 2013
Recommended by A. Karimi/D.W. Clarke
Available online 9 May 2013

Keywords:
Indirect adaptive regulation
Active vibration control
Inertial actuators
Multiple narrow-band disturbances

ABSTRACT

The paper presents an indirect adaptive regulation algorithm for the attenuation of unknown narrow-band disturbances. The main features of this new scheme are (i) the use of adaptive Band-stop Filters (BSFs) tuned at the frequencies of the disturbance and (ii) a procedure for direct identification of frequencies contained in the disturbance. The use of adaptive BSFs allows one to introduce the desired attenuation of the disturbance (instead of total rejection) and simplifies the shaping of the output sensitivity function (to meet the specification for the tolerated amplification outside the frequencies of the disturbance). The proposed approach is evaluated on the benchmark simulator and on the benchmark active vibration control system.

1. Introduction

The present benchmark concerns attenuation of unknown and time varying narrow-band disturbances without an explicit measurement of the disturbance [13]. Only the residual force measurement is provided. Therefore, a feedback approach has to be considered for disturbance attenuation. In general, one considers the disturbances as being a white noise or a Dirac impulse passed through a filter which characterizes the model of the disturbance. For the purpose of this paper, the disturbances are considered to be unknown and/or time varying multiple narrow-band disturbances, in other words their model has time varying coefficients. Adaptive feedback control methods can then be used either in a direct scheme that updates the parameters of a controller at each sampling time or when the disturbance changes or in an indirect scheme that treats the problems of disturbance estimation and controller updating separately.

Various design procedures have been described in the scientific literature: (i) the internal model principle (IMP) [11,2,14], (ii) the disturbance observer [20,9], and (iii) the use of the phase-locked loop structure [7,6]. A popular methodology for this adaptive regulation problem is the design of a controller that incorporates the model of the disturbance (internal model principle). Using the Youla–Kučera parametrization of the controller a direct adaptation technique can be implemented. Using the IMP principle, the complete rejection of the disturbances is attempted (asymptotically). In the case of several narrow-band disturbances, the "water bed" effect on the output sensitivity function (amplification introduced at the other frequencies than those of the disturbances) using IMP may become unacceptable in terms of performance as well as in terms of robustness (unacceptable profile of the output sensitivity function).

In practice however, and in particular for the present benchmark, we do not need a complete rejection of the narrow-band disturbances but just a level of attenuation (IMP does too much!). Introducing only a level of attenuation combined with an appropriate controller design will reduce the "water bed" effect on the output sensitivity function improving both robustness and performance (by reducing the unwanted amplification of the noise). This will become particularly useful in the case of multiple narrow-band disturbances.

In this paper, an indirect adaptive regulation method is presented that is capable of introducing a desired level of attenuation on the disturbances. The most important advantage of this scheme is that the loss of robustness due to the "water bed" effect on the Bode integral of the output sensitivity function can be easily controlled by the design parameters of the new controller. The proposed procedure is based on the shaping of the output sensitivity function using band stop-filters (BSFs) centred at the frequencies corresponding to spikes in the spectrum of the disturbance. One interesting fact that should be mentioned is that the zeros of these BSFs are implemented in the controller while their poles are introduced as desired poles of the closed loop (see also [24,16]). Reduction of the complexity of the computations has been achieved by considering the Youla–Kučera (YK) parametrization of the controller [31,10,29]. This is very important in the perspective of using this controller design procedure in an adaptive scheme. It is important to underline that previous approaches for indirect adaptive regulation were still based on the use of the

* Corresponding author.
E-mail addresses: tudor-bogdan.airimitoaie@gipsa-lab.grenoble-inp.fr (T.-B. Airimiţoaie), abraham.castellanos-silva@gipsa-lab.grenoble-inp.fr (A. Castellanos Silva), ioan-dore.landau@gipsa-lab.grenoble-inp.fr, ioan.landau@gmail.com (I. Doré Landau).

0947-3580/$ - see front matter © 2013 European Control Association. Published by Elsevier Ltd. All rights reserved.
http://dx.doi.org/10.1016/j.ejcon.2013.05.011

IMP and the identification of a model of the disturbance was enough for implementing the procedure [14].

In order to use adaptive BSFs for disturbance attenuation, it is necessary to estimate the frequencies of the narrow-band signals in the disturbance. Therefore, a procedure for the direct estimation of the frequencies of the disturbance has been implemented. Several methods have been proposed by the signal processing community for solving the problem of frequencies estimation from a narrow-band signal [30]. In a continuous time framework and for a small number of disturbances recent solutions have been described in [19,4,5,25]. For estimation using discrete time signals and a theoretically unlimited number of narrow-band spikes, the adaptive notch filter (ANF) approach has been proposed in [22,21] and analysed in a statistical framework in [28]. Revised and improved versions have also been proposed in a number of articles [26,27,8,18,12,23]. In this paper, the estimation approach presented in [28,21] will be used. Combining the frequency estimation procedure and the control design procedure, an indirect adaptive regulation system for attenuation of multiple unknown and/or time varying narrow-band disturbances is obtained, which will be denoted IBSF in the remainder of this paper.

The paper is organized as follows. Section 2 presents the general plant and controller structure in the context of the YK parametrization. To better understand the proposed approach, the linear controller design is presented in Section 3 considering, temporarily, constant and known frequencies of the narrow-band disturbances. Then in Section 4 the frequency estimation technique based on ANF is recalled. It can be combined with the linear controller design technique from the previous section to complete the indirect adaptive controller scheme. Section 5 discusses briefly the design of the central controller and simulation results are shown in Section 6. Experimental results are given in Section 7 where also a comparison with simulation results is performed. Concluding remarks are presented in Section 8.

2. Plant representation and controller structure

The structure of the LTI discrete time model of the plant, also called *secondary path*, used for controller design is

$$G(z^{-1}) = \frac{z^{-d}B(z^{-1})}{A(z^{-1})} = \frac{z^{-d-1}B^*(z^{-1})}{A(z^{-1})}, \tag{1}$$

where

$$A(z^{-1}) = 1 + a_1 z^{-1} + \cdots + a_{n_A} z^{-n_A}, \tag{2}$$

$$B(z^{-1}) = b_1 z^{-1} + \cdots + b_{n_B} z^{-n_B} = z^{-1} B^*(z^{-1}), \tag{3}$$

$$B^*(z^{-1}) = b_1 + \cdots + b_{n_B} z^{-n_B+1}, \tag{4}$$

and d is the plant pure time delay in a number of sampling periods.[1] In the context of this paper the hypothesis of constant dynamic characteristics of the AVC (Active Vibration Control) system is made and it is also supposed that the corresponding control model (secondary path) is accurately identified from input/output data.

The output of the plant $y(t)$ and the input $u(t)$ may be written as (see Fig. 1)

$$y(t) = \frac{q^{-d}B(q^{-1})}{A(q^{-1})} \cdot u(t) + p(t), \tag{5}$$

$$S(q^{-1}) \cdot u(t) = -R(q^{-1}) \cdot y(t), \tag{6}$$

[1] The complex variable z^{-1} will be used to characterize the system's behaviour in the frequency domain and the delay operator q^{-1} will be used for the time domain analysis.

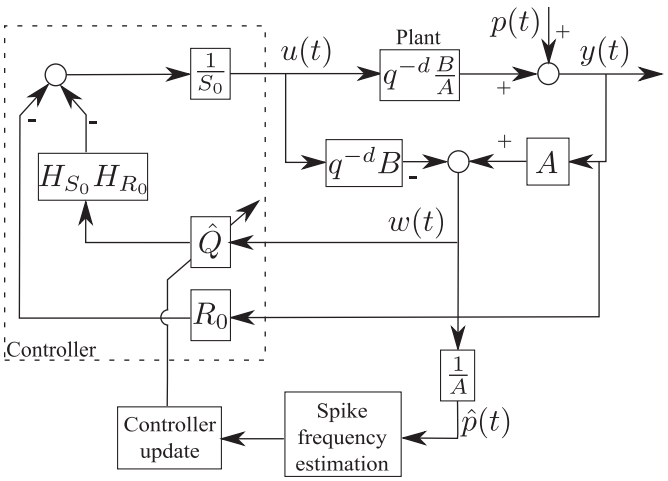

Fig. 1. Indirect adaptive regulation scheme using Youla–Kučera parametrized controller with adaptive $\hat{Q}$ filter.

with $p(t) = (N_p/D_p)\delta(t) + v(t)$, where $\delta(t)$ is the Dirac impulse passed through a model of the *primary path*, whose denominator, D_p, has all its zeroes on the unit circle, and $v(t)$ is a zero mean white noise.

In this paper, the Youla–Kučera parametrization [3,31] is used. Supposing a generalized infinite impulse response (IIR) representation of the adaptive Q filter

$$Q(z^{-1}) = \frac{B_Q(z^{-1})}{A_Q(z^{-1})}, \tag{7}$$

the controller's polynomials are[2]

$$R = R_0 A_Q + A B_Q H_{S_0} H_{R_0}, \tag{8}$$

$$S = S_0 A_Q - z^{-d} B B_Q H_{S_0} H_{R_0}. \tag{9}$$

where R_0 and S_0 define the central controller and have the expressions:

$$S_0 = 1 + s_1^0 z^{-1} + \ldots + s_{n_S}^0 z^{-n_S} = S'_0 \cdot H_{S_0}, \tag{10}$$

$$R_0 = r_0^0 + r_1^0 z^{-1} + \ldots + r_{n_R}^0 z^{-n_R} = R'_0 \cdot H_{R_0}. \tag{11}$$

Let define also the characteristic polynomial of the nominal system

$$P_0(z^{-1}) = A(z^{-1})S_0(z^{-1}) + z^{-d}B(z^{-1})R_0(z^{-1}), \tag{12}$$

which specifies the desired closed loop poles of the feedback loop composed only by the process and the central controller (see also [16]). The characteristic polynomial of the closed loop with Youla–Kučera parametrized controller becomes

$$P(z^{-1}) = A_Q(z^{-1})P_0(z^{-1}). \tag{13}$$

In (10) and (11), $H_{S0}(z^{-1})$ and $H_{R0}(z^{-1})$ represent pre-specified parts of the controller (used for example to incorporate the internal model of a disturbance or to open the loop at certain frequencies) and $S'_0(z^{-1})$ and $R'_0(z^{-1})$ are computed. The central controller is designed in order to fulfil desired specifications in the absence of the disturbance.

We define the output sensitivity function (the transfer function between the disturbance $p(t)$ and the output of the system $y(t)$) as

$$S_{yp}(z^{-1}) = \frac{A(z^{-1})S(z^{-1})}{P(z^{-1})} \tag{14}$$

[2] The argument (z^{-1}) will be omitted in some of the following equations to make them more compact.

and the input sensitivity function (the transfer function between the disturbance $p(t)$ and the control input $u(t)$) as

$$S_{up}(z^{-1}) = -\frac{A(z^{-1})R(z^{-1})}{P(z^{-1})}. \tag{15}$$

It is important to remark that one should only reject disturbances located in frequency regions where the plant model has enough gain. This can be seen by looking at Eq. (14) and noticing that perfect rejection at a certain frequency, ω_0, is obtained *iff* $S(e^{-j\omega_0}) = 0$. On the other hand, from Eq. (15) one can see that this has a bad effect on the control input if the gain of the secondary path is too small at ω_0, since at this frequency the modulus of the input sensitivity function becomes $|S_{up}(e^{-j\omega_0})| = |A(e^{-j\omega_0})/B(e^{-j\omega_0})|$. This implies that the robustness vs additive plant model uncertainties is reduced and the stress on the actuator will become important. Furthermore, it can be observed that serious problems will occur if $B(z^{-1})$ has complex zeros close to the unit circle at frequencies where an important attenuation of disturbances is introduced. It is mandatory to avoid attenuation of disturbances at these frequencies [14].

In addition to what has already been specified, it is also important to have a low magnitude of the input sensitivity function outside the region of attenuation in order to avoid amplification of noise and to have a good robustness with respect to model uncertainties.

3. Indirect adaptive regulation based on BSFs for disturbance attenuation

In this section, a technique of output sensitivity function shaping for narrow-band disturbance attenuation is presented. The controller parameters computation procedure will be presented considering constant and known frequencies of the narrow-band disturbances $\omega_i, \forall i \in \{1, \ldots, n\}$ where n (number of spikes in the disturbance's spectral characteristic) is also known (a technique for estimating the frequencies is presented in Section 4).

The design uses BSFs to shape the output sensitivity function. Following [16,24], there exist digital filters H_{S_i}/P_{F_i}, which will assure the desired attenuation of a narrow-band disturbance. The numerators of these filters are directly included in the controller. The denominators specify a factor in the desired closed loop characteristic polynomial. The transfer function of the BSFs is

$$\frac{S_{BSF_i}(z^{-1})}{P_{BSF_i}(z^{-1})} = \frac{1 + \beta_1^i z^{-1} + \beta_2^i z^{-2}}{1 + \alpha_1^i z^{-1} + \alpha_2^i z^{-2}}, \tag{16}$$

resulting from the discretization of a continuous filter (see also [24,16])

$$F_i(s) = \frac{s^2 + 2\zeta_{n_i}\omega_i s + \omega_i^2}{s^2 + 2\zeta_{d_i}\omega_i s + \omega_i^2} \tag{17}$$

using the bilinear transformation. This filter introduces an attenuation of

$$M_i = -20\log_{10}\left(\frac{\zeta_{n_i}}{\zeta_{d_i}}\right) \tag{18}$$

at the frequency ω_i. Positive values of M_i denote attenuations ($\zeta_{n_i} < \zeta_{d_i}$) and negative values denote amplifications ($\zeta_{n_i} > \zeta_{d_i}$).[3] For n narrow-band disturbances, n BSFs will be used

$$H_{BSF}(z^{-1}) = \frac{S_{BSF}(z^{-1})}{P_{BSF}(z^{-1})} = \frac{\prod_{i=1}^{n} S_{BSF_i}(z^{-1})}{\prod_{i=1}^{n} P_{BSF_i}(z^{-1})}. \tag{19}$$

Remark: The design parameters for each BSF are the desired attenuation (M_i), the central frequency of the filter ($\hat{\omega}_i$) and the damping of the denominator (ζ_{d_i}). The denominator damping is used to adjust the frequency bandwidth of the BSF. For very small values of the frequency bandwidth the influence of the filters on frequencies other than those defined by $\hat{\omega}_i$ is negligible. Therefore, the number of BSFs and subsequently that of the narrow-band disturbances that can be compensated can be as large as necessary.[4]

Next, the computation of the controller's $S(z^{-1})$ and $R(z^{-1})$ polynomials Eqs. ((8) and (9)) is described taking into account that at the end the BSFs have to become part of the output sensitivity function. Without considering the Youla–Kučera parametrization, the controller is computed as solution of a Bezout equation $P(z^{-1}) = A(z^{-1})S(z^{-1}) + z^{-d}B(z^{-1})R(z^{-1})$, where

$$R(z^{-1}) = H_R(z^{-1})R'(z^{-1}), S(z^{-1}) = H_S(z^{-1})S'(z^{-1}), \tag{20}$$

and $P(z^{-1})$ is given by

$$P(z^{-1}) = P_0(z^{-1})P_{BSF}(z^{-1}). \tag{21}$$

In the last equation, P_{BSF} is the combined denominator of all the BSFs (19), and P_0 can define any other poles, e.g., from an initial robust control design as in (12). The fixed part of the controller denominator H_S is in turn factorized into

$$H_S(z^{-1}) = S_{BSF}(z^{-1})H_{S_0}(z^{-1}), \tag{22}$$

where S_{BSF} is the combined numerator of the BSFs (19), and H_{S_0} is the fixed part of the denominator in the initial robust controller (see (10)). The fixed part of R is equal to that used for the initial robust controller, i.e. $H_R = H_{R_0}$. It is easy to see that the output sensitivity function becomes

$$S_{yp}(z^{-1}) = \frac{A(z^{-1})S(z^{-1})}{P(z^{-1})} = \frac{AS'H_{S_0}S_{BSF}}{P_0P_{BSF}} \tag{23}$$

and the shaping effect of the BSFs upon the sensitivity functions is obtained.

The unknowns S' and R' are solutions of

$$P(z^{-1}) = P_0(z^{-1})P_{BSF}(z^{-1}) = A(z^{-1})H_S(z^{-1})S'(z^{-1}) + z^{-d}B(z^{-1})H_{R_0}(z^{-1})R'(z^{-1}) \tag{24}$$

and can be computed by putting (24) into a matrix form (see also [16]). The size of the matrix equation that needs to be solved is given by

$$n_{Bez} = n_A + n_B + d + n_{H_{S_0}} + n_{H_{R_0}} + 2\cdot n - 1, \tag{25}$$

where n_A, n_B, and d are respectively the order of the plant's model denominator, numerator, and delay (given in (2) and (3)), n_{HS0} and n_{HR0} are the orders of $H_{S0}(z^{-1})$ and $H_{R0}(z^{-1})$ respectively and n is the number of narrow-band disturbances. Eq. (24) has an unique minimal degree solution for S' and R', if

$$n_P \le n_{Bez}, \tag{26}$$

where n_P is the order of the pre-specified characteristic polynomial $P(q^{-1})$. Also, it can be seen from (24) and (22) that the minimal orders of S' and R' will be

$$n_{S'} = n_B + d + n_{H_{R_0}} - 1, \quad n_{R'} = n_A + n_{H_{S_0}} + 2\cdot n - 1. \tag{27}$$

Note that for real time applications, the diophantine equation (24) has to be solved either at each sampling time (adaptive operation) or each time when a change in the narrow-band disturbances' frequencies occurs (self-tuning operation).

The computational complexity related to the Bezout equation (24) is significant. We show next how the computation load of the

[3] For frequencies below $0.17f_s$ (f_s is the sampling frequency) the design can be done with a very good precision directly in discrete time [16].

[4] Of course, there is a compromise between the attenuation imposed and the number of narrow-band disturbances.

algorithm can be reduced by the use of the Youla–Kučera parametrization with IIR parameter (7). Using this, the initial robust controller from (10) and (11) becomes the central controller of the parametrization as in (8) and (9).

In (8) and (9), $A_Q(z^{-1})$ will be chosen as the cumulated denominator of the BSFs, $P_{BSF}(z^{-1})$, while $B_Q(z^{-1})$ is computed so that it allows one to introduce the BSFs' numerators into the fixed part of $S(z^{-1})$, as in (22). Taking into account (9), this is equivalent to find $B_Q(z^{-1})$ from the Bezout equation

$$S'_0 P_{BSF} = S_{BSF} S' + q^{-d} B H_{R_0} B_Q, \tag{28}$$

where the common term $H_{S0}(z^{-1})$ has been eliminated.

In the last equation, the left side of the equal sign is known and on its right side only $S'(z^{-1})$ and $B_Q(z^{-1})$ are unknown. This is also a Bezout equation which can be solved by finding the solution to a matrix equation of dimension

$$n_{Bez_{YK}} = n_B + d + n_{H_{R_0}} + 2 \cdot n - 1. \tag{29}$$

As it can be observed, the size of the new Bezout equation is reduced in comparison to (25) by $n_A + n_{H_{S_0}}$. For systems with large dimensions, this has a significant influence on the computation time (in Sections 6 and 7, $n_A = 22$ and $n_{HS0} = 0$). Taking into account that the central controller is a unique and minimal degree solution of the Bezout equation (12), we find that the left hand side of (28) is a polynomial of degree

$$n_{S'_0} + 2 \cdot n = 2 \cdot n + n_B + d + n_{H_{R_0}} - 1 \tag{30}$$

which is equal to the quantity given in (29). Therefore, the solution of the simplified Bezout equation (28) is unique and of minimal degree. Furthermore, the order of the B_Q FIR filter is equal to $2 \cdot n - 1$ (where n is the number of narrow-band signals in the disturbance).

4. Frequency estimation using adaptive notch filters

In order to use the proposed control strategy in the presence of unknown and/or time varying narrow-band disturbances, one needs an estimation in real time of the spikes' frequencies in the spectrum of the disturbance. In the framework of narrow-band disturbance rejection, it is usually supposed that the disturbances are in fact sinusoidal signals with variable frequencies. As specified in the introduction, it is assumed that the number of narrow-band disturbances n is known (similar to [15,14,9]). A technique based on ANFs will be used to estimate the frequencies of the sinusoidal signals in the disturbance (more details can be found in [22,21]). Under the hypothesis that the plant model parameters are constant and that an accurate identification experiment can be run, a reliable estimate $\hat{p}(t)$ of the disturbance signal can be obtained by using the disturbance observer

$$\hat{p}(t+1) = y(t+1) - q^{-d} \frac{B^*(q^{-1})}{A(q^{-1})} u(t). \tag{31}$$

The signal $\hat{p}(t)$ can then be used to estimate the spike frequencies ($\hat{\omega}_i$) with adaptive notch filters (ANF) as will be described in Section 4. The general form of an ANF is

$$H_f(z^{-1}) = \frac{A_f(z^{-1})}{A_f(\rho z^{-1})}, \tag{32}$$

where the polynomial $A_f(z^{-1})$ is such that the zeros of the transfer function $H_f(z^{-1})$ lie on the unit circle. A necessary condition for a monic polynomial to satisfy this property is that its coefficients have a mirror symmetric form

$$A_f = 1 + a_1^f z^{-1} + \cdots + a_n^f z^{-n} + \cdots + a_1^f z^{-2n+1} + z^{-2n}. \tag{33}$$

Another requirement is that the poles of the ANF should be on the same radial lines as the zeros but slightly closer to the origin of the unit circle. Using filter denominators of the general form $A_f(\rho z^{-1})$ with ρ being a positive real number smaller but close to 1, the poles have the desired property and are in fact located on a circle of radius ρ [22].

The estimation algorithm will be detailed next. It is assumed that the disturbance signal (or a good estimation) is available. A cascade construction of second order ANF filters is considered. Their number is given by the number of narrow-band signals whose frequencies have to be estimated. The main idea behind this algorithm is to consider the signal $\hat{p}(t)$ as having the form

$$\hat{p}(t) = \sum_{i=1}^{n} c_i \sin(\omega_i \cdot t + \beta_i) + v(t), \tag{34}$$

where $v(t)$ is the noise affecting the measurement.

The ANF cascade form will be given by (this is an equivalent representation of Eqs. (32) and (33))

$$H_f(z^{-1}) = \prod_{i=1}^{n} H_f^i(z^{-1}) = \prod_{i=1}^{n} \frac{1 + a^{f_i} z^{-1} + z^{-2}}{1 + \rho a^{f_i} z^{-1} + \rho^2 z^{-2}}. \tag{35}$$

Next, the estimation of one spike's frequency is considered, assuming convergence of the other $n-1$, which can thus by filtered out of the estimated disturbance signal, $\hat{p}(t)$, by applying

$$\hat{p}^j(t) = \prod_{\substack{i=1 \\ i \neq j}}^{n} \frac{1 + a^{f_i} z^{-1} + z^{-2}}{1 + \rho a^{f_i} z^{-1} + \rho^2 z^{-2}} \hat{p}(t). \tag{36}$$

The prediction error is obtained from

$$\epsilon(t) = H_f(z^{-1}) \hat{p}(t) \tag{37}$$

and can be computed based on one of the $\hat{p}^j(t)$ to reduce the computation complexity. Each cell can be adapted independently after prefiltering the signal by the others. Following the Recursive Prediction Error (RPE) technique, the gradient is obtained as

$$\Psi^j(t) = -\frac{\partial \epsilon(t)}{\partial a^{f_j}} = \frac{(1-\rho)(1-\rho z^{-2})}{1 + \rho a^{f_j} z^{-1} + \rho^2 z^{-2}} \hat{p}^j(t). \tag{38}$$

The parametric adaptation algorithm can be summarized as

$$\hat{a}^{f_j}(t) = \hat{a}^{f_j}(t-1) + F(t-1) \cdot \Psi^j(t) \cdot \epsilon(t) \tag{39}$$

$$F(t) = \frac{F(t-1)}{\lambda + F(t-1) \Psi^j(t)^2}. \tag{40}$$

where $\hat{a}^{f_j}$ are the estimations of the true a_j^f, which are connected to the narrow-band signals' frequencies by $\omega_{f_j} = f_s \arccos(-a^{f_j}/2)$, where f_s is the sampling frequency.

Combining the linear controller design presented in Section 3 with the spike frequency estimations presented here, an indirect adaptive regulation scheme is obtained. A stability proof for this scheme has been given in [1].

5. Central controller design

A key element of the IBSF is the central controller, which is presented in Eqs. (10) and (11). Its aim is to ensure closed loop robustness with respect to model uncertainties and noise outside the attenuation region. The design of the central controller is described in this section. The main tool used has been the sensitivity functions shaping. As there exist uncertainties in the estimated parameters of the system, an important aspect is that of minimizing the effect of possibly undesired dynamics and unmodelled noise [17]. Therefore, outside the frequency region of interest for control (the disturbances are located between 50 and 95 Hz) the input sensitivity (15) function is reduced.

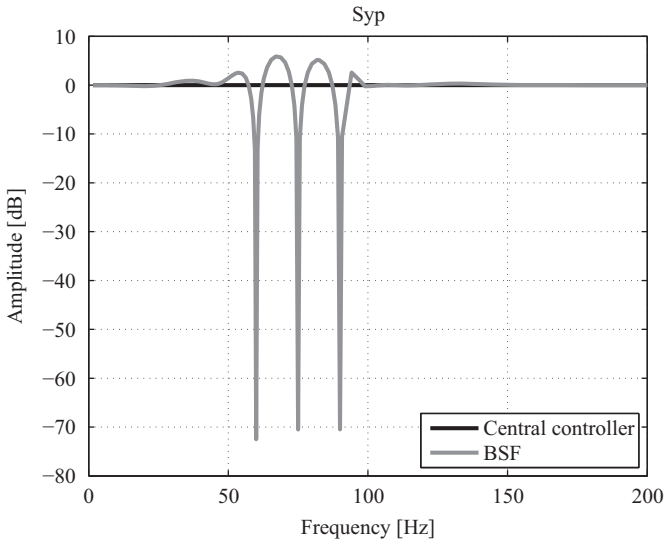

Fig. 2. Output sensitivity functions comparison for a central controller and a BSF controller designed to attenuate disturbances at 60, 75, and 90 Hz.

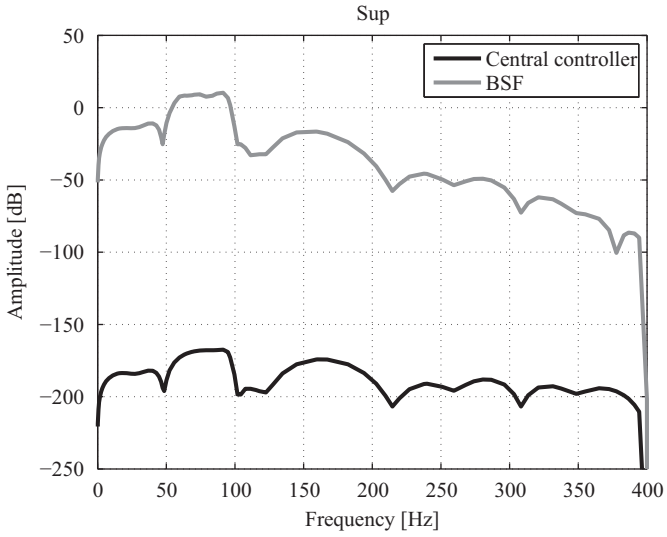

Fig. 3. Input sensitivity functions comparison for a central controller and a BSF controller designed to attenuate disturbances at 60, 75, and 90 Hz.

For the specific case that was the benchmark active vibration control system, first all the poles of the secondary path are conserved as poles of the closed loop (the system is stable). In addition, two pairs of complex fixed *auxiliary* low damped poles are introduced near to the limits of the frequency region of interest, at 50 and at 95 Hz, in order to improve the system's robustness. The effect is the decrease of the magnitudes of the sensitivity functions outside this region.

Finally, fixed parts are introduced in the central controller's numerator, $R_0(z^{-1})$, for opening the loop at $0f_s$ and $0.5f_s$ (required by the benchmark specifications). No fixed parts were considered for $S_0(z^{-1})$.

Given the characteristics of the BSFs, the design of the central controller is simplified since the shape of the sensitivity functions (i.e., the robustness of the closed loop system) is only slightly modified when the BSFs for attenuation are introduced. Therefore, a single central controller can be designed for the three levels of the benchmark.

Fig. 2 shows a comparison of the output sensitivity functions obtained with the central controller presented previously and a controller that introduces in addition 3 BSFs to attenuate narrowband disturbances at 60, 75, and 90 Hz. For the BSFs, an attenuation of 80 dB and a damping of the denominator of 0.09 have been used. It can be observed that only a minor increase in the output sensitivity function is introduced for the desired level of attenuation, which proves that the proposed method is capable of offering satisfactory robust performance. For the same situation, the input sensitivity function is shown in Fig. 3. It can be seen that the transfer from disturbance to control signal is significantly below 0 dB outside the frequency region of interest even when the BSFs are introduced. As a consequence, the residual noise is not amplified and a good robustness with respect to plant model uncertainties is assured.

6. Simulation results

Regarding the parameters used in the IBSF, through all the simulation and experimental tests, the ANFs use a ρ of 0.92 and the BSFs have been chosen with an attenuation of 80 dB and a denominator damping of 0.09.

The IBSF approach was tested first in simulation and the results are presented in the following subsections. The benchmark considers three levels in terms of the number of unknown narrowband disturbances. For each level, according to the benchmark specifications, there are three tests. For each one, specifications have been set for the frequency and time domains. For the frequency domain, we evaluate global attenuation (GA, in dB), disturbance attenuation (DA, in dB) and maximum amplification (MA) outside the attenuation frequencies (in pairs of dB@Hz). In the time domain, evaluation is done for: maximum value during the chirp (in V) and transient performance.

The basic specification for transient performance is the requirement that the transient duration (TD) when a disturbance is applied, be smaller than 2 s. Details of the measurement procedure can be found in [13]. From the point of view of the benchmark, this means that 2 s after application of a disturbance, the square of the truncated two norm has to be equal or smaller than 1.21 of the steady state value of the square of the truncated two norm of the residual force. The square of the truncated two norm is evaluated over an interval of 3 s both for transient and steady state, taking in account that disturbance is applied at $t=5$ s and that steady state is evaluated between 17 and 20 s. The square of the truncated two norms is denoted as $N2T(v{:}w)$, where v and w define the interval of computation. One defines

$$TD_i = \frac{N2T(7:10)}{N2T(17:20)} \tag{41}$$

$$\Delta Trans_i = TD_i - 1.21 \quad \text{if } TD_i > 1.21 \tag{42}$$

$$\Delta Trans_i = 0 \quad \text{if } TD_i \le 1.21,\ \forall\, i = 1,\ldots,M \tag{43}$$

If TD_i is smaller than 1.21 it means that the specifications for transient duration are satisfied (less or equal to 2 s).

Other measurements are also considered in order to asses the performance of the approach. Such measurements include quadratic norm of the transient and the residual (once the algorithm converges), the maximum value during the transient and the mean-square error during the chirp.

6.1. Level 1

For level one of the benchmark, the results, in the presence of a constant frequency disturbance (called *Simple Step Test*), are summarized in Table 1. As it can be seen, in general, all the specifications were fulfilled (one notices however a global attenuation below the required value of 24 dB at 95 Hz). Since

Table 1
Simulation results—Simple Step Test.

Frequency (Hz)	Global (dB)	Dist. Atten. (dB)	Max. Amp. (dB@Hz)	Norm^2 Trans. ($\times 10^{-3}$)	Norm^2 Res. ($\times 10^{-3}$)	Max. Val. ($\times 10^{-3}$)	TD (ratio)
Level 1							
50	34.52	46.78	6.41@59.38	21.01	3.60	18.09	1.085
55	34.47	50.04	4.21@68.75	24.14	3.65	20.70	1.081
60	34.40	48.10	3.89@68.75	25.66	3.68	21.84	1.089
65	34.40	48.52	3.59@76.56	18.87	3.74	19.36	1.073
70	34.47	54.06	2.84@79.69	11.26	3.75	21.26	1.067
75	34.84	54.26	3.06@67.19	7.84	3.68	22.82	1.067
80	35.12	49.11	3.34@67.19	7.61	3.52	23.51	1.083
85	34.88	49.97	3.40@70.31	8.69	3.50	23.55	1.091
90	32.69	43.65	4.06@78.13	149.86	3.70	40.94	1.078
95	23.78	40.36	7.86@87.50	200.93	4.60	38.80	1.073
Level 2							
50–70	39.68	45.48–50.32	7.54@59.38	115.56	4.01	43.13	1.063
55–75	39.98	48.18–50.82	6.29@67.19	261.46	3.94	51.75	1.066
60–80	40.51	45.91–46.35	5.76@68.75	476.28	3.68	53.36	1.101
65–85	40.36	46.28–47.42	5.65@73.44	375.31	3.71	49.41	1.090
70–90	38.99	52.14–43.25	5.36@76.56	245.35	3.98	42.43	1.065
75–95	35.25	52.02–40.49	8.50@87.50	144.05	4.68	49.25	10.110
Level 3							
50–65–80	43.28	44.04–42.67–43.58	7.52@56.26	29.80	3.99	50.43	1.068
55–70–85	43.26	46.34–47.80–45.53	6.63@62.50	56.60	3.98	53.31	1.075
60–75–90	42.61	45.40–50.13–42.07	6.78@68.75	131.40	4.07	65.38	1.075
65–80–95	40.48	45.29–42.19–38.66	8.62@87.50	205.41	4.36	82.05	1.068

Table 2
Simulation results—Level 1—Step Frequency Changes Test.

Frequency (Hz)	Norm^2 Trans. ($\times 10^{-3}$)	Max. Val. ($\times 10^{-3}$)
Sequence 1		
60→70	43.25	23.22
70→60	40.17	21.01
60→50	31.51	18.76
50→60	50.93	30.19
Sequence 2		
75→85	44.71	21.24
85→75	52.24	21.29
75→65	45.09	19.87
65→75	43.27	22.94
Sequence 3		
85→95	56.03	23.15
95→85	104.22	36.57
85→75	51.71	22.15
75→85	44.10	21.12

Table 3
Simulation results—Level 1—Chirp Test.

	Error-mean square value ($\times 10^{-6}$)	Error-maximum value ($\times 10^{-3}$)
↗	39.229	13.228
↘	53.673	18.688

this approach uses the frequency estimation described in [22,21], the performance of the control scheme relies on how fast the frequency is estimated, thereby the transient duration results are strongly linked to this issue. For the case when step changes in the frequency of the disturbance occur (called *Step Frequency Changes Test*), the results are shown in Table 2. The results for the chirp disturbance test (called *Chirp Test*) are summarized in Table 3. ↗ denotes linearly increasing frequency chirp disturbance, while ↘ is used to denote the disturbance with linearly decreasing frequencies. The maximum value during the chirp periods did not exceed the imposed limit of 0.1 V.

Table 4
Simulation results—Level 2—Step Frequency Changes Test.

Frequency (Hz)	Norm^2 Trans. ($\times 10^{-3}$)	Max. Val. ($\times 10^{-3}$)
Sequence 1		
[55, 75]→[60, 80]	37.65	34.75
[60, 80]→[55, 75]	36.85	33.37
[55, 75]→[50, 70]	38.40	32.51
[50, 70]→[55, 75]	43.66	36.21
Sequence 2		
[70, 90]→[75, 95]	40.40	28.90
[75, 95]→[70, 90]	64.08	40.62
[70, 90]→[65, 85]	38.14	31.23
[65, 85]→[70, 90]	37.38	31.43

Table 5
Simulation results—Level 2—Chirp Test.

	Error-mean square value ($\times 10^{-6}$)	Error-maximum value ($\times 10^{-3}$)
↗	25.998	13.416
↘	29.678	16.466

6.2. Level 2

For the second level of the benchmark, the results of the proposed approach during the Simple Step Test are shown in Table 1. Almost all the benchmark specifications were satisfied, the only criterion which is not met being the maximum amplification and the transient duration ratio at 75–95 Hz. The other values for the TD ratio are within the requirements for the benchmark. For Step Frequency Changes Test and Chirp Test, the limits were respected as it can be seen in Tables 4 and 5.

6.3. Level 3

On the third level, for Simple Step Test, only at 95 Hz the disturbance attenuation requirement was not achieved as imposed by the benchmark specifications (see Table 1). The Step Frequency Changes and Chirp Tests results are shown in Tables 6 and 7.

7. Experimental results

Using the same central controller and frequency estimation configuration (Section 5), the following real-time results were obtained.

Table 6
Simulation results—Level 3—Step Frequency Changes Test.

Frequency (Hz)	Norm^2 Trans. ($\times 10^{-3}$)	Max. Val. ($\times 10^{-3}$)
Sequence 1		
[55, 70, 85]→[60, 75, 90]	84.74	58.41
[60, 75, 90]→[55, 70, 85]	86.05	59.28
[55, 70, 85]→[50, 65, 80]	90.77	58.00
[50, 65, 80]→[55, 70, 85]	91.86	63.18
Sequence 2		
[60, 75, 90]→[65, 80, 95]	85.96	53.62
[65, 80, 95]→[60, 75, 90]	113.25	62.22
[60, 75, 90]→[55, 70, 85]	85.49	60.84
[55, 70, 85]→[60, 75, 90]	84.16	58.74

Table 7
Simulation results—Level 3—Chirp Test.

	Error-mean square value ($\times 10^{-6}$)	Error-maximum value ($\times 10^{-3}$)
↗	15.830	12.494
↘	17.190	12.783

7.1. Level 1 results

In Table 8, the experimental results for Simple Step Level 1 are summarized. The most important differences between these results and the ones obtained in simulation concern the maximum amplification (this is due probably to the model uncertainties, some small error in the estimation of the frequency of the disturbances, and also to the measurement noise present in the

Table 9
Experimental results—Level 1—Step Frequency Changes Test.

Frequency (Hz)	Norm^2 Trans. ($\times 10^{-3}$)	Max. Val. ($\times 10^{-3}$)
Sequence 1		
60→70	49.83	24.68
70→60	50.84	24.68
60→50	63.82	23.46
50→60	81.38	39.39
Sequence 2		
75→85	47.40	20.99
85→75	52.77	20.993
75→65	52.55	23.44
65→75	48.34	24.66
Sequence 3		
85→95	59.21	15.79
95→85	95.33	32.01
85→75	52.48	19.75
75→85	46.39	19.75

Table 10
Experimental results—Level 1—Chirp Test.

	Error-mean square value ($\times 10^{-6}$)	Error-maximum value ($\times 10^{-3}$)
↗	31.783	16.730
↘	35.878	11.828

Table 8
Experimental results—Simple Step Test.

Frequency (Hz)	Global (dB)	Dist. Atten. (dB)	Max. Amp. (dB@Hz)	Norm^2 Trans. ($\times 10^{-3}$)	Norm^2 Res. ($\times 10^{-3}$)	Max. Val. ($\times 10^{-3}$)	TD (ratio)
Level 1							
50	36.17	37.54	11.61@65.63	62.06	6.61	23.57	1.013
55	38.50	49.35	8.15@120.31	33.31	3.60	21.81	1.310
60	36.74	49.20	9.53@46.88	26.13	4.11	20.59	1.088
65	36.25	48.45	8.03@134.38	15.17	3.56	22.35	0.875
70	34.23	52.76	10.66@134.38	9.88	3.67	19.37	1.097
75	33.31	46.91	5.99@134.38	8.45	3.64	18.62	1.029
80	32.65	48.32	7.48@276.56	16.05	3.65	20.56	0.985
85	32.58	48.07	12.03@73.44	20.85	3.55	22.33	1.120
90	31.19	47.38	8.49@14.06	21.18	3.64	24.79	1.071
95	28.83	38.52	10.85@82.21	21.32	3.71	27.22	1.094
Level 2							
50–70	38.44	39.73–47.27	9.29@56.25	50.36	7.68	34.56	0.983
55–75	40.22	48.89–40.72	9.05@270.31	435.20	4.74	63.44	0.982
60–80	39.07	49.94–47.17	9.96@68.75	51.69	3.54	35.96	0.939
65–85	35.86	43.67–43.89	9.75@104.69	25.08	5.13	48.52	0.939
70–90	35.44	47.23–39.01	8.70@134.38	230.78	4.22	84.22	0.923
75–95	35.44	47.23–39.01	8.40@81.25	131.21	4.02	37.69	1.019
Level 3							
50–65–80	41.87	32.47–34.95–43.68	8.02@71.69	44.00	6.46	45.72	1.052
55–70–85	42.53	46.70–46.16–48.35	10.99@62.50	92.26	4.93	58.58	0.890
60–75–90	40.77	49.59–42.09–42.37	8.70@67.19	173.46	5.40	64.68	0.972
65–80–95	41.43	44.85–43.74–36.49	9.88@87.50	340.05	4.47	57.37	0.973

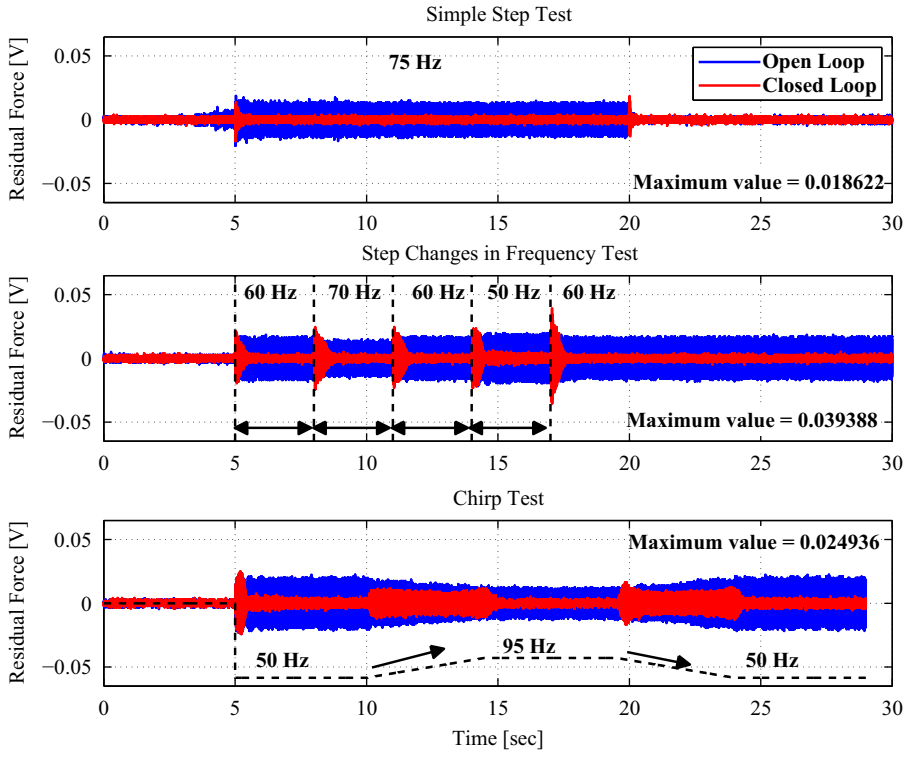

Fig. 4. Time response results for Level 1—experimental.

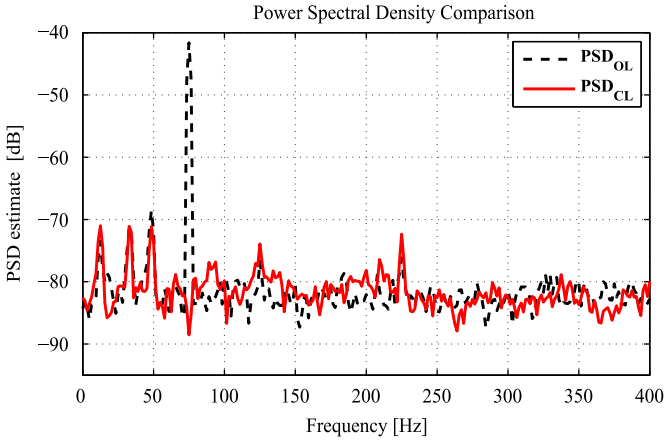

Fig. 5. PSD of the open loop disturbance (black dashed line) and effective attenuation (red line) for 75 Hz—experimental. (For interpretation of the references to color in this figure legend, the reader is referred to the web version of this article.)

Table 11
Experimental results—Level 2—Step Frequency Changes Test.

Frequency (Hz)	**Norm^2 Trans.** ($\times 10^{-3}$)	**Max. Val.** ($\times 10^{-3}$)
Sequence 1		
[55, 75]→[60, 80]	46.39	19.75
[60, 80]→[55, 75]	33.71	37.39
[55, 75]→[50, 70]	50.66	36.70
[50, 70]→[55, 75]	45.62	41.61
Sequence 2		
[70, 90]→[75, 95]	44.15	35.49
[75, 95]→[70, 90]	54.60	36.82
[70, 90]→[65, 85]	38.19	34.26
[65, 85]→[70, 90]	41.22	34.37

Table 12
Experimental results—Level 2—Chirp Test.

	Error-mean square value ($\times 10^{-6}$)	**Error-maximum value** ($\times 10^{-3}$)
↗	34.007	16.307
↘	35.600	16.307

real time evaluations which is not the same as the one used in simulations). Except that the results are close to those obtained in simulation.

Table 9 shows the Step Frequency Changes Test results for this level. In most of the cases, one obtains faster transients in real-time than in simulation. Also for the Chirp Test, the results are generally better than in simulation (Table 10).

The time responses of the system in open loop and in closed loop with the proposed disturbance attenuation approach are shown in Fig. 4 for specific disturbance characteristics (see figure for details). A sufficient level of attenuation is observed in all of the tests. In the case of the simple step test, the power spectral density (PSD) estimate of the open loop and the effective attenuation are shown in Fig. 5. The tests shown in these figure have been selected to be the same for all the participants in order to help evaluate the various approaches.

7.2. Level 2 results

Simple Step Test results for this level are shown in Table 8 and it can be noticed that the algorithm provides in general good results within the specifications of the benchmark with the exception of the maximum amplification which is over the limit. Tables 11 and 12 show the results for the Step Frequency Changes and the Chirp Test.

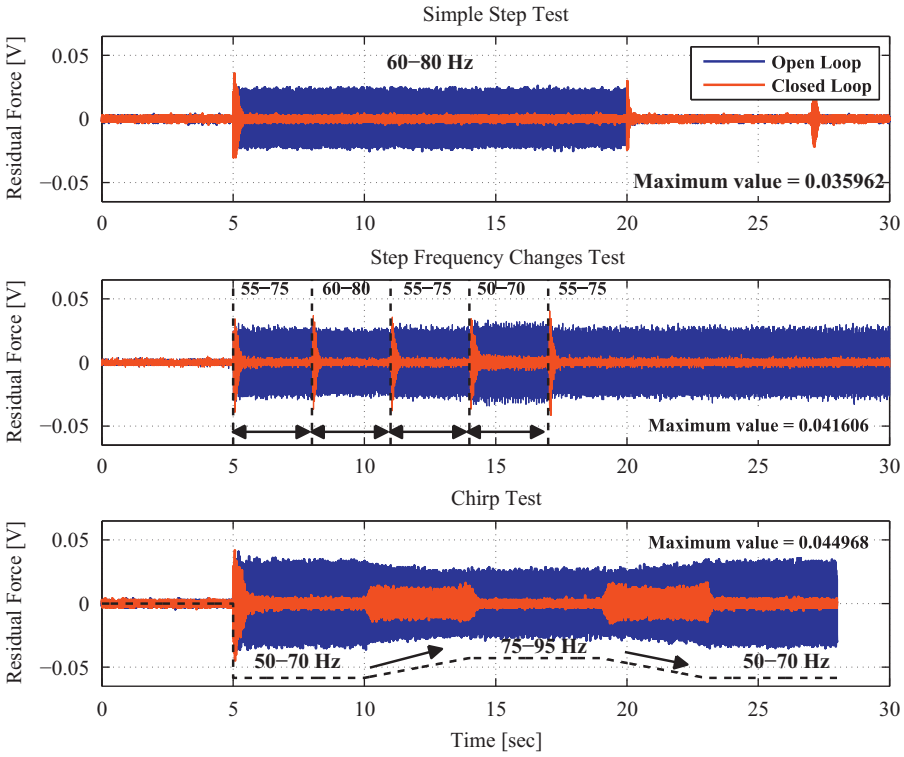

Fig. 6. Time response results for Level 2—experimental.

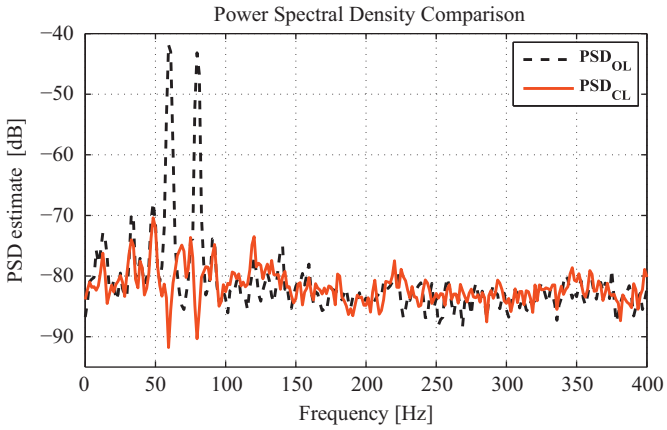

Fig. 7. PSD of the open loop disturbance (black dashed line) and effective attenuation (red line) for 60–80 Hz—experimental. (For interpretation of the references to color in this figure legend, the reader is referred to the web version of this article.)

Table 13
Experimental results—Level 3—Step Frequency Changes Test.

Frequency (Hz)	**Norm² Trans.** ($\times 10^{-3}$)	**Max. Val.** ($\times 10^{-3}$)
Sequence 1		
[55, 70, 85]→[60, 75, 90]	97.33	65.06
[60, 75, 90]→[55, 70, 85]	86.38	64.84
[55, 70, 85]→[50, 65, 80]	103.87	62.61
[50, 65, 80]→[55, 70, 85]	115.15	68.74
Sequence 2		
[60, 75, 90]→[65, 80, 95]	96.45	57.76
[65, 80, 95]→[60, 75, 90]	100.68	61.44
[60, 75, 90]→[55, 70, 85]	85.00	61.44
[55, 70, 85]→[60, 75, 90]	96.50	63.57

Table 14
Experimental results—Level 3—Chirp Test.

	Error-mean square value ($\times 10^{-6}$)	**Error-maximum value** ($\times 10^{-3}$)
↗	19.874	13.749
↘	20.479	13.749

The time responses of the system in open loop and in closed loop with the proposed disturbance attenuation approach are shown in Fig. 6 for specific disturbance characteristics. A sufficient level of attenuation is observed in all of the tests. In the case of the simple step test, the power spectral density (PSD) estimate of the open loop and the effective attenuation are shown in Fig. 7.

7.3. *Level 3 results*

In the most challenging level, the good performance of the algorithm is proved since the benchmark specifications are passed for all the objectives in the Simple Step Test (Table 8). Table 13 shows the results for the Step Frequency Changes Test. It can be observed that both the two norm transient and the maximum value are worse than for the previous level but the values are still acceptable from the benchmark specifications point of view. Meanwhile, in Table 14 the Chirp Test evaluation is shown and the result is even better than for the previous level.

The time responses of the system in open loop and in closed loop with the proposed disturbance attenuation approach are shown in Fig. 8 for specific disturbance characteristics. A sufficient level of attenuation is observed in all of the tests. In the case of the simple step test, the power spectral density (PSD) estimate of the open loop and the effective attenuation are shown in Fig. 9.

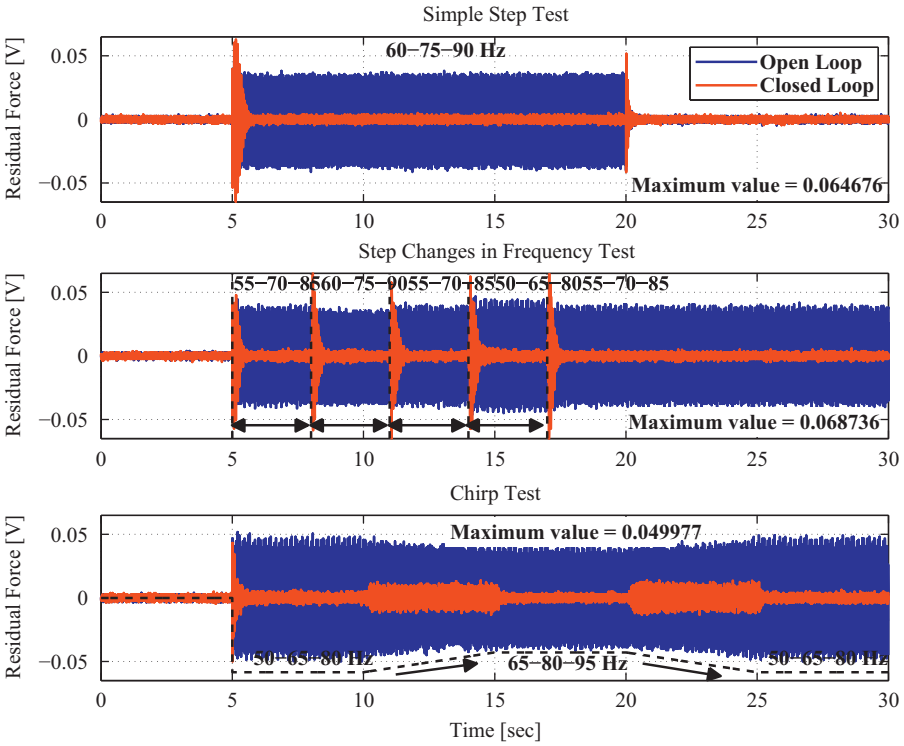

Fig. 8. Time response results for Level 3—experimental.

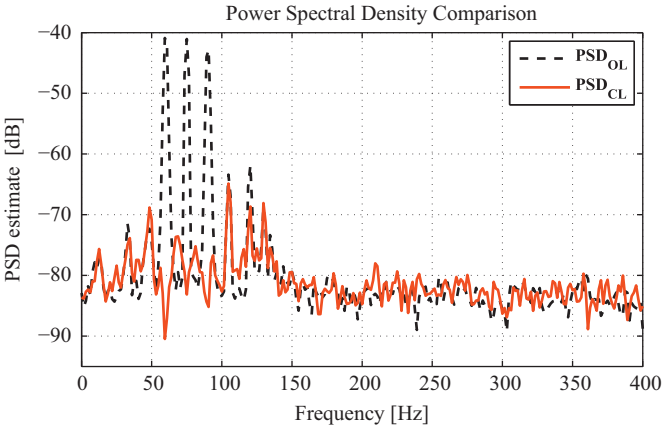

Fig. 9. PSD of the open loop disturbance (black dashed line) and effective attenuation (red line) for 60–75–90 Hz—experimental. (For interpretation of the references to color in this figure legend, the reader is referred to the web version of this article.)

7.4. Comparison with simulation results

The comparison of the GA, DA, MA and TD between simulation (Table 1) and experimental (Table 8) results for the Single Step Test is shown in Fig. 10 for Level 1 of the benchmark, in Fig. 11 for Level 2, and in Fig. 12 for Level 3. The interpretation of these results is given next. For Level 1, one observes in Fig. 10 very similar results with respect to global attenuation and disturbance attenuation. However, for the MA the results obtained experimentally are worse than those obtained in simulation and the main reason for this is that the measurement noise used in simulations is not representative of the one on the real time system (see also [17]) but also to possible model uncertainties. Nevertheless, a modified design of the central controller, which decreases even more the input sensitivity function's amplitude above 100 Hz (by introduction of four additional BSFs in the input sensitivity function). Such a central controller has improved the performances for the Level 1 but not for Levels 2 and 3. With respect to the TD ratio (i.e., ratio between the squared two norm of the residual force from 7 to 10 s and the squared two norm of the residual force from 17 to 20 s, as described by Eqs. (41)–(43)), the experimental results seem overall better than those obtained in simulation (especially for Levels 2, Fig. 11, and 3, Fig. 12).

Another aspect is the maximum amplification, which, by analysing the Level 3 comparison in Fig. 12, is significantly improved with respect to the previous two levels and very close to the simulation results with the single exception of the rejection of a disturbance composed of sinusoids at 55, 70, and 85 Hz.

To complete the comparison, particular disturbance configurations are chosen and further analysed. In Fig. 13, the PSD estimates of the effective attenuation/amplification of the residual during the Simple Step Test are shown.[5] It can be seen that measurement noise is present in the experimental results but the level of the noise in closed loop remains below the benchmark specifications (i.e., below the accepted MA). For the Step Frequency Changes Test, Fig. 14 shows very close results between simulation and real time and a satisfactory level of attenuation for both. The frequency estimation comparison is shown in Fig. 15 for the same protocol as in Fig. 14. It is notable that transient durations in Fig. 14 are related to those in Fig. 15. Finally, a Chirp Test comparison is provided in Fig. 16 and allows one to conclude that both in simulation and in real time the proposed approach gives satisfactory results. Robustness is also shown by the similarity of the simulation and real time results.

[5] Note that the two PSDs are computed with 512 points windows and do not allow one to view the attenuations of 80 dB introduced by the BSFs.

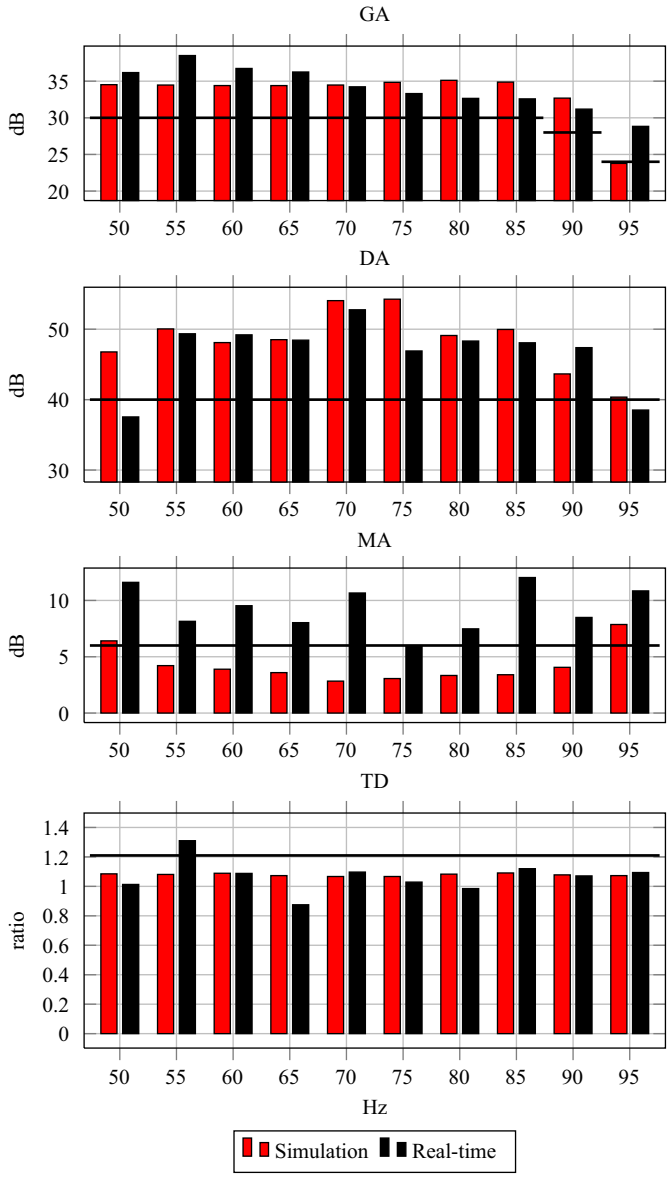

Fig. 10. Level 1 comparison between simulation and experimental results.

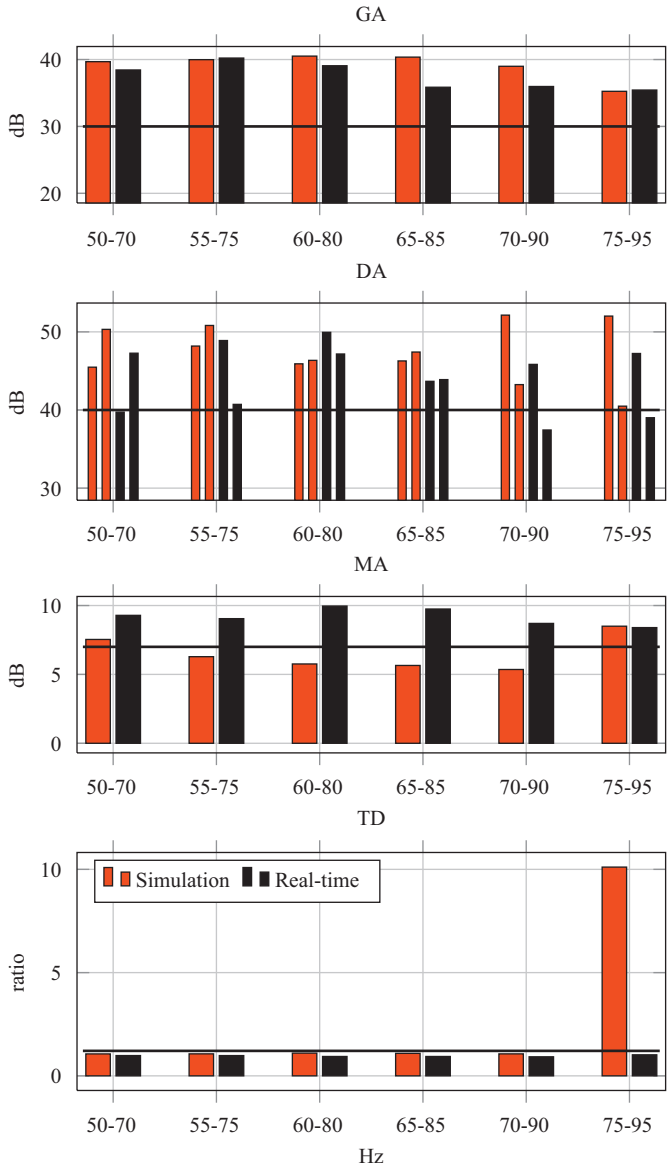

Fig. 11. Level 2 comparison between simulation and experimental results.

8. Concluding remarks

The idea of designing an adaptive controller on which the value of the attenuation can be imposed, proved to be efficient in practice. A single central controller has been used for the three levels of the benchmark in both simulation and in real time.

Experimental results on the benchmark platform have shown a reasonable good coherence between simulation and real time results. The IBSF simplifies the design, since it allows one to obtain good results without the redesign of the central controller for each benchmark level, and seems to be less sensitive with respect to controller design, plant model uncertainties at various frequencies, and to measurement noise. In terms of computational complexity, indirect adaptive control approaches are in general more demanding than direct adaptive control approaches [14], but the compromise between robust performance and computational complexity makes it appealing for the rejection of multiple narrow-band disturbances.

Among the advantages of this approach we should mention an easy and systematic controller design assuring simultaneously a good profile for the sensitivity functions in order to guarantee a good robustness with respect to plant model uncertainties and low noise amplification outside the region of attenuation.

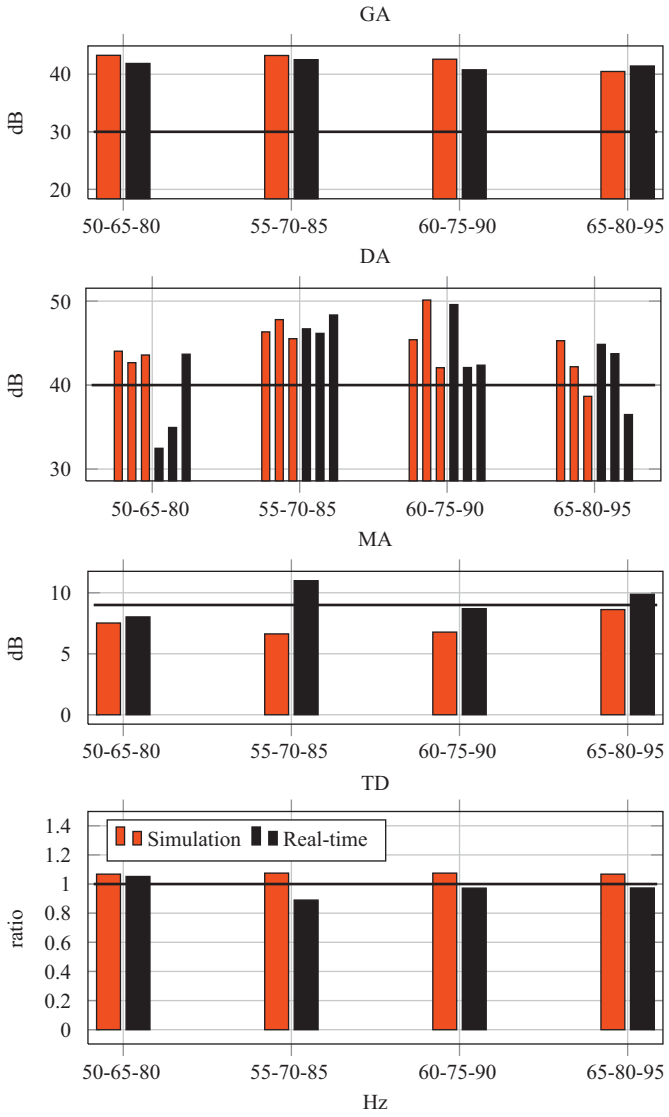

Fig. 12. Level 3 comparison between simulation and experimental results.

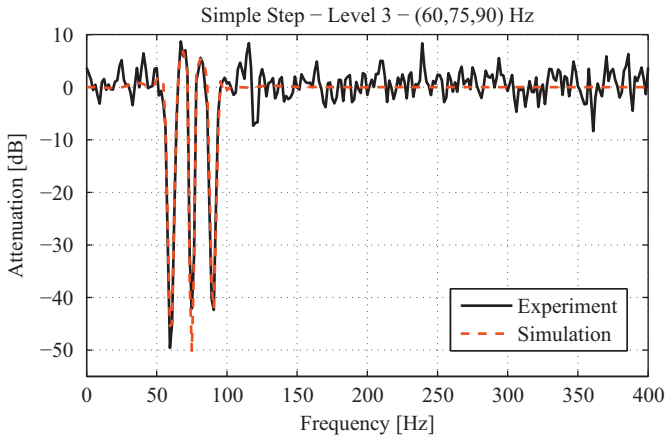

Fig. 13. Effective residual attenuation/amplification PSD estimates computed as the difference between the open loop PSD and the closed loop PSD. Comparison between the simulation and the real-time result for the Simple Step Test with three narrow-band disturbances at 60, 75, and 90 Hz.

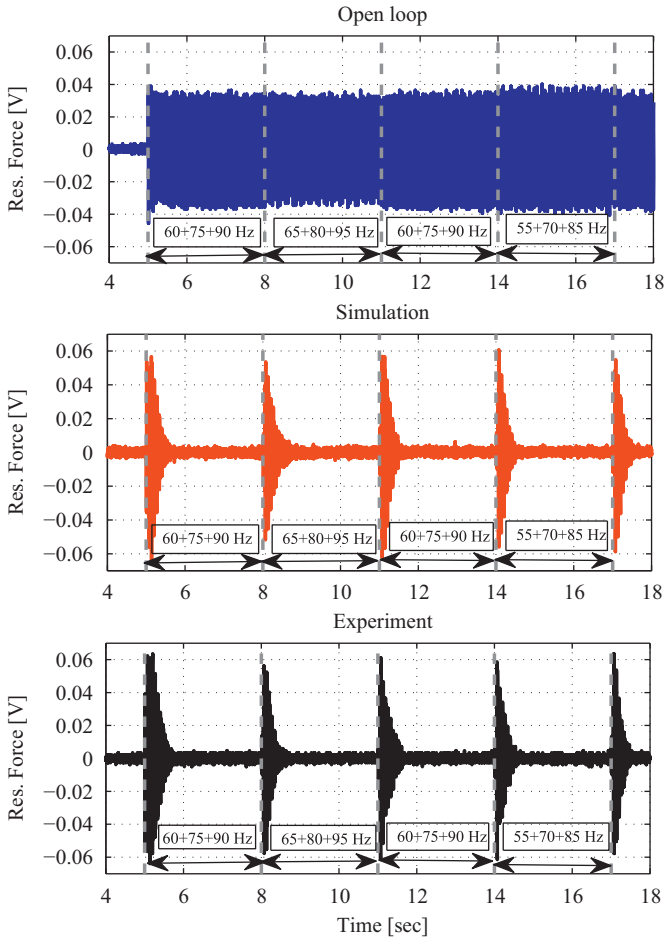

Fig. 14. Time response comparison between the open loop (top), simulation (middle), and the real-time results (bottom) for the Step Frequency Changes Test —Sequence 2.

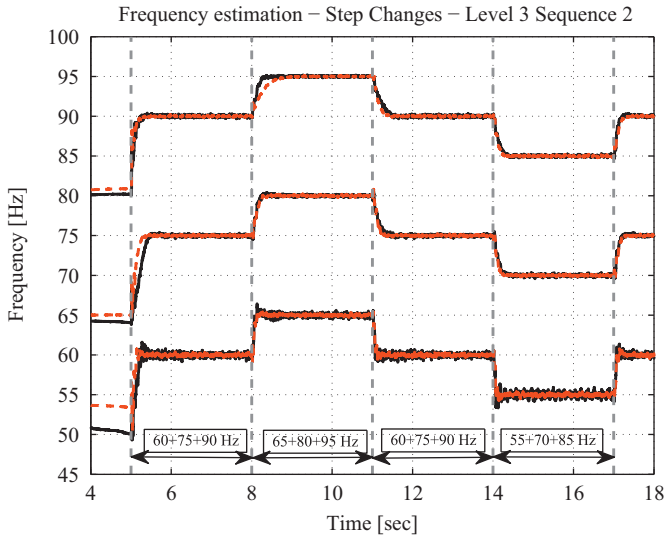

Fig. 15. Frequency estimation for the sequence 2 in real time (solid line) and in simulation (dashed line).

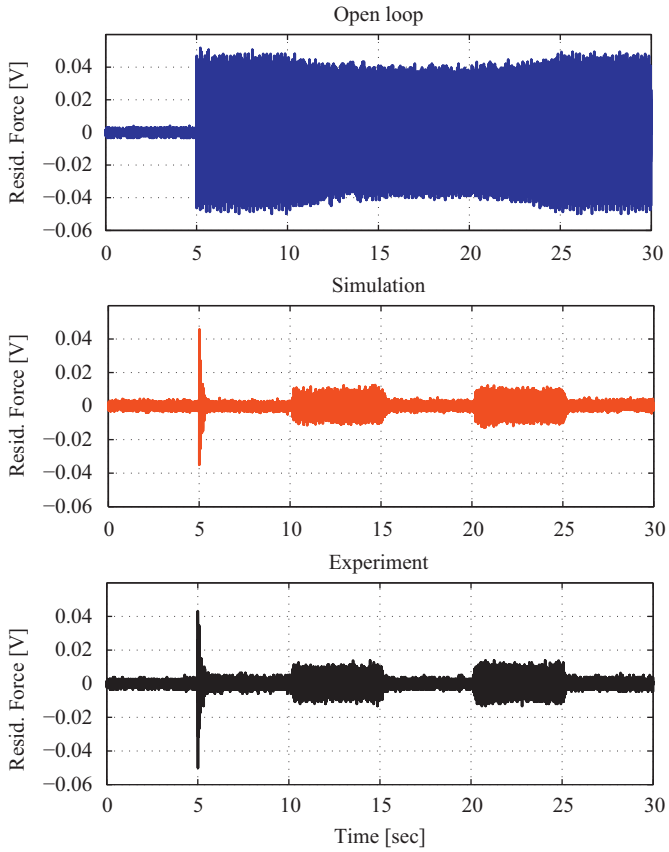

Fig. 16. Time response comparison between the open loop (top), simulation (middle), and real-time (bottom) results for the Chirp Test.

References

[1] T.-B. Airimitoaie, I.D. Landau, Indirect adaptive attenuation of multiple narrow-band disturbances applied to active vibration control, IEEE Transactions on Control Systems Technology, in press, http://dx.doi.org/10.1109/TCST.2013.2257782.

[2] F. Ben Amara, P.T. Kabamba, A.G. Ulsoy, Adaptive sinusoidal disturbance rejection in linear discrete-time systems—Parts I and II, Journal of Dynamic Systems Measurement and Control 121 (1999) 648–659.

[3] B.D.O. Anderson, From Youla–Kucera to identification, adaptive and nonlinear control, Automatica 34 (1998) 1485–1506.

[4] Alexey A. Bobtsov, Denis Efimov, Anton A. Pyrkin, Ali Zolghadri, Switched algorithm for frequency estimation with noise rejection, IEEE Transactions on Automatic Control 57 (9) (2012) 2400–2404.

[5] Alexey A. Bobtsov, Anton A. Pyrkin, Cancelation of unknown multiharmonic disturbance for nonlinear plant with input delay, International Journal of Adaptive Control and Signal Processing 26 (4) (2012) 302–315.

[6] M. Bodson, Rejection of periodic disturbances of unknown and time-varying frequency, International Journal of Adaptive Control and Signal Processing 19 (2005) 67–88.

[7] M. Bodson, S.C. Douglas, Adaptive algorithms for the rejection of sinusoidal disturbances with unknown frequency, Automatica 33 (1997) 2213–2221.

[8] Bor-Sen Chen, Tsang-Yi Yang, Bin-Hong Lin, Adaptive notch filter by direct frequency estimation, Signal Processing 27 (2) (1992) 161–176.

[9] Xu Chen, M. Tomizuka, A minimum parameter adaptive approach for rejecting multiple narrow-band disturbances with application to hard disk drives, IEEE Transactions on Control Systems Technology 20 (March (2)) (2012) 408–415.

[10] Raymond A. de Callafon, Charles E. Kinney, Robust estimation and adaptive controller tuning for variance minimization in servo systems, Journal of Advanced Mechanical Design, Systems, and Manufacturing 4 (1) (2010) 130–142.

[11] B.A. Francis, W.M. Wonham, The internal model principle of control theory, Automatica 12 (5) (1976) 457–465.

[12] Liu Hsu, Romeo Ortega, Gilney Damm, A globally convergent frequency estimator, IEEE Transactions on Automatic Control 4 (4) (1999) 698–713.

[13] I.D. Landau, T.-B. Airimiţoaie, A. Castellanos Silva, G. Buche, Benchmark on adaptive regulation, URL: http://www.gipsa-lab.grenoble-inp.fr/ĩoandore.landau/benchmark_adaptive_regulation/.

[14] I.D. Landau, M. Alma, J.J. Martinez, G. Buche, Adaptive suppression of multiple time-varying unknown vibrations using an inertial actuator, IEEE Transactions on Control Systems Technology 19 (November (6)) (2011) 1327–1338.

[15] I.D. Landau, A. Constantinescu, D. Rey, Adaptive narrow band disturbance rejection applied to an active suspension—an internal model principle approach, Automatica 41 (4) (2005) 563–574.

[16] I.D. Landau, G. Zito, Digital Control Systems—Design, Identification and Implementation, Springer, London, 2005.

[17] Ioan Doré Landau, Abraham Castellanos-Silva, Tudor-Bogdan Airimiţoaie, Gabriel Buche, Mathieu Noe, Benchmark on adaptive regulation—rejection of unknown/time-varying multiple narrow band disturbances, European Journal of Control (2013), this issue.

[18] Gang Li, A stable and efficient adaptive notch filter for direct frequency estimation, IEEE Transactions on Signal Processing 45 (August (8)) (1997) 2001–2009.

[19] R. Marino, G.L. Santosuosso, P. Tomei, Output feedback stabilization of linear systems with unknown additive output sinusoidal disturbances, European Journal of Control 14 (2) (2008) 131–148.

[20] Riccardo Marino, Giovanni L. Santosuosso, Patrizio Tomei, Robust adaptive compensation of biased sinusoidal disturbances with unknown frequency, Automatica 39 (2003) 1755–1761.

[21] N.K. M'Sirdi, H.R. Tjokronegoro, I.D. Landau, An RML algorithm for retrieval of sinusoids with cascaded notch filters, in: 1988 International Conference on Acoustics, Speech, and Signal Processing, ICASSP-88, April 1988, vol. 4, pp. 2484–2487.

[22] A. Nehorai, A minimal parameter adaptive notch filter with constrained poles and zeros, IEEE Transactions on Acoustics, Speech and Signal Processing 33 (1985) 983–996.

[23] G. Obregon-Pulido, B. Castillo-Toledo, A. Loukianov, A globally convergent estimator for n-frequencies, IEEE Transactions on Automatic Control 47 (5) (2002) 857–863.

[24] H. Prochàzka, I.D. Landau, Pole placement with sensitivity function shaping using 2nd order digital notch filters, Automatica 39 (6) (2003) 1103–1107.

[25] Anton A. Pyrkin, Adaptive algorithm to compensate parametrically uncertain biased disturbance of a linear plant with delay in the control channel, Automation and Remote Control 71 (8) (2010) 1562–1577.

[26] D.B. Rao, Sun-Yuan Kung, Adaptive notch filtering for the retrieval of sinusoids in noise, IEEE Transactions on Acoustics, Speech and Signal Processing 32 (August (4)) (1984) 791–802.

[27] Phillip A. Regalia, An improved lattice-based adaptive IIR notch filter, IEEE Transactions on Signal Processing 9 (September (9)) (1991) 2124–2128.

[28] Petre Stoica, Arye Nehorai, Performance analysis of an adaptive notch filter with constrained poles and zeros, IEEE Transactions on Acoustics, Speech and Signal Processing 36 (6) (1988) 911–919.

[29] T.T. Tay, I.M.Y. Mareels, J.B. Moore, High Performance Control, Birkhauser, Boston, 1997.

[30] Petr Tichavský, Arye Nehorai, Comparative study of four adaptive frequency trackers, IEEE Transactions on Automatic Control 45 (6) (1997) 1473–1484.

[31] Y.Z. Tsypkin, Stochastic discrete systems with internal models, Journal of Automation and Information Sciences 29 (4 & 5) (1997) 156–161.

Appendix D

Benchmark on Adaptive Regulation - Rejection of Unknown/Time-varying Multiple Narrow Band Disturbances

Authors: Ioan Doré Landau, Abraham Castellanos Silva, Tudor-Bogdan Airimiţoaie, Gabriel Buche and Mathieu Noé
Journal: European Journal of Control 19(4) (2013) 237–252
Type of submission: Regular paper

European Journal of Control 19 (2013) 237–252

Contents lists available at SciVerse ScienceDirect

European Journal of Control

journal homepage: www.elsevier.com/locate/ejcon

Benchmark on adaptive regulation—rejection of unknown/time-varying multiple narrow band disturbances

Ioan Doré Landau [a,*], Abraham Castellanos Silva [a], Tudor-Bogdan Airimitoaie [a], Gabriel Buche [a], Mathieu Noë [b]

[a] Control System Department of GIPSA-LAB, St. Martin d'héres 38402, France
[b] Paulstra S.A.; Vibrachoc Division, France

ARTICLE INFO

Article history:
Received 1 March 2013
Accepted 5 May 2013
Recommended by J. Maciejowski/D.W. Clarke
Available online 9 May 2013

Keywords:
Adaptive regulation
Active vibration control
Inertial actuators
Multiple narrow band disturbances
Youla–Kučera parametrization
Internal model principle

ABSTRACT

Adaptive regulation is an important issue with a lot of potential for applications in active suspension, active vibration control, disc drives control and active noise control. One of the basic problems from the "control system" point of view is the rejection of multiple unknown and time varying narrow band disturbances without using an additional transducer for getting information upon the disturbances. An adaptive feedback approach has to be considered for this problem. Industry needs to know the *state of the art* in the field based on a solid experimental verification on a representative system using currently available technology. The paper presents a benchmark problem for suppression of multiple unknown and/or time-varying vibrations and an associated active vibration control system using an inertial actuator with which the experimental verifications have been done. The objective is to minimize the residual force by applying an appropriate control effort through the inertial actuator. The system does not use any additional transducer for getting real-time information about the disturbances.

The benchmark has three levels of difficulty and the associated control performance specifications are presented. A simulator of the system has been used by the various contributors to the benchmark to test their methodology. The procedure for real-time experiments is briefly described.[1] The performance measurement methods used will be presented as well as an extensive comparison of the results obtained by various approaches.[2]

1. Introduction

One of the basic problems in active vibration control (AVC) and active noise control (ANC) is the (strong) attenuation of multiple narrow band disturbances[3] with unknown and varying frequencies.

Solutions for this problem using adaptive feedforward compensator techniques have been proposed by signal processing community (see for example [13,29]). These solutions ignore the possibilities offered by feedback and require additional transducers for obtaining correlated measurements with the disturbance (they should provide the "reference" for the feedforward compensator). This approach has a number of disadvantages: (1) it requires the use of additional transducers; (2) implies often a difficult choice for the location of this additional transducers in order to get a relevant image of the disturbance; (3) In many situations the interaction between the compensator system and the measurement of the disturbance cannot be avoided (positive feedback causing stability problems—see [20, Chapter 15]); (4) it requires adaptation of many parameters.

However it is possible to achieve attenuation (rejection) of narrow band disturbances without measuring them by using a feedback approach. A common framework is the assumption that the disturbance is the result of a white noise or a Dirac impulse passed through the *model of the disturbance*. The knowledge of this model allows the design of an appropriate controller. When considering the model of a disturbance, one has to address two issues: (1) its structure (complexity, order of the parametric model) and (2) the values of the parameters of the model. In general, one can assess from data the structure for such *model of disturbance* (using spectral analysis or order estimation techniques) and assume that the structure does not change. However the parameters of the model are unknown and may be time varying. This will require the use of an adaptive feedback approach.[4]

* Corresponding author.
E-mail addresses: ioan-dore.landau@gipsa-lab.grenoble-inp.fr, ioan-dore.landau@gipsa-lab.grenoble-inp.fr (I.D. Landau), abraham.castellanos-silva@gipsa-lab.grenoble-inp.fr (A. Castellanos Silva), tudor-bogdan.airimitoaie@gipsa-lab.grenoble-inp.fr (T.-B. Airimitoaie), Gabriel.Buche@gipsa-lab.grenoble-inp.fr (G. Buche).

[1] The GIPSA-LAB team has done the experiments for all the contributors.

[2] Simulation and Real-time results are presented by each contributor in their papers [3,11,17,30,10,1,7].

[3] Called "tonal" disturbances in active noise control.

[4] Since it is not possible to design a robust controller which introduces a strong attenuation over a large frequency region as a consequence of the Bode Integral (water bed effect), one can not construct a single controller achieving strong attenuation of disturbances with varying frequencies.

0947-3580/$ - see front matter © 2013 European Control Association. Published by Elsevier Ltd. All rights reserved.
http://dx.doi.org/10.1016/j.ejcon.2013.05.007

The classical adaptive control paradigm deals essentially with the construction of a control law when the parameters of the plant dynamic model are unknown and time varying [20]. However, in the present context, the plant dynamic model is almost invariant and it can be identified. The objective then is the rejection of disturbances characterized by unknown and time varying disturbance models. It seems reasonable to call this paradigm as *adaptive regulation*. In classical "adaptive control" the objective is tracking/disturbance attenuation in the presence of unknown and time varying plant model parameters. Therefore adaptive control focuses on adaptation with respect to plant model parameter variations. The model of the disturbance is assumed to be known and invariant. Only a level of attenuation in a frequency band is imposed (with the exception of DC disturbances where the controller may include an integrator). In *adaptive regulation* the objective is to asymptotically suppress (attenuate) the effect of unknown and time-varying disturbances. Therefore *adaptive regulation* focuses on adaptation of the controller parameters with respect to variations in the disturbance model parameters. The plant model is assumed to be known. It is also assumed that the possible small variations or uncertainties of the plant model can be handled by a robust control design. The problem of adaptive regulation as defined above has been previously addressed in a number of papers [26–28,6,4,12,15,16,24,18,2,9,14,5,8] among others. Ref. [19] presents a survey of the various techniques (up to 2010) used in adaptive regulation as well as a review of a number of applications.

Industry needs to know the *state of the art* in the field based on a solid experimental verification on a benchmark. The objective of the proposed benchmark is to evaluate on an experimental basis the available techniques for adaptive regulation in the presence of unknown/time varying multiple narrow band disturbances. Active vibration control constitutes an excellent example of a field where this situation occurs. But similar situations occur in disc drive control and active noise control. Solutions for this problem in active vibration control can be extrapolated to the control of disc drives and active noise control (see for example the applications described in [19]). The benchmark will effectively test various approaches in the specific context of an active vibration control system which will be used as a test bed.

The scientific objective of the benchmark is to evaluate current available procedures for adaptive regulation which may be applied in the presence of unknown/time varying multiple narrow band disturbances. The benchmark specifically will focus in testing: (1) performance, (2) robustness and (3) complexity.

The test bed is an active vibration control system using an inertial actuator and equipped with a shaker and a measurement of the residual force. It is located at GIPSA-Lab, Grenoble (France).[5] The test bed is representative of many situations encountered in practice and in particular of light weighted mechanical structures featuring strong resonance and antiresonance behavior[6] and impacted by vibration sources of different frequencies.

The paper is organized as follows. Section 2 gives a description of the active vibration control system used, as well as some information about the simulator. Section 3 gives the basic equations describing the system and the disturbance along with some information upon the identified models. Section 4 presents the control specifications as well as the protocols used on the benchmark. Section 5 describes some differences found between the simulator and the real plant and how these were taken into account. A methodological comparison of the various approaches is made in Section 6. The description of the measurements used for the analysis is given in Section 7. Section 8 gives the evaluation criteria defined with respect to the benchmark specifications as well as a comparison of obtained results. The complexity evaluation is done in Section 9 and the performance robustness with respect to experimental protocol changes is analyzed in Section 10. The main conclusions for this benchmark are given in Section 11. Appendix A presents a comparison of the adaptation algorithms used by the various contributors.

[5] A first version of the test bed and benchmark specifications has been made available in 2010. Unfortunately because of some hardware and mechanical problems the test bed was redesigned and rebuilt. In this initial benchmark project J. Martinez-Molina, M. Alma and A.Karimi have been involved.

[6] I.e. very low damped complex poles and zeros.

2. An active vibration control system using an inertial actuator

2.1. System structure

The basic structure of an active vibration control system using an inertial actuator is shown in Fig. 1. The inertial actuator will create vibrational forces which can counteract the effect of vibrational disturbances (inertial actuators use a similar principle as loudspeakers). A general view of the benchmark system including the testing equipment is shown Fig. 2. It consists of a passive damper, an inertial actuator, a mechanical structure, a transducer for the residual force, a controller, a power amplifier and a shaker. The mechanical construction is such that the vibrations produced by the shaker, fixed to the ground, are transmitted to the upper side, on top of the passive damper. The inertial actuator is fixed to the chassis where the vibrations should be attenuated. The controller, through the power amplifier, generates current in the moving coil which produces motion in order to reduce the residual force. The equivalent control scheme is shown in Fig. 3. The system input, $u(t)$ is the position of the mobile part (magnet) of the inertial actuator (see Figs. 1, 3 and 4), the output $y(t)$ is the residual force measured by a force sensor. The transfer function $(q^{-d_1}C/D)$, between the disturbance force, $u_p(t)$, and the residual force $y(t)$ is called *primary path*. In our case (for testing purposes), the primary force is generated by a shaker driven by a signal delivered by the computer. The plant transfer function $(q^{-d}B/A)$ between the input of the inertial actuator, $u(t)$, and the residual force is called *secondary path*. Since the input of the system is a position and the output a force, the secondary path transfer function has a double differentiator behavior.

The block diagram of the active vibration control system emphasizing the hardware aspects is shown in Fig. 4.

The control objective is to reject the effect of unknown narrow band disturbances on the output of the system (residual force), i.e. to attenuate the vibrations transmitted from the machine to the chassis. This requires that the compensator system (the secondary path) has enough gain in the frequency range where the narrow band disturbances are located [22]. The physical parameters of the system are not available. The system has to be considered as a *black box* and the corresponding models for control design should be identified. The sampling frequency is $F_s = 800$ Hz.

Data used for system identification as well as the models identified from these data by the organizers are available on the benchmark website (http://www.gipsa-lab.grenoble-inp.fr/~ioandore.landau/benchmark_adaptive_regulation/index.html).

2.2. Simulator

A *black box* discrete time simulator of the active suspension built on MATLAB© Simulink (2007 version) has been provided (can be downloaded from the benchmark website). It uses the models identified by the organizers.

The control scheme (*Controller*) should be built around the given simulator. The simulator has been used by the participants to the benchmark to set the appropriate control scheme and test the performance.

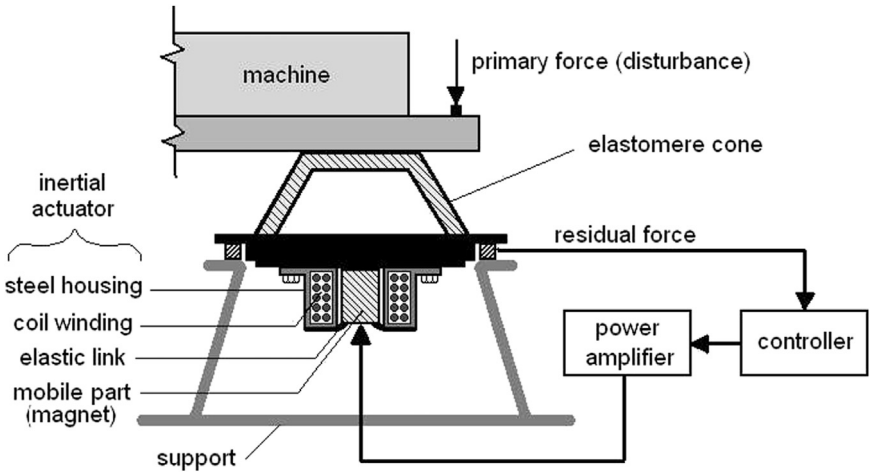

Fig. 1. Active vibration control using an inertial actuator (scheme).

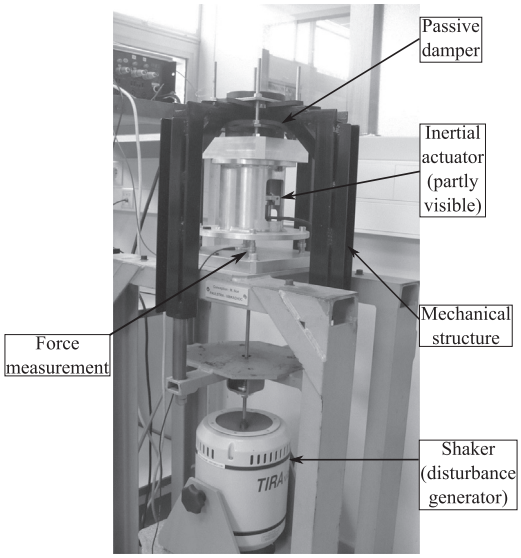

Fig. 2. The benchmark active vibration control system (photo).

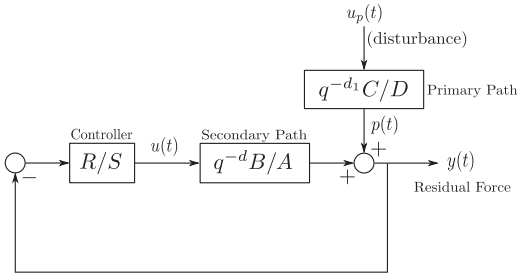

Fig. 3. Block diagram of the benchmark active vibration control systems.

2.3. Real time implementation

The real time implementation uses the MATLAB xPC Target environment (2007). The PC for program development is a Dell© Optiplex 760. The PC target (Dell Optiplex GX270 with Pentium© 4 at 2.86 GHz) is equipped with I/O data acquisition board, A/D and D/A converters. The controller algorithms are compiled directly from the Simulink diagrams provided by the participants. The experiments on the benchmark test bed (for all the contributions) have been done by the organizers of the benchmark. More details on the system, the data acquisition and the simulator can be found on the benchmark website:

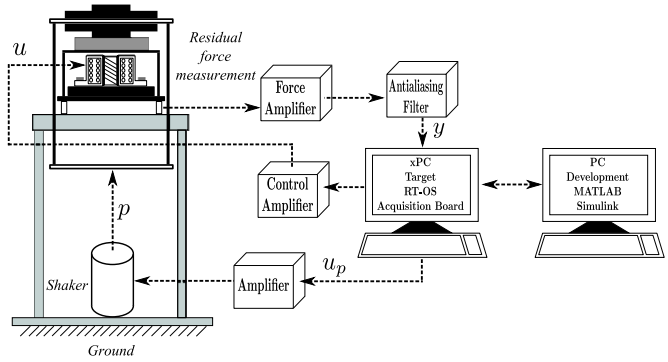

Fig. 4. The benchmark active vibration control system—hardware configuration.

http://www.gipsa-lab.grenoble-inp.fr/~ioandore.landau/benchmark_adaptive_regulation/index.html.

3. Plant/disturbance representation and controller structure

The structure of the linear time invariant discrete time model of the plant – the secondary path – used for controller design is

$$G(z^{-1}) = \frac{z^{-d}B(z^{-1})}{A(z^{-1})} = \frac{z^{-d-1}B^*(z^{-1})}{A(z^{-1})}, \tag{1}$$

with

d = the plant pure time delay in number of sampling periods

$$A = 1 + a_1 z^{-1} + \cdots + a_{n_A} z^{-n_A};$$
$$B = b_1 z^{-1} + \cdots + b_{n_B} z^{-n_B} = z^{-1} B^*;$$
$$B^* = b_1 + \cdots + b_{n_B} z^{-n_B+1},$$

where $A(z^{-1})$, $B(z^{-1})$, $B^*(z^{-1})$ are polynomials in the complex variable z^{-1} and n_A, n_B and n_B-1 represent their orders.[7] The model of the plant may be obtained by system identification. Details on system identification of the models considered in this paper can be found in [25,23,22].

Since the benchmark is focused on regulation, the controller to be designed is a *RS*-type polynomial controller (or an equivalently state space controller+observer) ([20,25]—see also Fig. 3).

[7] The complex variable z^{-1} will be used for characterizing the system's behavior in the frequency domain and the delay operator q^{-1} will be used for describing the system's behavior in the time domain.

The output of the plant $y(t)$ and the input $u(t)$ may be written as

$$y(t) = \frac{q^{-d}B(q^{-1})}{A(q^{-1})} \cdot u(t) + p(t); \tag{2}$$

$$S(q^{-1}) \cdot u(t) = -R(q^{-1}) \cdot y(t), \tag{3}$$

where q^{-1} is the delay (shift) operator ($x(t) = q^{-1}x(t+1)$) and $p(t)$ is the resulting additive disturbance on the output of the system. $R(z^{-1})$ and $S(z^{-1})$ are polynomials in z^{-1} having the orders n_R and n_S, respectively, with the following expressions:

$$R(z^{-1}) = r_0 + r_1 z^{-1} + \cdots + r_{n_R} z^{-n_R} = R'(z^{-1}) \cdot H_R(z^{-1}); \tag{4}$$

$$S(z^{-1}) = 1 + s_1 z^{-1} + \cdots + s_{n_S} z^{-n_S} = S'(z^{-1}) \cdot H_S(z^{-1}), \tag{5}$$

where H_R and H_S are pre-specified parts of the controller (used for example to incorporate the internal model of a disturbance or to open the loop at certain frequencies).

We define the following sensitivity functions:

- Output sensitivity function (the transfer function between the disturbance $p(t)$ and the output of the system $y(t)$):

$$S_{yp}(z^{-1}) = \frac{A(z^{-1})S(z^{-1})}{P(z^{-1})}; \tag{6}$$

- Input sensitivity function (the transfer function between the disturbance $p(t)$ and the input of the system $u(t)$):

$$S_{up}(z^{-1}) = -\frac{A(z^{-1})R(z^{-1})}{P(z^{-1})}, \tag{7}$$

where

$$\begin{aligned} P(z^{-1}) &= A(z^{-1})S(z^{-1}) + z^{-d}B(z^{-1})R(z^{-1}) \\ &= A(z^{-1})S'(z^{-1}) \cdot H_S(z^{-1}) + z^{-d}B(z^{-1})R'(z^{-1}) \cdot H_R(z^{-1}) \end{aligned} \tag{8}$$

defines the poles of the closed loop (roots of $P(z^{-1})$).

In pole placement design, the polynomial $P(z^{-1})$ specifies the desired closed loop poles and the controller polynomials $R(z^{-1})$ and $S(z^{-1})$ are minimal degree solutions of (8) where the degrees of P, R and S are given by $n_P \leq n_A + n_B + d - 1$, $n_S = n_B + d - 1$ and $n_R = n_A - 1$.

Using Eqs. (2) and (3), one can write the output of the system as

$$y(t) = \frac{A(q^{-1})S(q^{-1})}{P(q^{-1})} \cdot p(t) = S_{yp}(q^{-1}) \cdot p(t). \tag{9}$$

For more details on *RS*-type controllers and sensitivity functions see [25].

Suppose that $p(t)$ is a deterministic disturbance, so it can be written as

$$p(t) = \frac{N_p(q^{-1})}{D_p(q^{-1})} \cdot \delta(t), \tag{10}$$

where $\delta(t)$ is a Dirac impulse and $N_p(z^{-1})$, $D_p(z^{-1})$ are coprime polynomials in z^{-1}, of degrees n_{N_p} and n_{D_p}, respectively. In the case of persistent (stationary) disturbances the roots of $D_p(z^{-1})$ are on the unit circle (which will be the case for the disturbances considered in the benchmark). The energy of the disturbance is essentially represented by D_p. The contribution of the terms of N_p is weak compared to the effect of D_p, so one can neglect the effect of N_p. Fig. 5 gives the frequency characteristics of the identified parametric models for the primary and secondary paths (the excitation signal was a PRBS). The system itself in the absence of the disturbances features a number of low damped vibration modes as well as low damped complex zeros (anti-resonance). This makes the design of the controller difficult for rejecting disturbances close to the location of low damped complex zeros. The most significant are those near 50 Hz (secondary path) and 100 and 120 Hz (primary and secondary paths) (see the zoom of the frequency characteristics of the secondary path in Fig. 6). The range of frequencies for the disturbances considered in the benchmark is from 50 Hz to 95 Hz. Note that the design of a linear controller for rejecting a disturbance at 95 Hz is difficult since this frequency is close to a pair of very low damped zeros. The parametric models of both the secondary and primary paths are of significant high order ($n_A = 23$, $n_B = 26$ and $n_C = 17$, $n_D = 16$ respectively). Data used for system identification are available on the website. The contributors had the possibility to use the models provided on the website or to identify models from the data provided (only Callafon et al. took this opportunity). They were also entitled to ask for a special experiment (nobody took this opportunity). The organizers provided an additional model for the

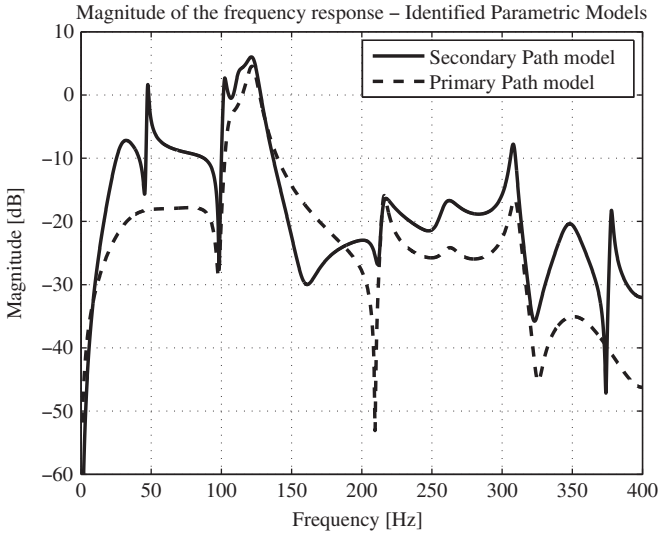

Fig. 5. Magnitude of the frequency response for the primary and secondary path identified models.

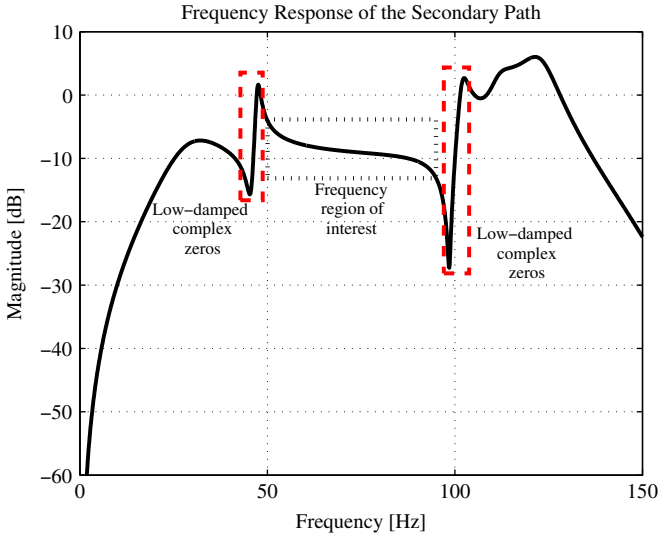

Fig. 6. Zoom at the magnitude of the secondary path's frequency response, between 0 and 150 Hz (website model).

secondary path obtained under different experimental conditions corresponding to a lower level of noise (by modifying the scaling of the A/D converter—however this does not correspond to the benchmark operating conditions). Fig. 7 shows a comparison of the frequency characteristics of the two models. Some of the participants used this second model for tuning their controller for the real-time experiments (Aranovskiy et al., Callafon et al.).

It was assumed that all the contributors were familiar with the design of linear controllers in the presence of very low damped complex zeros and the uncertainty generally associated with the value of the identified damping. No constraints have been imposed by the benchmark on the input sensitivity function.

4. Control specifications

The narrow band disturbances are located in the range 50–95 Hz. It is important to take into account the fact that the secondary path (the actuator path) has no gain at very low frequencies and very low gain in high frequencies near $0.5F_s$. Therefore the control system has to be designed such that the gain of the controller be very low (or zero) in these regions (preferably 0 at $0.5F_s$). Not taking into account these constraints can lead to undesirable stress on the actuator.

There are three levels of difficulty corresponding to one, two or three unknown time varying narrow band disturbances:

- *Level* 1: Rejection of a single time varying sinusoidal disturbance within 50 and 95 Hz.
- *Level* 2: Rejection of two time varying sinusoidal disturbances within 50 and 95 Hz.
- *Level* 3: Rejection of three time varying sinusoidal disturbances within 50 and 95 Hz.

The control objectives for all levels are summarized in Table 1. Level 3 is particularly difficult in terms of tolerated amplification (at other frequencies than those of the disturbances) and transient requirements.

In order to test the required performances, 3 protocols have been defined:

Protocol 1. Tuning capabilities: Evaluation in steady state operation after application of the disturbance once the adaptation settles. *This is the most important aspect of the benchmark.*

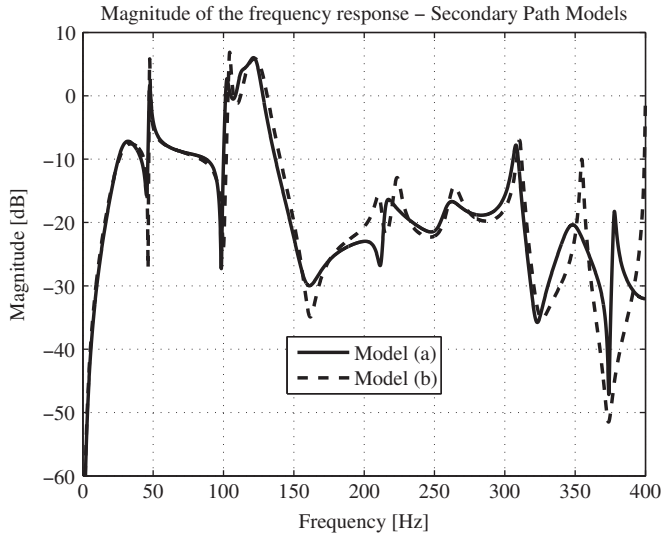

Fig. 7. Comparison between the magnitude of the frequency response for the identified models of the secondary path—(a) website model, (b) additional model.

Table 1
Control specifications in the frequency domain.

Control specifications	Level 1	Level 2	Level 3
Transient duration	≤2 s	≤2 s	≤2 s
Global attenuation	≥30 dB[a]	≥30 dB	≥30 dB
Minimum disturbance attenuation	≥40 dB	≥40 dB	≥40 dB
Maximum amplification	≤6 dB	≤7 dB	≤9 dB
Chirp speed	10 Hz/s	6.25 Hz/s	3 Hz/s
Maximum value during chirp	≤0.1 V	≤0.1 V	≤0.1 V

[a] For this level, the specification of 30 dB is for the range between 50 and 85 Hz, for 90 Hz is 28 dB and for 95 Hz is 24 dB.

Test 1: The steady state performance in time domain will be evaluated by measuring the mean square value of the residual force which will be compared with the value of the residual force in open loop (providing a measure of the global attenuation).

Test 2: Power spectral density performances. For constant frequency disturbances, once the adaptation transient is settled, the performance with respect to the open loop will be evaluated as follows:

- Attenuation of the disturbances (with respect to the open loop) should be larger than the specified value.
- Amplification at other frequencies (with respect to the open loop) should be less than the specified value.

Protocol 2. Transient performance in the presence of step application of the disturbance and step changes in the frequency of the disturbances.

Test 1: Step application of the disturbances.

Test 2: Step changes in the frequencies of the disturbances. The frequencies of the disturbances around specified central values are changed by ± 5 Hz. An upper bound for the duration of the adaptation transient was imposed (2 s). However it was not possible to define a reliable test for measuring the duration of the transient for Test 2. The quantities which have been measured for the purpose of performance evaluation are:

- the square of the truncated two-norm of the residual force over a time horizon;
- the maximum value of the residual force during transient.

Protocol 3. Chirp changes in frequency.

Linear time varying frequency changes between two situations are considered. The maximum value of the residual force during the chirp has been measured as well as the mean square value of the residual force.

The loop is closed before the disturbances are applied for all the above tests.

Supplementary tests:

- The operation of the system should remain stable for all the levels if one, two or three sinusoidal disturbances are applied simultaneously.
- The operation of the loop should remain stable if the disturbance is applied simultaneously with the closing of the loop.

Routines for executing the protocols and the measurements have been provided (see website).

The complexity of the procedures proposed has been evaluated by measuring the average *Task Execution Time* on the real-time system.

Additional tests in simulation and real time have been done by the organizers in order to test the tuning capabilities and transient

performance within the range of frequencies considered in the benchmark but with different experimental protocols (testing others values for the frequencies within the given range, changing the spacing between the narrow band disturbances in the case of Levels 2 and 3, changing the time of application of the disturbances).

Global criteria have been used to assess the performance of each procedure and to allow a comparison between the various schemes (see Section 8).

5. Coherence of simulation results and experimental results

There were some differences between the real plant and the simulator. They can be summarized as follows:

- A small bias in the force measurement is present on the real system (easy to compensate).
- The noise in the simulator was a sample of the noise measured on the real system in the absence of signals. Some differences occur in the presence of disturbance and compensation. This can be explained by the presence of some harmonics of the disturbances (a low level) since neither the disturbance generator nor the inertial actuator are perfectly linear.
- Uncertainties in the estimation of the frequency and damping of the very low damped complex zeros (see Fig. 7) located near 50 Hz and 95 Hz.
- Some uncertainties on the model in the frequency region over 150 Hz (see Fig. 7).

In the first experiments, some of the contributors got significant differences between simulation results and real-time results. These differences can be classified in two categories:

1. instabilities in some situations,
2. significant differences in performance in other situations.

In fact these problems have been easily solved by imposing on *tuned* controllers a very low level of the input sensitivity function around the low damped complex zeros located close to the border of the operation region and outside the operation region (which implies very good robustness with respect to additive uncertainties as well as $|S_{yp}|\cong 1$). One can conclude that the basic rule is to have gain in the controller only in the frequency region of operation (50–95 Hz) and very low gain outside.

6. Methodological comparison

Before evaluating the performance of the various approaches, it is important to assess from a methodological point of view what are the resemblances and the differences between the various approaches proposed. Most of the proposed approaches use implicitly or explicitly a *Youla–Kučera* parametrization of the controller. This also leads to the presence of an observer for the (non-measurable) disturbance, which uses the measurements of the input and the output of the system (see Fig. 8).

However, the *Youla–Kučera* parametrization is not unique, it depends on the right coprime factorization selected $G=ND^{-1}$.

For the benchmark problem where the plant is SISO, four factorizations have been considered by the various contributors:

Factorization 1

$$N=G;\quad D=I. \tag{11}$$

This factorization leads to an *output error* disturbance observer (see Fig. 9) with

$$w_{OE}=y-Gu. \tag{12}$$

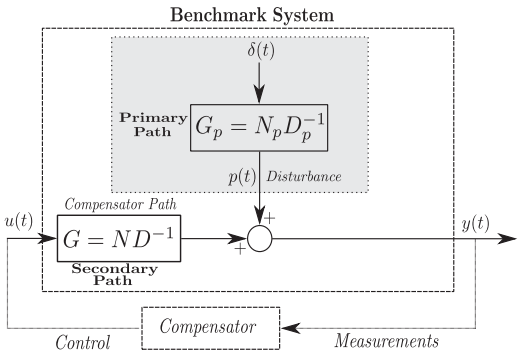

Fig. 8. General scheme for the benchmark system.

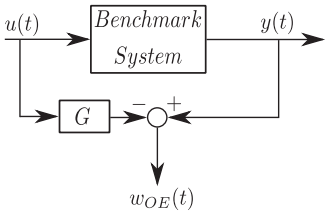

Fig. 9. Output error factorization scheme.

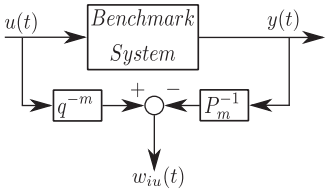

Fig. 10. Input error factorization scheme.

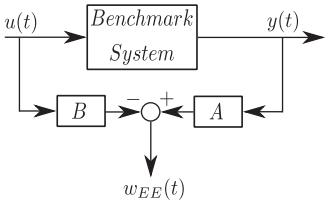

Fig. 11. Equation error factorization scheme.

Factorization 2

$$N=z^{-m};\quad D=P_m \quad \text{with } G\approx z^{-m}P_m. \tag{13}$$

This factorization leads in fact to an *input error* observer (see Fig. 10) with

$$w_{iu}=q^{-m}u-P_m^{-1}y. \tag{14}$$

Factorization 3

$$N=B;\quad D=A \quad \text{with } G=B/A. \tag{15}$$

This factorization leads to an *equation error* disturbance observer (see Fig. 11) with

$$w_{EE}=Ay-Bu. \tag{16}$$

Factorization 4

$$N=BF;\quad D=AF \quad \text{with } G=B/A;\quad F=F_N/F_D, \tag{17}$$

with F and F^{-1} asymptotically stable. This factorization leads to a *filtered equation error* disturbance observer (see Fig. 12) with

$$w_{FEE} = AFy - BFu = Fw_{EE}. \tag{18}$$

The filtered equation error disturbance observer can be obtained either by using the filtered factors or using the equation error disturbance observer and filtering this quantity by F (see Fig. 12 (a) and (b) respectively). Implicitly those configurations which use the equation error disturbance observer but include a fixed filter in cascade with the Q filter correspond in fact to a filtered equation error observer configuration.

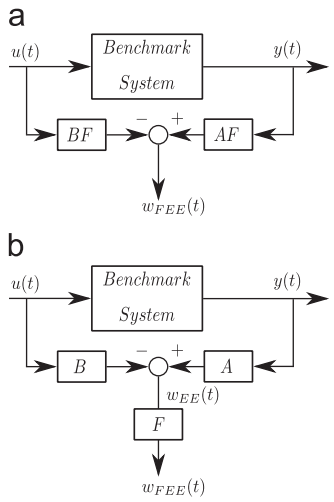

Fig. 12. Filtered equation error factorization—two equivalent schemes.

Table 2 tries to emphasize the characteristics of each proposed approach for the benchmark. The presence (or absence) of the *central controller* (controller used in the absence of disturbance) is indicated as well as the design method used for the central controller. The list of acronyms used is given below.

List of acronyms for Table 2.

IMP	internal model principle
TF	transfer function
FIR	finite impulse response
IIR	infinite impulse response
LQR	linear quadratic regulator
LPV	linear parameter varying control
n	number of narrow band (sinusoidal) disturbances
a.s.	asymptotically stable

Callafon et al. and Wu et al. provided a single controller configuration valid for all the three levels. Aranovskiy et al. provided both a single controller configuration valid for all three levels as well as specific configurations for each level. It was found that in real time the specific configurations gave better performance than the single configuration and therefore the results are given for the case of specific configuration for each level. Airimitoaie et al. provided a single central controller but the frequency estimator was different for each level. The other contributors provided a specific controller configuration for each level (in terms of central controller and parameter estimator).

All participants except Aranovskiy et al. and Callafon et al. provided the same controller for simulations and real-time experiments. Aranovskiy et al. and Callafon et al. have used the model of the secondary path given on the website for the implementation

Table 2
Comparative table for the different approaches used in the benchmark.

Participant	Plant factorization $G = ND^{-1}$	Disturbance observer for control	YK parametrization	Type of Q filter	Central controller design	Disturbance rejection method	Type of adaptation	Number of parameters to adapt	Error signal for adaptation
Aranovskiy et al.	$N=P$ $D=I$ $P=G$ or *a.s. T.F.*	Output error	Yes	FIR filter cascaded with fixed filter or Bank of weighted parallel filters (IIR/FIR)	No central controller (can be added)	IMP	Direct	$2n$	Disturbance estimation (OE)
Callafon et al.	$N=BF$ $D=AF$ $F=F_N/F_D$ or 1 $F, F^{-1} = a.s.$	Equation error	Yes	FIR	H_2	H_2	Direct	Any. Benchmark: 29	Performance indicator *vector* (crit. arg)
Karimi et al.	$N=B$ $D=A$	No	No	No	No	H_∞ + IMP	Indirect (LPV with interpol.) Gain Sche.	n	Disturbance estimation (OE)
Wu et al.	$N=B$ $D=A$	Equation error	Yes	FIR filter cascaded with fixed BP filter	LQR	IMP	Direct	$2n$	Residual error estimation
Xu et al.	$N=z^{-m}$ $D=P_m^{-1}$ $G \approx z^{-m}P_m$	Input error	Yes	IIR (notch filter structure)	Stability	Plant Model Approx. Inversion (IMP)	Direct	n	Disturbance estimation (OE)
Airimitoaie et al.	$N=B$ $D=A$	Equation error	Yes	IIR filter cascaded with fixed filter	Pole Placement	Output sensitivity shaping	Indirect	n	Disturbance estimation (OE)
Castellanos et al.	$N=B$ $D=A$	Equation error	Yes	FIR filter cascaded with fixed filter	Pole placement	IMP	Direct	$2n$	Residual error estimation

of the controllers used in simulation and the additional model of the secondary path (see Fig. 7) for the implementation of the controllers used in real time.

7. Measurements for performance analysis

In order to assess the performance of the proposed approaches, measurement procedures have been defined. These measurements will give information both for *steady state* and *transient* behavior.

7.1. Measurements for simple step test

For step application of the disturbance, measurements for the transient behavior and steady state behavior (tuning capabilities) have been defined. The benchmark protocol for the *Simple Step* test defines the time period for the disturbance application. The disturbance is applied at $t=5$ s, while the entire experiment duration is 30 s. In this context, the *transient* behavior will be considered in the first 3 s after the disturbance is applied. For measuring the *steady state* behavior the last 3 s of the test (before the disturbance is removed) will be used since it is expected that the algorithm has converged at this time.

The measurements considered in the time domain are:

- The *square of the truncated two norm* of the residual force defined by

  $$N^2\,T=\sum_{i=1}^{m} y(i)^2,$$

  where $y(i)$ is a sample of the discrete-time signal to evaluate. This quantity indicates the *energy* contained in the measured signal.
- The *maximum value* measured in millivolts and defined by

  $$MV=\max_m |y(i)|.$$

The measurements in the frequency domain (steady state behavior) are:

- *Global attenuation* (*GA*) measured in dB and defined by

  $$GA=20\log_{10}\frac{N^2Y_{ol}}{N^2Y_{cl}},$$

  where N^2Y_{ol} and N^2Y_{cl} correspond to the square of the truncated two norm of the measured residual force in open and closed loop, respectively, evaluated during the last 3 s of the experiment.
- *Disturbance attenuation* (*DA*) measured in dB and defined as the minimum value of the difference between the estimated PSD[8] of the residual force in closed loop and in open loop:

  $$DA=\min(\mathrm{PSD}_{cl}-\mathrm{PSD}_{ol}).$$

- *Maximum amplification* (*MA*), measured in dB, is defined as the maximum value of the difference between the estimated PSD of the residual force in closed and open loop:

  $$MA=\max(\mathrm{PSD}_{cl}-\mathrm{PSD}_{ol}).$$

For all the frequency domain measurements, only the last 3 s of the test are considered.

[8] Power spectral density.

7.2. Measurements for step frequency changes

For the *Step frequencies changes* only time domain measurements were considered. Based on the protocol for this test, a frequency step change occurs every 3 s. During this time period the following measurements are considered:

- Square of the truncated two norm of the transient N^2T.
- Maximum value of the transient *MV*.

7.3. Chirp frequency change

For the *Chirp* test only time domain measurements were considered. The measurements are:

- Mean Square of the residual force defined as

  $$MSE=\frac{1}{m}\sum_{i=1}^{m} y(i)^2=\frac{1}{m}N^2\,T,$$

  where m correspond to the number of output samples evaluated.
- Maximum value *MV* measured in millivolts.

8. Evaluation criteria

The results of each group will be evaluated with respect to the benchmark specifications. However, for some performance indices no bounds have been set in the benchmark and the comparison will be done between the various indices obtained. To summarize, two types of criteria will be considered:

- criteria for taking into account the fact that not all the specifications have been satisfied (when applicable),
- normalized quantitative criteria for comparison of performance indices for which benchmark specifications were not available.

Evaluation of the performances will be done for both simulation and real-time results. The simulation results will give us information upon the potential of the design methods under the assumption: *design model=true plant model*. The real-time results will tell us in addition what is the robustness of the design with respect to plant model uncertainties and real noise. These criteria are given next.

8.1. Steady state performance (tuning capabilities)

As mentioned earlier, these are the most important performances. Only if a good tuning for the attenuation of the disturbance can be achieved, it makes sense to examine the transient performance of a given scheme. For the steady state performance, which is evaluated only in the *simple step test*, the variable k, with $k=1,\ldots,3$, will indicate the *level* of the benchmark. In several criteria a mean of certain variables will be considered. The number of distinct experiments, M, is used to compute the mean. This number depends upon the level of the benchmark as follows:

$M=10$ if $k=1$
$M=6$ if $k=2$
$M=4$ if $k=3$

The performances can be evaluated with respect to the benchmark specifications. The benchmark specifications will be in the form: *XXB*, where *XX* will denote the evaluated variable and *B* will

indicate the benchmark specification. ΔXX will represent the error with respect to the benchmark specification.

(1) *Global attenuation* (*GA*): The benchmark specification corresponds to $GAB_k = 30$ dB, for all the levels and frequencies, except for 90 Hz and 95 Hz at $k=1$, for which GAB_1 is 28 dB and 24 dB respectively.

Error:

$$\Delta GA_i = GAB_k - GA_i \quad \text{if } GA_i < GAB_k$$
$$\Delta GA_i = 0 \quad \text{if } GA_i \geq GAB_k$$

with $i=1,\ldots,M$.

Global attenuation criterion

$$J_{\Delta GA_k} = \frac{1}{M}\sum_{i=1}^{M} \Delta GA_i \tag{19}$$

(2) *Disturbance attenuation* (*DA*): The benchmark specification corresponds to $DAB = 40$ dB, for all the levels and frequencies.

Error:

$$\Delta DA_{ij} = DAB - DA_{ij} \quad \text{if } DA_{ij} < DAB$$
$$\Delta DA_{ij} = 0 \quad \text{if } DA_{ij} \geq DAB$$

with $i=1,\ldots,M$ and $j=1,\ldots,j_{max}$, where $j_{max}=k$.

Disturbance attenuation criterion

$$J_{\Delta DA_k} = \frac{1}{M}\sum_{i=1}^{M}\sum_{j=1}^{j_{max}} \Delta DA_{ij} \tag{20}$$

(3) *Maximum amplification* (*MA*): The benchmark specifications depend on the level, and are defined as

$$MAB_k = 6 \text{ dB} \quad \text{if } k=1$$
$$MAB_k = 7 \text{ dB} \quad \text{if } k=2$$
$$MAB_k = 9 \text{ dB} \quad \text{if } k=3$$

Error:

$$\Delta MA_i = MA_i - MAB_k \quad \text{if } MA_i > MAB_k$$
$$\Delta MA_i = 0 \quad \text{if } MA_i \leq MAB_k$$

with $i=1,\ldots,M$.

Maximum amplification criterion

$$J_{\Delta MA_k} = \frac{1}{M}\sum_{i=1}^{M} \Delta MA_i \tag{21}$$

(4) *Global criterion of steady state performance for one level*:

$$J_{SS_k} = \tfrac{1}{3}[J_{\Delta GA_k} + J_{\Delta DA_k} + J_{\Delta MA_k}] \tag{22}$$

(5) *Benchmark satisfaction index for steady state performance*: Following the procedure for the *robust digital control benchmark* [21] a *Benchmark Satisfaction Index* can be defined.

The *Benchmark Satisfaction Index* is a performance index computed from the *average* criteria $J_{\Delta GA_k}$, $J_{\Delta DA_k}$ and $J_{\Delta MA_k}$. The *Benchmark Satisfaction Index* is 100%, if these quantities are "0" (full satisfaction of the benchmark specifications) and it is 0% if the corresponding quantities are half of the specifications for *GA*, and *DA* or twice the specifications for *MA*. The corresponding reference error quantities are summarized below:

$$\Delta GA_{index} = 15,$$
$$\Delta DA_{index} = 20,$$

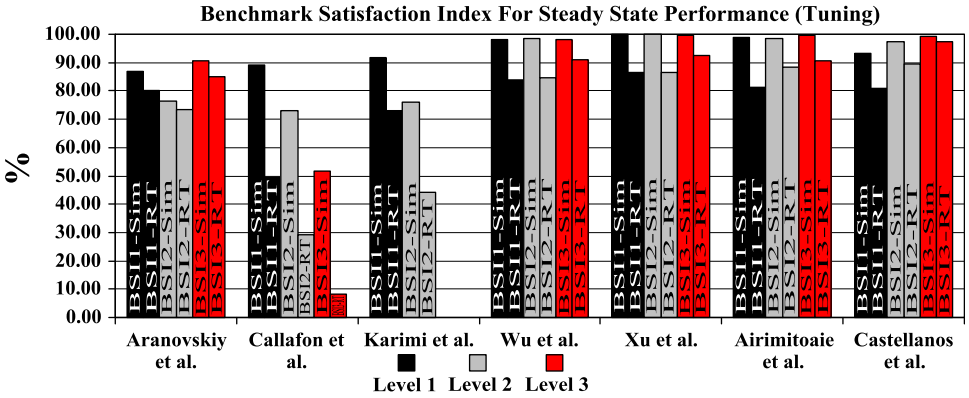

Fig. 13. Benchmark Satisfaction Index (*BSI*) for all levels and all participants, both in simulation and real-time.

Table 3
Benchmark Satisfaction Index for all the participants.

Participant	LEVEL 1				LEVEL 2				LEVEL 3			
	Simulation		Real time		Simulation		Real time		Simulation		Real time	
	J_{SS_1}	BSI_1 (%)	J_{SS_1}	BSI_1 (%)	J_{SS_2}	BSI_2 (%)	J_{SS_2}	BSI_2 (%)	J_{SS_3}	BSI_3 (%)	J_{SS_3}	BSI_3 (%)
Aranovskiy et al.	0.87	86.94	1.20	80.22	1.77	76.33	2.04	73.58	0.84	90.65	1.41	84.89
Callafon et al.	2.12	89.21	6.74	49.37	5.02	72.89	11.01	29.08	17.14	51.74	31.47	8.40
Karimi et al.	1.33	91.92	2.17	72.89	3.42	76.13	7.43	44.33	–	–	–	–
Wu et al.	0.11	98.31	1.31	**83.83**	0.13	98.48	1.35	84.69	0.18	98.01	1.34	91.00
Xu et al.	**0.00**	**100.00**	**1.00**	**86.63**	**0.00**	**100.00**	1.37	**86.65**	**0.04**	**99.78**	1.45	92.52
Airimitoaie et al.	0.08	98.69	1.23	81.11	0.11	98.38	**0.94**	**88.51**	0.11	99.44	1.58	90.64
Castellanos et al.	0.50	93.30	1.35	80.87	0.29	97.29	1.20	**89.56**	0.17	99.13	**0.43**	**97.56**

$\Delta MA_{index,1} = 6 \quad \text{if } k = 1,$
$\Delta MA_{index,2} = 7 \quad \text{if } k = 2,$
$\Delta MA_{index,3} = 9 \quad \text{if } k = 3.$

The computation formulas are

$$GA_{index,k} = \left(\frac{\Delta GA_{index} - J_{\Delta GA_k}}{\Delta GA_{index}}\right)100\%$$
$$DA_{index,k} = \left(\frac{\Delta DA_{index} - J_{\Delta GA_k}}{\Delta DA_{index}}\right)100\%$$
$$MA_{index,k} = \left(\frac{\Delta MA_{index,k} - J_{\Delta MA_k}}{\Delta MA_{index,k}}\right)100\%.$$

Then the *Benchmark Satisfaction Index* (*BSI*) is defined as

$$BSI_k = \frac{GA_{index,k} + DA_{index,k} + MA_{index,k}}{3} \tag{23}$$

The results for BSI_k obtained both in simulation and real-time for each participant and all the levels are summarized in Table 3, and represented graphically in Fig. 13. Table 3 shows also the J_{SS_k} for all the levels and contributors. Low values of J_{SS_k} indicate an "average" good performance. However Benchmark Satisfaction Index (BSI_k) allows a better characterization of the performance with respect to the various benchmark specifications. The results obtained in simulation allow the characterization of the performance of the proposed design under the assumption that *design model=true plant model*. Therefore in terms of capabilities of a design method to meet the benchmark specification the simulation results are fully relevant. It is also important to recall that Level 3 of the benchmark is the most important. The results obtained in real time, more exactly the difference between the simulation results and real time results, allow one to characterize the robustness in performance with respect to uncertainties on design model and noise model (for those who used the same controller in simulation and in real time).

8.2. Simulation results

Consider the *simulation results* in terms of the BSI. Clearly the *benchmark specifications* are achievable since Xu et al. have achieved 100% for Levels 1 and 2 and for Level 3 Xu et al. and Airimitoaie et al. have achieved respectively 99.78% and 99.44%. If we look for those who achieved at least 97% of the benchmark specifications, for Level 1 we find Xu et al., Airimitoaie et al. and Wu et al. For Levels 2 and 3, we find Xu et al., Airimitoaie et al. and Wu et al. and Castellanos et al. These designs feature a number of common properties as well as some differences.

- They all use a Youla Kučera parametrization.
- Xu et al., and Wu et al. and Castellanos et al. use the IMP and direct adaptation with very similar parameter adaptation algorithms (see Appendix A).
- Airimitoaie et al. use shaping of the output sensitivity function and indirect adaptation.

The approach of Callafon et al. has been probably handicapped by the fact that the real-time control system did not allow to use more than 29 adjustable parameters and this number has been used also in simulations. One also has to mention that Karimi et al., who use a convex optimization procedure, were not able to provide controllers for Level 3.

8.3. Real time results

Rigourously the same algorithms and tunings from simulation have been used for the real time experiments by all the participants except Aranovskiy et al. and Callafon et al. (which use different models for building the controllers for simulation and real time experiments).

The physical system cannot be considered as a "deterministic system" in particular concerning the noise (but not only that). Therefore a very precise evaluation of the performance would require that an average of several repetitive tests (let say 10) be considered as the relevant information. Unfortunately this was not possible to be done taking into account the large number of trials to be done. However for one situation (Level 3) and for one controller configuration but considering two protocols, multiple experiments have been conducted and the results have been analyzed. The conclusion is that the results which are provided for the BSI in Table 3 have to be considered with an associated uncertainty of about $\pm 4\%$. The consequence is that we cannot classify results within this uncertainty range.

From Table 3 it results that for Level 1 the best results have been obtained by Xu et al. and Wu et al. For Level 2 the best results have been obtained by Castellanos et al., Airimitoaie et al. and Xu et al. For Level 3 the best results have been obtained by Castellanos et al.[9]

Since there are differences between simulation results and real time results it is interesting to assess the robustness with respect to model uncertainties.

8.4. Robustness with respect to model uncertainties

As was mentioned earlier there are uncertainties on the plant model used for design. These uncertainties come mostly from the difficulty of correctly identifying very low damped complex zeros. The identification results concerning the low damped complex zeros are influenced by the level of noise. As mentioned earlier (see Section 5) also the noise is different in the simulator with respect to the real system. The contributors were aware of these problems and the final designs did not show any instability going from the simulation scheme to the real system.

However the loss in performance moving from simulation to real time experiments is obvious as can be seen in Table 3. Therefore an important point is to assess the robustness in performance for those who uses the same controller in simulation and in real time. This will be done by defining the *Normalized Performance Loss*.

For each level one defines the *Normalized Performance Loss* as

$$NPL_k = \left(\frac{BSI_{ksim} - BSI_{kRT}}{BSI_{ksim}}\right)100\% \tag{24}$$

and the global *NPL* is given by

$$NPL = \frac{1}{M}\sum_{k=1}^{M} NPL_k \tag{25}$$

where $N=3$ for all the participants except for Karimi et al., since they provided only solutions for Levels 1 and 2; for them $N=2$.

Table 4 gives the normalized performance loss for all the participants and levels. Fig. 14 summarizes these results in a bar graph. The results for Aranovskiy et al. and Callafon et al. are given for information only since the controllers are not the same in simulation and real time.

For the Levels 1, 2 and 3, the design of Castellanos et al. has the minimum $NPL_{1,2,3}$. The minimum averaged *NPL* has been obtained by Castellanos et al. For Callafon et al. the explanation of a high loss in performance comes from the fact that the controller gain in high frequencies (over 100 Hz) has not been reduced enough.

[9] All these mentioned results differ by less than 4% with respect to the highest value obtained.

8.5. Transient performance

Transient performances will be evaluated for:

- Simple Step Test (application of the disturbance).
- Step Changes in the frequencies.
- Chirp Changes in the frequencies.

We will consider first the case of the *simple step test*.

(1) *Simple step test*: The basic specification for transient performance is the requirement that the transient duration when a disturbance is applied, be smaller than 2 s. Similar to the steady state performance a BSI index for transient duration has been established (a transient duration of 4 s corresponds to 0%). From the point of view of the benchmark, this means that 2 s after application of a disturbance the square of the truncated two norm has to be equal or smaller than 1.21 of the steady state value of the square of the truncated two norm of the residual force. The square of the truncated two norm is evaluated over an interval of 3 s both for transient and steady state, taking into account that the disturbance is applied at $t=5$ s and that steady state is evaluated between 17 and 20 s. The square of the truncated two norm is denoted as $N2T(v:w)$ where v and w define the interval of computation.

One defines

$$\alpha_i = \frac{N^2\,T(7:10)}{N^2T(17:20)}$$

$$\Delta Trans_i = \alpha_i - 1.21 \quad \text{if } \alpha_i > 1.21$$

$$\Delta Trans_i = 0 \quad \text{if } \alpha_i \le 1.21 \quad i = 1,\ldots,M$$

$$J_{\Delta Trans_k} = \frac{1}{M}\sum_{i=1}^{M} \Delta Trans_i \tag{26}$$

$$BSI_{Trans_k} = \left(\frac{1.21 - J_{\Delta Trans_k}}{1.21}\right)100\% \quad k = 1,\ldots,3 \tag{27}$$

where M is given by

$M=10$ if $k=1$
$M=6$ if $k=2$
$M=4$ if $k=3$

Table 5 gives the results obtained for the various approaches. Most of the approaches have met the specifications or are very close.

The transient performances have been further investigated in order to compare the various approaches. Simple step test, step changes in frequencies and chirp tests have been considered. Two quantities have been defined:

- Square of the truncated-two norm of residual force N^2T.
- Maximum value during transient MV.

Note: In order to introduce "normalized" criteria (maximum value $=1$) one has to define for these 2 quantities the $(Max)_{\max}$ within the results provided by all the participants. These quantities will be called $(J^U_{NT_k})_{\max}$, $(J^U_{MV_k})_{\max}$, where the U stands for *un-normalized*.

$$J^U_{NT_k} = \frac{1}{M}\sum_{i=1}^{M} N^2T(i)$$

$$J^U_{MV_k} = \frac{1}{M}\sum_{i=1}^{M} MV(i)$$

$$J_{NT_k} = \frac{J^U_{NT_k}}{(J^U_{NT_k})_{\max}}$$

$$J_{MV_k} = \frac{J^U_{MV_k}}{(J^U_{MV_k})_{\max}}$$

Table 4
Normalized Performance Loss for all the participants.

Participant	NPL_1 (%)	NPL_2 (%)	NLP_3 (%)	NPL (%)
Aranovskiy et al.	7.73*	3.61*	6.35*	5.90*
Callafon et al.	44.66*	60.11*	83.77*	62.85*
Karimi et al.	20.70	41.77	–	31.24
Wu et al.	14.73	14.01	7.16	11.96
Xu et al.	13.37	13.35	7.28	11.33
Airimitoaie et al.	17.81	10.03	8.85	12.23
Castellanos et al.	**13.32**	**7.95**	**1.58**	**7.62**

Table 5
Benchmark Satisfaction Index for Transient Performance (for simple step test).

Participant	Index					
	$\mathbf{BSI_{Trans_1}}$ (%)		$\mathbf{BSI_{Trans_2}}$ (%)		$\mathbf{BSI_{Trans_3}}$ (%)	
	Simulation	Real time	Simulation	Real time	Simulation	Real time
Aranovskiy et al.	100	100	100	100	100	100
Callafon et al.	100	100	100	100	100	92.35
Karimi et al.	100	97.69	100	91.79	–	–
Wu et al.	100	99.86	94.85	100	100	92.40
Xu et al.	100	100	100	100	100	100
Airimitoaie et al.	100	99.17	83.33	100	100	100
Castellanos et al.	100	96.45	100	95.74	100	100

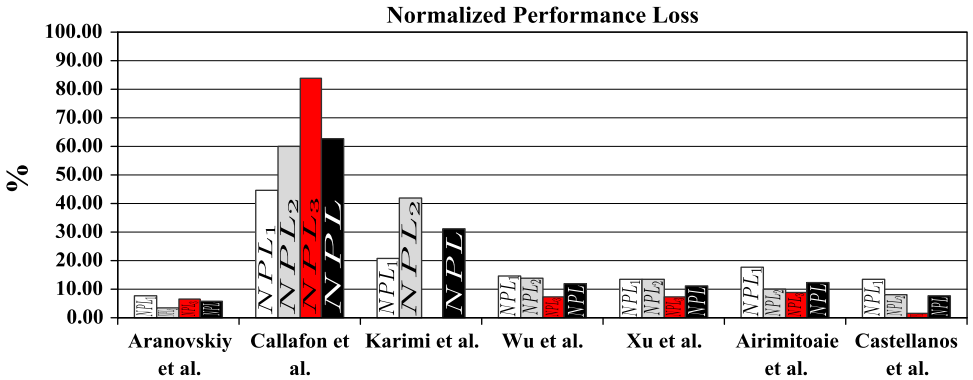

Fig. 14. Normalized Performance Loss (NPL) for all levels and all participants (smaller=better).

Table 6
Average global criterion for transient performance for all the participants.

Participant	JTRAV1		JTRAV2		JTRAV3	
	Simulation	Real time	Simulation	Real time	Simulation	Real time
Aranovskiy et al.	0.76	0.89	0.57	0.72	0.51	0.61
Callafon et al.	0.44	0.54	**0.26**	**0.40**	**0.22**	0.52
Karimi et al.	**0.35**	**0.40**	0.34	0.49	–	–
Wu et al.	0.50	0.56	0.36	0.46	0.34	**0.37**
Xu et al.	0.39	0.55	0.76	0.81	0.63	0.74
Airimitoaie et al.	0.93	0.85	0.60	0.71	0.42	0.49
Castellanos et al.	0.55	0.61	0.48	0.60	0.90	0.98

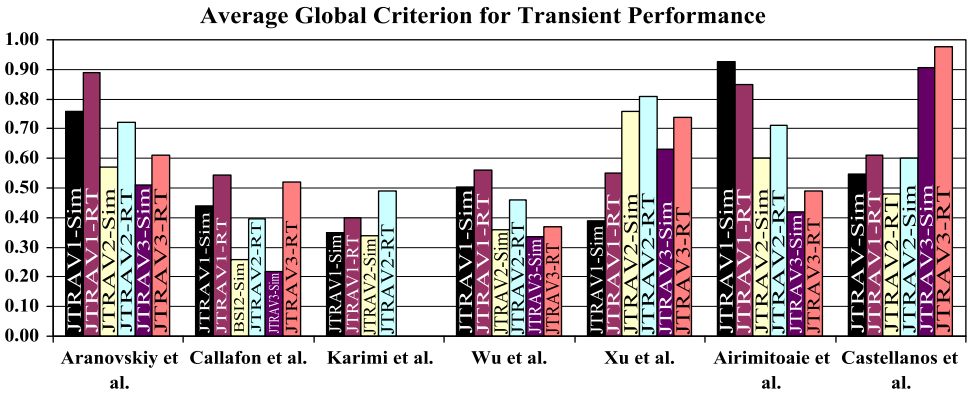

Fig. 15. Average global criterion for transient performance (J_{TRAV}) for all levels and all participants (smaller=better).

where M is given by

$M=10$ if $k=1$
$M=6$ if $k=2$
$M=4$ if $k=3$

Global criterion for transient evaluation for simple step test:

$$J_{TR_k}=\tfrac{1}{2}[J_{NT_k}+J_{MV_k}] \tag{28}$$

(2) *Step frequency changes test*: Only the square of the norm of the residual force and the maximum value during transient will be considered (similar case to the simple step test). The corresponding criteria are given below:

$$J^U_{SNT_k}=\frac{1}{M}\sum_{i=1}^{M}N^2T_i$$

$$J^U_{SMV_k}=\frac{1}{M}\sum_{i=1}^{M}MV_i$$

$$J_{SNT_k}=\frac{J^U_{SNT_k}}{(J^U_{SNT_k})_{\max}}$$

$$J_{SMV_k}=\frac{J^U_{SMV_k}}{(J^U_{SMV_k})_{\max}}$$

where M is given by

$M=12$ if $k=1$
$M=8$ if $k=2$
$M=8$ if $k=3$

Global criterion for transient performance evaluation-step changes in frequencies:

$$J_{STR_k}=\tfrac{1}{2}\left[J_{SNT_k}+J_{SMV_k}\right] \tag{29}$$

(3) *Chirp test*: As for the step frequencies changes, the maximum values among all the participants will be used to normalize the results. For each level two measurements have been done for:

- Mean square of the residual force (*MSE*),
- Maximum value of the residual force (*MV*),

during the periods of application of the chirp. They are denoted by *up* when the frequencies increase and *down* when the frequencies decrease.

One defines the criterion for the mean square error (for each level) for all the levels ($k=1,\ldots,3$) as follows[10]:

$$J^U_{MSE_k}=\tfrac{1}{2}[MSE_{up}+MSE_{down}]$$

$$J_{MSE_k}=\frac{J^U_{MSE_k}}{(J^U_{MSE_k})_{\max}}$$

The benchmark specifications for the *maximum value* were far too conservative. However, a comparison between the various approaches has to be done.

For the maximum value one defines the criterion

$$J^U_{MV_k}=\tfrac{1}{2}[MV_{up}+MV_{down}]$$

$$J_{MV_k}=\frac{J^U_{MV_k}}{(J^U_{MV_k})_{\max}}$$

Global criterion for chirp disturbance:

$$J_{chirp_k}=\tfrac{1}{2}[J_{MSE_k}+J_{MV_k}] \tag{30}$$

An average global criterion for transient performance is defined for each level as:

[10] The results are exactly the same for the normalized values J_{MSE_k} if one uses N^2T instead of *MSE*.

(4) *Average global criterion for transient performance* (*one level*):

$$J_{TRAV_k} = \frac{1}{3}[J_{TR_k} + J_{STR_k} + J_{chirp_k}] \quad (31)$$

Table 6 gives the values of J_{TRAV_k} for all levels and participants, both in simulation and real-time. For this criterion lower values mean a better transient behavior. A graphic representation of these results is given in Fig. 15. Best results in simulation are obtained by Karimi et al. (Level 1), Callafon et al. (Levels 2 and 3). In real time the best results are obtained by Karimi et al. (Level 1), Callafon et al. (Level 2) and Wu et al. (Level 3). The results of Karimi et al. can be explained by the fact that it is an interpolation between a set of stored controller and the parameters for interpolation are rapidly identified for Levels 1 and 2 as well as by the design method used which minimizes the infinity norm of the transients. However as has been mentioned earlier, since the steady state performance is the most important, it is interesting to compare the transient behavior of those designs which achieved at least 97% of the benchmark specifications in simulation. For Level 1 the best transient performance (simulation and real-time) is achieved by Xu et al. For Levels 2 and 3 the best transient performance (simulation and real-time) is achieved by Wu et al. To a large extent these results confirm the known fact that direct adaptive configurations provide in general better transients than indirect adaptive configurations.

9. Evaluation of the complexity

For complexity evaluation, the measure of the *Task Execution Time* (TET) in the xPC Target environment will be used. This is the time required to perform all the calculations on the host target PC for each method. Such process has to be done on each sample time. The more complex is the approach, the bigger is the TET. One can argue that the TET depends also on the programming of the algorithm. However this may change the TET by a factor of 2–4 but not by an order of magnitude. The xPC Target MATLAB environment delivers an *average* of the TET (*ATET*). It is however interesting to assess the TET specifically associated with the controller by subtracting from the measured TET in closed loop operation, the average TET in open loop operation.

The following criteria to compare the complexity between all the approaches are defined:

$$\Delta TET_{Simple,k} = ATET_{Simple,k} - ATET_{OL_{Simple,k}} \quad (32)$$

$$\Delta TET_{Step,k} = ATET_{Step,k} - ATET_{OL_{Step,k}} \quad (33)$$

$$\Delta TET_{Chirp,k} = ATET_{Chirp,k} - ATET_{OL_{Chirp,k}} \quad (34)$$

where $k = 1, \ldots, 3$. The symbols *Simple, Step* and *Chirp* are associated respectively with Simple Step Test (application of the disturbance), Step Changes in Frequency and Chirp Changes in Frequency. The global ΔTET_k for one level is defined as the average of the above computed quantities:

$$\Delta TET_k = \frac{1}{3}(\Delta TET_{Simple,k} + \Delta TET_{Step,k} + \Delta TET_{Chirp,k}) \quad (35)$$

where $k = 1, \ldots, 3$. Table 7 and Fig. 16 summarize the results obtained by each participant for all the levels. All the values are in microseconds. Higher values indicate higher complexity. If we set three intervals : < 5 μs, between 5 and 15 μs and over 200 μs, one can conclude that the lowest complexity structures for Level 1 are provided by Karimi et al., Xu et al., Castellanos et al. and Aranovskiy et al., for Level 2 by Karimi et al., Castellanos et al. and Aranovskiy et al. and for Level 3 by Aranovskiy et al. and Castellanos et al. The large values of the ΔTET (over 200 μs) can be explained for Callafon et al. by the large number of parameters to adapt and for Airimitoaie et al. by the fact that a Bezout equation has to be solved at each sampling instant. It seems that a good compromise between good steady state performance and complexity has been provided by Castellanos et al., Xu et al., Wu et al. and Aranovskiy et al.

Table 7
Task Execution Time for all levels and participants.

Participant	ΔTET (microseconds)		
	L1	L2	L3
Aranovskiy et al.	3.71	4.18	**4.92**
Callafon et al.	210.68	209.90	212.62
Karimi et al.	**2.37**	4.08	–
Wu et al.	14.73	14.65	14.74
Xu et al.	2.96	9.11	14.27
Airimitoaie et al.	254.24	203.83	241.22
Castellanos et al.	3.26	**3.90**	5.60

10. New protocol test

The benchmark specifications have been measured under prespecified experimental protocols in terms of: (1) values of frequencies, (2) difference in frequency between two neighbor disturbances, (3) time of application of the disturbances and (4) magnitude of the step changes in frequencies. An obvious question is: what happens if the experimental protocols are changed (but maintaining the range of operation in the frequency domain)? Since the systems are adaptive, these changes should not have too much influence upon the results.

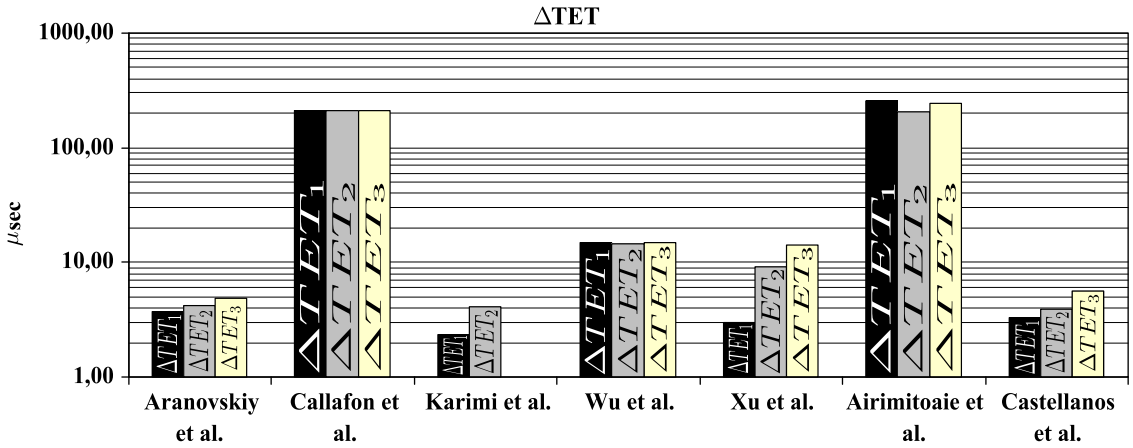

Fig. 16. The controller average Task Execution Time (ΔTET) for all the participants.

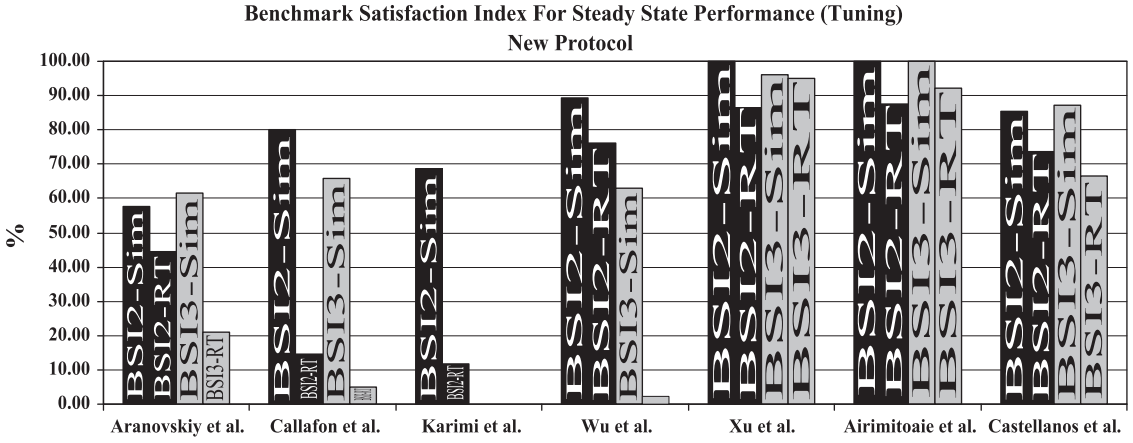

Fig. 17. Comparison of the Benchmark Satisfaction Index (*BSI*) for benchmark protocol and new protocol.

Table 8
Benchmark Satisfaction Index for all the participants for the new protocol.

Participant	LEVEL 2				LEVEL 3			
	Simulation		Real time		Simulation		Real time	
	J_{SS_2}	BSI_2 (%)	J_{SS_2}	BSI_2 (%)	J_{SS_3}	BSI_3 (%)	J_{SS_3}	BSI_3 (%)
Aranovskiy et al.	4.55	57.78	8.52	44.65	5.26	61.62	15.55	20.92
Callafon et al.	3.33	79.95	16.75	14.55	5.56	65.68	16.14	5.13
Karimi et al.	5.39	68.76	17.99	11.89	–	–	–	–
Wu et al.	0.74	89.48	1.68	76.00	3.88	62.90	33.79	0.00
Xu et al.	**0.00**	**100.00**	0.94	**86.63**	0.81	95.96	0.70	**95.05**
Airimitoaie et al.	**0.00**	**100.00**	**0.86**	**87.71**	**0.00**	**100.00**	**0.69**	**92.30**
Castellanos et al.	1.01	85.57	1.85	73.52	1.14	87.30	3.69	66.67

Only two tests have been conducted for each participant, *Simple Step Test* and *Step Changes in Frequency Test*. Only Levels 2 and 3 of the benchmark are considered.

In the original protocol, the separation (in Hz) between the sinusoidal disturbances was 20 Hz for Level 2 and 15 Hz for Level 3. For this *new* protocol, 10 Hz of separation is considered both for Levels 2 and 3. The (central) frequencies chosen (expressed in Hz) are in addition nonintegers[11] with the following values:

- 61.5 Hz–71.5 Hz for Level 2.
- 61.5 Hz–71.5 Hz–81.5 Hz for Level 3.

For *Simple Step Test*, only the central frequencies are applied while for *Step Changes in Frequencies Test*, variations of ± 5 Hz of the central frequencies are considered (as in the benchmark protocol, in order to compare transient results).

The application time of the first disturbance was changed from 5 s to 3.75 s for both tests, but the duration of the steps in frequencies was kept at 3 s, in order to be able to compare the new transient results with the previous results. The measurements defined in Section 7 and the criteria from Section 8 have been used.

Table 8 gives the summary of the results concerning tuning capabilities (steady state performances) and Fig. 17 gives the corresponding graphic representation. Among the designs of Wu et al., Xu et al., Airitimioaie et al. and Castellanos et al.

[11] In the benchmark protocols only integer values have been considered.

Table 9
Benchmark Satisfaction Index for transient performance (for simple step test). New protocol.

Participant	Index			
	BSI_{Trans_2} (%)		BSI_{Trans_3} (%)	
	Simulation	Real time	Simulation	Real time
Aranovskiy et al.	100	100	100	100
Callafon et al.	100	100	100	100
Karimi et al.	100	78.53	–	–
Wu et al.	83.02	100	100	100
Xu et al.	100	100	0	100
Airimitoaie et al.	100	100	100	100
Castellanos et al.	100	100	100	100

which provided the best results in simulation for the benchmark protocol, it appears that the designs of Airimitoaie et al. and Xu et al. are less sensitive to changes of the experimental protocols since they succeed to achieve a BSI of 100% (Airimitoaie et al. for Levels 2 and 3 and Xu et al. for Level 2). For these two designs the changes in real time performances with respect to the case of benchmark protocols (compare with Table 3) are small and an improvement in performance is obtained. A significant loss in performance both in simulation and in real time occurs for the design of Wu et al. at Level 3. A possible explanation is the design considered for the central controller (they provided a single controller configuration for all the levels). The design of Castellanos et al. shows also a important loss in performance in real-time operation for Level 3.

Table 9 gives the BSI_{trans} for the case of the new protocol. One can see that most of the designs meet the benchmark specification for maximum transient duration in real-time. However in simulation the results for Xu et al. show a surprisingly slow adaptation at Level 3 while the results in real-time are good.

Taking into account both the steady state performance and transient performance one can say that some of the designs are insensitive to the change of the testing protocols (i.e. different operational conditions).

11. Conclusion

This benchmark has offered the opportunity to assess the state of the art in the field of Adaptive Regulation for the case of rejection of multiple narrow band disturbances. It is the

Table 10
Parameter adaptation algorithm.

Participant	Adaptation matrix	Observation matrix (vector)	Notation
Aranovskiy et al.	$\zeta(t)=\frac{1+\Phi^T(t+1)F(t)\Phi(t+1)}{\lambda+\Phi^T(t+1)F(t)\Phi(t+1)}$ $\lambda_1(t)=\lambda$ $\lambda_2(t)=1$	$\Phi(t+1)=[F_0L\hat{p}(t+1),\cdots]^T$ $q=1$	$\Phi(t+1)=x(t+1)$ $\hat{\theta}(t)=\hat{k}(t)$ $F(t)=P(t)$
Callafon et al.	$\zeta(t)=1$ $\lambda_1(t)=1$ $\lambda_2(t)=1$	$\Phi(t+1)=\begin{bmatrix}\gamma WD\\ N\end{bmatrix}w(t+1),\cdots]^T$ $q=2$	$\Phi(t+1)=\phi(t+1)$ $\epsilon^0(t+1)=\epsilon(t,\hat{\theta}(t))$ $F(t)=P(t)$
Karimi et al.	$\zeta(t)=1$	$\Phi(t+1)=\frac{1}{N_p}[-\hat{p}(t+1),\epsilon(t+1),\epsilon(t)]^T$ $q=1$	$\Phi(t+1)=\psi_f(t+1)$ $\hat{\theta}(t)=\hat{\Theta}(t)$
Wu et al.	$\zeta(t)=1$ $\lambda_1(t)=\lambda(t)$ $\lambda_2(t)=\lambda_1(t)$	$\Phi(t+1)=[T_{12}F(y(t+1)-\hat{y}(t+1)),\cdots]^T$ $q=1$	$\Phi(t+1)=\phi(t+1)$ $\epsilon^0(t+1)=\tilde{e}(t+1)$ $F(t)=P(t)$
Xu et al.	$\zeta(t)=1$ $\lambda_1(t)=\lambda(t)$ $\lambda_2(t)=1$	$\Phi_1(t+1)=[\psi_i(t+1),\cdots,\psi_n(t+1)]^T$ $q=1$ $\Phi_2(t+1)=[\phi_1(t+1),\ldots,\phi_n(t+1)]^T$ $q=1$	$\Phi_1(t+1)=\psi(t+1)$ $F(t)=P(t)$ $\Phi_2(t+1)=\phi(t+1)$ $\epsilon^0(t+1)=v^0(t+1)$ $F(t)=P(t)$
Arimitoaie et al.	Scalar version $\zeta(t)=1+\Phi^T(t+1)F(t)\Phi(t+1)$ $\lambda_1(t)=\lambda$ $\lambda_2(t)=1$	$\Phi(t+1)=H_f\hat{p}^j(t+1)$ $q=1$	$\Phi(t+1)=\Psi^j(t+1)$ $\hat{\theta}(t)=\hat{a}^{f_j}(t)$ $\epsilon^0(t+1)=\epsilon(t+1)$
Castellanos et al.	$\zeta(t)=1$	$\Phi(t+1)=\frac{q^{-d}B^*H_{S_0}H_{R_0}}{P}\left[w(t+1),\cdots\right]^T$ $q=1$	$\Phi(t+1)=\phi(t+1)$

opinion of the organizers that the active vibration control system used as the support of this benchmark was relevant for the difficulties which can be encountered in practice (in particular the presence of very low damped complex zeros). Steady state performance, transient performance, robustness with respect to plant model uncertainties and complexity have been evaluated. This will allow potential users to select the appropriate approach taking into account their specific constraints. Clearly not all the problems which can be encountered in the attenuation of multiple unknown time varying narrow band disturbances have been covered by the benchmark. Among future directions of research and benchmarking we mention the case of multiple narrow band disturbances with very small frequency intervals between them[12] and the tuning of the active vibration control systems in the presence of variations of the plant model.

Appendix A. Comparison of adaptive algorithms used

To summarize the adaptive algorithms used for each participant, the following notations have been considered:

- $p\in\mathbb{R}$ is the number of parameters to adapt.[13]
- $q\in\mathbb{R}$ is the dimension of the observation matrix.[14]
- $\hat{\theta}(t)\in\mathbb{R}_{p\times 1}$ is the vector of parameters to adapt.
- $F(t)\in\mathbb{R}_{p\times p}$ is the adaptation matrix.
- $\Phi(t)\in\mathbb{R}_{p\times q}$ is the observation matrix.
- $\epsilon^0(t)\in\mathbb{R}_{q\times 1}$ is the *a priori* error prediction function.
- $\zeta(t)\in\mathbb{R}_{1\times 1}$ is an auxiliary variable defined according to the participant approach.

In general all the participants use a parameter adaptation algorithm having the form

$$\hat{\theta}(t+1)=\hat{\theta}(t)+\zeta(t)\frac{F(t)\Phi(t+1)}{1+\Phi^T(t+1)F(t)\Phi(t+1)}\epsilon^0(t+1) \tag{36}$$

$$\epsilon^0(t+1)=\varsigma(t+1)-\Phi^T(t+1)\hat{\theta}(t) \tag{37}$$

$$F(t+1)=\frac{1}{\lambda_1(t)}\left[F(t)-\frac{F(t)\Phi(t+1)\Phi^T(t+1)F(t)}{\frac{\lambda_1(t)}{\lambda_2(t)}+\Phi^T(t+1)F(t)\Phi(t+1)}\right] \tag{38}$$

where the parameter vector is updated using the previous value of the parameter vector and adding a correcting term which contains, the adaptation matrix, the observation matrix and the error prediction function. It is in the adaptation matrix calculations and the error prediction functions where the particularities of each contribution can be found. The error prediction function uses a signal ($\varsigma(t+1)$), which could be a disturbance prediction (as in Aranovskiy et al., Karimi et al., Wu et al. and Airimitoaie et al.), an input error prediction (as in Xu et al.), an equation error prediction (as in Castellanos et al.) or an output filtered prediction (as in Callafon et al.). This is related also to the factorization presented in Section 6. Regarding the adaptation matrix, various profiles for the adaptation gains are obtained depending on the values assigned to $\lambda_1(t)$ and $\lambda_2(t)$, see details in [25]. Table 10 summarizes the characteristics of the parameter adaptation algorithm used by each participant.

[12] Less than 10% of the disturbance frequencies.
[13] For each case consider Table 2 in Section 6.
[14] In order to consider a general parametrization, $q=1$ is a special case.

References

[1] T.-B. Airimitoaie, A. Castellanos Silva, I.D. Landau, Indirect adaptive regulation strategy for the rejection of time varying narrow-band disturbances applied to a benchmark problem, European Journal of Control, http://dx.doi.org/10.1016/j.ejcon.2013.05.011, this issue.

[2] S. Aranovskiy, A. Bobtsov, A. Kremlev, N. Nikolaev, O. Slita, Identification of frequency of biased harmonic signal, European Journal of Control (5) (2010) 129–139.

[3] S. Aranovskiy, L.B. Freidovich, Adaptive compensation of disturbances formed as sums of sinusoidal signals with application to an active vibration control benchmark, European Journal of Control, http://dx.doi.org/10.1016/j.ejcon.2013.05.008, this issue.

[4] F. Ben Amara, P.T. Kabamba, A.G. Ulsoy, Adaptive sinusoidal disturbance rejection in linear discrete-time systems—Part I: Theory, Journal of Dynamic Systems Measurement and Control 121 (1999) 648–654.

[5] A.A. Bobtsov, S.A. Kolyubin, A.S. Kremlev, A.A. Pyrkin, An iterative algorithm of adaptive output control with complete compensation for unknown sinusoidal disturbance, Automation and Remote Control 73 (8) (2012) 1327–1336.

[6] M. Bodson, S.C. Douglas, Adaptive algorithms for the rejection of sinusoidal disturbances with unknown frequency, Automatica 33 (1997) 2213–2221.

[7] A. Castellanos Silva, I.D. Landau, T.-B. Airimitoaie, Direct adaptive rejection of unknown time-varying narrow band disturbances applied to a benchmark problem, European Journal of Control, http://dx.doi.org/10.1016/j.ejcon.2013.05.012, this issue.

[8] F. Celani, Output regulation for the tora benchmark via rotational position feedback, Automatica 47 (3) (2011) 584–590.

[9] X. Chen, M. Tomizuka, A minimum parameter adaptive approach for rejecting multiple narrow-band disturbances with application to hard disk drives, IEEE Transactions on Control System Technology 20 (March (2)) (2012) 408–415.

[10] X. Chen, M. Tomizuka, Adaptive model inversion for time-varying vibration rejection on an active suspension benchmark, European Journal of Control, http://dx.doi.org/10.1016/j.ejcon.2013.04.002, this issue.

[11] R.A. de Callafon, H. Fang, Adaptive regulation via weighted robust estimation and automatic controller tuning, European Journal of Control, http://dx.doi.org/10.1016/j.ejcon.2013.05.009, this issue.

[12] Z. Ding, Global stabilization and disturbance suppression of a class of linear systems with uncertain internal model, Automatica 39 (3) (2003) 471–479.

[13] S. Elliott, Signal Processing for Active Control, Academic Press, San Diego, California, 2001.

[14] Z. Emedi, A. Karimi, Fixed-order lpv controller design for rejection of a sinusoidal disturbance with time-varying frequency, in: 2012 IEEE Multi-Conference on Systems and Control, Dubrovnik, 2012.

[15] T. Gouraud, M. Gugliemi, F. Auger, Design of robust and frequency adaptive controllers for harmonic disturbance rejection in a single-phase power network, in: Proceedings of the European Control Conference, Bruxelles, 1997.

[16] G. Hillerstrom, J. Sternby, Rejection of periodic disturbances with unknown period—a frequency domain approach, in: Proceedings of American Control Conference, Baltimore, 1994, pp. 1626–1631.

[17] A. Karimi, Z. Emedji, H-inf gain-scheduled controller design for rejection of time-varying narrow-band disturbances applied to a benchmark problem, European Journal of Control, http://dx.doi.org/10.1016/j.ejcon.2013.05.010, this issue.

[18] C.E. Kinney, H. Fang, R.A. de Callafon, M. Alma, Robust estimation and automatic controller tuning in vibration control of time varying harmonic disturbances, in: Proceedings of 18th IFAC World Congress, Milano, Italy, 2011, pp. 5401–5406.

[19] I.D. Landau, M. Alma, A. Constantinescu, J.J. Martinez, M. Noë, Adaptive regulation—rejection of unknown multiple narrow band disturbances (a review on algorithms and applications), Control Engineering Practice 19 (10) (2011) 1168–1181.

[20] I.D. Landau, R. Lozano, M. M'Saad, A. Karimi, Adaptive Control, 2nd ed., Springer, London, 2011.

[21] I.D. Landau, D. Rey, A. Karimi, A. Voda, A. France, A flexible transmission system as a benchmark for robust digital control, European Journal of Control 1 (2) (1995) 77–96.

[22] I.D. Landau, M. Alma, J.J. Martinez, G. Buche, Adaptive suppression of multiple time-varying unknown vibrations using an inertial actuator, IEEE Transactions on Control Systems Technology 19 (November (6)) (2011) 1327–1338.

[23] I.D. Landau, A. Constantinescu, P. Loubat, D. Rey, A. Franco, A methodology for the design of feedback active vibration control systems, in: Proceedings of the European Control Conference 2001, Porto, Portugal.

[24] I.D. Landau, A. Constantinescu, D. Rey, Adaptive narrow band disturbance rejection applied to an active suspension—an internal model principle approach, Automatica 41 (4) (2005) 563–574.

[25] I.D. Landau, G. Zito, Digital Control Systems—Design, Identification and Implementation, Springer, London, 2005.

[26] R. Marino, G.L. Santosuosso, P. Tomei, Robust adaptive compensation of biased sinusoidal disturbances with unknown frequency, Automatica 39 (2003) 1755–1761.

[27] R. Marino, G.L. Santosuosso, P. Tomei, Output feedback stabilization of linear systems with unknown additive output sinusoidal disturbances, European Journal of Control 14 (2) (2008).

[28] S. Valentinotti, Adaptive Rejection of Unstable Disturbances: Application to a Fed-Batch Fermentation. Thèse de doctorat, École Polytechnique Fédérale de Lausanne, April 2001.

[29] B. Widrow, S.D. Stearns, Adaptive Signal Processing, Prentice-Hall, Englewood Cliffs, New Jersey, 1985.

[30] Z. Wu, F. Ben Amara, Youla parametrized adaptive regulation against sinusoidal exogenous inputs applied to a benchmark problem, European Journal of Control, http://dx.doi.org/j.ejcon.2013.04.001, this issue.

Appendix E

Direct Adaptive Regulation in the Vicinity of Low Damped Complex Zeros - Application to Active Vibration Control

Authors: Abraham Castellanos Silva, Ioan Doré Landau and Petros Ioannou
Conference: 22nd Mediterranean Conference on Control and Automation (MED)
Year: 2014
City: Palermo, Italy
Type of submission: Regular paper

2014 22nd Mediterranean Conference on Control and Automation (MED)
University of Palermo. June 16-19, 2014. Palermo, Italy

Direct adaptive regulation in the vicinity of low damped complex zeros - Application to active vibration control

Abraham Castellanos Silva*, Ioan Doré Landau*,
Petros Ioannou†.

***Abstract*—The adaptive feedback approach is now widely used for the rejection of multiple narrow band disturbances with unknown and time varying frequencies in Active Vibration Control (AVC) and Active Noise Control (ANC). The approach is based directly or indirectly on the use of the Internal Model Principle and the Youla-Kučera parametrization combined with an adaptive law. All the algorithms associated with the approach make the assumption that the plant zeros are different from the poles of the disturbance model in order to achieve disturbance compensation. However in practice the problem is more intricate since it is not clear what happens if the plant have very low damped complex zeros (often encountered in mechanical structures) and the frequency of the disturbance is close to the anti-resonance frequency (the resonance frequency of the plant zeros). A recent international investigation on adaptive regulation in the presence of unknown time varying disturbances [16] has considered such a situation for a benchmark example. Several solutions have been proposed and the most successful has been based on the appropriate choice of the desired closed loop poles to be achieved by the Youla-Kučera central controller [5] using a Q FIR filter with the minimum number of parameters. Recently in [12] it was suggested that over parametrization of the Q (FIR) filter can enhance the robustness of the linear and adaptive scheme in the vicinity of plant complex zeros. The present paper compares these two approaches using the same benchmark example as in [16]. The results from simulations and real time experiments used to evaluate the two approaches are presented.**

***Index Terms*—Adaptive Regulation, Active Vibration Control, Inertial Actuators, Multiple Narrow Band Disturbances, Youla-Kučera Parametrization, Internal Model Principle**

I. Introduction

The basic problem in active vibration control (AVC) and active noise control (ANC) is the *strong* attenuation of multiple narrow band disturbances[1] with unknown and varying frequencies. An adaptive feedback approach (adaptive regulation) is now widely accepted as the most effective approach for solving this class of problems. The disturbance model is assumed to be either a function equal to the sum of sinusoids with unknown frequencies, amplitudes and phases or equivalently, a transfer function with unknown complex poles on the unit circle with white noise or a Dirac impulse as an input. In general, one can assess from data the structure for such *model of disturbance* (using spectral analysis or order estimation techniques) and assume that the structure does not change. However, the parameters of the model are unknown and may be time varying. This will require the use of an adaptive feedback approach in order to adapt to changes in parameters.

It is also assumed that the plant model is stable and this property could be the result of a robust control design that is already incorporated in the system under consideration. The problem of disturbance rejection and adaptive regulation as defined above has been previously addressed in a number of papers ([4], [2], [24], [22], [8], [10], [11], [20], [14], [1], [7], [9], [3], [23], [6]) among others. [15] presents a survey of the various techniques (up to 2010) used as well as a review of a number of applications.

Among them, the *Internal Model Principle* implemented through a Youla-Kučera parametrization arises as a very attractive and efficient solution, since it allows to introduce the model of the disturbance in the controller without modifying the *desired* closed loop poles, defined by the designer [24], [20], [5]. This parametrization allows to obtain a direct adaptive scheme. The number of parameters to adapt is defined by the complexity of the assumed disturbance model. An international competition benchmark example on adaptive rejection of narrow band disturbances has been organized and the results are published in a special issue of the European Journal of Control [16].

A common challenge of all the up to date efforts and proposed methods is the following: the disturbance is considered to be periodic, i.e. the poles of the disturbance models are on the unit circle. All the adaptation algorithms make the assumption that the plant zeros are different from the poles of the disturbance model in order to achieve disturbance compensation. However in practice the problem is more intricate since it is not clear what happens if the plant has very low damped complex zeros (often encountered in mechanical structures) and the frequency of the disturbance is close to the anti-resonance frequency (the resonance frequency of the plant zeros). Obviously even in the linear case with known parameters the design of the controller in this region is difficult for robustness reasons. In the international benchmark example on adaptive regulation in the presence of unknown time varying disturbances [16] such a situation has been explicitly considered. Several solutions have been proposed and the most successful has been based on the appropriate choice of the desired closed loop poles to be achieved by the Youla-Kučera central controller [5] and by using a Q-FIR filter with the minimum number of parameters. Recently [12] it was suggested that

[1]Called *tonal* disturbances in active noise control.

978-1-4799-5899-3/14/$31.00 ©2014 IEEE

XPL:978-1-4799-5901-3/14/$31.00 ©2014 IEEE

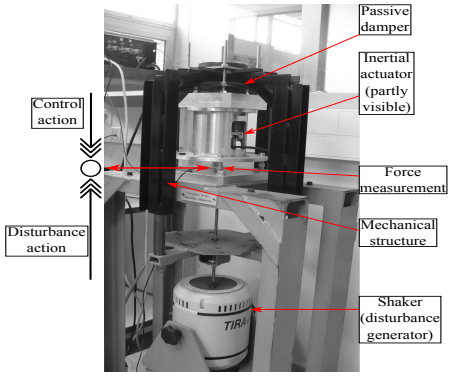

Fig. 1. Active vibration control using an inertial actuator (photo).

over parametrization of the Q-(FIR) filter can enhance the robustness of the linear and adaptive scheme in the vicinity of plant complex zeros[2]. In this paper these two approaches are compared using the benchmark example and the simulation and real time results are presented.

II. An Active Vibration Control System Using an Inertial Actuator

A. System structure

The photo of the active vibration control experimental set up used in this study is presented in fig. 1. Figure 1 also shows the description of the basic actions. The shaker acts as a disturbance source by introducing vibration forces and the inertial actuator can be used to counteract them by introducing vibrational forces in the opposite direction (inertial actuators use a similar principle as loudspeakers). This test bed was used in the international benchmark in adaptive regulation, whose results were published in [16]. The equivalent control scheme is shown in figure 2. The system input, $u(t)$ is the position of the mobile part (magnet) of the inertial actuator, the output $y(t)$ is the residual force measured by a force sensor. The transfer function ($H = q^{-d_1}\frac{C}{D}$), between the disturbance force, $\delta(t)$, and the residual force $y(t)$ is called *primary path*. In our case (for testing purposes), the primary force is generated by a shaker driven by a signal delivered by the computer. The plant transfer function ($G = q^{-d}\frac{B}{A}$) between the input of the inertial actuator, $u(t)$, and the residual force is called *secondary path*. The sampling frequency is $F_s = 800$ Hz.

Figure 3 gives the frequency characteristics of the identified parametric model for the secondary path (the excitation signal was a PRBS). The system itself in the absence of the disturbances features a number of low damped vibration modes as well as low damped complex zeros (anti-resonance). This makes the design of the controller difficult

[2]This idea has not been explored by the participants to the benchmark. Note that the over parametrization of the Q filter for robustness with respect to uncertainties in the plant model has been proposed in [24], [12], however, here the objective of over parametrization is different.

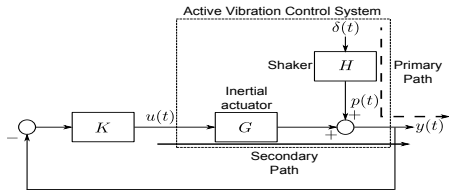

Fig. 2. Active suspension system (scheme).

for rejecting disturbances close to the location of low damped complex zeros (low or no system gain). The most significant are those near 50, 100 and 110 Hz (see the zoom of the frequency characteristics of the secondary path in figure 3). Note that the design of a linear controller for rejecting a disturbance at 95 Hz (as required by the benchmark) is difficult since this frequency is close to a pair of very low damped zeros (around of 0.005). The parametric model of the secondary path has a significant order, $n_A = 22$ and $n_B = 25$.

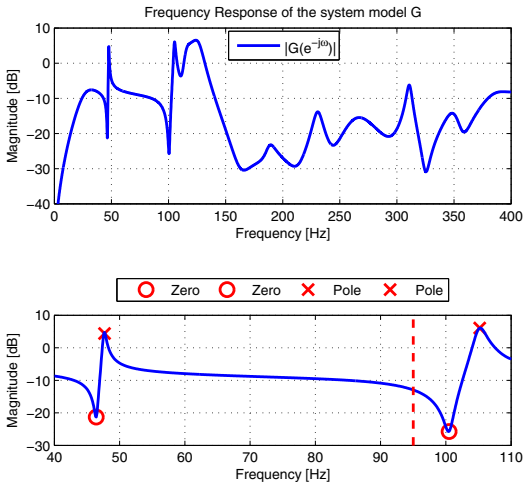

Fig. 3. Magnitude of the frequency response for secondary path model (top). Zoom at the low damped complex poles and zeros (bottom).

III. Plant/Disturbance Representation and Controller Structure

The structure of the linear time invariant discrete time model of the plant - the secondary path - used for controller design is:

$$G(z^{-1}) = \frac{z^{-d}B(z^{-1})}{A(z^{-1})} = \frac{z^{-d-1}B^*(z^{-1})}{A(z^{-1})}\ , \qquad (1)$$

with:

$$d = \text{the plant pure time delay in number of sampling periods}$$

$$A = 1 + a_1 z^{-1} + \cdots + a_{n_A} z^{-n_A}\ ;$$
$$B = b_1 z^{-1} + \cdots + b_{n_B} z^{-n_B} = z^{-1}B^*\ ;$$
$$B^* = b_1 + \cdots + b_{n_B} z^{-n_B+1}\ ,$$

where $A(z^{-1})$, $B(z^{-1})$, $B^*(z^{-1})$ are polynomials in the complex variable z^{-1} and n_A, n_B and n_B-1 represent their orders[3]. The model of the plant may be obtained by system identification. Details on system identification of the models considered in this paper can be found in [21], [19], [18].

Since the control objective is focused on regulation, the controller to be designed (K) corresponds to a RS polynomial digital controller, ([17], [21] - see also figure 2). The controller is $K=\frac{R}{S}$, where $R(z^{-1})$ and $S(z^{-1})$ are polynomials in z^{-1} having the orders n_R and n_S, respectively, with the following expressions:

$$R(z^{-1}) = r_0 + r_1 z^{-1} + \ldots + r_{n_R} z^{-n_R} = R'(z^{-1}) \cdot H_R(z^{-1}) \; ; \quad (2)$$

$$S(z^{-1}) = 1 + s_1 z^{-1} + \ldots + s_{n_S} z^{-n_S} = S'(z^{-1}) \cdot H_S(z^{-1}) \; , \quad (3)$$

where H_R and H_S are pre-specified parts of the controller (used for example to incorporate the internal model of a disturbance or to open the loop at certain frequencies).

The output of the plant $y(t)$ and the input $u(t)$ may be written as:

$$y(t) = \frac{q^{-d}B(q^{-1})}{A(q^{-1})} \cdot u(t) + p(t) \; ; \quad (4)$$

$$S(q^{-1}) \cdot u(t) = -R(q^{-1}) \cdot y(t) \; , \quad (5)$$

where q^{-1} is the delay (shift) operator ($x(t) = q^{-1}x(t+1)$) and $p(t)$ is the resulting additive disturbance on the output of the system.

We define the following sensitivity functions:

- Output sensitivity function (the transfer function between the disturbance $p(t)$ and the output of the system $y(t)$):

$$S_{yp}(z^{-1}) = \frac{1}{1+GK} = \frac{A(z^{-1})S(z^{-1})}{P(z^{-1})} \; ; \quad (6)$$

- Input sensitivity function (the transfer function between the disturbance $p(t)$ and the input of the system $u(t)$):

$$S_{up}(z^{-1}) = \frac{-K}{1+GK} = -\frac{A(z^{-1})R(z^{-1})}{P(z^{-1})} \; , \quad (7)$$

where

$$\begin{aligned} P(z^{-1}) &= A(z^{-1})S(z^{-1}) + z^{-d}B(z^{-1})R(z^{-1}) \\ &= A(z^{-1})S'(z^{-1}) \cdot H_S(z^{-1}) + z^{-d}B(z^{-1})R'(z^{-1}) \cdot H_R(z^{-1}) \end{aligned} \quad (8)$$

defines the poles of the closed loop (roots of $P(z^{-1})$).
In pole placement design, the polynomial $P(z^{-1})$ specifies the desired closed loop poles and the controller polynomials $R(z^{-1})$ and $S(z^{-1})$ are minimal degree solutions of (8) where the degrees of P, R and S are given by: $n_P \leq n_A + n_B + d - 1$, $n_S = n_B + d - 1$ and $n_R = n_A - 1$.
Using equations (4) and (5), one can write the output of the system as:

$$y(t) = \frac{A(q^{-1})S(q^{-1})}{P(q^{-1})} \cdot p(t) = S_{yp}(q^{-1}) \cdot p(t) \; . \quad (9)$$

[3]The complex variable z^{-1} will be used for characterizing the system's behaviour in the frequency domain and the delay operator q^{-1} will be used for describing the system's behaviour in the time domain.

For more details on RS-type controllers and sensitivity functions see [21].

Suppose that $p(t)$ is a deterministic disturbance, so it can be written as

$$p(t) = \frac{N_p(q^{-1})}{D_p(q^{-1})} \cdot \delta(t) \; , \quad (10)$$

where $\delta(t)$ is a Dirac impulse and $N_p(z^{-1})$, $D_p(z^{-1})$ are coprime polynomials in z^{-1}, of degrees n_{N_p} and n_{D_p}, respectively. In the case of persistent (stationary) disturbances the roots of $D_p(z^{-1})$ are on the unit circle (which will be the case for this work). The energy of the disturbance is essentially represented by D_p. The contribution of the terms of N_p is weak compared to the effect of D_p, so one can neglect the effect of N_p.

IV. Low damped complex zeros

An important remark is that in order to be able to reject the disturbance introduced by the primary path, the secondary path has to provide enough gain. Looking at eq. (6), total rejection at a frequency ω is achieved when

$$S_{yp}(e^{-j\omega}) = 0 \quad \rightarrow \quad S(e^{-j\omega}) = 0, \quad (11)$$

nevertheless, in such case the modulus of the input sensitivity function (eq. (7)) becomes

$$\left|S_{up}(e^{-j\omega})\right| = \left|\frac{A(e^{-j\omega})}{B(e^{-j\omega})}\right|, \quad (12)$$

meaning that the robustness against additive plant model uncertainties is reduced and the stress on the actuator will be important if low damped complex zeros are located near or at the frequency ω. Therefore, the cancelation (or in general an important attenuation) of disturbance effect on the output should be done only in frequency regions where the system gain is large enough.

In [16], several approaches were used in the benchmark example to reject a disturbance at 95 Hz. It was found that stability and performance issues arises due the proximity of the low damped zeros; furthermore, if the gain of the input sensitivity function is not low enough (below -10 dB) above 100 Hz, important amplifications (and even instability) can appear on the real system. One of the best results was presented in [5], using a Yula-Kučera (YK) parametrization of the controller, a specific choice for the desired closed loop poles location and a direct adaptive approach.

V. Direct Adaptive Feedback Regulation - A Youla-Kučera Approach

The YK-parametrization proposed is depicted in the fig. 4, where both fixed and adaptive parts are pointed out. For this paper a YK-parametrization using an equation-error disturbance observer is used, along with a finite impulse response (FIR) filter representation of the optimal Q filter

$$Q(z^{-1}) = q_0 + q_1 z^{-1} + \cdots + q_{n_Q} z^{-n_Q}. \quad (13)$$

XPL:978-1-4799-5901-3/14/$31.00 ©2014 IEEE

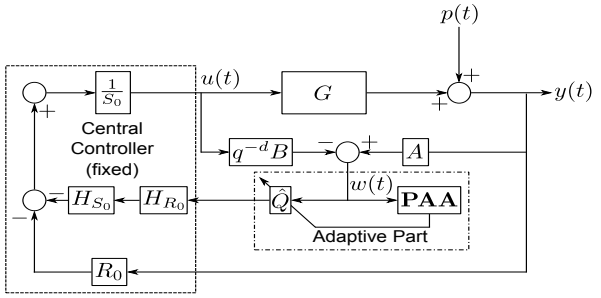

Fig. 4. Direct adaptive scheme using a YK-parametrization of the controller. Dashed box: fixed part, Point-dash box: adaptive part.

TABLE I
FREQUENCY DOMAIN RESULTS IN SIMULATION AND REAL TIME

	Closed Loop Poles	Case 1 Plant Poles + 12 real poles					Case 2 Plant Poles + 2 pairs of resonant poles + 4 real poles	
		a)	**b)**				**a)**	**b)**
	$n_Q =$	1	2	3	4	5	1	5
GA	RT	1.2	6.5	8.0	13.0	11.7	21.0	22.0
	SIM	9.8	15.6	16.1	16.1	17.0	25.4	27.3
DA	RT	4.5	6.7	8.2	11.6	12.5	39.4	38.0
	SIM	9.5	15.2	15.6	15.9	16.8	39.8	46.5
MA	RT	30.8	26.3	19.4	15.6	18.3	8.1	7.2
	SIM	21.0	16.9	15.7	16.5	15.4	10.0	8.5

RT: Real time, SIM: Simulation, GA: Global attenuation, DA: Disturbance attenuation, MA: Maximum amplification, **a)**: minimal solution and **b)**: augmented solution.

Using this parametrization, the controller polynomials R and S are defined by[4]

$$R(z^{-1}) = R_0 + H_{S_0}H_{R_0}QA \tag{14}$$

$$S(z^{-1}) = S_0 - H_{S_0}H_{R_0}Qz^{-d}B, \tag{15}$$

It is easy to show that for any arbitrary $Q(z^{-1})$, the closed loop poles remain unchanged; they are defined by

$$P(z^1) = A(z^{-1})S_0(z^{-1}) + z^{-d}B(z^{-1})R_0(z^{-1}). \tag{16}$$

A. Internal Model Principle

Looking at the output sensitivity function (eq. (6)) and the assumed model of the disturbance (eq. (10)), total rejection of a disturbance is possible if $S(z^{-1}) = S'(z^{-1}) \cdot D_p(z^{-1})$, meaning that the controller incorporates the model of the disturbance (internal model principle).
Consider eq. (9) and eq. (15), then the output of the system can be expressed as follows:

$$y(t) = \frac{A\left[S_0 - H_{S_0}H_{R_0}Qq^{-d}B\right]}{P} \cdot p(t). \tag{17}$$

In order that the numerator polynomial contains the model of the disturbance, the following diophantine equation has to be solved

$$S'D_p + H_{S_0}H_{R_0}Qz^{-d}B = S_0 \tag{18}$$

where D_p, H_{S_0}, H_{R_0}, d, B and S_0 are known, and S' and Q are unknown. Eq. (18) has a unique and minimal degree solution for S' and Q with $n_{S_0} \leq n_{D_p} + n_B + d - 1$, $n_{S'} = n_B + d + n_{H_{R_0}} + n_{H_{S_0}} - 1$ and $n_Q = n_{D_p} - 1$.
Remark: It is assumed that D_p and B do not have common factors but nothing is said of the feasibility of the solution if some complex zeros of D_p are very close to some low damped complex zeros of B (of course the Bezout equation to be solved will be "ill conditioned" as we approach cancellation).

From eqs. (17) and (18), and using a standard parameter adaptation algorithm (PAA) as explained in [21], a direct adaptive algorithm for the rejection of multiple unknown time-varying narrow band disturbances can be developed, by considering an adaptive $\hat{Q}$ filter of the form

$$\hat{Q}(z^{-1}) = \hat{q}_0 + \hat{q}_1 z^{-1} + \cdots + \hat{q}_{n_Q} z^{-n_Q}. \tag{19}$$

The details of the adaptation algorithm are given in [18] and a stability analysis is provided in [20].

VI. Adaptive regulation in the vicinity of low damped zeros

Eq. (18) has a unique and minimal solution for $Q(z^{-1})$ when the roots of $D_p(z^{-1})$ are not contained in $B(z^{-1})$, nevertheless the modulus of the output sensitivity function $S_{yp}(z^{-1})$ may becomes larger, specially when $B(z^{-1})$ has roots close to those of $D_p(z^{-1})$, e.g. presence of low damped zeros in the system at frequencies where attenuation is introduced. To overcome such situation, in [12] the augmentation of the order of the polynomial $\hat{Q}(z^{-1})$ is proposed, claiming that if the solution of (18) is not unique, and an infinity possible values for the coefficients $Q(z^{-1})$ exist to have the internal model as a factor, then there is a structural freedom to choose the optimum set of coefficients that provide the best performance by minimizing the output sensitivity function, (e.g. the modulus margin will be minimized)[5]. Note that the controller considered in [12] uses an "output error" type Youla-Kučera disturbance observer[6].

In [5] it was shown that using the plant model information (frequency characteristics), it is possible to *keep* the modulus of $S_{yp}(z^{-1})$ under an imposed maximum value by choosing appropriately the desired closed loop poles in $P(z^{-1})$. In this approach the minimal degree for the polynomial $\hat{Q}(z^{-1})$ is maintained and an "equation error" Youla-Kučera observer is used.

The objective will be subsequently to compare the two approaches in the context of the international benchmark on adaptive regulation. The experiments were conducted in

[4]The arguments (z^{-1}) and (q^{-1}) will be omitted in some of the following equations to make them more compact.

[5]$\left|S_{yp}(e^{-j\omega})\right|_{\max}$ corresponds to the H_∞ norm of the output sensitivity function.

[6]For a definition of the various types of Youla-Kučera disturbance observers see [16].

XPL:978-1-4799-5901-3/14/$31.00 ©2014 IEEE

the international test bed proposed in [16], where a single sinusoidal disturbance at 95 Hz will be introduced.

VII. Comparison of the two approaches - simulation and real time results

The comparison of the two approaches has been done on the active vibration control system described in Section II. Two main cases have been considered, with two options each:

1) $P(z^{-1})$ contains the stable poles **(SP)** of the plant model along with 12 real poles **(RP)** (This will reduce the modulus of $S_{up}(z^{-1})$ in high frequencies. Without these poles the control signal is saturated in the real-time application due to the presence of the harmonics of the disturbance).
   - a) With the minimal solution $n_Q = n_{D_p} - 1$.
   - b) With an augmented solution $n_Q > n_{D_p} - 1$.
2) $P(z^{-1})$ has the stable poles **(SP)** of the plant along with some auxiliary poles **(AP)**: 2 pairs of low damped complex poles and 4 real poles.
   - a) With the minimal solution $n_Q = n_{D_p} - 1$.
   - b) With an augmented solution $n_Q > n_{D_p} - 1$.

Simulations **(SIM)** and real-time **(RT)** experiments were conducted using both approaches. The results were classified in frequency and time domain. Time domain results are provided only for real-time experiments.

Table I summarizes the results in frequency domain (measured in dB) obtained for simulations and real-time experiments. The objective is to strongly attenuate the disturbance with a limited amplification of the other frequencies. To evaluate the performance three indicators have been defined together with there target values according to [16]: Disturbance Attenuation (**DA**) (min = 40 dB), Global Attenuation (**GA**) (min = 25 dB), and Maximum Amplification (**MA**) (max = 6 dB)[7]. The effects of the vicinity of the low damped complex zeros is noted for the *Case 1 a)*, where the global attenuation is minimum and a significant amplification was found, both for RT and SIM. For *Case 1 b)* with $n_Q = 5$, the improvements of the augmentation of the size of $\hat{Q}(z^{-1})$ are evident. Better attenuation and decreasing of the unwanted amplification are obtained[8]. When AP are used with a minimal solution (*Case 2 a)*), the results are significantly improved for the three specifications. It is important to observe that for the *Case 2 b)*, augmenting the size of the Q-filter improves further all the performance indicators in simulation. In real time the performance is improved by reducing the maximum of the unwanted amplification and augmenting the global attenuation, however the disturbance attenuation is slightly lower with respect to the case of minimal order for the $\hat{Q}(z^{-1})$.

[7]GA and MA give indication about the quality of the control which is supposed to introduce a very limited amplification at frequencies difeerent from the frequency of the disturbance

[8]Due to the presence of harmonics of the disturbance in real time experiments, differences arise between the RT and SIM results for the *Case 1* since the gain of $S_{up}(z^{-1})$ above 100 Hz is not low enough.

TABLE II
Time domain results

	Case 1 SP+RP					Case 2 SP+AP	
	a)	**b)**				**a)**	**b)**
$nQ =$	1	2	3	4	5	1	5
TE %	0	97.21	96	72.84	97.78	100	100
CT μs	2.8	3.0	3.5	3.8	4.5	2.8	4.2

TE: transient behaviour indicator (desired = 100%). CT: computation time.

Table II summarizes the results obtained in real-time with respect to the transient performance and computation time. Two specifications were considered according to [16]: a Transient Evaluation (**TE** in %) and the Computation Time (**CT** in μs). The transient evaluation criterion establishes that the transient duration when a disturbance is applied, has to be smaller than 2 s. A percentage was established for the fulfilment of this criterion. TE = 0% indicates a transient duration of 4 s and TE = 100% a transient duration smaller than 2 s. The detailed computation formulas can be found in [16].

The computation time is calculated from the Task Execution Time evaluated in the MATLAB©'s xPC-Target environment. The computational time only consider the closed loop calculations[9].

The use of **SP+AP** shows its efficiency since 100% fulfilment of the transient evaluation criterion is achieved. The results are slightly less good when augmentation of the size of the $\hat{Q}(z^{-1})$ is considered. As was expected, the increase of the number of parameters (order of $\hat{Q}$) implies an increase in the computation time, but this effect is not very significant.

Figure 5 shows the disturbance attenuation comparison between the two cases with the minimal ($n_Q = 1$) and highest order ($n_Q = 5$) solution. The figure shows real-time experimental results. As can be seen in the figure, some improvements are introduced when the order of Q is increased, such as lower amplifications in high frequencies and a larger attenuation (differences between the dashed blue line and dotted red line). Nevertheless, choosing appropriately the fixed closed loop poles (*Case 2, a) and b)*), the adaptive scheme introduce a significant attenuation with a minimum amplification. This can be seen also in the resulting output sensitivity function calculated with the estimated parameters of $\hat{Q}(z^{-1})$ for each case, from the real-time experiments. Figure 6 displays the modulus of each sensitivity function. It is noticed that passing from the *Case 2 a)* to *Case 2 b)* the characteristics of the output sensitivity function remains almost unchanged in high frequencies, while the maximum amplification is reduced. keeping the *water bed effect* bounded in the frequency zone of interest [5].

VIII. Concluding remarks

Careful selection of the closed loop poles for the design of the central controller combined with a minimum order

[9]The CT for an open loop test is 12.9 μs.

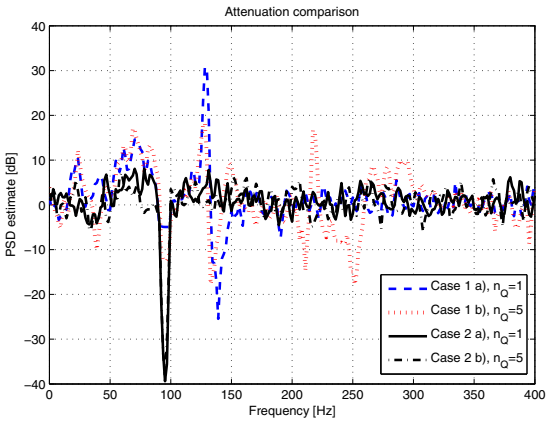

Fig. 5. Disturbance attenuation comparison between the three cases, real-time results.

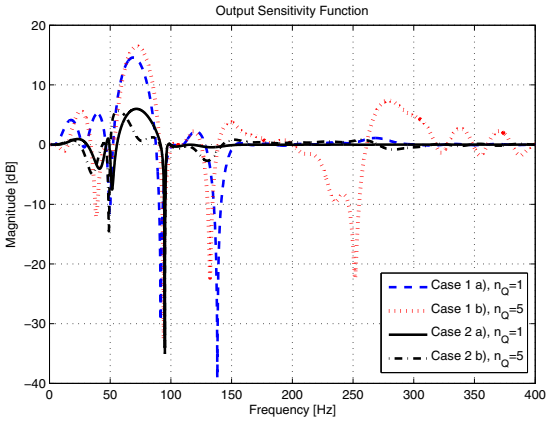

Fig. 6. Output Sensitivity Function comparison between the three cases, real-time results.

adaptive Q filter or over parametrization of the adaptive Q filter are two interesting solutions for improving the performance of adaptive regulation schemes in the vicinity of low damped complex zeros. The two approaches can also be combined. However over parametrization of the Q filter will require to use robust parameter estimation in order to avoid parameter drift. This case has been considered in a recent paper [13].

REFERENCES

[1] S. Aranovskiy, A. Bobtsov, A. Kremlev, N. Nikolaev, and O. Slita. Identification of frequency of biased harmonic signal. *European Journal of Control*, (5):129–139, 2010.

[2] F. Ben Amara, P.T. Kabamba, and A.G. Ulsoy. Adaptive sinusoidal disturbance rejection in linear discrete-time systems - Part I: Theory. *Journal of Dynamic Systems Measurement and Control*, 121:648–654, 1999.

[3] A.A. Bobtsov, S.A. Kolyubin, A.S. Kremlev, and A.A. Pyrkin. An iterative algorithm of adaptive output control with complete compensation for unknown sinusoidal disturbance. *Automation and Remote Control*, 73(8):1327–1336, 2012.

[4] M. Bodson and S.C. Douglas. Adaptive algorithms for the rejection of sinusosidal disturbances with unknown frequency. *Automatica*, 33:2213–2221, 1997.

[5] A. Castellanos Silva, I. D. Landau, and T.-B. Airimitoaie. Direct adaptive rejection of unknown time-varying narrow band disturbances applied to a benchmark problem. *European Journal of Control*, 19(4), 2013.

[6] F. Celani. Output regulation for the tora benchmark via rotational position feedback. *Automatica*, 47(3):584–590, 2011.

[7] X. Chen and M. Tomizuka. A minimum parameter adaptive approach for rejecting multiple narrow-band disturbances with application to hard disk drives. *IEEE Transactions on Control System Technology*, 20(2):408–415, Mar. 2012.

[8] Z. Ding. Global stabilization and disturbance suppression of a class of nonlinear systems with uncertain internal model. *Automatica*, 39(3):471 – 479, 2003.

[9] Z. Emedi and A. Karimi. Fixed-order lpv controller design for rejection of a sinusoidal disturbance with time-varying frequency. *2012 IEEE Multi-Conference on Systems and Control, Dubrovnik,*, 2012.

[10] T. Gouraud, M. Gugliemi, and F. Auger. Design of robust and frequency adaptive controllers for harmonic disturbance rejection in a single-phase power network. *Proceedings of the European Control Conference, Bruxelles*, 1997.

[11] G. Hillerstrom and J. Sternby. Rejection of periodic disturbances with unknown period - a frequency domain approach. *Proceedings of American Control Conference, Baltimore*, pages 1626–1631, 1994.

[12] Saeid Jafari, Petros Ioannou, Ben Fitzpatrick, and Yun Wang. Robust stability and performance of adaptive jitter supression in laser beam pointing. In *52nd IEEE Conference on Decision and Control*, Florence, Italy, December 10-13 2013.

[13] Saeid Jafari, Petros Ioannou, Ben Fitzpatrick, and Yun Wang. Robustness and performance of adaptive suppresion of unknown periodic disturbances. *Automatic Control, IEEE Transactions on*, 2013. Under review.

[14] C.E. Kinney, H.Fang, R.A. de Callafon, and M. Alma. Robust estimation and automatic controller tuning in vibration control of time varying harmonic disturbances. *Prepr. 18th IFAC World Congress,Milano, Italy*, pages 5401–5406, 2011.

[15] I. D. Landau, M. Alma, A. Constantinescu, J. J. Martinez, and M Noë. Adaptive regulation-rejection of unknown multiple narrow band disturbances (a review on algorithms and applications). *Control Engineering Practice*, 19(10):1168 – 1181, 2011.

[16] I. D. Landau, A. Castellanos Silva, T.-B. Airimitoaie, G. Buche, and N. Mathieu. Benchmark on adaptive regulation - rejection of unknown/time-varying multiple narrow band disturbances. *European Journal of Control*, 19(4), 2013.

[17] I. D. Landau, R. Lozano, M. M'Saad, and A. Karimi. *Adaptive control*. Springer, London, 2nd edition, 2011.

[18] I.D. Landau, M. Alma, J.J. Martinez, and G. Buche. Adaptive suppression of multiple time-varying unknown vibrations using an inertial actuator. *Control Systems Technology, IEEE Transactions on*, 19(6):1327 –1338, nov. 2011.

[19] I.D. Landau, A. Constantinescu, P. Loubat, D. Rey, and A. Franco. A methodology for the design of feedback active vibration control systems. *Proceedings of the European Control Conference 2001*, 2001. Porto, Portugal.

[20] I.D. Landau, A. Constantinescu, and D. Rey. Adaptive narrow band disturbance rejection applied to an active suspension - an internal model principle approach. *Automatica*, 41(4):563–574, 2005.

[21] I.D. Landau and G. Zito. *Digital Control Systems - Design, Identification and Implementation*. Springer, London, 2005.

[22] R. Marino, G.L. Santosuosso, and P. Tomei. Robust adaptive compensation of biased sinusoidal disturbances with unknown frequency. *Automatica*, 39:1755–1761, 2003.

[23] R. Marino, G.L. Santosuosso, and P. Tomei. Output feedback stabilization of linear systems with unknown additive output sinusoidal disturbances. *European Journal of Control*, 14(2), 2008.

[24] S. Valentinotti. *Adaptive Rejection of Unstable Disturbances: Application to a Fed-Batch Fermentation*. Thèse de doctorat, École Polytechnique Fédérale de Lausanne, April 2001.

Bibliography

[Airimiţoaie, 2012] Airimiţoaie, T.-B. (2012). *Commande robuste et calibrage des systèmes de contrôle actif de vibrations*. PhD thesis, Université de Grenoble.

[Airimitoaie et al., 2013] Airimitoaie, T.-B., Castellanos Silva, A., and Landau, I. D. (2013). Direct and indirect adaptive regulation strategies for rejection of time varying narrow band disturbances applied to a benchmark problem. In *Control Conference (ECC), 2013 European*, pages 2885–2890. IEEE.

[Airimiţoaie et al., 2013] Airimiţoaie, T.-B., Castellanos Silva, A., and Landau, I. D. (2013). Indirect adaptive regulation strategy for the attenuation of time varying narrow-band disturbances applied to a benchmark problem. *European Journal of Control*, 19(4):313–325.

[Airimitoaie and Landau, 2014] Airimitoaie, T.-B. and Landau, I. D. (2014). Indirect adaptive attenuation of multiple narrow-band disturbances applied to active vibration control. *Control Systems Technology, IEEE Transactions on*, 22(2):761–769.

[Airimitoaie et al., 2013] Airimitoaie, T.-B., Landau, I. D., Dugard, L., Alma, M., Castellanos Silva, A., Buche, G., and Noé, M. (2013). Algorithme de commande anticipatrice adaptative et contreréaction fixe pour le contrôle actif de vibrations en présence du couplage mécanique interne. In *4émes Journées Démonstrateurs 2013*.

[Alma, 2011] Alma, M. (2011). *Rejet adaptatif de perturbations en contrôle actif de vibrations*. PhD thesis, Université de Grenoble.

[Amara et al., 1999a] Amara, F. B., Kabamba, P., and Ulsoy, A. (1999a). Adaptive sinusoidal disturbance rejection in linear discrete-time systems - Part I: Theory. *Journal of Dynamic Systems Measurement and Control*, 121:648–654.

[Amara et al., 1999b] Amara, F. B., Kabamba, P., and Ulsoy, A. (1999b). Adaptive sinusoidal disturbance rejection in linear discrete-time systems - Part II: Experiments. *Journal of Dynamic Systems Measurement and Control*, 121:655–659.

[Anderson, 1998] Anderson, B. (1998). From Youla-Kucera to identification, adaptive and nonlinear control. *Automatica*, 34:1485–1506.

[Aranovskiy and Freidovich, 2013] Aranovskiy, S. and Freidovich, L. B. (2013). Adaptive compensation of disturbances formed as sums of sinusoidal signals with application to an active vibration control benchmark. *European Journal of Control*, 19(4):253–265.

[Åström and Murray, 2008] Åström, K. and Murray, R. (2008). *Feedback Systems: An Introduction for Scientists and Engineers*. Princeton University Press.

[Åström et al., 1984] Åström, K. J., Hagander, P., and Sternby, J. (1984). Zeros of sampled systems. *Automatica*, 20(1):31–38.

[Bengtsson, 1977] Bengtsson, G. (1977). Output regulation and internal models—a frequency domain approach. *Automatica*, 13(4):333 – 345.

[Beranek and Ver, 1992] Beranek, L. and Ver, I. (1992). *Noise and Vibration Control Engineering: Principles and Applications*. Wiley, New York.

[Bodson, 2005] Bodson, M. (2005). Rejection of periodic distrubances of unknown and time-varying frequency. *Int. J. of Adapt. Contr. and Sign. Proc.*, 19:67–88.

[Bodson and Douglas, 1997] Bodson, M. and Douglas, S. (1997). Adaptive algorithms for the rejection of sinusosidal disturbances with unknown frequency. *Automatica*, 33:2213–2221.

[Castellanos Silva et al., 2013a] Castellanos Silva, A., Airimitoaie, T.-B., Landau, I. D., Dugard, L., Buche, G., and Noé, M. (2013a). Stratégies directes et indirectes de régulation adaptative du rejet de perturbations variables à bande étroite appliqués à un benchmark international. In *4émes Journées Démonstrateurs*.

[Castellanos Silva et al., 2013b] Castellanos Silva, A., Landau, I. D., and Airimiţoaie, T.-B. (2013b). Direct adaptive rejection of unknown time-varying narrow band disturbances applied to a benchmark problem. *European Journal of Control*, 19(4):326–336.

[Castellanos Silva et al., 2014] Castellanos Silva, A., Landau, I. D., and Ioannou, P. (2014). Direct adaptive regulation in the vicinity of low damped complex zeros - application to active vibration control. In *22nd Mediterranean Conference on Control and Automation (MED)*, pages 255–260.

[Chen and Tomizuka, 2012] Chen, X. and Tomizuka, M. (2012). A minimum parameter adaptive approach for rejecting multiple narrow-band disturbances with application to hard disk drives. *Control Systems Technology, IEEE Transactions on*, 20(2):408 –415.

[Chen and Tomizuka, 2013a] Chen, X. and Tomizuka, M. (2013a). Control methodologies for precision positioning systems. In *2013 American Control Conference (ACC)*, pages 3704–3711.

[Chen and Tomizuka, 2013b] Chen, X. and Tomizuka, M. (2013b). Selective model inversion and adaptive disturbance observer for time-varying vibration rejection on an active-suspension benchmark. *European Journal of Control*, 19(4):300–312.

[Chen and Tomizuka, 2014] Chen, X. and Tomizuka, M. (2014). New repetitive control with improved steady-sate performance and accelerated transient. *Control Systems Technology, IEEE Transactions on*, 22(2):664–675.

[Coanda, 1930] Coanda, H. (1930). Procédé de protection contre les bruits. French Patent FR 722.274.

[de Callafon and Fang, 2013] de Callafon, R. A. and Fang, H. (2013). Adaptive regulation via weighted robust estimation and automatic controller tuning. *European Journal of Control*, 19(4):266–278.

[Ding, 2003] Ding, Z. (2003). Global stabilization and disturbance suppression of a class of nonlinear systems with uncertain internal model. *Automatica*, 39(3):471 – 479.

[Doyle et al., 2013] Doyle, J. C., Francis, B. A., and Tannenbaum, A. R. (2013). *Feedback control theory*. Courier Dover Publications.

[Elliott, 2001] Elliott, S. (2001). *Signal processing for active control*. Academic Press.

[Elliott and Nelson, 1993] Elliott, S. and Nelson, P. (1993). Active noise control. *Signal Processing Magazine, IEEE*, 10(4):12 –35.

[Elliott and Sutton, 1996] Elliott, S. and Sutton, T. (1996). Performance of feedforward and feedback systems for active control. *Speech and Audio Processing, IEEE Transactions on*, 4(3):214 –223.

[Fleming et al., 2007] Fleming, A., Niederberger, D., Moheimani, S., and Morari, M. (2007). Control of resonant acoustic sound fields by electrical shunting of a loudspeaker. *Control Systems Technology, IEEE Transactions on*, 15(4):689 –703.

[Forssell and Ljung, 1999] Forssell, U. and Ljung, L. (1999). Closed-loop identification revisited. *Automatica*, 35(7):1215–1241.

[Francis and Wonham, 1976] Francis, B. and Wonham, W. (1976). The internal model principle of control theory. *Automatica*, 12(5):457 – 465.

[Fuller et al., 1997] Fuller, C., Elliott, S., and Nelson, P. (1997). *Active Control of Vibration*. Academic Press, New York.

[Fuller and von Flotow, 1995] Fuller, C. and von Flotow, A. (1995). Active control of sound and vibration. *Control Systems, IEEE*, 15(6):9 –19.

[Gevers, 1993] Gevers, M. (1993). Towards a joint design of identification and control? In *Essays on Control*, pages 111–151. Springer.

[Gouraud et al., 1997] Gouraud, T., Gugliemi, M., and Auger, F. (1997). Design of robust and frequency adaptive controllers for harmonic disturbance rejection in a single-phase power network. *Proceedings of the European Control Conference, Bruxelles*.

[Guicking, 2007] Guicking, D. (2007). Active control of sound and vibration history – fundamentals – state of the art. Festschrift DPI, 1–32, Herausgeber (ed.), Universitätsverlag Göttingen 2007.

[Gustavsson et al., 1977] Gustavsson, I., Ljung, L., and Söderström, T. (1977). Identification of processes in closed loop?identifiability and accuracy aspects. *Automatica*, 13(1):59–75.

[Hillerstrom and Sternby, 1994] Hillerstrom, G. and Sternby, J. (1994). Rejection of periodic disturbances with unknown period - a frequency domain approach. *Proceedings of American Control Conference, Baltimore*, pages 1626–1631.

[Hjalmarsson et al., 1996] Hjalmarsson, H., Gevers, M., and De Bruyne, F. (1996). For model-based control design, closed-loop identification gives better performance. *Automatica*, 32(12):1659–1673.

[Johnson, 1976] Johnson, C. (1976). Theory of disturbance-accomodating controllers. In *Control and Dynamical Systems* (C. T. Leondes, Ed.). Vol. 12, pp. 387-489.

[Junger and Feit, 1972] Junger, M. C. and Feit, D. (1972). *Sound, structures, and their interaction*, volume 240. MIT press Cambridge, MA.

[Karimi and Emedi, 2013] Karimi, A. and Emedi, Z. (2013). H-inf gain-scheduled controller design for rejection of time-varying narrow-band disturbances applied to a benchmark problem. *European Journal of Control*, 19(4):279–288.

[Karnopp et al., 1974] Karnopp, D., Crosby, M. J., and Harwood, R. A. (1974). Vibration control using semi-active force generators. *Journal of Manufacturing Science and Engineering*, 96(2):619 – 626.

[Kucera, 1975] Kucera, V. (1975). Stability of discrete linear feedback systems. In *Proc. 6th IFAC World Congress*, volume 1.

[Landau et al., 2011a] Landau, I., Alma, M., and Airimiţoaie, T. (2011a). Adaptive feedforward compensation algorithms for active vibration control with mechanical coupling. *Automatica*, 47(10):2185 – 2196.

[Landau et al., 2011b] Landau, I., Alma, M., Martinez, J., and Buche, G. (2011b). Adaptive suppression of multiple time-varying unknown vibrations using an inertial actuator. *Control Systems Technology, IEEE Transactions on*, 19(6):1327 –1338.

[Landau et al., 2005] Landau, I., Constantinescu, A., and Rey, D. (2005). Adaptive narrow band disturbance rejection applied to an active suspension - an internal model principle approach. *Automatica*, 41(4):563–574.

[Landau and Karimi, 1997] Landau, I. and Karimi, A. (1997). Recursive algorithms for identification in closed loop. a unified approach and evaluation. *Automatica*, 33(8):1499–1523.

[Landau and Zito, 2005] Landau, I. and Zito, G. (2005). *Digital Control Systems - Design, Identification and Implementation*. Springer, London.

[Landau et al., 2011c] Landau, I. D., Alma, M., Constantinescu, A., Martinez, J. J., and Noë, M. (2011c). Adaptive regulation: Rejection of unknown multiple narrow band disturbances (a review on algorithms and applications). *Control Engineering Practice*, 19(10):1168 – 1181.

[Landau et al., 2013a] Landau, I. D., Castellanos Silva, A., Airimitoaie, T.-B., Buche, G., et al. (2013a). Benchmark on adaptive regulation: rejection of unknown/time-varying multiple narrow band disturbances. *European Journal of Control*, 19(4):237–252.

[Landau et al., 2013b] Landau, I. D., Castellanos Silva, A., Airimitoaie, T.-B., Buche, G., and Noe, M. (2013b). An active vibration control system as a benchmark on adaptive regulation. In *Control Conference (ECC), 2013 European*, pages 2873–2878. IEEE.

[Landau and Karimi, 1999] Landau, I. D. and Karimi, A. (1999). A recursive algorithm for armax model identification in closed loop. *Automatic Control, IEEE Transactions on*, 44(4):840–843.

[Landau et al., 2011d] Landau, I. D., Lozano, R., M'Saad, M., and Karimi, A. (2011d). *Adaptive control*. Springer, London, 2nd edition.

[Landau et al., 1995] Landau, I. D., Rey, D., Karimi, A., Voda, A., and France, A. (1995). A flexible transimission system as a benchmark for robust digital control. *European Journal of Control*.

[Ljung, 1999] Ljung, L. (1999). *System Identification - Theory for the User*. Prentice Hall, Englewood Cliffs, second edition.

[Lueg, 1934] Lueg, P. (1934). Process of silencing sound oscillations. US Patent 2,043,416.

[Marcos, 2000] Marcos, T. (2000). The straight attraction. *Motion control*, 13:29–33.

[Marino et al., 2003] Marino, R., Santosuosso, G., and Tomei, P. (2003). Robust adaptive compensation of biased sinusoidal disturbances with unknown frequency. *Automatica*, 39:1755–1761.

[Marino and Tomei, 2007] Marino, R. and Tomei, P. (2007). Output regulation for linear minimum phase systems with unknown order exosystem. *Automatic Control, IEEE Transactions on*, 52(10):2000 –2005.

[Mårtensson and Hjalmarsson, 2005] Mårtensson, J. and Hjalmarsson, H. (2005). Closed loop identification of unstable poles and non-minimum phase zeros.

[Mårtensson and Hjalmarsson, 2009] Mårtensson, J. and Hjalmarsson, H. (2009). Variance-error quantification for identified poles and zeros. *Automatica*, 45(11):2512–2525.

[Martensson et al., 2005] Martensson, J., Jansson, H., and Hjalmarsson, H. (2005). Input design for identification of zeros. In *World Congress*, volume 16, pages 78–78.

[Nehorai, 1985] Nehorai, A. (1985). A minimal parameter adaptive notch filter with constrained poles and zeros. *IEEE Trans. Acoust., Speech, Signal Processing*, ASSP-33:983–996.

[Olson and May, 1953] Olson, H. F. and May, E. G. (1953). Electronic sound absorber. *The Journal of the Acoustical Society of America*, 25(6):1130–1136.

[Procházka and Landau, 2003] Procházka, H. and Landau, I. D. (2003). Pole placement with sensitivity function shaping using 2nd order digital notch filters. *Automatica*, 39(6):1103 – 1107.

[Serrani, 2006] Serrani, A. (2006). Rejection of harmonic disturbances at the controller input via hybrid adaptive external models. *Automatica*, 42(11):1977 – 1985.

[Snyder, 2000] Snyder, S. D. (2000). *Active Noise Control Primer*. Springer Verlag.

[Söderström and Stoica, 1988] Söderström, T. and Stoica, P. (1988). *System identification*. Prentice-Hall, Inc.

[Stoica and Nehorai, 1988] Stoica, P. and Nehorai, A. (1988). Performance analysis of an adaptive notch filter with constrained poles and zeros. *IEEE Trans. Acoust., Speech, Signal Processing*, 36(6):911 – 919.

[Tsypkin, 1997] Tsypkin, Y. (1997). Stochastic discrete systems with internal models. *Journal of Automation and Information Sciences*, 29(4&5):156–161.

[Valentinotti, 2001] Valentinotti, S. (2001). *Adaptive Rejection of Unstable Disturbances: Application to a Fed-Batch Fermentation*. Thèse de doctorat, École Polytechnique Fédérale de Lausanne.

[Valentinotti et al., 2003] Valentinotti, S., Srinivasan, B., Holmberg, U., Bonvin, D., Cannizzaro, C., Rhiel, M., and von Stockar, U. (2003). Optimal operation of fed-batch fermentations via adaptive control of overflow metabolite. *Control Engineering Practice*, 11(6):665 – 674.

[Van den Hof, 1998] Van den Hof, P. (1998). Closed-loop issues in system identification. *Annual reviews in control*, 22:173–186.

[Van Den Hof and Schrama, 1995] Van Den Hof, P. M. and Schrama, R. J. (1995). Identification and control-closed-loop issues. *Automatica*, 31(12):1751–1770.

[Vinnicombe, 1993] Vinnicombe, G. (1993). Frequency domain uncertainty and the graph topology. *Automatic Control, IEEE Transactions on*, 38(9):1371 –1383.

[Widrow and Stearns, 1985] Widrow, B. and Stearns, S. (1985). *Adaptive Signal Processing*. Prentice-Hall, Englewood Cliffs, New Jersey.

[Wu and Ben Amara, 2013] Wu, Z. and Ben Amara, F. (2013). Youla parameterized adaptive regulation against sinusoidal exogenous inputs applied to a benchmark problem. *European Journal of Control*, 19(4):289–299.

[Youla et al., 1976] Youla, D. C., Jabr, H., and Bongiorno, J. J. (1976). Modern wiener-hopf design of optimal controllers–part ii: The multivariable case. *Automatic Control, IEEE Transactions on*, 21(3):319–338.

[Zhou et al., 1996] Zhou, K., Doyle, J. C., and Glover, K. (1996). *Robust and optimal control*. Prentice Hall, Upper Saddle River, New Jersey.

Compensation adaptative par feedback pour le contrôle actif de vibrations en présence d'incertitudes sur les paramètres du procédé

Résumé : Dans cette thèse, nous proposons des solutions pour la conception de systèmes de contrôle actif de vibration robustes (AVC). Le manuscrit de thèse comporte deux grandes parties.

Dans la première, les problèmes d'incertitude paramétrique dans les systèmes de contrôle actif de vibration sont étudiés. En plus des incertitudes sur la fréquence des perturbations, nous avons trouvé que la présence de zéros complexes peu amortis soulevait des problèmes de conception difficiles, même pour des systèmes et des modèles parfaitement connus. Dans ce contexte, nous avons proposé des solutions pour le problème linéaire. Une procédure améliorée d'identification en boucle fermée a été développée pour réduire les incertitudes dans l'identification de ces zéros. Pour traiter les incertitudes sur la perturbation, l'adaptation de la fréquence est de toute façon incontournable.

La seconde partie est consacrée au développement et/ou à l'amélioration de deux algorithmes, désormais classiques, de compensation par feedback adaptatif direct, fondés sur la paramétrisation de Youla-Kučera. Le premier résulte de l'amélioration d'un précédent travail (Landau et al., 2005); les contributions concernent la synthèse du contrôleur central robuste et l'utilisation optionnelle de la surparamétrisation du filtre Q-FIR (réponse à temps fini) pour minimiser l'effet « waterbed » sur la fonction de sensibilité de sortie. Le second algorithme présente une structure hybride directe/indirecte qui utilise un filtre Q-IIR (à temps de réponse infini). Les améliorations sont dues principalement au dénominateur du filtre, obtenu à partir d'une estimation de la perturbation. Cette solution permet également de simplifier la conception du contrôleur central.

Les algorithmes ont été testés, comparés et validés sur un procédé réel du laboratoire Gipsa-lab, dans le cadre d'un benchmark international.

Mots clés : Contrôle actif de vibration, paramétrisation de Youla-Kučera, commande échantillonnée robuste, identification paramétrique, compensation par feedback adaptatif, calibrage de fonction de sensibilité.

Feedback Adaptive Compensation for Active Vibration Control in the presence of plant parameter uncertainties

Abstract: In this thesis, solutions for the design of robust Active Vibration Control (AVC) systems are presented. The thesis report is composed of two main parts.

In the first part of the thesis, uncertainties issues in Active Vibration Control systems are examined. In addition to the uncertainties on the frequency of the disturbances, it has been found that the presence of low damped complex zeros raises difficult design problems even if plant and models are perfectly known. Solutions for the linear control in this context have been proposed. In order to reduce the uncertainties in the identification of low damped complex zeros, an improved closed loop identification procedure has been developed. To handle the uncertainties on the disturbance, frequency adaptation has to be used anyway.

The second part deals with further developments and/or improvements of the now classical direct adaptive feedback compensation algorithms using the Youla-Kučera controller parameterization. Two new solutions have been proposed in this context. The first one results from the improvement of a previous work (Landau et al., 2005). The contributions are a new robust central controller design and the optional use of overparameterization of the Q-FIR filter which aims to ensure a small waterbed effect for the output sensitivity function, reducing therefore the unwanted amplification. The second algorithm presents a mixed direct/indirect structure which uses a Q-IIR filter. The improvements are mainly due to the effect of the Q filter denominator, obtained from a disturbance identification. This solution, in addition, drastically simplifies the design of the central controller.

The algorithms have been tested, compared and validated on an international benchmark setup available at the Control Systems Department of GIPSA-Lab, Grenoble, France.

Keywords: Active vibration control, Youla-Kučera parameterization, robust digital control, parametric identification, adaptive feedback compensation, sensitivity function shaping.